European Commission

Advanced zinc-based hot dip coatings for the automotive application

(AUTOCOAT)

Research and Innovation

EUR 26323 EN

EUROPEAN COMMISSION
Directorate-General for Research and Innovation
Directorate G — Industrial Technologies
Unit G.5 — Research Fund for Coal and Steel

E-mail: rtd-steel-coal@ec.europa.eu
RTD-PUBLICATIONS@ec.europa.eu

Contact: RFCS Publications

European Commission
B-1049 Brussels

European Commission

Research Fund for Coal and Steel

Advanced zinc-based hot dip coatings for the automotive application

(AUTOCOAT)

N. Le Bozec, D. Thierry
Institut de la Corrosion SAS
220 rue Rivoalon, 29200 Brest, FRANCE

M. Rohwerder
MPIE für Eisenforschnung GmbH
Max-Planck Str. 1, 40237 Düsseldorf, GERMANY

A. Kovacs
Limedion GmbH
Augarten Str. 110, 68165 Mannheim, GERMANY

A. Peltola
Ruukki Metals Oy
Suolakivenkatu, 008110 Helsinki, FINLAND

G. Luckeneder
voestalpine Stahl GmbH
voest-alpine Str. 3, 4020 Linz, AUSTRIA

L. Luxem
Thyssen Krupp Steel Europe AG
Eberhard Str. 12, 44145 Dortmund, GERMANY

G. Marchiaro
Centro Ricerche FIAT
Corso Giovanni Agnelli 200, 10135 Torino, ITALY

Grant Agreement RFSR-CT-2009-00014
1 September 2009 to 28 February 2013

Final report

Directorate-General for Research and Innovation

2013

EUR 26323 EN

Europe Direct is a service to help you find answers to your questions about the European Union

Freephone number (*)**:**

00 800 6 7 8 9 10 11

(*) Certain mobile telephone operators do not allow access to 00 800 numbers or these calls may be billed.

More information on the European Union is available on the Internet (http://europa.eu).

Cataloguing data can be found at the end of this publication.

Luxembourg: Publications Office of the European Union, 2013

ISBN 978-92-79-34587-6
doi:10.2777/50368

Printed in Luxembourg

PRINTED ON WHITE CHLORINE-FREE PAPER

Table of Content

1 Final summary

The project has been successful in achieving almost all the planned objectives as summarized below:

Technological aspects

- Data on long term field exposures of ZnMgAl coatings in various configurations (painted, unpainted in open and confined situations, galvanic conditions) have been obtained as well as their behaviour in accelerated corrosion tests commonly used by the automotive industry.
- The application properties of these novel coatings have been tested with regards to formability and joining with spot welding and adhesive bonding techniques.
- The influence of phosphatation parameters on ZnMgAl coatings has been investigated in order to assess their robustness to process variation.
- Guidelines for the application of advanced ZnMgAl coatings in the manufacturing of car have been issued in a comprehensive way. These guidelines can also be used for other applications such as building or infrastructure.

Scientific aspects

- The outcomes of the laboratory tests in particular on the influence of carbon dioxide have helped in a better understanding of the mechanisms of atmospheric corrosion of ZnMgAl materials.
- The delamination behavior of painted ZnMgAl coatings has been studied and compared to conventional coating. A paint system without phosphatation has also been investigated.

1.1 WP 1 Project management

Management of the project was carried out by IC which ensured the communication with TGS5 by reporting and attending meetings. No major problems that would have affected the project occurred. Regular meetings of the consortium were organized in order to ensure smooth progression of the project, to present and discuss data, to solve the problems etc. Modifications of the Grant Agreement were also made as a consequence of change of legal structures at three beneficiaries.

1.2 WP2 Material selection, preparation and characterization

The objectives of WP 2 were to finalize the selection of material and provide them for the project, to characterize the materials and to prepare them in various configurations upon WPs.

Line hot dip metallic coatings including three novel Zn-Mg-Al ‘ZMA’ compositions available at steel suppliers involved in the project and four conventional zinc coatings (GI, GE, Galfan and Galvannealed steel) were supplied as planned. Novel ZMA included ZnMg1%Al1% from TKSE, ZnMg2%Al2% from voestalpine and ZnMg1.5%Al1.5% from Ruukki. In addition, five Rhesca coatings which composition varied from 1 to 4% of Al and Mg were produced by Ruukki. All novel ZMA materials were characterized as regards to the coating thickness, surface microstructure, composition and distribution of elements (cross-section and GDOES profile). Evidence of Al-Mg rich phase was shown on ZMA coatings at the interface with steel. Rather similar structure was observed on all ZMA coatings with an obvious tendency to increase the binary and ternary eutectic structures compared to primary zinc globules when increasing the content of Mg and Al in the coating.
Line hot dip materials were further prepared for being tested in situations for automotive applications: cosmetic situation (e.g. painted), unpainted in open and hem-flange configurations and in galvanic state with bolts. Formability and joining was obviously carried out on bare metallic coatings. The samples were distributed to the different partners upon tasks distribution.
Two coating compositions (ZnMg1%Al1% and ZnMg4%Al4%) produced by physical vapour deposition (PVD) were initially planned at Limedion. However, despite many different trials at LMI and at another place (JKU), no satisfying ternary PVD coatings could be produced within the time schedule of the project. As the production of PVD coatings was only a minor task of the project, the absence of such coating has not affected the achievement of the project tasks and objectives.

1.3 WP3 Surface oxides, pre-treatment optimization and mechanism of paint delamination

The objectives of WP 3 were to assess the effect of surface oxide composition and structure on paint adhesion and cathodic delamination in view of optimization of phosphataion or avoiding it, to study and understand the corrosion mechanisms of bare and painted ZMA coatings in atmosphere, focusing on the initial stages of corrosion.

The composition of the native oxide on the different line hot dip ZMA coatings as well as on the Rhesca ZMA coatings was investigated by means of XPS and sputter depth profiling. SKP technique was used to assess the surface potential. The results indicated that during the galvanizing process of the Zn-Mg-Al metallic coatings, a segregation of the minor alloying elements e.g. Mg and Al takes place towards the surface. The composition of the coatings´ outer surface scale was rather different than the chemical composition of the bath used. More interestingly, all Rhesca simulator samples showed more or less similar surface compositions, which differed especially in the Zn concentration from the production line coatings ZMA1 and ZMA2, which might be attributed to the history of the production process itself.

As regards to paint delamination, although an enrichment in alloying elements to the surface and surface near region was observed, i.e. a significant coverage by high band gap oxides was present on the surface, this was not sufficient to provide a significant improvement in the delamination behaviour over standard materials such as GE or GI. The reason for this is for one thing that potential inversion between corrosion potential in the defect and at the intact interface that was found for Zn-Mg alloys with higher Mg-contents, such as $MgZn_2$, does not occur, most likely because of too low levels of Mg. Hence, the inherent delamination resistance that was observed on such high Mg-containing alloys as a consequence of this potential inversion, was not available for the ZMAs investigated here. However, one would expect that the presence of high band gap oxides should have a greater impact on delamination rate. The reason for the relatively low impact was suggested to lie in the microstrucure of the ZMA coatings: great Zn-rich phases are present in these materials that may serve as fast delamination pathways, lowering the possible impact of the more insulating oxides on the higher alloyed phases. Summarizing, the oxide layers on the investigated ZMAs do not provide a meaningful protection against delamination and do not provide any advantages when it is planned to skip phosphatation. The influence of phosphatation parameters (bath temperature, treatment time and free acid) was additionally studied using a model and commercial solution. The results showed that ZMA are suitable for phosphation processes in automotive industry with good robustness to process variation.

1.4 WP4 Long term corrosion properties

The objectives of WP 4 were to obtain reliable and full-scale data on the performance of ZMA hot dip coated materials in a wide variety of reals conditions including mobile exposures.

The corrosion performance of line hot dip materials including conventional coatings (GI, GE, GA and Galfan) and new ZMA coatings (ZnMg1-2%Al1-2%) after field exposures in three stationary sites and two mobile situations on operating vehicle (Fiat proving ground and under a truck driving in Switzerland) was studied regarding cosmetic corrosion and corrosion in hem-flanges and open situations. From the results, the following conclusions may be drawn:

- No improvement of ZMA coatings in comparison to conventional ones was observed on **painted cosmetic samples** (creep from the scribe line) after two years of exposure in atmospheric field sites or under the trailer driving in Switzerland. The most important degradations were observed in the marine site of Brest while the sites of Dortmund and Linz were significantly less aggressive as well as the mobile exposure. The results should however be consolidated with longer exposure durations.
- The better performance of painted ZMA coatings after Fiat proving ground test (with about twice less creep than conventional coatings) was typical of their behavior in accelerated corrosion tests with important salt load. This is not surprising when examining the different phases of the proving ground.
- A beneficial effect of Mg and Al alloying elements by a factor of 1.5 to 2 was however noticed when considering **unpainted metallic coatings** in **open configurations** exposed at stationary field sites.

This improvement factor was significantly better on mobile exposure: whereas a factor of about 6 was found after 1 year, it decreases to 2.5-3 after 2 years. Same improvement factor was also observed after Fiat proving ground test with however significant deviation upon the position of the samples to the road.

- More corrosion was globally observed in the selected **hem-flange designs** than in open configurations, whatever the metallic coating and exposure conditions. In such confined situations, the improvement of ZMA coating compared to conventional zinc coatings was not obvious either after field exposures or Fiat proving ground test. In some cases, significant scattering of the data were also observed. However, ZMA1.5 and ZMA2 showed better performance after 2 years of exposure under the truck.
- No major difference was observed upon Al and Mg content whatever the configuration and field exposure conditions.

It is however recommended to consolidate the present results with data from longer exposure durations.

1.5 WP5 Application properties

The objectives of WP 5 were to obtain evidence that ZMA coatings can be applied in mass automotive production as regards to coating formability and joining tecnhnology.

The application properties of ZMA coating compositions ranging from 1 to 2% of alloying elements were tested as regards to formability and joining with spot welding and adhesive bonding techniques.

Concerning **formability** of ZMA coatings, the following conclusions may be drawn:

- ZMA coatings were more prone to cracking compared to HDG coating. Cracking of ZMA coating was observed in severe forming situation on cross die sample and on cup of 4.3 and 6.5 mm in height in particular. The crack networks covered the whole coating and went through it down to the steel substrate. A tendency to form larger cracks was observed on the thickest ZMA coating (ZMA1.5). No influence of the content of alloying element (1 to 2%) was however noted.
- Despite the presence of cracks in ZMA coatings on formed samples, no increase of the corrosion risk was observed in accelerated corrosion tests.
- Regarding friction coefficients, slightly lower values were measured on line hot dip ZMA than on HDG coating presumably attributed to surface roughness.

As regards to **joining** properties of ZMA coatings, the following observations were made:

- The addition of Mg and Al from 1 to 2 % in the coating gave rather comparable welding properties as for conventional zinc coating when similar welding parameters were applied. The welding properties appeared to be more sensitive to welding parameters and to coating/steel thickness than to coating composition.
- Despite slightly lower mechanical properties of adhesive bonded joints on ZMA coating compared to HDG one, acceptable results fulfilling FIAT requirements were however obtained.

Thus, ZMA coatings with alloying elements ranging from 1 and 2% showed similar application properties than HDG coating both regarding formability, spot welding and adhesive bonding which obviously constitutes crucial properties for manufacturing vehicles.

1.6 WP6 Cosmetic corrosion and protection in hem flange

The objectives of WP 6 were to evaluate the corrosion performance of ZMA coatings in several accelerated corrosion tests currently used by car manufacturers considering cosmetic corrosion (painted surface) and perforation corrosion (hem-flanges).

The corrosion resistance of line hot dip ZMA coatings was evaluated in accelerated corrosion tests namely Volvo ACT STD423-0014, VDA 621-415 and New VDA test considering painted cosmetic

samples and unpainted coatings in open and hem flange configurations. The results were compared to conventional zinc coatings (GI, GE, GA and Galfan).
From the results, the behaviour of ZMA coating in accelerated corrosion automotive tests seemed to be dependent on the testing conditions as well as the configuration of the samples e.g. cosmetic and hem-flange. Thus, ZMA coatings provided significant improvement in comparison to conventional coatings in tests involving significant salt loads such as VDA or neutral salt spray tests especially on cosmetic and open samples.
On the contrary, the beneficial effect of ZMA coatings was inferior in tests with lower salt load (New VDA and Volvo test), particularly when considering cosmetic corrosion on painted samples and corrosion in confinement.
On the influence of Al and Mg content in the metallic coating of line hot dip coatings, no significant differences were observed unless on bare material in open configuration where ZMA2 showed a somewhat better improvement than ZMA1. This was validated when testing a larger range of Mg and Al composition (e.g. from 1 to 4 wt%) as prepared using a galvanising simulator. The corrosion resistance was clearly increasing with the increasing concentration of Magnesium and Aluminium in the coating at least in open configuration.

1.7 WP7 Galvanic protection by Zn-Al-Mg coatings and effect of carbon dioxide

The objectives of WP 7 were to evaluate the effect of carbon dioxide on the corrosion performance of ZMA coated steel and to assess the galvanic effect of ZMA coating in contact with steel and other coatings for fasteners.

For the first time, the **effect of CO_2** on the atmospheric corrosion of line hot dip ZMA coatings was investigated under carefully controlled conditions at ambient concentration of CO_2 (approx. 350 ppm) and low CO_2 (<3 ppm) as a function of chloride concentration. Two temperatures 20 and 30°C were also tested and two conventional zinc coatings GI and Galfan were also included in the study as reference materials.
From this investigation, the absence of CO_2 clearly enhanced the average corrosion of all zinc coatings and the metal loss increased with the concentration of chloride and the temperature. Interestingly, ZMA coatings were clearly more affected than conventional GI coating. While GI was approximately twice more corroded in the absence of CO_2 compared to ambient concentration, ZMA was 12 times more affected when exposed to low CO_2 conditions, particularly at high concentration of chloride. An obvious pH effect in the absence of CO_2 was underlined. The analysis of corrosion products by FTIR and XRD indicated the presence of layered double hydroxide (LDH), ZnO and simonkolleite on ZMA2 in the absence of CO_2 while hydroxycarbonate and simonkolleite were dominating in ambient air.

The **galvanic protection** of ZMA coating was compared to conventional zinc coating in assemblies with fasteners of different nature (steel, stainless steel and different zinc coated steels) in order to simulate on-vehicle situations. The results were depending on testing conditions e.g. field or laboratory tests. Considering the strongest galvanic coupling obtained with steel fasteners where significant corrosion occurred, rather comparable behaviour of ZMA and conventional GI coating was observed when considering field exposures both stationary and mobile exposure (truck) while in accelerated corrosion test (such as New VDA), ZMA coating tend to be more protective than conventional GI for similar coating thickness. In all situations, GE showed the poorest protective ability. Same conclusions were also observed when stainless steel fasteners were used with however much less corrosion extent of the metallic coatings, while no or extremely low corrosion was developed with zinc coated fasteners. The observed results were also confirmed by electrochemical investigations regarding the galvanic current.

1.8 WP8 Modelling, life prediction and application guidelines

The objectives of WP 8 were to compile data from laboratory and field tests in guidelines for the industry and to propose mechanisms of metal and paint degradation in order to formulate models describing the corrosion mechanisms of ZMA coatings.

Simple guidelines for the industry have been written as regards to automotive process for phosphatation, forming, spot welding and adhesive bonding. Concerning the corrosion performance of ZMA, the variety of testing conditions including accelerated tests and exposures in real environments (static and mobile situations) have allowed to draw useful corrosion guidelines which estimate the corrosion behaviour of ZMA compared to conventional zinc coatings.

The possible mechanisms of corrosion protection ZMA coatings, based on the results obtained in WP3 - WP7, were analysed and models for corrosion at initial and later stages proposed. The analysis was divided in three subgroups: cathodic protection (delamination from scribe down to steel and cut edge performance), metal loss of the zinc (alloy) coating and appearance of red rust.

For the delamination from scribes and at cut edges, the explanation for the superior performance of ZMA coatings over GI and Galfan at initial stages of corrosion and especially under very aggressive corrosion conditions is suggested to be in line with a recently published work where the already important effect of zinc cations on the exposed steel surface is enhanced by precipitation of MgO in initial stages of the corrosion process. At these initial stages, the main effect of the zinc cations is the replacement of active Fe^{2+} sites in the iron oxide prevailing at the high alkaline pH levels during cathodic protection even at the low potentials of the corroding zinc. This replacement of the active surface sites by zinc cations seems to be enhanced by the precipitation of MgO. This effect is already present for low Mg contents in the ZMA coating, as clearly shown in accelerated corrosion testing. The results of the accelerated tests also show that this is really an effect due to Mg and not Al. After longer exposure times, when thicker corrosion product layers have formed on the surface and the electrochemical activity is already significantly reduced, the synergetic effect of Mg becomes unimportant. This is in accordance with long time exposure tests where the superior performance of ZMA becomes significantly reduced.

The superior corrosion performance of the coating itself, evaluated as metal loss of the zinc (alloy) coating is proposed to be mainly due to the effect of the alloying elements on the microstructure of the coatings. This should have an effect on the formation of local cathodes and anodes: with decreasing feature size of the microstructure, more anodes are expected to form as the Mg-containing intermetallics are more reactive than the zinc phase. This provides by far a higher density of corrosion initiation sites when compared to GE or GI, where the corrosion phenomenon is more a “statistical effect”. Similar to pitting corrosion, the statistical initiation sites on GE or GI coatings are stabilised by the related pH changes (less alkaline at the anodes, more alkaline at the cathodes). Hence, on GI coating, large anodes and cathodes are established while on ZMA coating, the size of anodes and cathodes is much smaller. This will lead to less extreme alkalinity on the cathodes of ZMA coating. This buffering effect is even more important when the corrosion activity is high (i.e. more alkaline pH). This is in accordance with the observation that for ZMA the performance gain over GI or GE increases with increasing aggressiveness of the corrosion test. Possibly, for ZMA, this microstructure related buffering effect, which is already effective at relatively low alloying degrees, is further enhanced by a buffering effect through Mg cations, but most likely only at the initial stages of the corrosion process, as Mg is quickly de-alloyed from the surface region.

At later stages of the corrosion such as after 1 to 2 years of field exposures, no Mg effect can be discerned as Galfan always performs better than the ZMA samples. The main reason for this is that the role of distribution of active sites at the metal surface becomes less important on less active surfaces, i.e. when they are covered by thick layers.

In CO_2-reduced atmospheres, such as e.g. in hem flange conditions, ZMA coatings, but also Galfan, can perform inferior to GE and GI. This is attributed to the much more alkaline values in the absence of the buffering effect of CO_2 and the correlated breakdown of Al-rich phases.

Concerning the appearance of red rust on the coating itself, it is proposed that the cathodic protection enhancement that is observed at the cut edge and at the scribe and the decreased metal loss of the alloy coating are combined leading to a significant improvement under very aggressive conditions.

2 Scientific and technical description of the results

2.1 Objectives of the project

The aims of the project may be summarized as follows as regards to two major aspects:

Technological innovative aspects

- To study the long term corrosion properties of ZMA coating in field exposure
- To study the application properties of ZMA coatings, such as formability and joining
- To investigate the effect of phosphatation parameters in a view of possibly escape the phosphatation process.
- To assess the performance of ZMA coating in hem-flanges (perforation corrosion) as well in cosmetic configuration
- To issue guidelines for the application of advanced ZMA coatings in the manufacturing of cars

Scientific aspects

- To better understand the mechanisms of atmospheric corrosion of ZMA materials
- To understand the mechanisms of the cathodic delamination of painted ZMA and tailoring of oxide properties
- To identify the role of alloying elements in corrosion mechanisms

2.2 Comparison of initially planned activities and work accomplished

The activities in the project are summarised in the bar chart planning shown below. The work has been conducted in agreement with the initially planned activities whereas some delays in the achievement of some tasks can be observed. This concerns tasks 4.1, 4.2, 5.1 and 5.2 in particular, but the objectives of these tasks have been reached. It should be pointed out that problems were encountered by LMI in producing adequate ternary PVD coatings in task 2.5. Whereas this task has been unsuccessful, the project was not affected and valuable results were obtained.

WPs	*Work packages' title*	Year 1				Year 2				Year 3				Year 4		Status
		I	II	III	IV	I	II	III	IV	I	II	III	IV	I	II	
WP1	**Project management**															
WP2	**Material preparation**															
T2.1	Update planning															Finished (D1)
T2.2	Line hot dip materials															Finished (D2)
T2.3	Galvanizing simulator															Finished (D3)
T2.4	Material characterization															Finished (D4)
T2.5	Model PVD materials															Unsuccessful (D6)
WP3	**Oxides & pretreatment**															
T3.1	Phosphatation optimiz.															Finished (D7)
T3.2	Properties of oxide films															Finished (D11)
T3.3	Oxide and paint stability															
WP4	**Long-term corr. pr.**															
T4.1	Testing at field stations															Finished (D5, D12)
T4.2	On-vehicle testing															
WP5	**Application properties**															
T5.1	Formability															Finished (D9)
T5.2	Joining															
WP6	**Acc. corrosion tests**															
T6.1	Cosmetic corrosion															Finished (D10)
T6.2	Perforation corrosion															
WP7	**Specific aspects**															
T7.1	Effect of carbon dioxide															Finished (D13)
T7.2	Galvanic protection															
WP8	**Modelling, guidelines**															
T8.1	Mechanism & modelling															Finished (D14)
T8.2	Prediction & guidelines															Finished (D15)

2.3 Description of activities and discussion

2.3.1 WP 1 Project management

The objectives of work package WP1 were to maintain communications with the European Commission, to ensure smooth progression of the project and to establish good communication strategies and enable effective sharing of information, rapid auditing of project performance, and solving of problems. Six joint project meetings were planned and realized. (see Table 1). Minutes were provided as additional deliverables to the working group.

Table 1: list of meetings organised in Autocoat project

Meeting Nr	Date	Location
1 (Kickoff)	22/09/2009	Paris
2	26/01/2010	Linz
3	28/09/2010	Dortmund
4	8 & 9 /03 /2011	Paris
5	12 & 13 /09 /2011	Helsinki
5	12 & 13/03/2012	Torino
6	12 & 13/11/2012	Brest

Moreover, the grant agreement was modified through the amendment n°1 which included the following:
-Addition of beneficiary Centro Ricerche FIAT in replacement of FIAT
-Transfer of rights and obligations: DOC to TKSE and Rautaruukki to Ruukki Metals.

2.3.2 WP2 Material selection, preparation and characterization

The objective of WP2 was to specify technical details and prepare detail work plan (D1), to finalize the material selection and provide materials for the project (line hot dip materials, PVD and Rhesca samples), to characterize the materials, and to prepare samples for WP3–WP7.

2.3.2.1 Task 2.1: Technological framework update and detail work planning

The objective of this task was to prepare a detail work plan of the project including an update of the state of the art as well as technical details and specifications resulting from cross consultations and kick off meeting. This was summarised in the first **deliverable D1**.

2.3.2.2 Task 2.2: Preparation of line hot dip materials

The line hot dip ZnMgAl coated steel samples selected for the project are presented in Table 2 and the reference zinc coated materials in Table 3, together with the suppliers of the different materials.

It should be pointed out that the thickness of steel panels from hot dip galvanising lines of the three steel suppliers was unfortunately different and obviously difficult to solve due to availability of materials of the different suppliers. Whereas steel thickness has no impact on cosmetic corrosion or in hem-flange configurations, it is important for corrosion at cut-edges but also on forming if ZMA coatings have to be compared to conventional zinc coating. Thus, for formability tests in task 5.1, similar steel grade and thickness was used both with ZMA and conventional zinc (GI) coating.

Table 2: list of line hot dip ZMA materials

Label	Material	Steel (thickness)	Exp. Metallic coating thickness, µm	Supplier
ZMA1	ZnMg1%Al1%	DX56D (0.9mm)	~7.5	TKSE
ZMA2	ZnMg2%Al2%	DX54D (0.79mm)	~7.5	voestalpine
ZMA1.5	ZnMg1.5%Al1.5%	S280 (0.50mm)	~10	Ruukki
ZMA1.5F	ZnMg1.5Al1.5%	DX53D (0.6mm)	~10	Ruukki

ZMA1.5F… for forming (T5.2)

Table 3: list of line zinc coated reference materials

Label	Material	Steel (thickness)	Exp. Metallic coating thickness, µm	Supplier
GE	Electrogalvanised steel	DC06 (0.75mm)	7µm	TKSE
GI	Hot dip galvanised steel (Zn0.2% Al)	DX56 (0.75mm)	7µm	voestalpine
GA	Galvannealed steel (Zn12% Fe)	DX56 (0.71mm)	~7 µm (hem flange)	voestalpine
	(Zn10% Fe)	DX56 (0.77mm)	~7.5µm	
GALF	Galfan coated steel (Zn5%Al)	DX54D (0.8mm)	~7µm (ZA95)	Ruukki

The materials were supplied in sufficient quantity and adequate size to produce different configurations of samples for WP3, WP4, WP5, WP6 and WP7. As indicated in Table 4, the materials were used both in bare and painted configurations.

Table 4: Description of samples design and size for the different work packages

Configuration	Size, (mm)	Workpackage/Task
Bare	100x200 or 100x50	WP3, WP4, WP6 T7.1
	100x50	WP4
	300x400	T5.2
	200x300	T5.1
	70x300	T7.2 (WP4, WP6)
E-coated cosmetic	100x200	WP6
Full painted cosmetic	100x100	WP4
Hem flange	100x75	WP4, WP6

For cosmetic corrosion, two size of samples were produced e.g. 100x200 mm for laboratory tests and 100x100mm for field exposures. The application of E-coat was performed by voestalpine according to conventional process: phosphating 956 from Henkel at 55°C, Ecoat EV2000 from PPG cured at 180°C. The thickness of the Ecoat was about 15-18 µm. Full painted cosmetic samples for field exposures were first E-coated at voestalpine and sent to FIAT for the application of clear-coat and top coat to get a total thickness of about 110 µm.

Prior to the tests and field exposures, cosmetic coated panels were scribed down to the steel substrate by TKSE. Two vertical scribes parallel to the longest side were applied at two different widths e.g. 1 mm (Sikkens) and 0.6 mm (Clemens). The length of the scribes was 100 mm for 200x100 mm samples and 70 mm for 100x100mm samples.

For the hem-flange samples, a design based on the standard SEP1160-2 was selected. However, a smaller size of sample was proposed so that it facilitates the exposure on-vehicle where the space is limited. Figure 1 presents a schematic drawing of the hem flange.

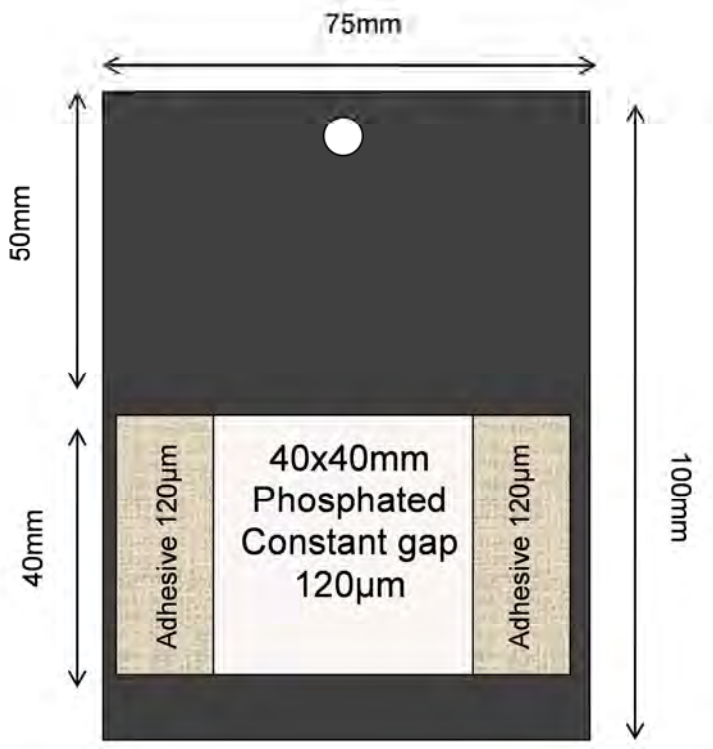

Figure 1: Schematic drawing of modified hem-flange design based on SEP1160 standard.

Line hot dip materials for long term field exposures and accelerated corrosion tests were delivered to the partners in March 2010 unless full painted panels which were ready in May 2010. This was described in **deliverable 2**.

2.3.2.3 Task 2.3: Preparation on hot dip materials in galvanising simulator

Rhesca hot dip galvanizing simulator of Ruukki was used to manufacture series of Zn-Mg-Al coated materials varying in the composition. 6 different compositions were selected as summarized in Table 5. Target coating thickness was 10 µm.

Table 5: list of Rhesca materials supplied by Ruukki

Label	Material	Steel	Exp. metal coat. Thickness, µm
ZMAR1	ZnMg1Al1	DX54D, 0.77mm	~10
ZMAR2	ZnMg2Al2		~10
ZMAR4	ZnMg4Al4		~10
ZMAR0.5	ZnMg0.5Al0.5	DX54D, 0.77mm	~10
ZMAR2/1	ZnMg2Al1		~10
ZMAR3	ZnMg3Al3		~10

Steel substrate was IF steel grade DX54 with thickness 0.77 mm. Steel substrate panels were in full hard condition and therefore contaminated with tandem mill rolling emulsion residues. They were cleaned with acetone and soft brush before annealing and coating in Rhesca simulator. Standard sample

size for Rhesca was 100x200 mm of which 100x160 mm area was coated. The following fixed parameters were used for all samples;

- heating 20 °C/s
- annealing temp 840 °C
- annealing atmosphere 80% N_2+20% H_2
- dew point -32 °C
- annealing time 50 s
- cooling before dipping 100 l/min N_2 (ave. -7 °C/s)
- pot temp 420 °C
- dipping time 3 s
- final cooling 200 l/min of nitrogen (ave. -4 °C/s)

The thickness of the coating was not uniform on the whole coated area and there were remarkable variation along the sample horizontally and also vertically. Based on previous experiences, the coating thickness was uniform on the area of 60x60 mm in the centre of the full sample (Figure 2).

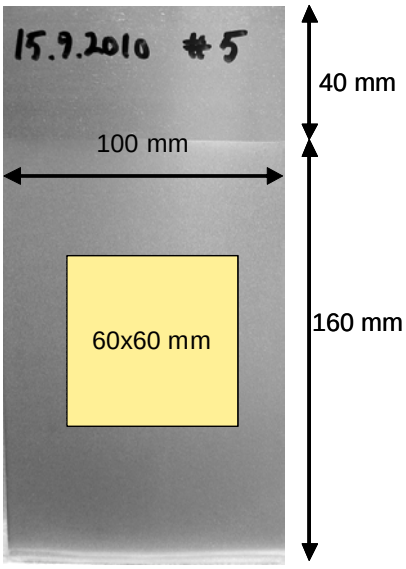

Figure 2: Dimensions of the coated Rhesca sample.

Contrary to the galvanising line coatings (WP2, T2.2), Rhesca coatings are not temper rolled and the surface roughness is therefore low which may have an effect at least on phosphatation behaviour when compared to the temper rolled line material.

- ZMAR1

The nominal coating bath composition was Zn - 1Mg - 1Al. The analysed composition was Zn - 0.9Mg - 1.0Al (before) and Zn - 1.0Mg - 0.9Al (after). The appearance of coated samples was acceptable. There were few bare spots (uncoated areas) near the edges and on the bottom area but coating on the centre was free of defects by the naked eye.

- ZMAR2

The nominal coating bath composition was Zn - 2Mg - 2Al. The analysed composition was Zn - 1.9Mg - 1.8Al (before) and Zn - 1.9Mg - 1.9Al (after). The appearance of coated samples was acceptable but some run off (sagging) of coating could not be avoided. There were few bare spots near the edges and on the bottom area but coating on the centre was free of defects by the naked eye.

- ZMAR4

The nominal coating bath composition was Zn - 4Mg - 4Al. The analysed composition was Zn - 4.2Mg - 3.5Al (before) and Zn - 4.2Mg - 3.5Al (after). The appearance of coated sample was acceptable but clearly different from that of ZMAR1 and ZMAR2. This is probably due to larger spangle size in ZMAR4. Coatings were free of defects by the naked eye.

- ZMAR0.5

The nominal coating bath composition was Zn - 0.5Mg - 0.5Al. The analysed composition was Zn - 0.5Mg - 0.5Al (before). The appearance of coated samples was not acceptable (details were given in **deliverable 4**). There were always bare areas and run off of coating on the whole panel area. Decent coatings were impossible to obtain as the coating thickness varied from 10 to 20 µm. Thus, this composition was excluded.

- ZMAR2/1

The nominal coating bath composition was Zn - 2Mg - 1Al. The analysed composition was Zn - 2.1Mg - 1.1Al (before) and Zn - 2.0Mg - 1.1Al (after). The appearance of coated samples was acceptable. There were few bare spots near the edges and on the bottom area but the coating on the centre was free of defects by naked eye.

- ZMAR3

The nominal coating bath composition was Zn - 3Mg - 3Al. The analysed composition was Zn - 3.1Mg - 3.1Al (before) and Zn - 3.1Mg - 3.0Al (after). The appearance of coated samples was acceptable. There were few bare spots near the edges and on the bottom area but coating on the centre was free of defects by naked eye. Some run off of coating could be observed on some of the samples..

2.3.2.4 Task 2.4: Material characterization

The objectives of WP2, T2.4 was to provide information on the structure of production line and Rhesca simulator ZMA coatings. Coatings surface and cross section were characterized using Scanning Electronic Microscopy coupled to an Electron Dispersive Spectrometer - SEM/EDS (performed at Ruukki and voestalpine) and Glow Discharge Optical Emission Spectroscopy - GDOES (performed at DOC). Rhesca coating ZMAR0.5 could be included in micro structural studies although preparing of decent coatings for other tasks was not possible.

2.3.2.4.1 Coating thickness

Measured coating thicknesses are shown in Table 6. The coating weight was measured by weighing method on one side. The coating thickness was calculated from the measured weight and calculated density. It must be noted that the density of the Rhesca coatings decreases with added Al and Mg. Coating thickness probably plays a role during solidification and thus may have an effect on the coating structure. The results obviously indicated significant variation of the thickness of Rhesca ZMA coating upon their composition that were unfortunately unsolvable with the equipment used. As Rhesca coatings were produced for selected experiences in view of better understanding the mechanisms of corrosion, it was believed that such heterogeneity of thicknesses would not be a problem as long as the time to red rust is not considered. Thus, ZMAR coatings were carefully considered.

Table 6: Measured and calculated coating thicknesses of zinc alloyed samples

Sample	Coating weight one side (g/m2)	Density	Calculated coating thickness (um)	Mg (%)	Al (%)
ZMA1	49.2	6.82	7.2	1	1
ZMA2	50.7	6.52	7.8	2	2
ZMA1.5	78.4	6.67	11.8	1.5	1.5
ZMA1.5F	77.4	6.67	11.6	1.5	1.5
ZMAR1	76.9	6.82	11.3	1	1
ZMAR2	88.8	6.52	13.6	2	2
ZMAR4	98.8	6.00	16.5	4	4
ZMAR2/1	95.8	6.62	14.5	2	1
ZMAR3	89.5	6.25	14.3	3	3
GALF	49.9	6.65	7.5	0	5

2.3.2.4.2 Production line coatings ZMA1, ZMA1.5 and ZMA2

2.3.2.4.2.1 Surface microstructure

Surface microstructure images of ZMA1, ZMA1,5 and ZMA2 are presented in Figure 3. The surface microstructure of ZMA coatings differs from ordinary hot dip galvanized material extremely in some points. For example, the grain size on a GI material is roughly 5 times larger than that of ZMA. The SEM pictures showed that large part of magnesium in form of $MgZn_2$ on the surface, because that is the part in the metal melt that was around the already frozen zinc dendrites at temperatures of 350-360 °C. The skin pass rolling caused a lot of little cracks into this very hard $MgZn_2$ phases – binary eutectic material. It is also plausible that ZMA1 shows more zinc dendrites on the surface than the other coating alloys.

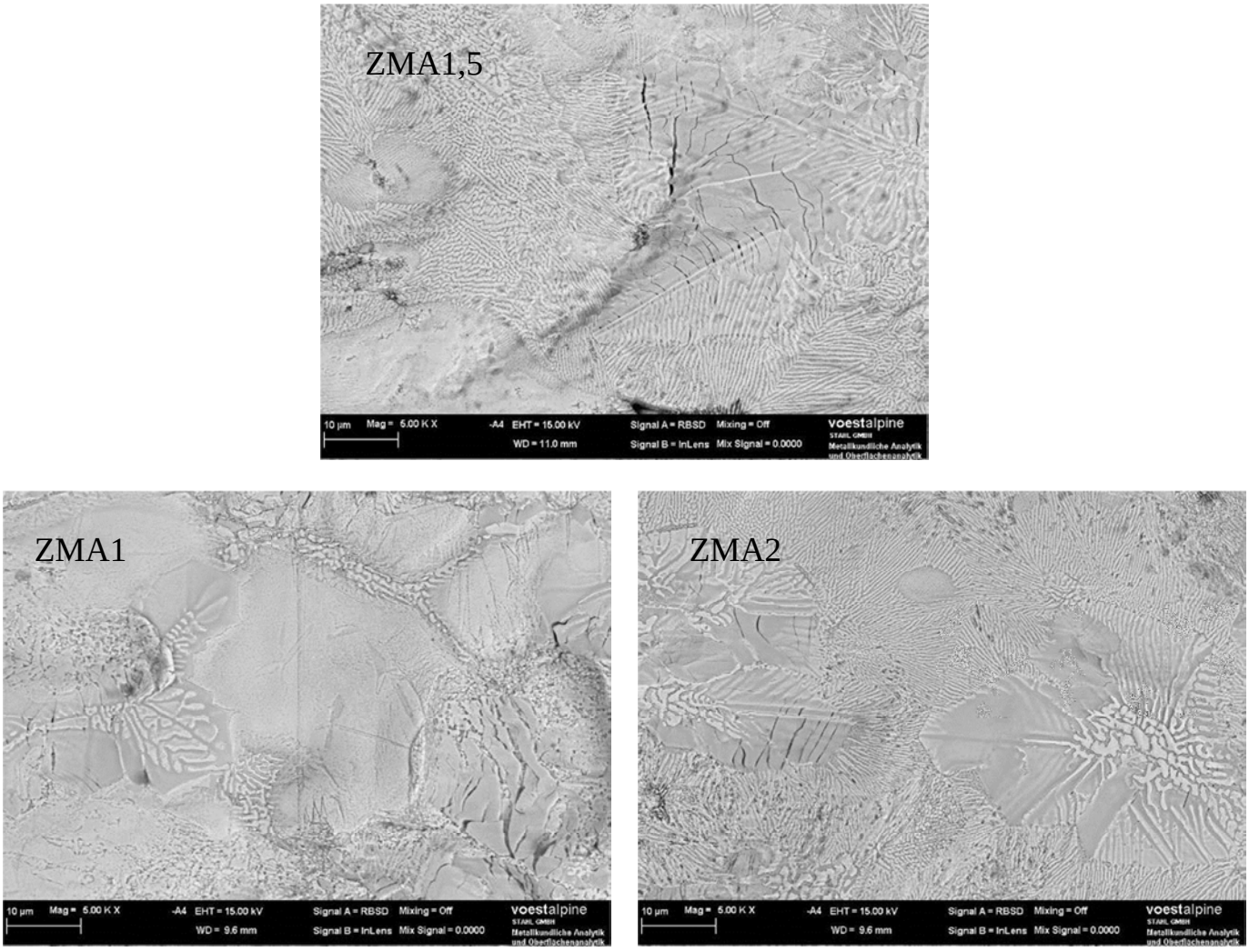

Figure 3: BSE images of the surfaces of the production line coatings.

2.3.2.4.2.2 Cross section investigations

Depending on the composition of the whole galvanizing melt, different amounts of nearly the same phases were created by the cooling process. It is clear that a layer with only the half of alloying elements (ZMA1 ↔ ZMA2) shows significant less binary and ternary eutectic structures (see Figure 4).

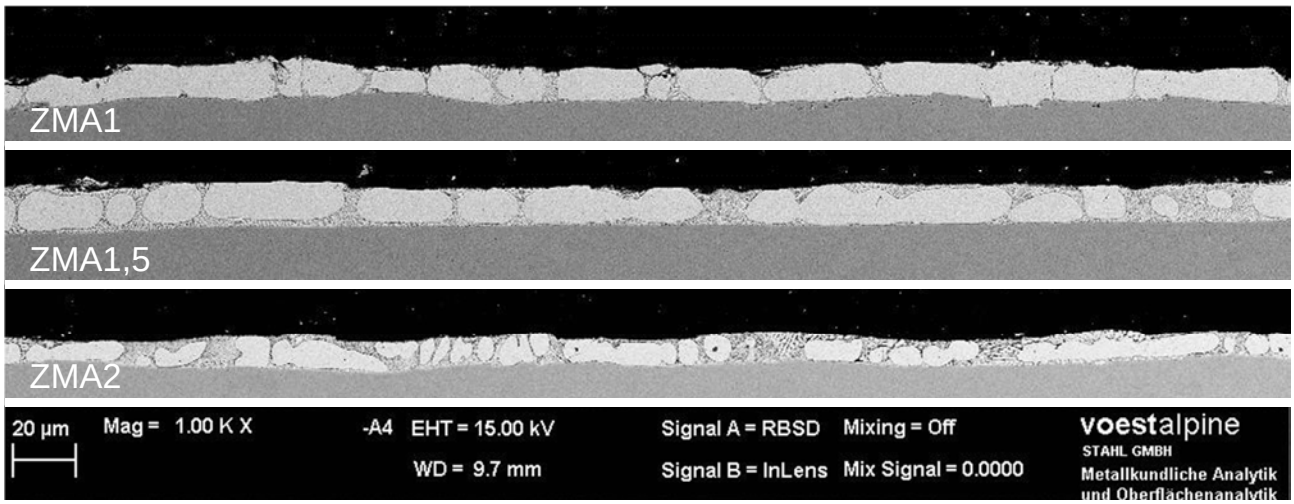

Figure 4: Cross-section polish of a typical ZMA1, ZMA1,5 and ZMA2 –layer after skin pass rolling.

From the detailed views of the structure presented in Figure 5 - Figure 6 for ZMA1, ZMA1.5 and ZMA2 respectively, the "history" of the cooling of the parts of layer may be observed. The first part, in this system with a very high concentration of zinc, is the zinc phase, this phase can solve small amounts of aluminium but normally no detectable amounts of magnesium (Figure 5). The second part which cools is a binary eutectic structure of zinc and $MgZn_2$. Sometimes, because of the very high cooling rate, aluminium dendrites grow. These dendrites solve a very high amount of zinc at the beginning, but when the temperature goes down, the solvability of zinc in aluminium shrinks. That causes sometimes a structure which looks like a binary eutectic, but in fact, it is an aluminium phase. The last part in the system is the ternary eutectic material. Because the ternary eutectic point is at ~3,9 % Al and ~2,4 % Mg (ThermoCalc), this part rises up by higher proportion of aluminium and/or magnesium. All cross-sections show similar structures, only the amount of the phases differs.

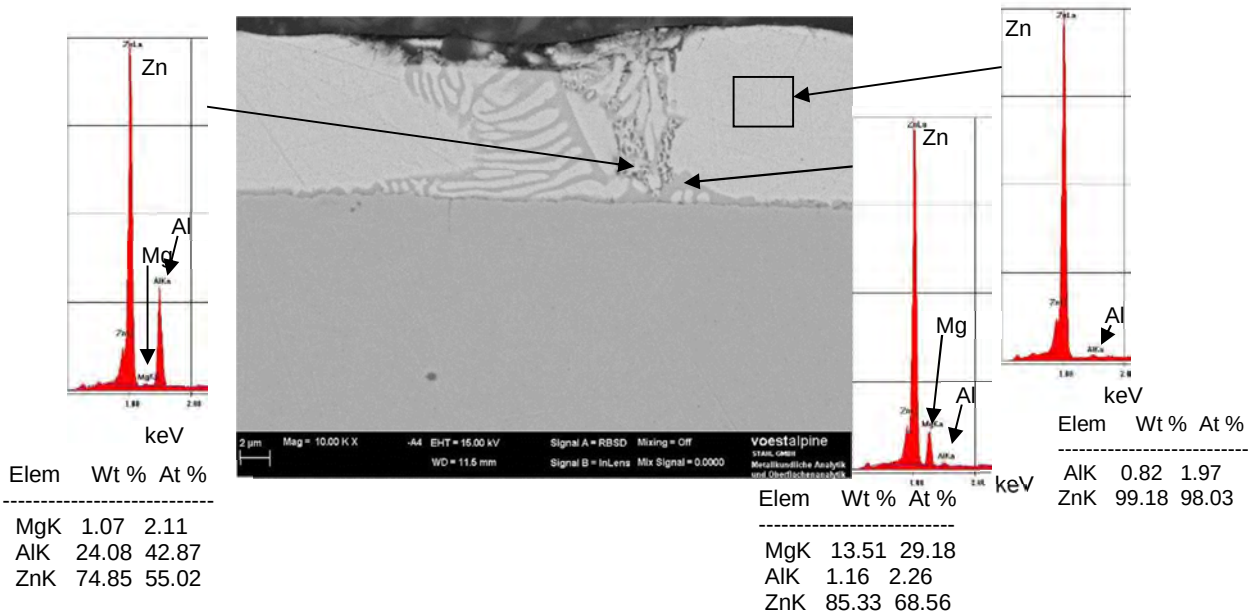

Figure 5: Cross-section of ZMA1 coating including EDX-analyses.

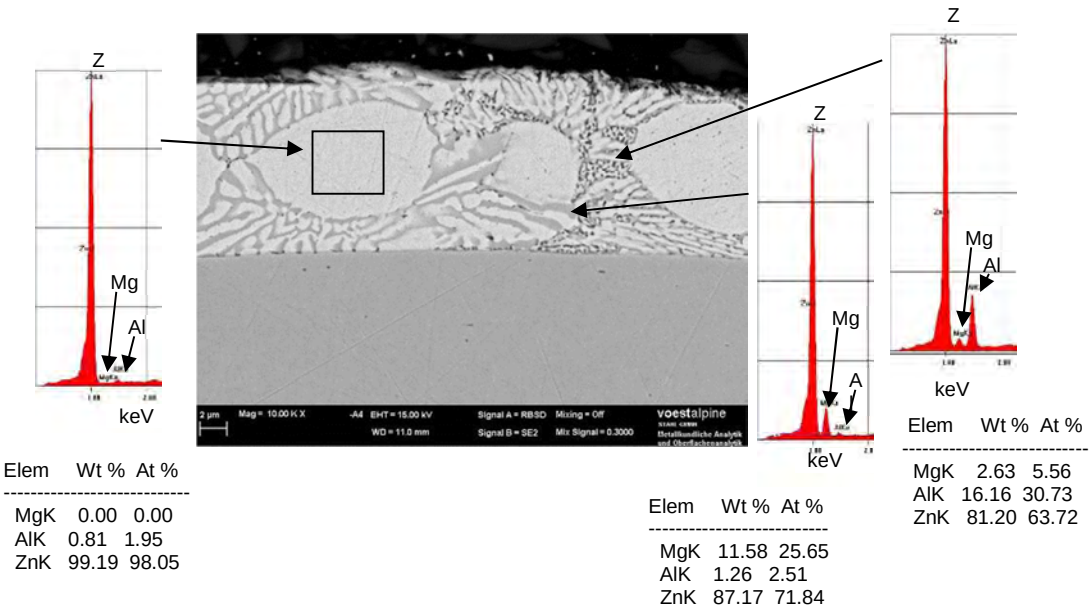

Elem	Wt %	At %
MgK	0.00	0.00
AlK	0.81	1.95
ZnK	99.19	98.05

Elem	Wt %	At %
MgK	11.58	25.65
AlK	1.26	2.51
ZnK	87.17	71.84

Elem	Wt %	At %
MgK	2.63	5.56
AlK	16.16	30.73
ZnK	81.20	63.72

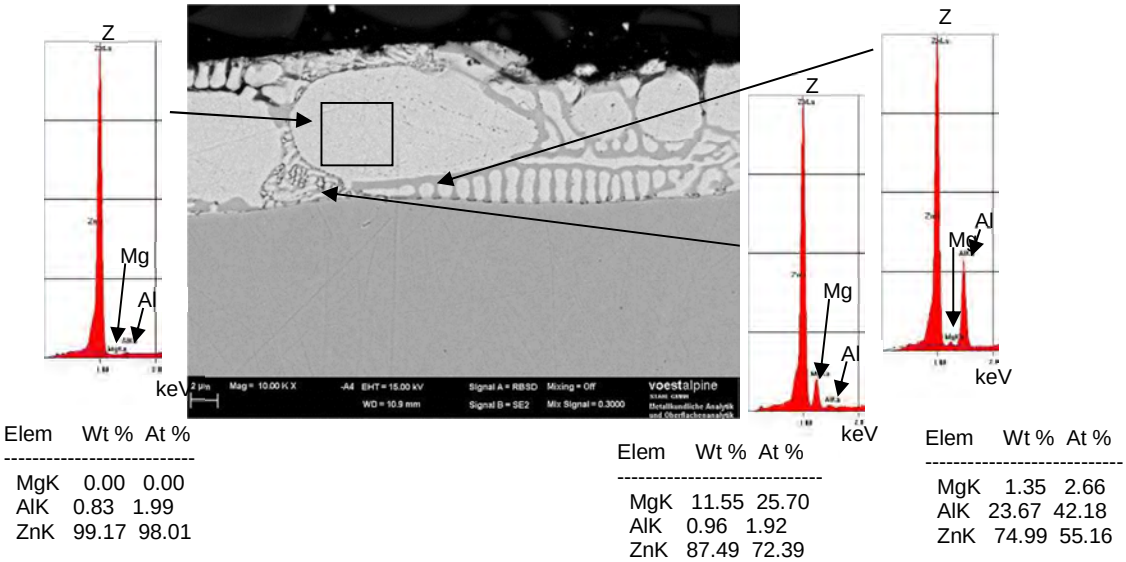

Elem	Wt %	At %
MgK	0.00	0.00
AlK	0.83	1.99
ZnK	99.17	98.01

Elem	Wt %	At %
MgK	11.55	25.70
AlK	0.96	1.92
ZnK	87.49	72.39

Elem	Wt %	At %
MgK	1.35	2.66
AlK	23.67	42.18
ZnK	74.99	55.16

Figure 6: Cross-section of ZMA1.5 (top) and ZMA2 (bottom) coating including EDX-analyses.

2.3.2.4.2.3 GDOES depth profile

GDOES depth profiling of all coatings was performed by TKSE. Profiles are presented in Figure 7 to Figure 9 for ZMA1, ZMA1.5 and ZMA2, respectively. Al and Mg enrichment on the coating surface can be noticed on all samples. Al and Mg enrichment is visible also on the interface of coatings containing Mg and Al up to 2 %.

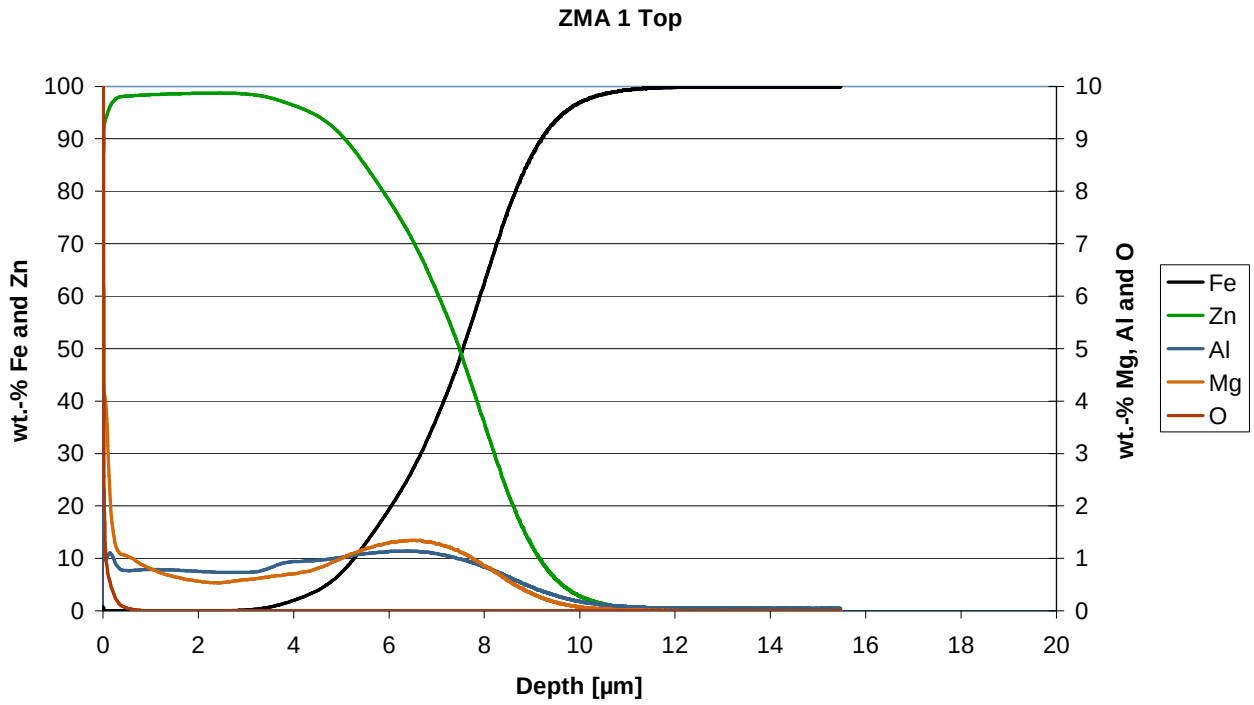

Figure 7: GDOES depth profile of coating ZMA1.

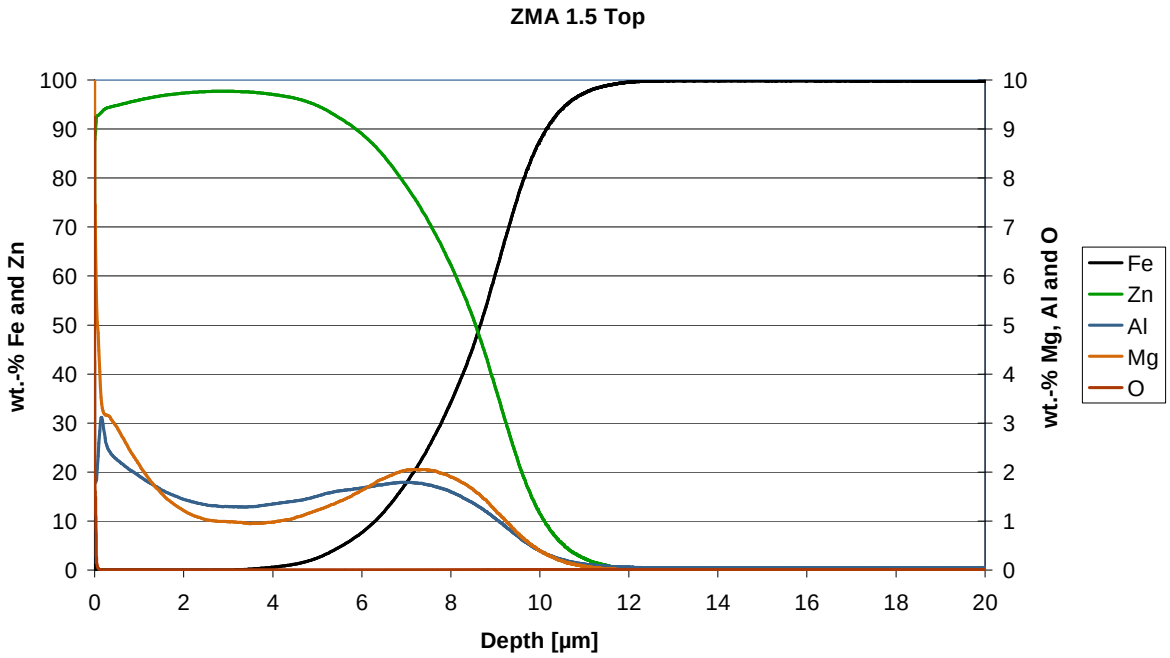

Figure 8: GDOES depth profile of coating ZMA1.5.

19

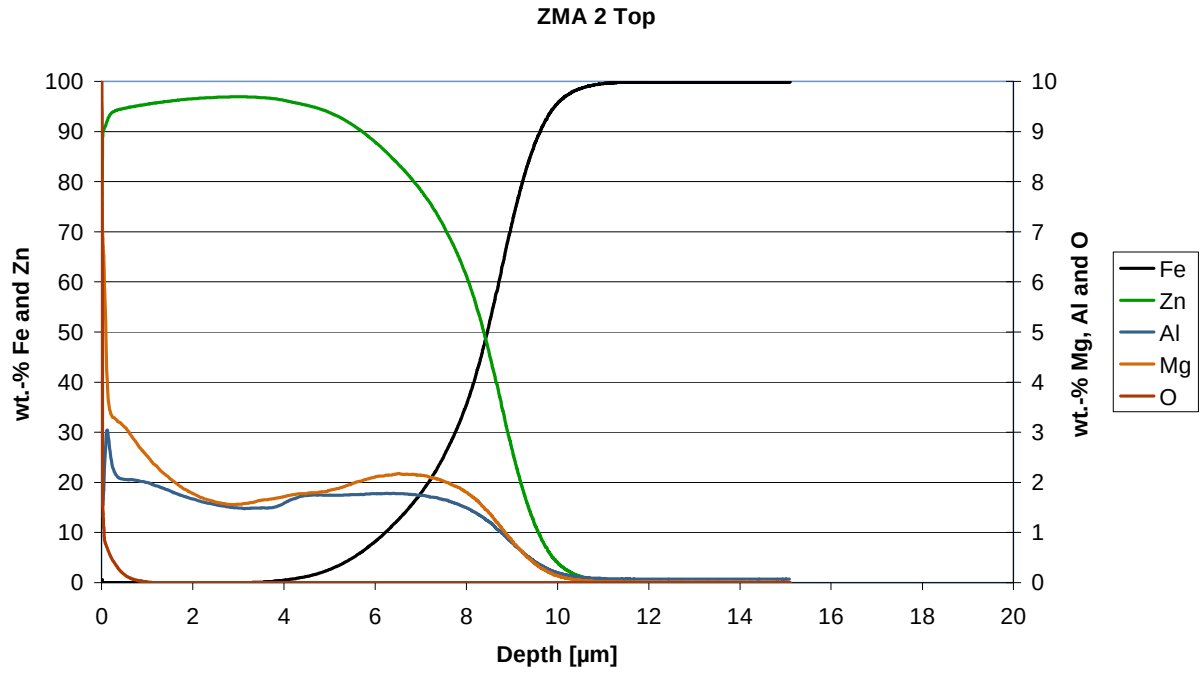

Figure 9: GDOES depth profile of coating ZMA2.

2.3.2.4.3 Rhesca simulator coatings

SEM images of Rhesca coatings are presented in Figure 10 at different magnifications and the cross-sections images are given in Figure 11.
From Figure 11, it can be observed that the number and size of primary zinc globules decreases with increasing Mg and Al content and a lamellar binary and ternary eutectic structures start to dominate. Because of the identical coating and cooling parameters, the differences seen in the coating structures can be said to originate from differences in the composition only. Some dross particles were observed in ZMAR4 coating (two angular particles on the left).

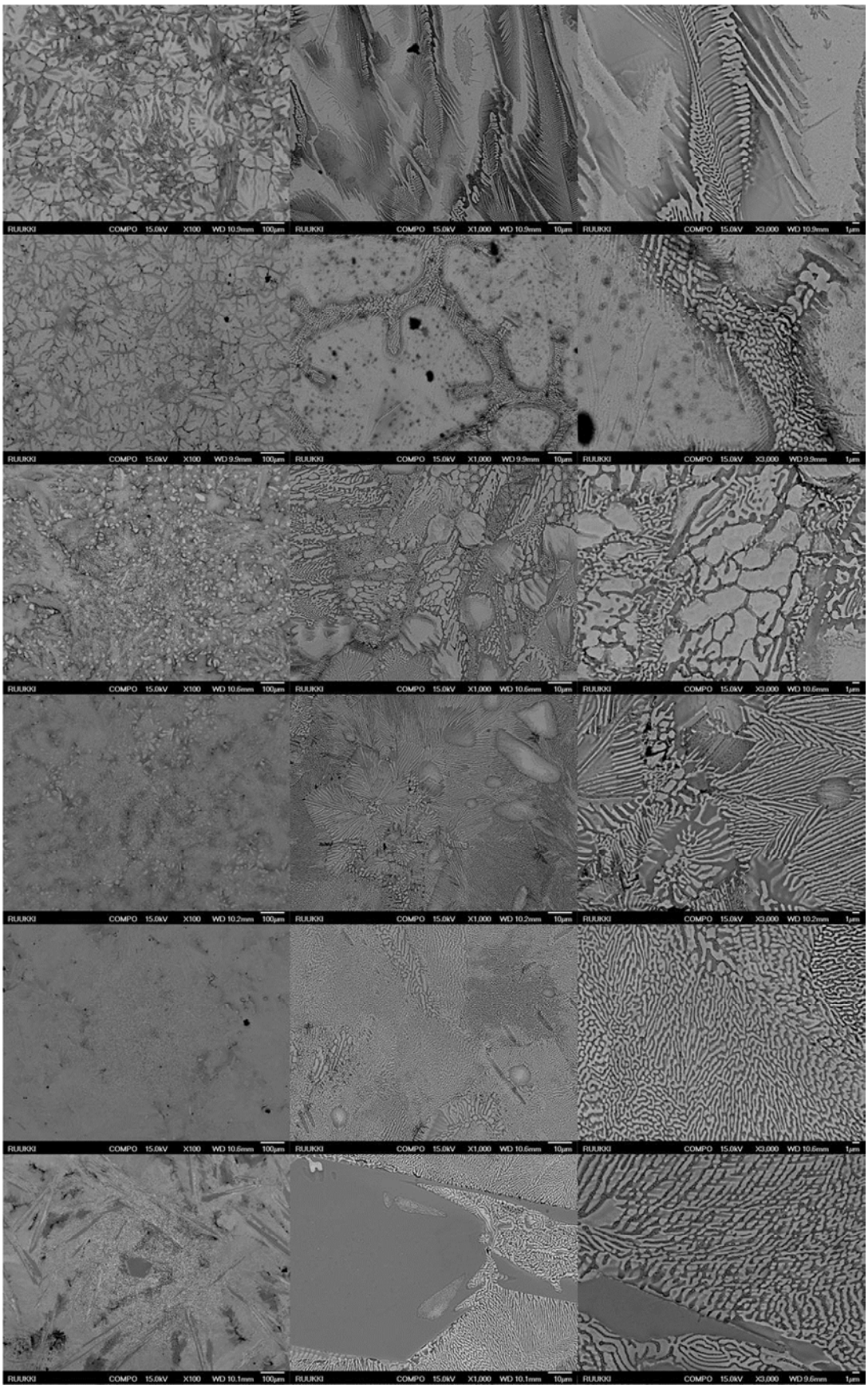

Figure 10: Surface images of Rhesca coatings. From top to bottom ZMAR0.5, ZMAR1, ZMAR2/1, ZMAR2, ZMAR3, ZMAR4. Magnification from left to right 100x, 1000x and 3000x.

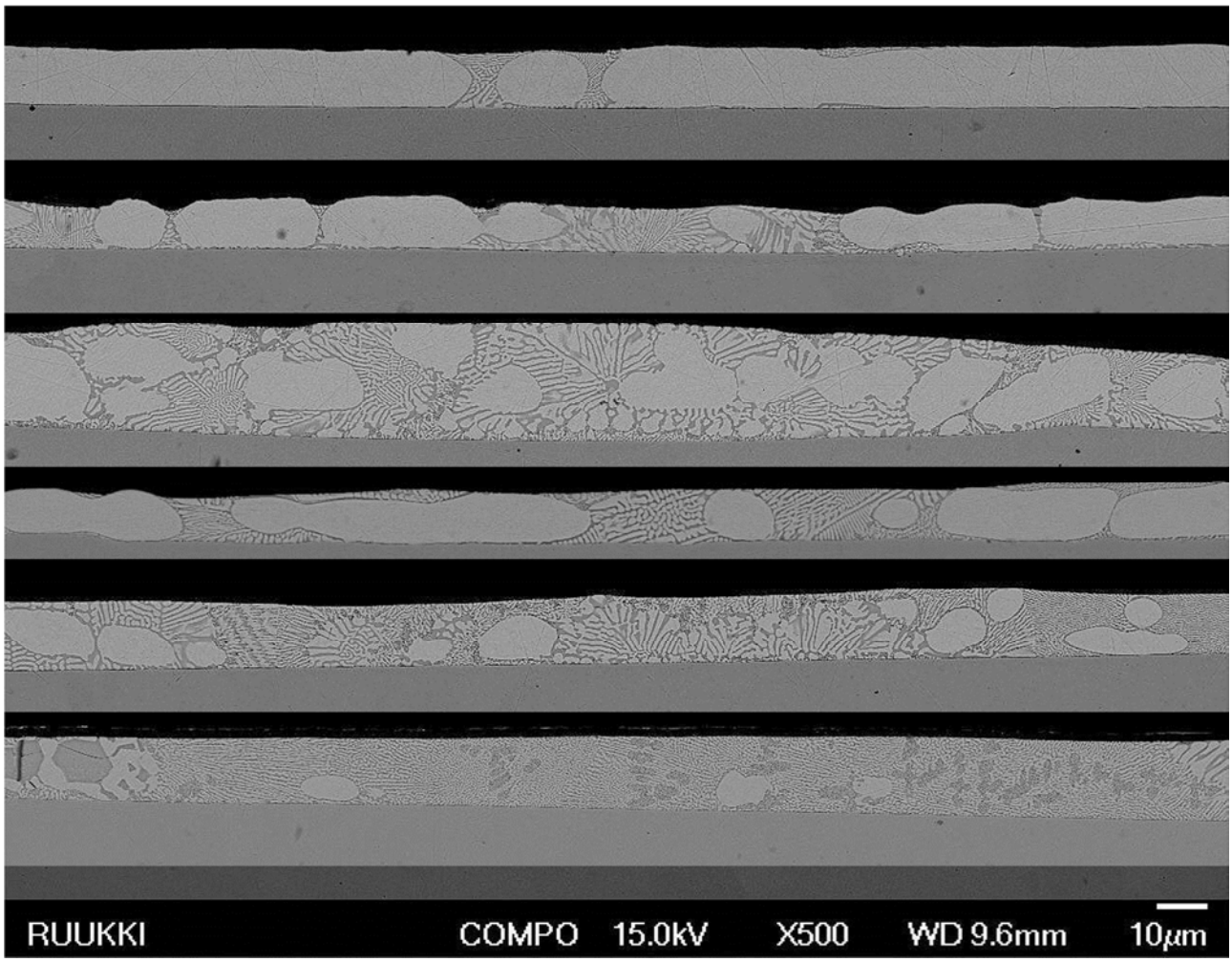

Figure 11: Cross section images of Rhesca coatings. From top to bottom ZMAR0.5, ZMAR1, ZMAR2/1, ZMAR2, ZMAR3, ZMAR4.

More detailed cross section images of Rhesca coatings including EDS analyses are presented in Figure 12 - Figure 13. Besides Zn, Mg and Al, few other elements e.g. O and Si with very low percentages were also identified but they are not shown in the results. Therefore, the sum of elements is not necessarily exactly 100 %. Basically, there were three different structures observed in all coatings: 1) primary Zn globules, 2) binary eutectic and 3) ternary eutectic. Only the ratio of these structures changes with composition. It was however not evident to calculate the relative proportion of the different structures inside the metallic coating. It is believed that the relative proportion of primary Zn globules and their repartition in the metallic coating can play an important role in the corrosion behaviour. All Rhesca simulator samples showed more or less similar surface compositions, which differed especially in the Zn concentration from the production line coatings ZMA1 and ZMA2. The reason for this difference is not clearly known, but it might be attributed to the history of the production process itself. As a consequence, Rhesca samples are not fully comparable because of higher Zn on the surface

It should also be noted that Rhesca coatings were wiped and cooled in nitrogen. Oxidation of elements was not expected to play an important role but it is not fully known, nor the oxygen level inside the simulator.

Detected Fe in all coatings (presented as normalized data) is very likely not correct as neither precipitations nor FeZn phases were observed. Fe seems to increase with depth which would indicate a possible analysis interaction with steel substrate. Moreover, XPS and GDOES analysis did not show any Fe content in the coatings.

(a)

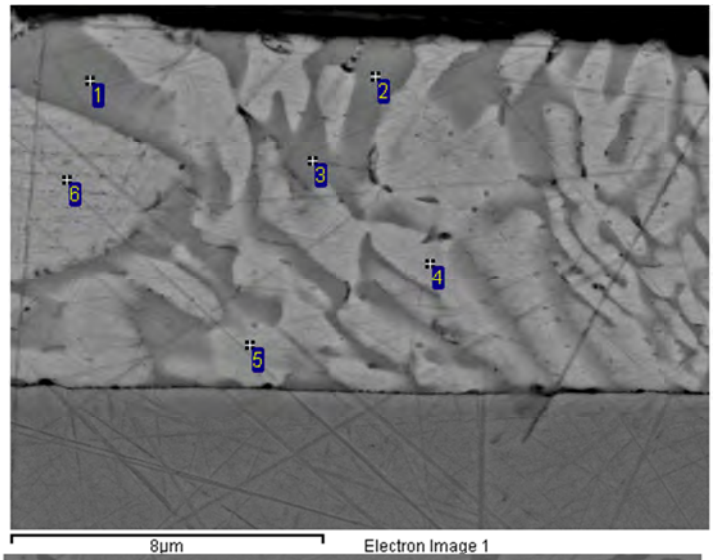

Spectrum	Mg	Al	Fe	Zn
1	12.95	0.86	1.12	84.99
2	13.47	1.07	1.02	84.37
3	12.51	0.72	1.35	85.30
4	0.77	0.23	2.09	96.86
5	0.34	0.21	3.04	96.33
6	0.09	0.61	1.55	97.69

All results in weight%

Spectrum	Mg	Al	Fe	Zn
1	28.22	1.69	1.06	68.88
2	29.07	2.08	0.96	67.75
3	27.45	1.42	1.29	69.61
4	2.02	0.55	2.40	94.92
5	0.91	0.50	3.50	94.90
6	0.23	1.46	1.78	96.36

All results in atomic%

(b)

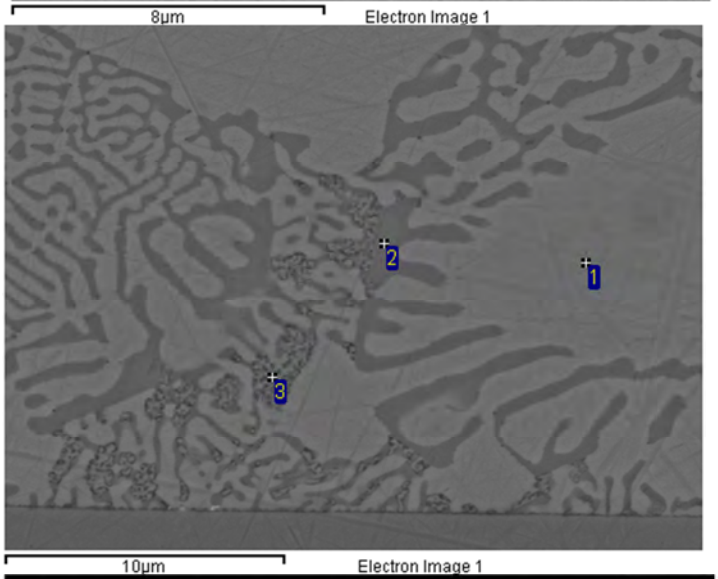

Spectrum	Mg	Al	Fe	Zn
1	-0.02	0.58	1.06	98.10
2	12.73	2.45	0.85	83.50
3	0.07	14.62	1.56	83.17

All results in weight%

Spectrum	Mg	Al	Fe	Zn
1	-0.04	1.37	1.22	96.33
2	27.04	4.68	0.79	65.98
3	0.15	28.80	1.48	67.63

All results in atomic%

(c)

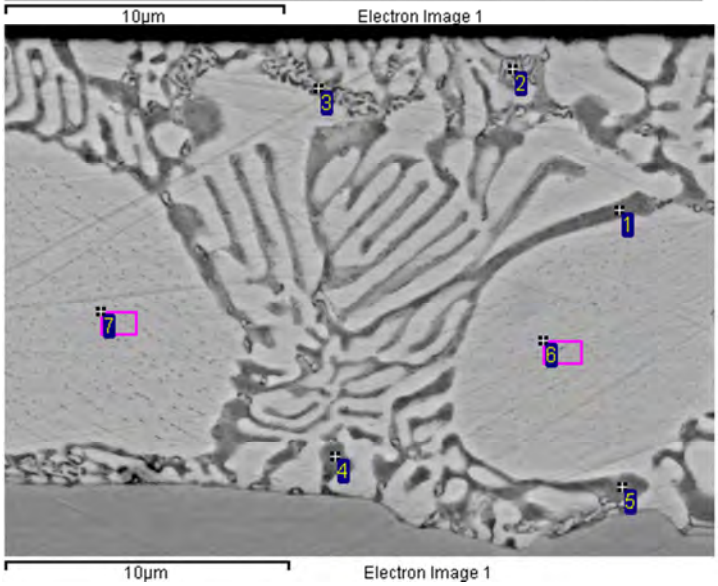

Spectrum	Mg	Al	Fe	Zn
1	7.44	0.88	1.10	90.54
2	1.43	12.95	0.54	85.03
3	0.24	20.18	0.49	79.02
4	10.73	2.03	2.96	84.24
5	10.55	1.73	3.57	84.06
6	0.03	0.82	1.52	97.56
7	0.01	0.89	1.42	97.63

All results in weight%

Spectrum	Mg	Al	Fe	Zn
1	17.54	1.87	1.13	79.39
2	3.17	25.92	0.52	70.27
3	0.50	37.82	0.44	61.12
4	23.73	4.04	2.85	69.30
5	23.45	3.47	3.46	69.47
6	0.08	1.96	1.76	96.06
7	0.02	2.11	1.64	96.11

All results in atomic%

Figure 12: EDS analysis of Rhesca coating ZMAR1 (a), ZMAR2/1 (b) and ZMAR2 (c) .

(a)

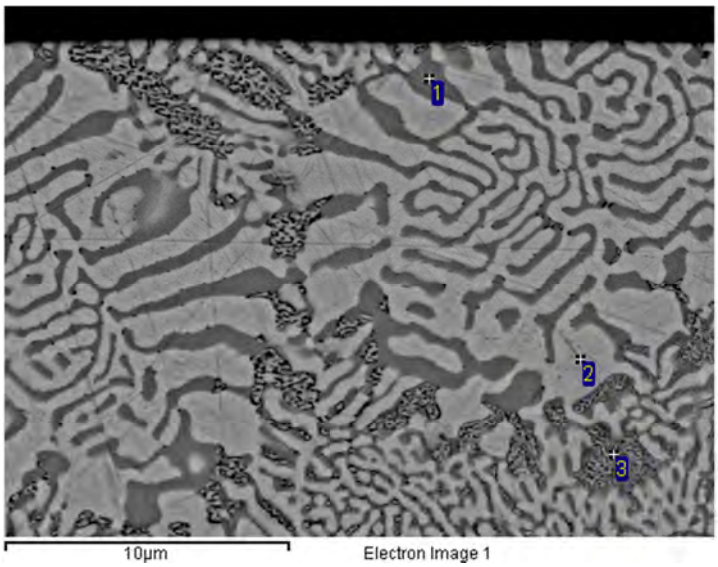

Spectrum	Mg	Al	Fe	Zn
1	13.48	0.93	0.51	84.55
2	-0.12	0.58	1.32	97.74
3	0.03	16.43	1.79	81.20

All results in weight%

Spectrum	Mg	Al	Fe	Zn
1	28.82	1.79	0.48	67.21
2	-0.31	1.37	1.51	95.53
3	0.06	31.73	1.67	64.73

All results in atomic%

(b)

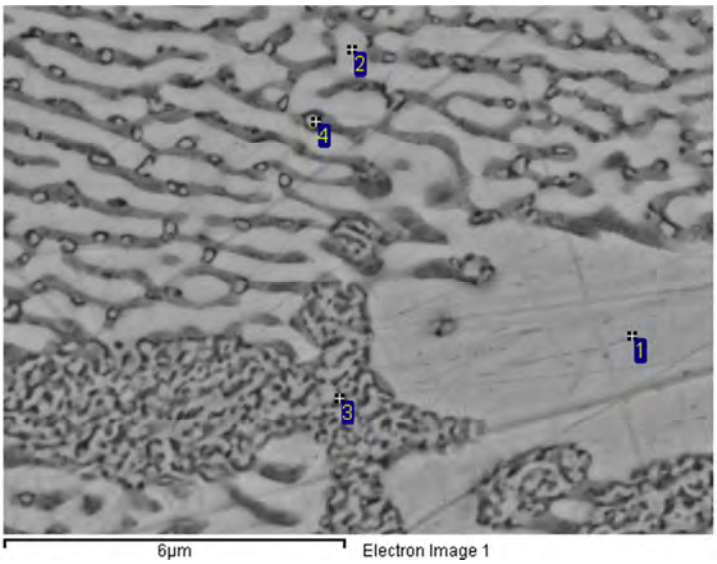

Spectrum	Mg	Al	Fe	Zn
1	-0.08	3.28	1.49	94.95
2	2.11	2.07	0.82	94.55
3	0.06	25.71	1.62	72.38
4	5.21	7.19	1.08	85.97

All results in weight%

Spectrum	Mg	Al	Fe	Zn
1	-0.20	7.51	1.65	89.66
2	5.24	4.64	0.89	87.53
3	0.11	45.25	1.37	52.58
4	11.58	14.40	1.04	71.10

All results in atomic%

Figure 13: EDS analysis of Rhesca coating ZMAR3 (a) and ZMAR4 (b).

GDOES depth profiling of Rhesca coatings are presented on Figure 14 to Figure 18. As for line hot dip coatings, an enrichment of Al and Mg is visible at the interface with steel substrate at least for composition up to 2%. The larger thickness of the metallic coating on the Rhesca samples is also obvious.

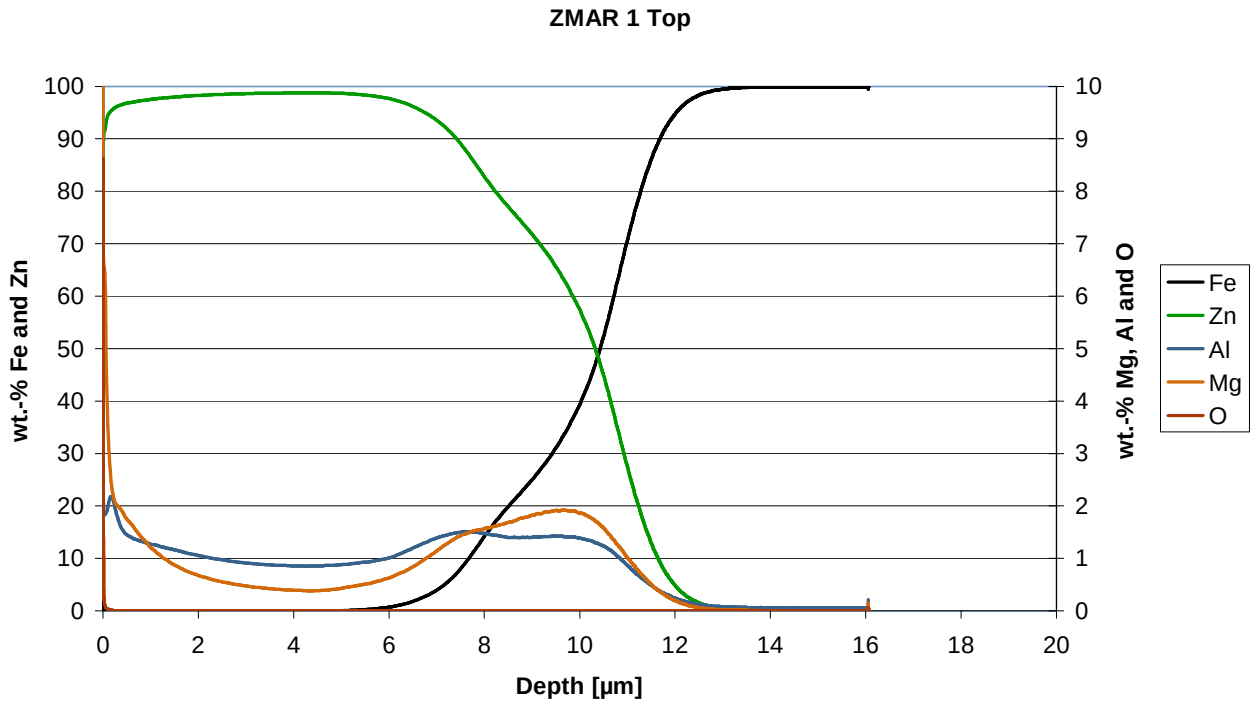

Figure 14: GDOES depth profile of coating ZMAR1.

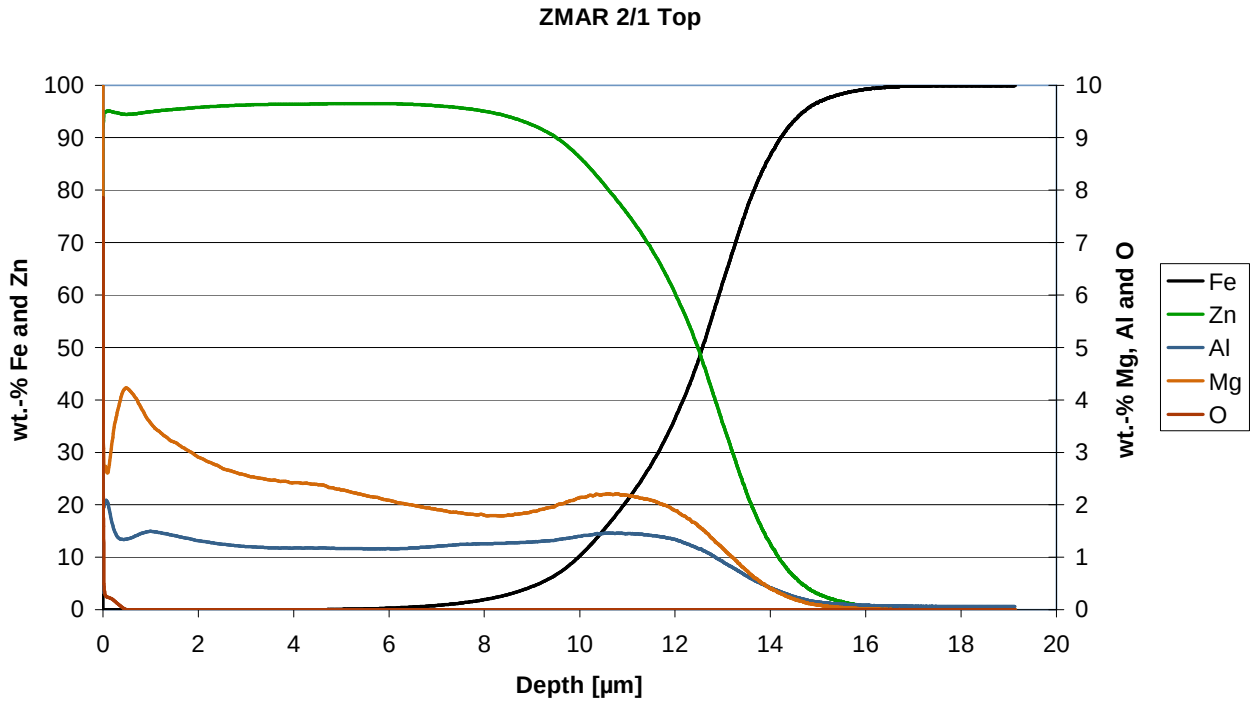

Figure 15: GDOES depth profile of coating ZMAR2/1.

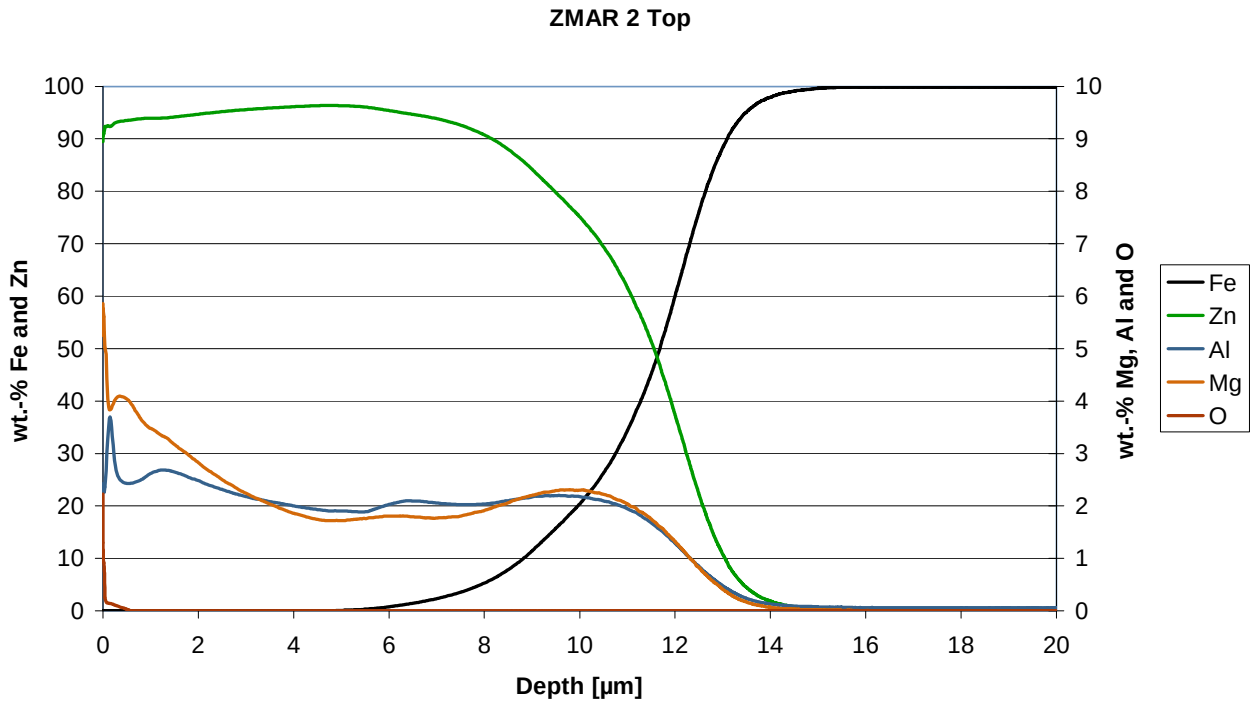

Figure 16: GDOES depth profile of coating ZMAR2.

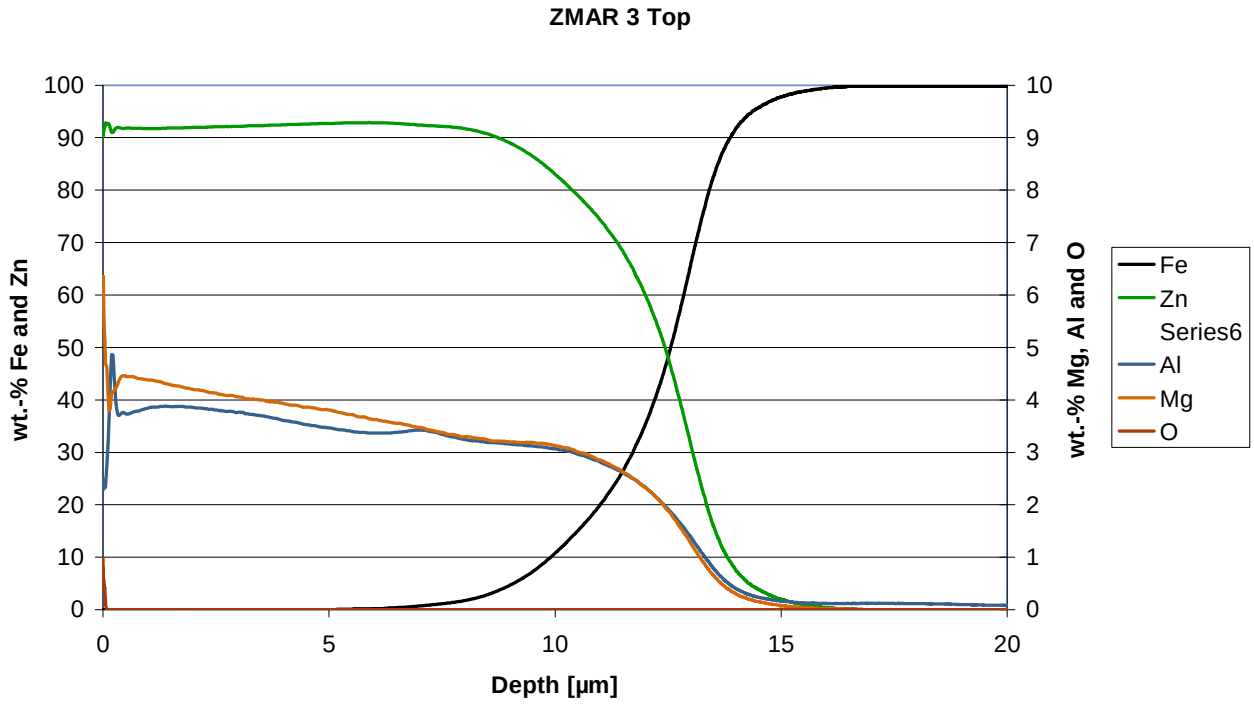

Figure 17: GDOES depth profile of coating ZMAR3.

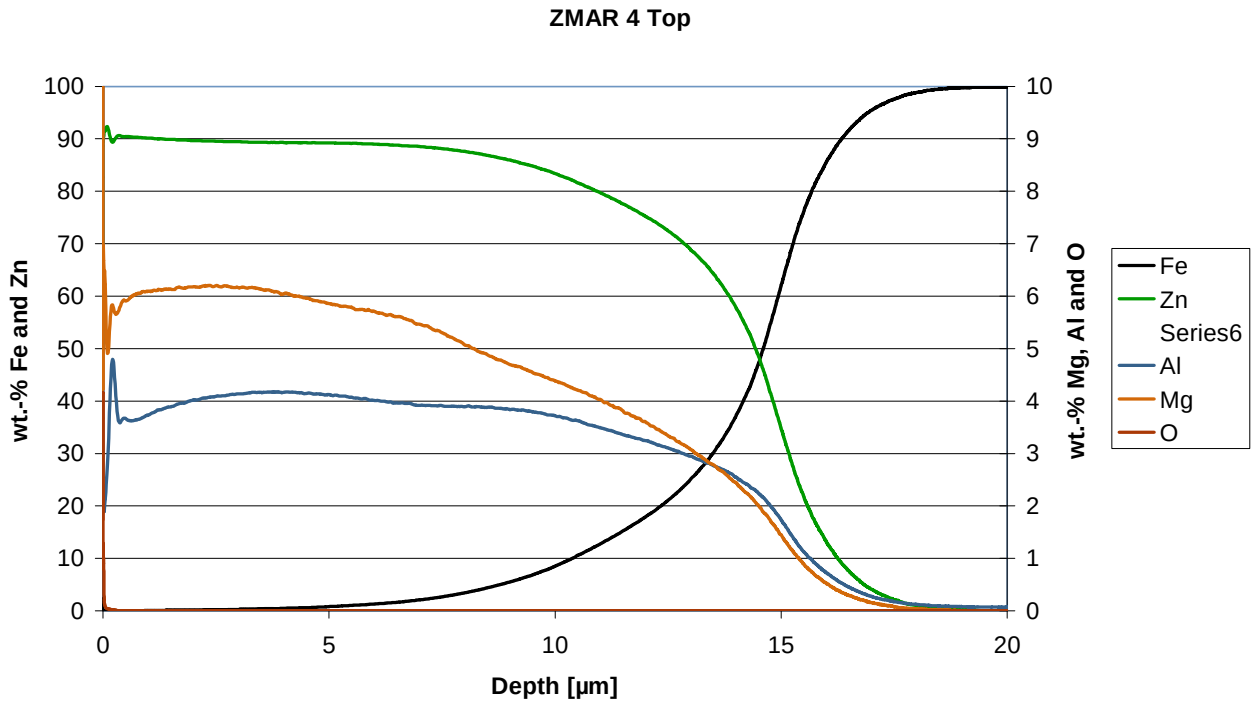

Figure 18: GDOES depth profile of coating ZMAR4.

2.3.2.5 Task 2.5: Preparation of model PVD materials

The objective of this task which was led by Limedion was to produce two model PVD coatings with a similar composition as two Rhesca samples. See Table 7.

Table 7: list of PVD materials expected to be produce by Limedion

Label	Material	Steel	Metal coat. thickness
ZMAP1	ZnMg1Al1	DX54D, or DX56D ~ 0.75mm	~7.5 µm
ZMAP4	ZnMg4Al4		~7.5 µm

Several approaches were made to deposit ternary 7.5 µm thick ZMAP1 and ZMAP4 well adhering coatings. The **first approach** to deposit from three evaporators led to a different stoichiometry, because the thickness monitors above the evaporators were interfering. Therefore, it was not possible to deposit coatings with the targeted concentration. In the **second approach**, a ZnMg mixture was evaporated from one crucible and Al from a second crucible. This led to an enrichment of Mg at the surface and the Mg concentration throughout the film was not constant. The **third approach** was to deposit multi-layers Zn-Mg-Al-Zn and to form the ternary alloy in a subsequent annealing procedure. Coatings deposited with this method showed only poor adhesion. In the **fourth approach**, an alloy of Zn-Mg-Al was produced by melting the three metals in certain concentrations in a vacuum oven. These ternary alloys were transferred into a crucible and coatings were deposited. A temper procedure for the production of the alloy was developed to assure a constant composition of the coating throughout the complete film. However, the alloyed materials seemed to concentrate in the remaining bead and it was necessary to prepare a new alloy block for each individual deposition. During the deposition, the substrates had to be heated, otherwise the adhesion was almost zero. Due to the substrate heating only one set of A4 and one 10x20cm panel could be coated simultaneously. Prior to deposition the panels were thoroughly pre-cleaned using a smooth alkaline cleaner and wiping the panels followed by wiping with an acetone/2-propanole mixture. After mounting into the vacuum chamber, the surface of the panels was sputter-cleaned using an argon ion beam. Then the deposition was started.

For ZMAP1 (Al1%, Mg1%), 4 A4 panels and 4 of 10x20 cm panels were coated. The coating thickness in all runs was 7.5 µm. For ZMAP4, 4 10x20cm panels were coated in two different runs. The deposition rate was reduced from 20nm (ZMAP1) to 15nm /s (ZMAP4) in order to get a better adhesion, but also this approach led to poor adhesion values. Obviously, with the given PVD device and the given substrate/coating combination and coating composition, no good adhesion was unfortunately possible.
MPIE did some characterisation on ZMAP1 coatings. The coatings were quite homogeneous in thickness. Magnesium seemed to be distributed uniformly. However, the coatings showed holes, some of these down to the substrate. The samples were also exposed in an accelerated corrosion test at IC which also showed the poor coating adhesion.
More details on the trials to produce ternary Zn-MG-Al coating by PVD may be found in **deliverable D6**.

Despite many trials, LMI could not produce satisfying PVD coatings, which underlines the difficulty of the task that was obviously not forecasted in the proposal enough. As indicated in the previous report, the production of ternary PVD coatings at another location (Johannes Kepler University of Linz, Austria) was tested and problems were also encountered. It was thus decided to stop the activity of the task 2.5, as it was believed that the absence of ZnMgAl applied by PVD would not compromise the project. **Deliverable D6** was submitted as a report summarising the different unsuccessful trials to produce PVD ZMA.

2.3.3 **WP3 Surface oxides, pre-treatment optimization and mechanism of paint delamination**

The aims of WP3 were to study and understand the corrosion mechanism of bare and painted Zn-Al-Mg coatings in atmospheric conditions, especially with respect to the initial stages of the corrosion process, which is supposed to help in understanding the fundamental principles governing the alloy stability.

2.3.3.1 **T3.1 Optimization of phosphatation and delamination behaviour of phosphated samples**

2.3.3.1.1 Experimental

Line hot dip ZMA1-2% coated steel samples with protected cut edges were used for the experiments. As reference sample, hot dip galvanized steel strip (GI) was used. All samples had a coating thickness of 7 µm, except of ZMA1.5 where the coating thickness was 10 µm.

The chemicals for the model phosphatation chemistry were all purchased in p.a. grade and the baths were set up according to Table 8. No commercial products were used for the first trials.

The selected variations of parameters are given in Table 9. Bath composition in respect to free acid, time of treatment and bath temperature were systematically varied. These parameters certainly are the most variable ones in industrial production and also are commonly agreed as the dominant influents of the phosphatation process. For a better control of the fluid flow, a construction with a flow channel was used. The thermostatic device pumped the phosphating solution to the bottom, then it flowed upward between the baffle and the sample. That set-up should improve the reproducibility of the flow in comparison to a simple stirred solution. Prior to phosphatation, for the activation of the surface Fixodine 50CF (1 g/l) was used for a duration of 10 seconds.

Table 8:Phosphating solution for first trials, without acid calibration with Na_2CO_3.

H_3PO_4 [ml/l]	ZnO [g/l]	NaF [g/l]	$Mn(NO_3)_2$ $4H_2O$ [g/l]	$Ni(NO_3)_2$ $6H_2O$ [g/l]	$NaNO_3$ [g/l]
11	1,25	0,8	4,6	5	6

Table 9: Parameters of the model phosphating solution for the sample production.

temperature [°C]	time [sec]	free acid points
40	20	0,636
50	5	0,636
50	20	0,636
50	40	0,636
60	20	0,636
40	20	1,14-1,19
50	5	1,14-1,19
50	20	1,14-1,19
50	40	1,14-1,19
60	20	1,14-1,19
40	20	1,49-1,63
50	5	1,49-1,63
50	20	1,49-1,63
50	40	1,49-1,63
60	20	1,49-1,63

The coating weight of the phosphate layers was determined by chemical analysis (pickling and subsequent determination of the phosphorus amount). Additionally, the composition of the layer was investigated by XPS.
The adhesion of the ED-paint applied on phosphated materials was measured by cross cut test. Scribe delamination was evaluated by exposure to the accelerated corrosion test New VDA test (VDA 233-102) which is described in WP 6. Details on scribe dimensions are given in WP 6.

Additionally, potential profiles during delamination under permanently humid conditions were recorded with the Scanning Kelvin Probe technique. Two extreme conditions were tested here by applying defects of either pure zinc or iron.

2.3.3.1.2 Results

The amount of phosphor on the surface was measured by x-ray fluorescence and is depicted in Figure 19 for the different bath variations. The standard free acid trials showed low dependence on time and temperature. Only for GI, a slight decrease of phosphate was observed for longer treatment times. The same was true for higher free acid levels, while all samples behaved very similar at low free acid levels.
The surface composition as function of the different model phosphating solutions was determined by means of XPS, as shown in Figure 20. Obviously, the phosphating parameters have an influence on the surface composition (esp. Na, P and Zn concentration), where a tendency to have more sodium in low free acid conditions in comparison to the standard one was observed. However, with the exception of the 50°C treatment for only 5 seconds, all samples showed a similar composition in the main elements.

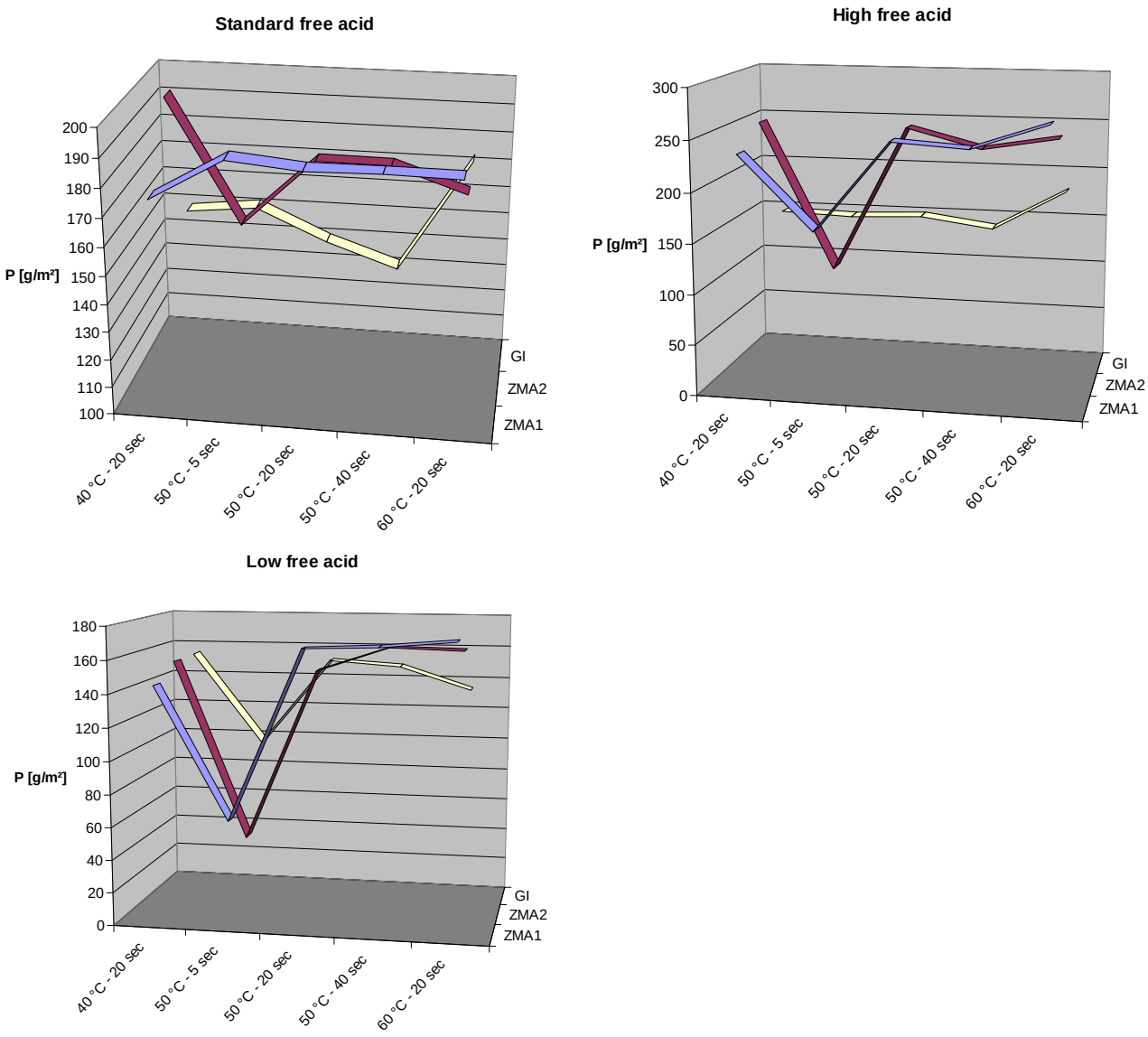

Figure 19: Phosphor deposition on different line hot dip coated steel (GI, ZMA1, ZMA2) as a function of temperature, time and free acid conditions.

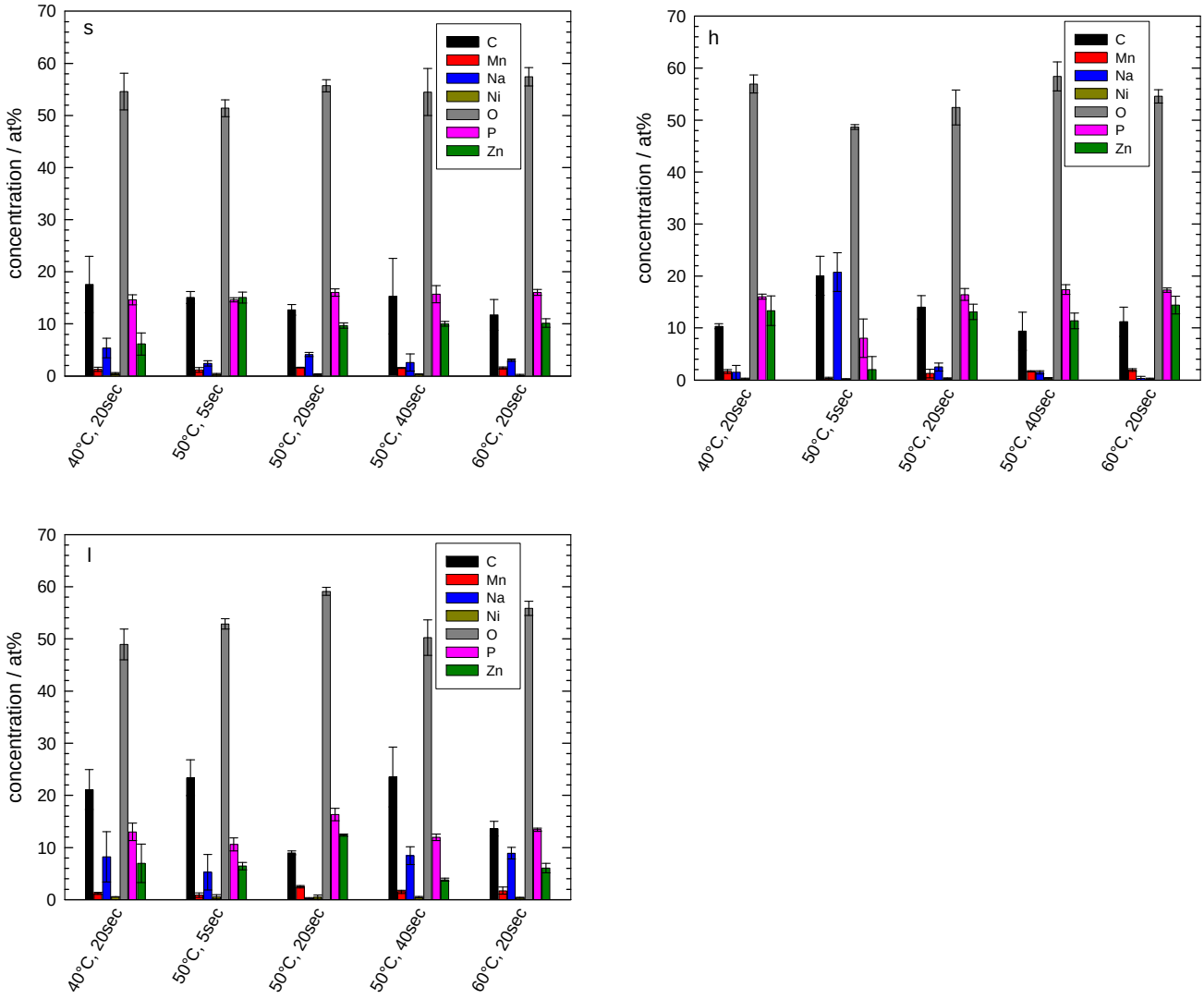

Figure 20: Surface composition of the phosphated ZMA2 samples (model phosphatation as given in Table 9) measured by means of XPS analysis. Standard free acid: s; Low free acid: l; and high free acid: h.

The adhesion of the ED-paint applied on phosphated materials measured by cross cut test (ISO 2409) was found to be within GT 2 for all parameters and no change was induced by exposure to accelerated corrosion testing. Scribe delamination was tested by exposure to the New VDA test. In addition, the delamination was quite homogeneous whatever the parameters. Therefore, the results were presented as an average value of all parameters of phosphatation given in Table 9. The average scribe delamination of ZMA and GI materials is presented as a function of exposure in the New VDA test in Figure 21, where comparable values were measured on both metallic coatings.

These results were compared with those obtained when all materials were phosphated following a standard phosphatation process by use of a commercial phosphatation bath (Granodine®). Once phosphated, all the samples were ED painted and the adhesion of the paint was verified before and after accelerated corrosion testing according to ISO 2409. Again, no influence on paint adhesion was detectable before and after corrosion testing (GT 0) whatever the phosphatation parameters. As can be observed in Figure 61 (WP 6), even a lower scribe creep was observed on the ZMA coatings whereas the delamination of GI showed similar values as in the model tests.

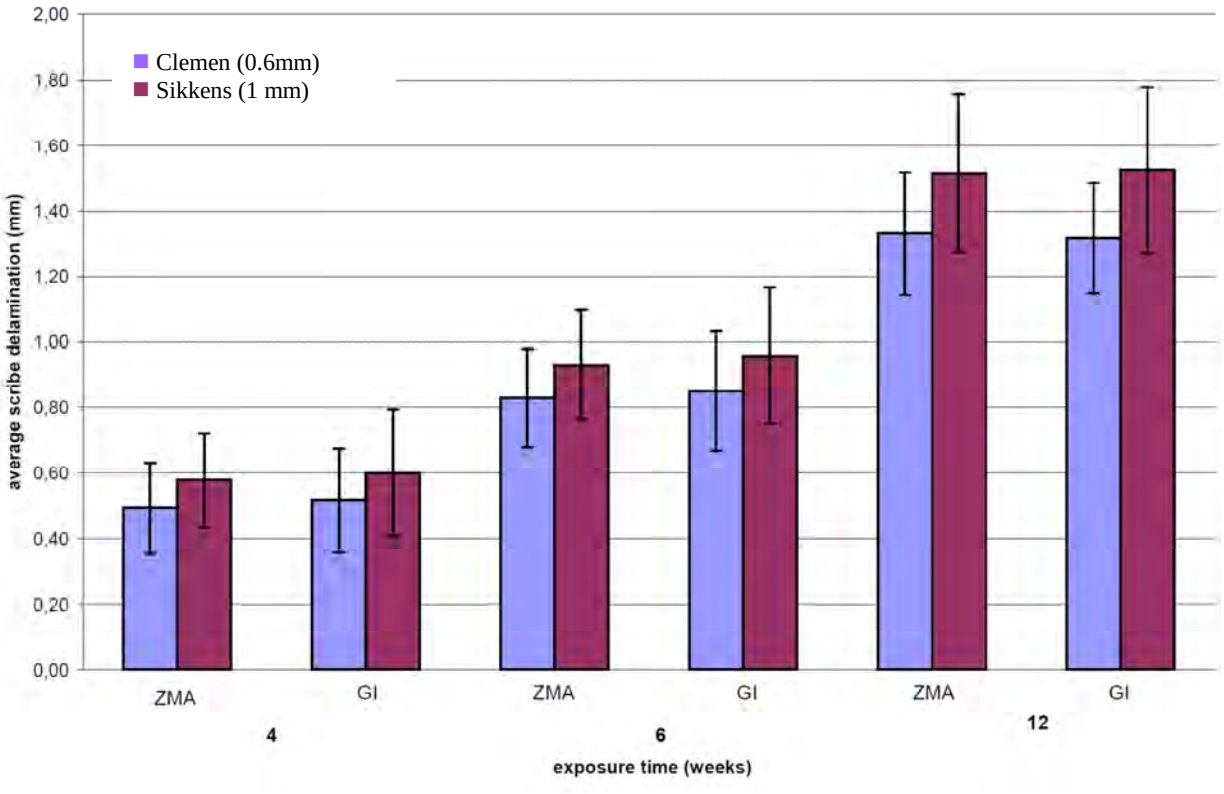

Figure 21: Average scribe delamination of ZMA and GI as a function of exposure to New-VDA test.

In a further experiment, the commercial phosphatation solution was used for varying parameters, for comparison of the effects with the results obtained with the model baths. This provided information about the robustness of ZMA coatings to common industrial phosphatation standards. Of course, in this case, no variation of the bath composition was possible, as this is know-how of the chemistry supplier. Hence, only temperature and time could be varied in the experiments. The resistance to scribe delamination after 6 weeks of new VDA testing was evaluated as a function of phosphatation conditions for the different ZMA coatings (ZMA 1, ZMA 1.5 and ZMA 2) previously covered with an electrocoat. Again, GI was used as a reference. As shown in Figure 22, the results again revealed that ZMA coated steel, without any representative differentiation between the alloying element concentration, showed rather low delamination values (~0.5mm mean scribe creep) with a slight tendency of improvement in comparison to GI (~1mm mean scribe creep). It should however be mentioned that the extent of delamination is rather marginal to point out significant difference between ZMA and GI. Regarding the effect of phosphatation conditions, an influence of the treatment time at 50°C may be noted when considering ZMA1.5 and ZMA2 to some extent. With the shortest treatment time of 5 seconds, no positive effect of ZMA coatings was observed in comparison to conventional zinc coating (GI). High free acid showed a tendency to enhance the robustness of the coatings.

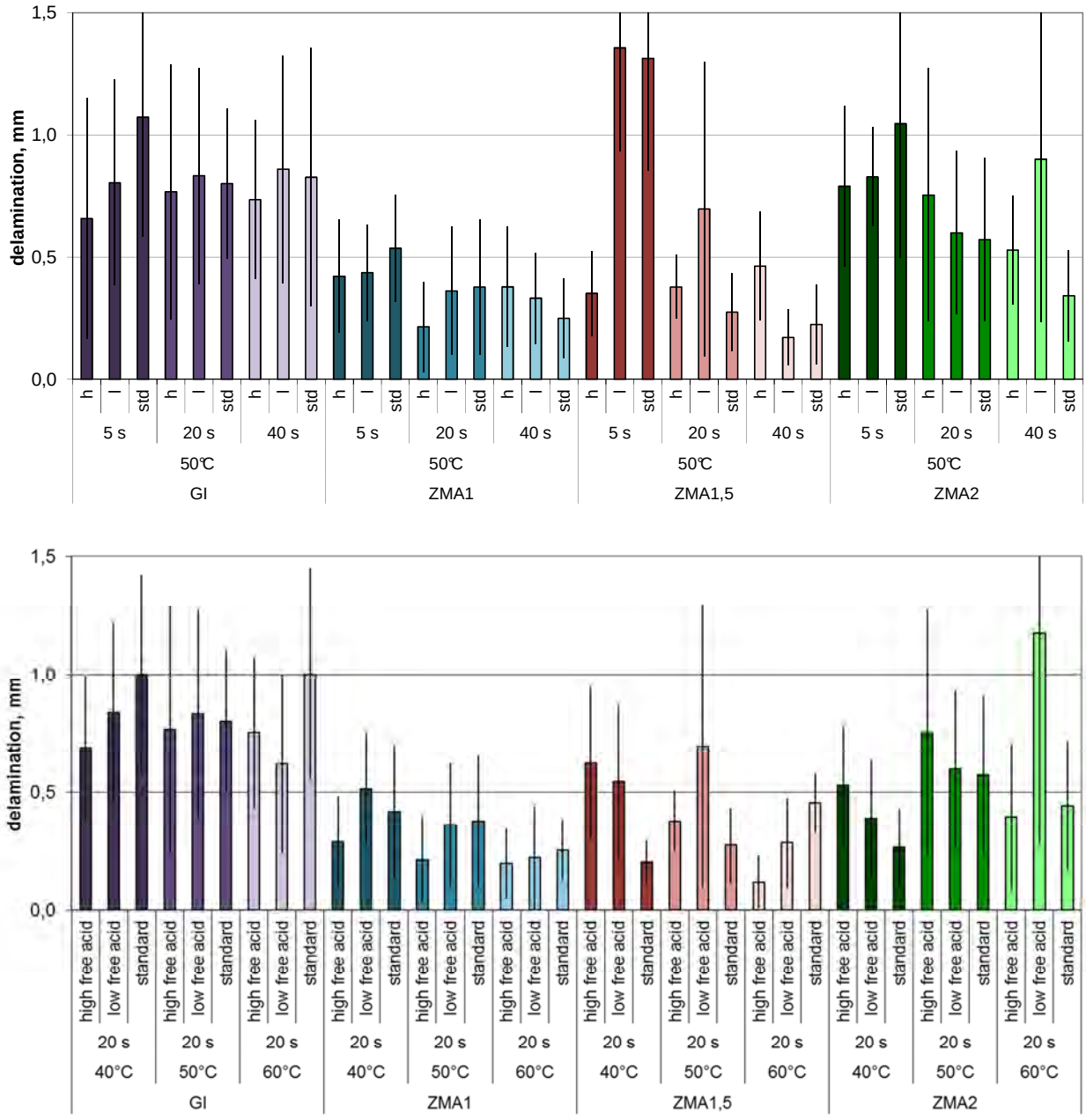

Figure 22: Influence of phosphatation conditions on the creep from scribe line after 6 weeks of exposure in New VDA test. ED-painted GI, ZMA1, ZMA1,5 and ZMA2. h: high free acid, l: low free acid, s: standard free acid. Top: influence of time at 50°C; bottom: influence of temperature.

2.3.3.2 T3.2 Composition and properties of native oxide films

The corrosion stability of Zn-Al, Zn-Mg, and Zn-Al-Mg alloys in initial stages of the corrosion process is probably connected to presence of oxide layers rich with the alloying elements with better protective properties than those of zinc-based oxide layers. The composition and properties of these layers are crucial for the paint stability as well. For instance, these parameters limit the rate of oxygen reduction and the rate of anodic dissolution. The exact nature of the protective films is not known yet. The aim of this task was to investigate the possible role of surface protective films.

In order to address the composition of the native oxide, scales of all coatings (see WP 2) were investigated by means of XPS (see Figure 23) and sputter depth profiling (see Figure 25 and 2.45). X-

ray photoelectron spectroscopy (XPS) was made using a Quantum 2000 equipment from Physical Electronics. The spectra were measured using a monochromatic Al (K_α) source at a 45° take-off angle and pass energies of 29.35 eV and 93.90 eV for the spectra during depth profiles and surveys, respectively. From all samples, at least three points were measured by survey scans. Calibration of the binding energy (BE) of the measured spectra was performed by the C1s peak of the adsorbed hydrocarbons (BE = 285 eV) as an internal reference.
Prior the XPS analysis, all coatings were ultrasonically cleaned in THF, acetone and isopropanol. In the case of Zn and Mg, the chemical shift between the metallic and oxidic state can be very small (usually around 0.1 eV at the Zn 2p3/2 and Mg 1s transition). Thus, the evaluation between metallic and oxidic bound Zn and Mg was done by means of XEAES taking the Mg KLL and Zn LMM transitions into account. For both metals, the chosen Auger transitions have a chemical shift of approx. 6 eV allowing a precise analysis of the oxidation state.

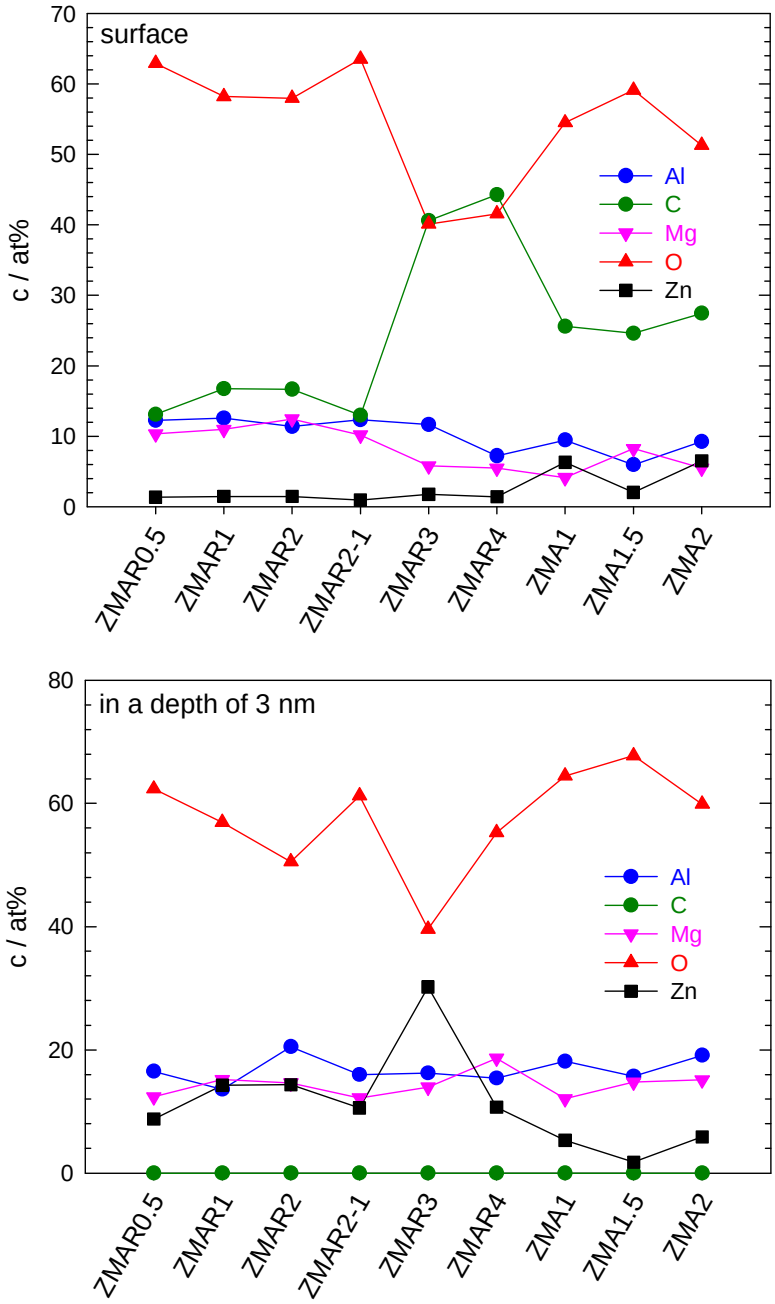

Figure 23: Composition of the production line coatings (ZMA) and Rhesca simulator coatings (ZMAR) at the surface and in a depth of 3 nm.

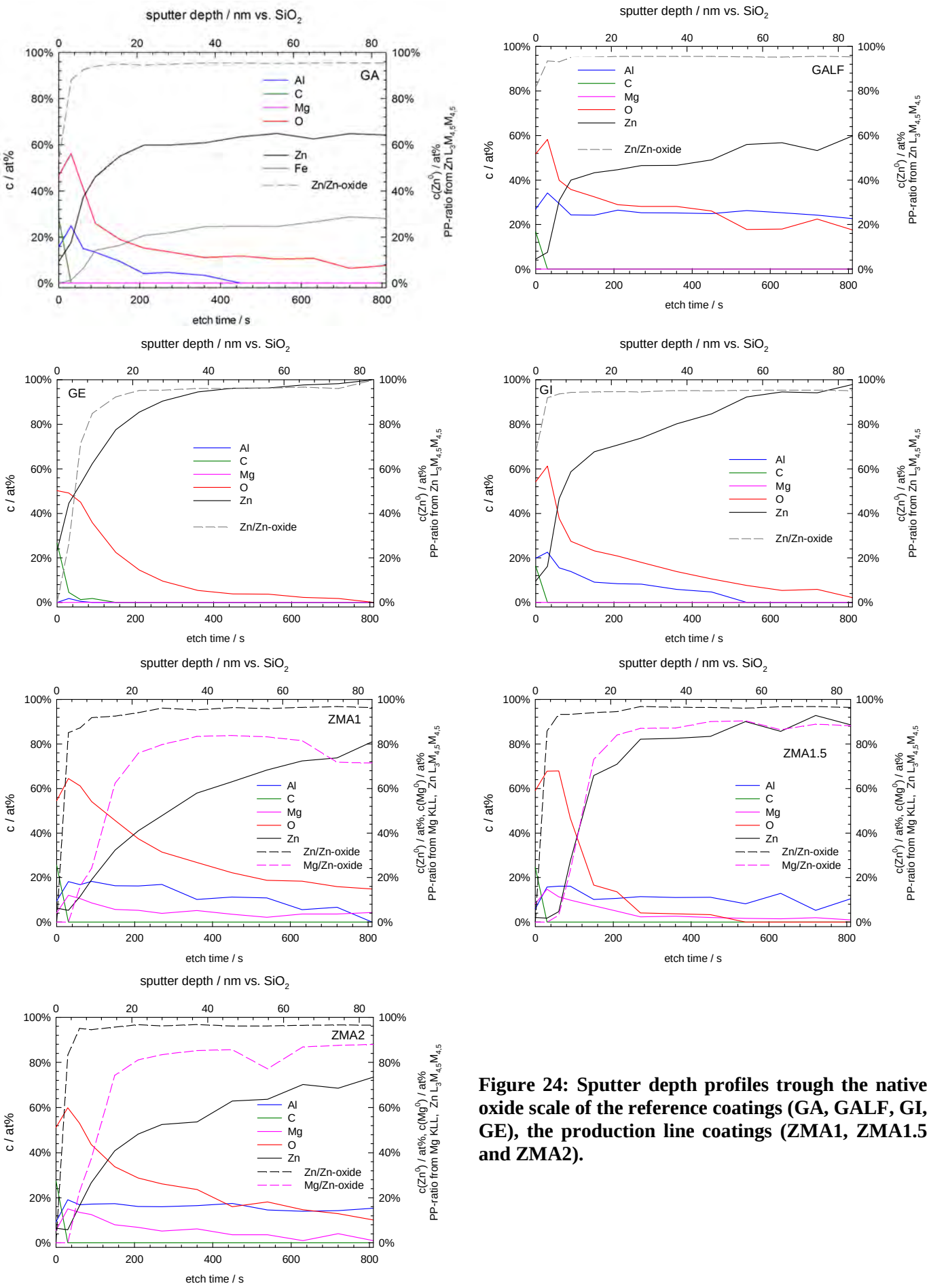

Figure 24: Sputter depth profiles trough the native oxide scale of the reference coatings (GA, GALF, GI, GE), the production line coatings (ZMA1, ZMA1.5 and ZMA2).

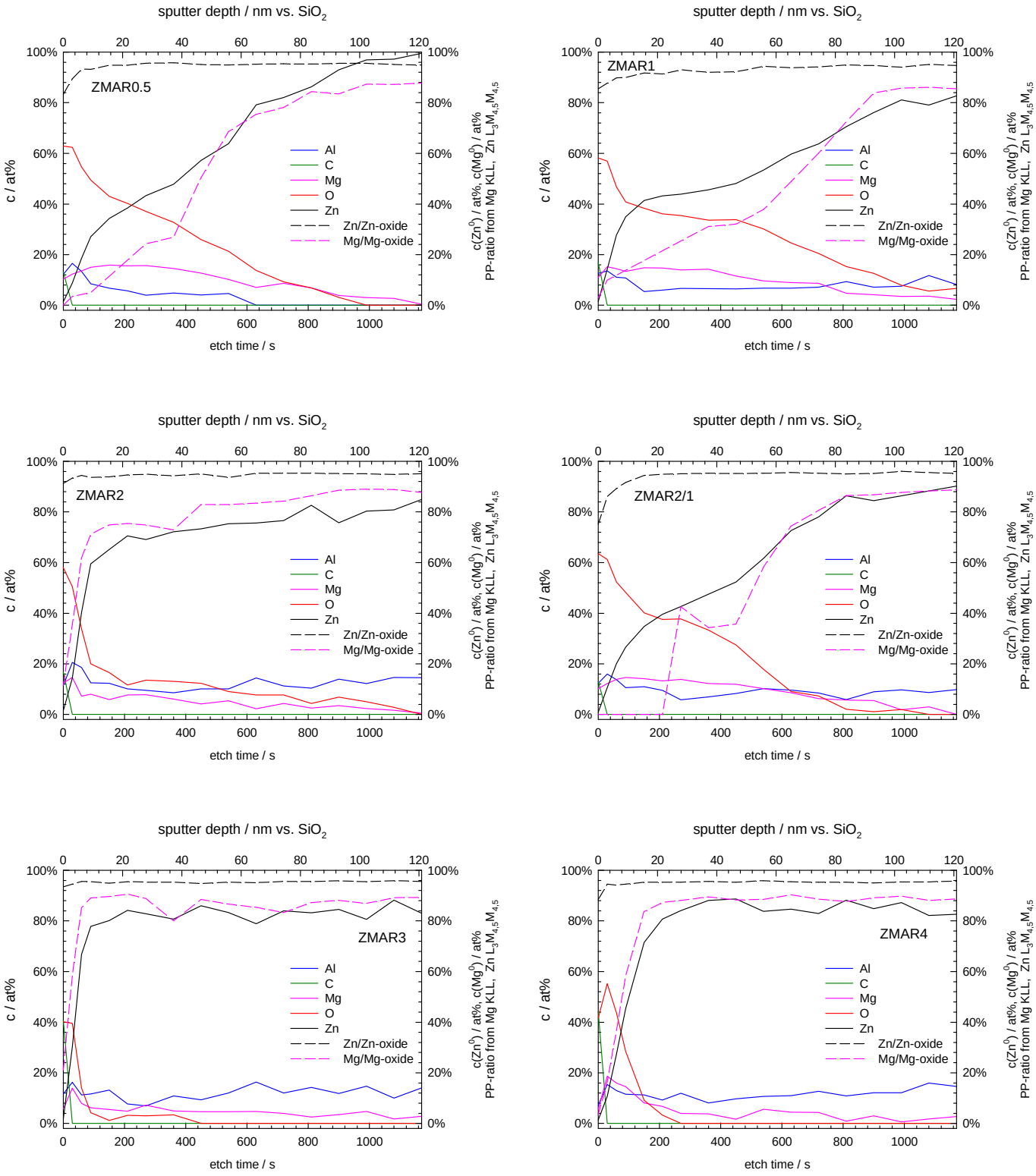

Figure 25: Sputter depth profiles trough the native oxide of Rhesca coatings (ZMAR1-4).

In general, all investigated specimens contain carbon contaminations on top of their surfaces originating from the contact with ambient atmospheres. The Zn-Mg-Al alloys show different kind of contamination levels although all investigated specimens were similar and simultaneously cleaned. All production line coatings show similar carbon concentrations of less than 30 at.%. In the case of the Rhesca simulator coatings, one can observe a reasonably low carbon contamination of less than 20 at.% and a significant higher concentration of more than 40 at.% for the samples ZMAR0.5 – ZMAR2/1 and ZMAR3 – ZMAR4, respectively. These differences are most likely related to the production history of the samples. In general, it can be seen that these considerable carbon contents are removed from the Zn-Mg-Al alloy and reference samples within the first sputter cycle that corresponds to a sputter depth of approx. 3 nm.

All references showed a relatively high oxygen concentration of around 50 at.% at the surface. The atomic concentration of Al (if present) at the surface was higher than Zn and amounts around 20%. The oxygen and aluminum concentrations fall rapidly within the sub surface region within the first 10 nm sputter depth indicating an native oxide scale of similar magnitude. Especially on the Galfan sample, the oxygen and aluminum signal which does not cease to be resent after more than 120 nm sputter depths may be attributed to the presence of residual oxygen in the analysis chamber that directly oxidizes the laid open aluminum surface. As the sputter depth increases, the oxygen signal decreases and zinc signal increases, whilst Zn is mostly present in its metallic form in the sub surface region. The iron concentration changes notably in the case of the galvannealed specimen. During approx. the first 6 nm of sputter depth profiling, the outer surface of the specimen is constituted by zinc (no Fe at the surface) or by a solid solution of iron or the ζ-phase in zinc (Fe/Zn ration around 0.05). In contrast, after a sputter depth of 20 nm till the end of the sputter profile, a Fe/Zn ration of approx. 0.4 could be detected. It is noteworthy, that iron is mostly present as Fe^0 in the analyzed depth area. In conclusion, one can observe a gradual transition in the phases formed with increasing distance from the surface of the GA specimen: The region 20 nm beneath the surface consists mainly of the Γ-phase (Fe/Zn ration approx. 0.4). On top of this phase, a thin layer is present, which is constituted mostly of pure Zn and its native oxide. In conclusion, the presented results are consistent with similar investigations of conventional GA, GALF, GE and GI coatings [1].
The XPS investigation of the Zn-Mg-Al alloy coated specimens indicated the presence of five main elements at the surface: Al, C, Mg, O and Zn (see Figure 23). Generally, the Zn concentration at the surface is relatively low, especially in case of the Rhesca simulator samples (< 2 at.%). The atomic concentration of Mg and Al is much higher than the concentration of Zn despite in the case of the production line samples ZMA1 and ZMA2, which show similar concentrations of Zn and Mg. Within the accuracy of the measurement technique, the Al concentration is similar or slightly higher than the Mg concentration, independent of the Al and Mg concentration of the chemical composition of the bath used. In general, the results obtained demonstrate that during the galvanizing process of the Zn-Mg-Al metallic coatings, a segregation of the minor alloying elements e.g. Mg and Al takes place towards the surface. The composition of the coatings´ outer surface scale is rather different than the chemical composition of the bath used. More interestingly, all Rhesca simulator samples showed more or less similar surface compositions, which differed especially in the Zn concentration from the production line coatings ZMA1 and ZMA2. The reason for this difference is not clearly known, but it might be attributed to the history of the production process itself.
One interesting feature of the Zn concentration can be seen in the XPS depth profiles for the Rhesca simulator samples as function of the minor alloying element concentration, especially for aluminum. The Zn concentration increases sharply to a saturation value within the first 10 nm beneath the surface for the samples produced from baths with higher concentrations of Al (ZMAR2, ZMAR3 and ZMA4). For samples produced from a lower bath concentration of Al (ZMAR0.5, ZMAR1 and ZMAR2/1), the depth profile of Zn looks completely different, more like a gradual increase to a saturation value till a distance of 80 nm to 100 nm beneath the surface. Within the sub surface region affected by this slow gradual increase, one can observe an enrichment of Mg. Both observations indicate a different segregation behavior of Mg and Al for low Al bath concentrations.

In order to study the corrosion products as function of exposure time (1 day, 7 days and 1 month) three different kinds of samples (Zn: as reference, ZMA1.5 and ZMA2 as cast) were exposed to a marine atmosphere environment in Brest. In the case of the production line coating ZMA1.5, all cut edges were

protected to avoid any contributions of the cut edges. The samples were analyzed by means of XPS to determine the surface composition. The survey and C1s detail spectra are shown in Figure 26 for the ZMA2 cast sample, exemplarily.

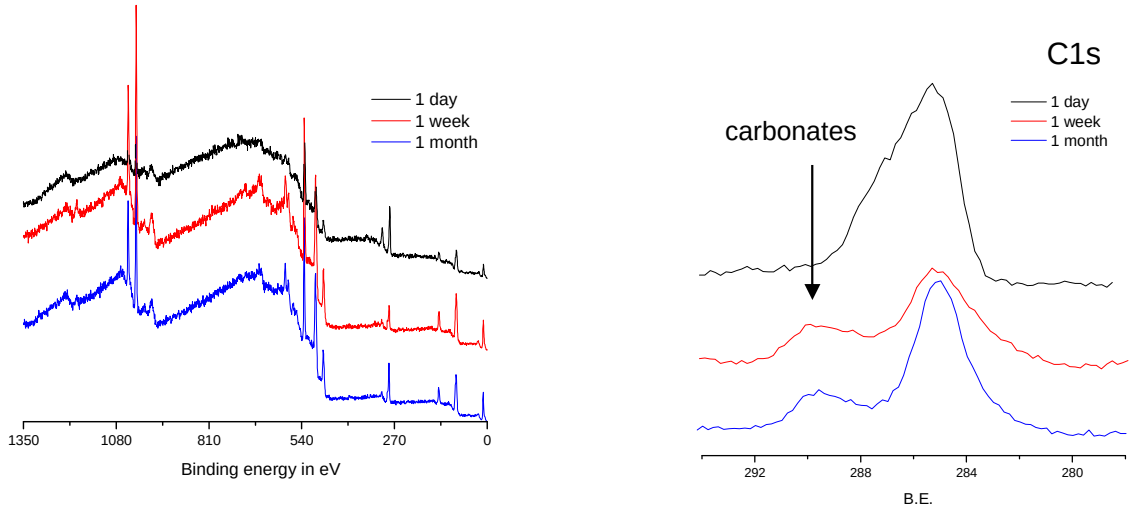

Figure 26: Survey and C1s detail spectra of the ZMA2 cast sample exposed to an marine atmosphere, as function of exposure time (as indicated).

As can be seen from the C1s detail spectra, carbonate species are forming on the surface after an exposure time of several days. The survey scan of the samples exposed for one day exibit a „bump"-like envelope structure, which is more pronounced in the case of the Zn reference and less pronounced in the case of the ZMA2 cast sample. Such kind of envelope structure is an indication for a low-Z and low density overlayer, most likely of organic nature. With increasing exposure time, this envelope structure vanishes and a pronounced carbonate species can be seen in the C1s detail spectra, indicating the transformation of the overlayer in a carbonate containing corrosion product scale. The increase of carbonate containing corrosion product was in agreement with FTIR measurement performed on identical samples. The complete surface composition of the samples is summarized in Figure 27. As can been seen in Figure 27, the amount of Zn and Mg is growing with time while the amount of C is falling. Interestingly, no residue of Al could be detected in the surface corrosion products already after one day of exposure.

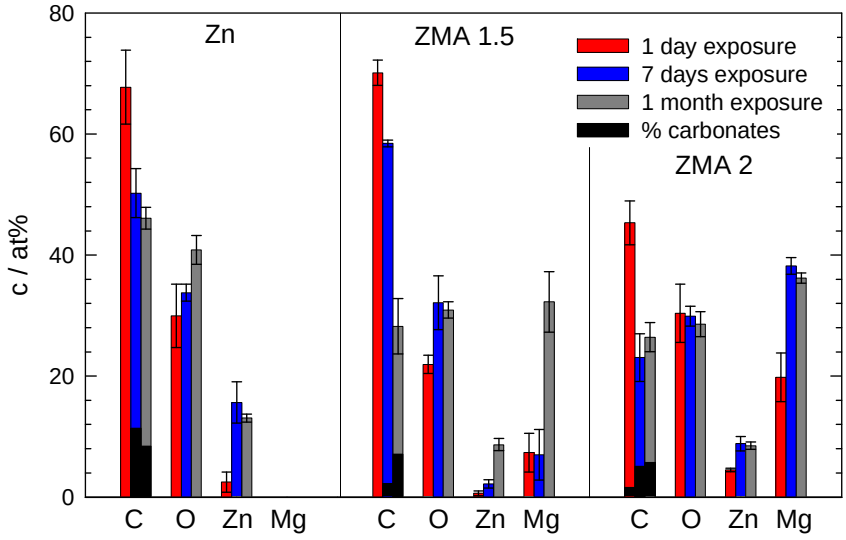

Figure 27: Surface composition determined by means of XPS of three different kinds of samples (Zn: as reference, ZMA1.5 and ZMA2 as cast) that were exposed to a marine atmosphere environment (as indicated). The carbonate concentration is shown as black bar within the overall carbon concentration.

2.3.3.3 T3.3 Surface oxide and paint stability

The aim of this task was to understand the effect of bulk and surface composition on the paint stability and paint delamination kinetics. The results obtained in former projects indicate that the distribution of the oxides on the surface plays a crucial role [2]. Hence, the aim of this task was to combine scanning Kelvin probe (SKP) delamination experiments and results on the oxide layer characterization from T2.4 and T3.2.
One key parameter that controls the formation of a local galvanic element during the deadhesion of paint from the steel specimen is the potential gradient between a defect in the paint (-800 mV_{SHE} (Zn/Zn^{2+})) and the intact metal oxide/polymer interface. Therefore, the surface potential of all samples (references (GA, GALF, GI, GE), production line coatings (ZMA1-2) and Rhesca simulator coatings (ZMAR1-4)) have been determined by means of the SKP technique as a first step. The measured potentials in a water saturated (94% R.H.) inert atmosphere (N_2) and air at over a 1000 µm x 1000 µm area are shown in appendix 1 on Figure 90, Figure 91 and Figure 92 for reference coatings (GA, GALF, GE and GI), line hot dip coatings (ZMA1, ZMA1.5 and ZMA2) and Rhesca samples respectively. The averaged values are summarized in Figure 28.

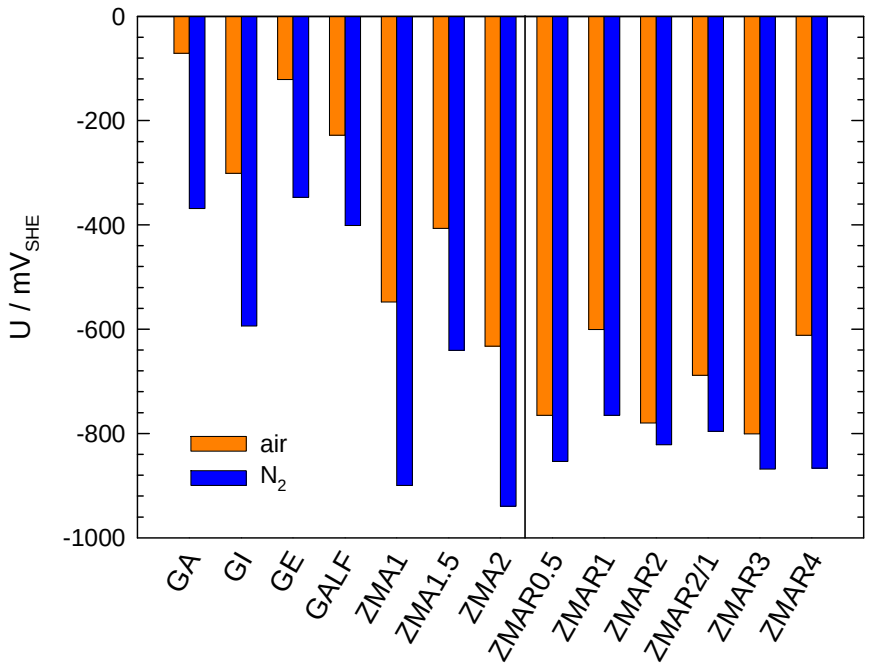

Figure 28: Averaged surface potential from the measurements shown in Figure 90 to 92.

Compared to the production line samples, the Rhesca simulator samples showed lateral inhomogeneous potential levels in air. This is most likely related to the inhomogeneous microstructure of the corresponding alloys (T 2.4) resulting in a lateral inhomogeneous surface oxide composition.

Compared to $ZnMg_2$ which potential is typically around -1.1 V_{SHE} (see Reference [3]), all measured potentials of all Zn-Mg-Al alloys are shifted in the anodic direction. Further, comparing the production line coatings, one can see differences between the ZMA1.5 and ZMA1 or ZMA2 coating. Obviously, these differences are related to the Fermi-level of the samples. The Fermi-level is directly influenced by the defect structure of the semiconducting surface oxide, e.g. the density of metallic Mg near the surface. To verify this assumption, very fine depth profiles have been performed, as shown in Figure 29.

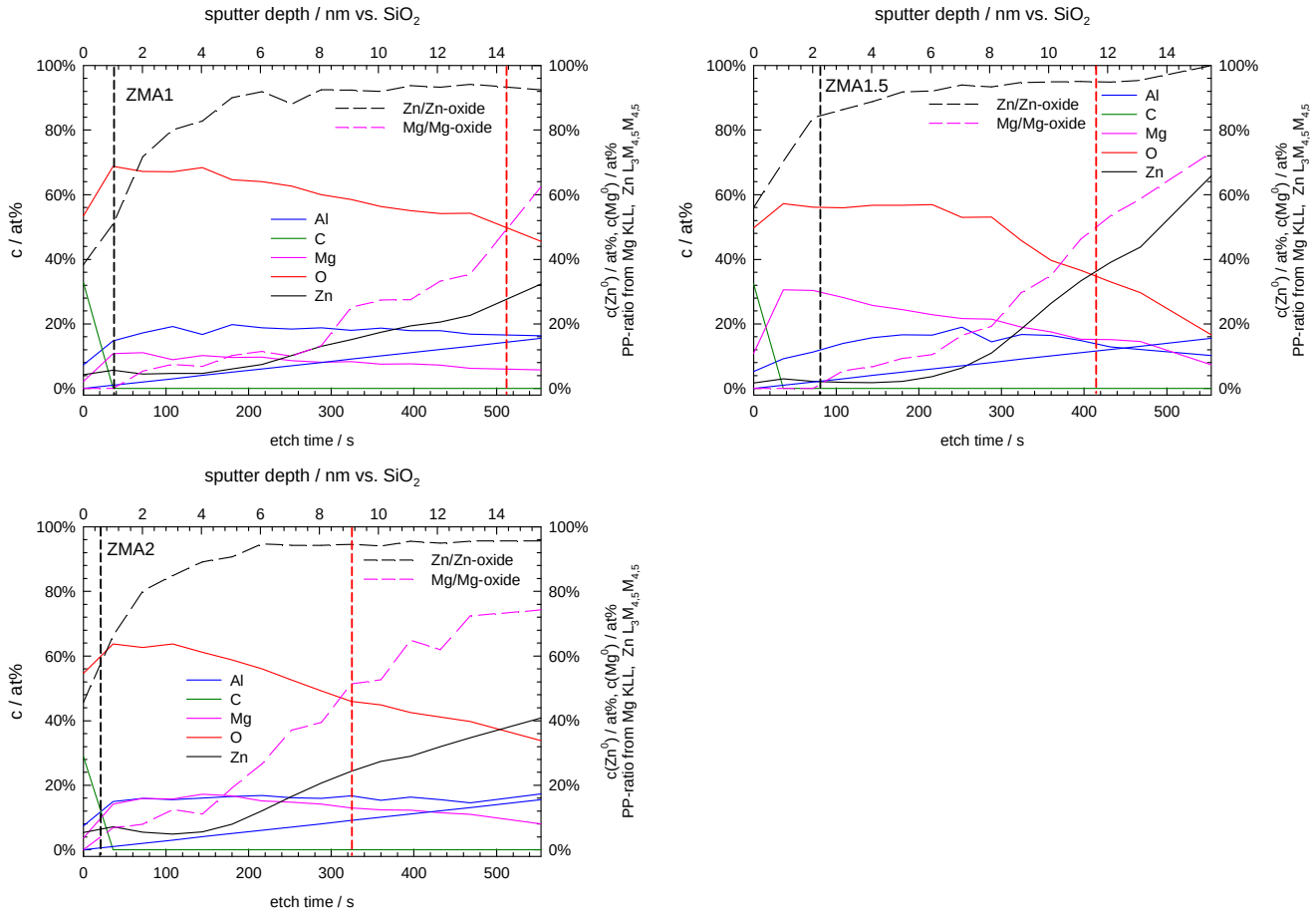

Figure 29: Sputter depth profiles through the first few nm of the native oxide scale of the production line coatings (ZMA1-2).The turning point of the Mg-oxide contribution and the onset of the metallic Mg contribution are indicated by the dashed red and black lines, respectively.

Obviously, the onset of the metallic Mg contribution differs between these two cases (ZMA1 and ZMA2 approx. 1nm; ZMA1.5 approx. 2.2 nm). This could explain the differences in measured potentials. This makes sense from a production line point of view, too. In the production process of the ZMA1.5 samples, an air wiping was indeed utilized, while for the other ones, a nitrogen wiping was used. Consequently, one could expect a thicker shell of the outer oxide on ZMA1.5 surface.

In general, the results summarized in Figure 28 show that for all cases, the observed potentials in air are above the corrosion potential of corroding zinc (about -800 mV_{SHE}) and hence an inherent delamination resistance as found for MgZn2 as a consequence of potential inversion between defect and intact interface (see again Reference [3]) will not be effective. However, it might well be that the high concentrations of Mg and Al found on the surface (see fig.1) may at least significantly slow down the delamination process.

In order to investigate that, first as a reference, the delamination of phosphated and ED coated samples was investigated. As different tests lead to different results, two extreme conditions were chosen for the delamination testing: large artificial defects 1) down to zinc and 2) down to steel. During delamination of zinc coated steel, a strong interplay between cathodic and anodic delamination mechanism is usually expected, i.e. also the corrosion behaviour of the zinc alloy plays a role, not only the delamination mechanism beneath the organic coating. Hence, two special sets of samples were prepared: ED coated phosphated samples were brought into contact with large (about 1 cm in width) artificial defects either of bare zinc or of bare steel, filled with 0.5 M NaCl (aq) solution (see Figure 30). For the first case, the corrosion potential, a key driving force for delamination, should be always the same for all samples. This way, differences especially of the processes at the interface are highlighted, i.e. here the focus is indeed mainly on the phosphate layer. Standard phosphatation was used for these experiments. The delamination was monitored by Kelvin probe.

As can be seen from the results, the differences in the delamination progress of the phosphated samples are small for this kind of defect (see Figure 30 and Figure 31). However, again the ZMA samples seem even to be slightly better.

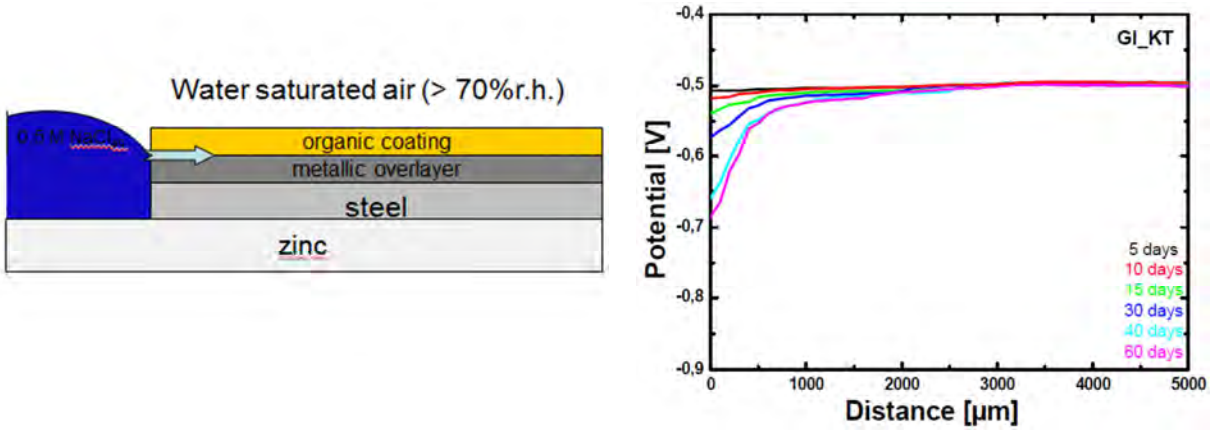

Figure 30: Evolution of the delamination distance from the defect (simulated by a large pure zinc surface, see sketch on the left) on ED coated phosphate GI as a function of exposure time in humid air. Potential profiles obtained by SKP in V/SHE.

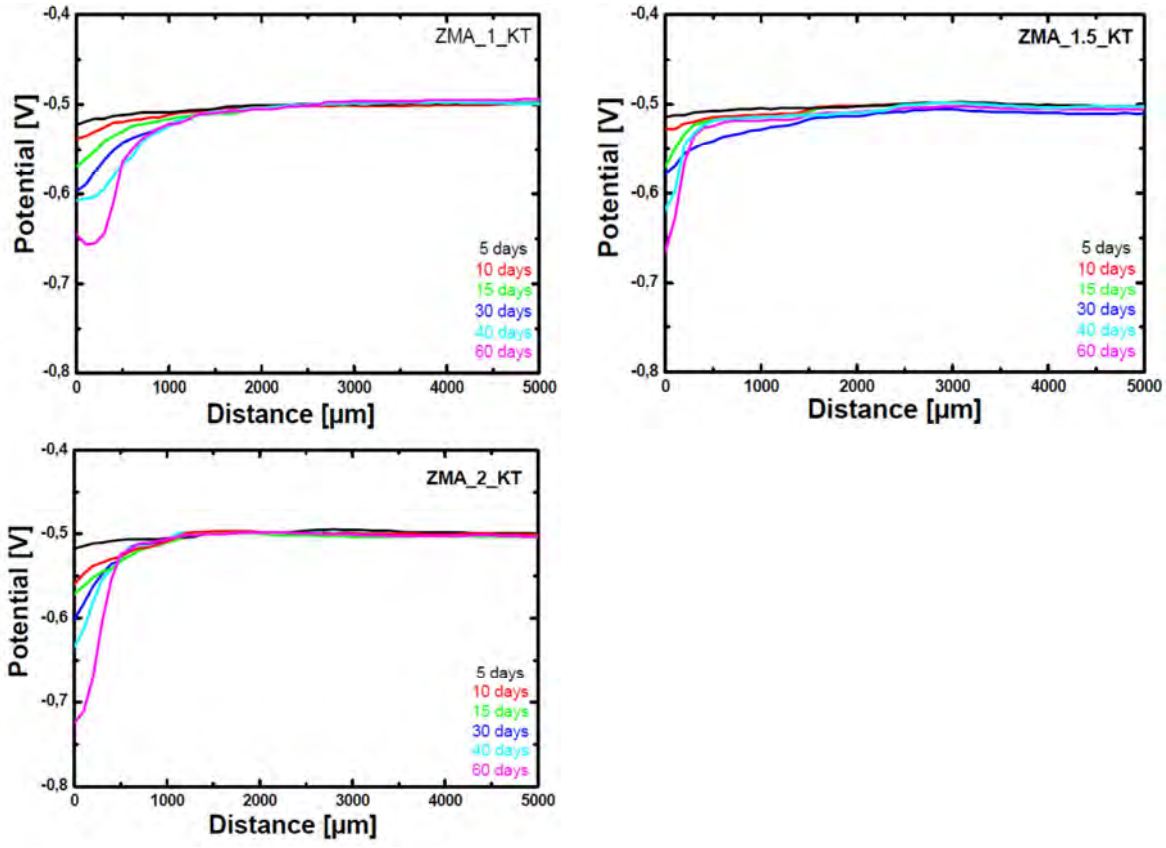

Figure 31: Evolution of the delamination distance from the defect (simulated by a large pure zinc surface) on ED coated phosphate ZMA1, ZMA1.5 and ZMA2 as a function of exposure time in humid air. Potential profiles obtained by SKP in V/SHE.

For the second kind of experiment, an extremely strong driving force for anodic delamination was exerted on the metallic coated samples by bringing the interfaces in contact with an extremely large iron surface, i.e. the coatings have to cathodically protect a very large steel defect. As shown on Figure 32, the performance of ZMA samples was again quite good and comparable with GI one where only minor

differences were found between the samples. This is in agreement with results reported in task 3.1 which indicated no problems of phosphatation of ZMA coatings. Despite the size of the exposed steel in the defect, the cathodic protection worked excellently for all samples, but, of course, the delamination progress was much faster in this case (about 3 mm in 7 days, compared to less than 1 mm in 60 days for the zinc defect). The delaminated area was indeed rather similar for all samples. In this case, however, slight differences in the shape of the measured delamination profiles can be observed but further underlying that certainly no problems with the phosphatation quality are caused by the Mg content.

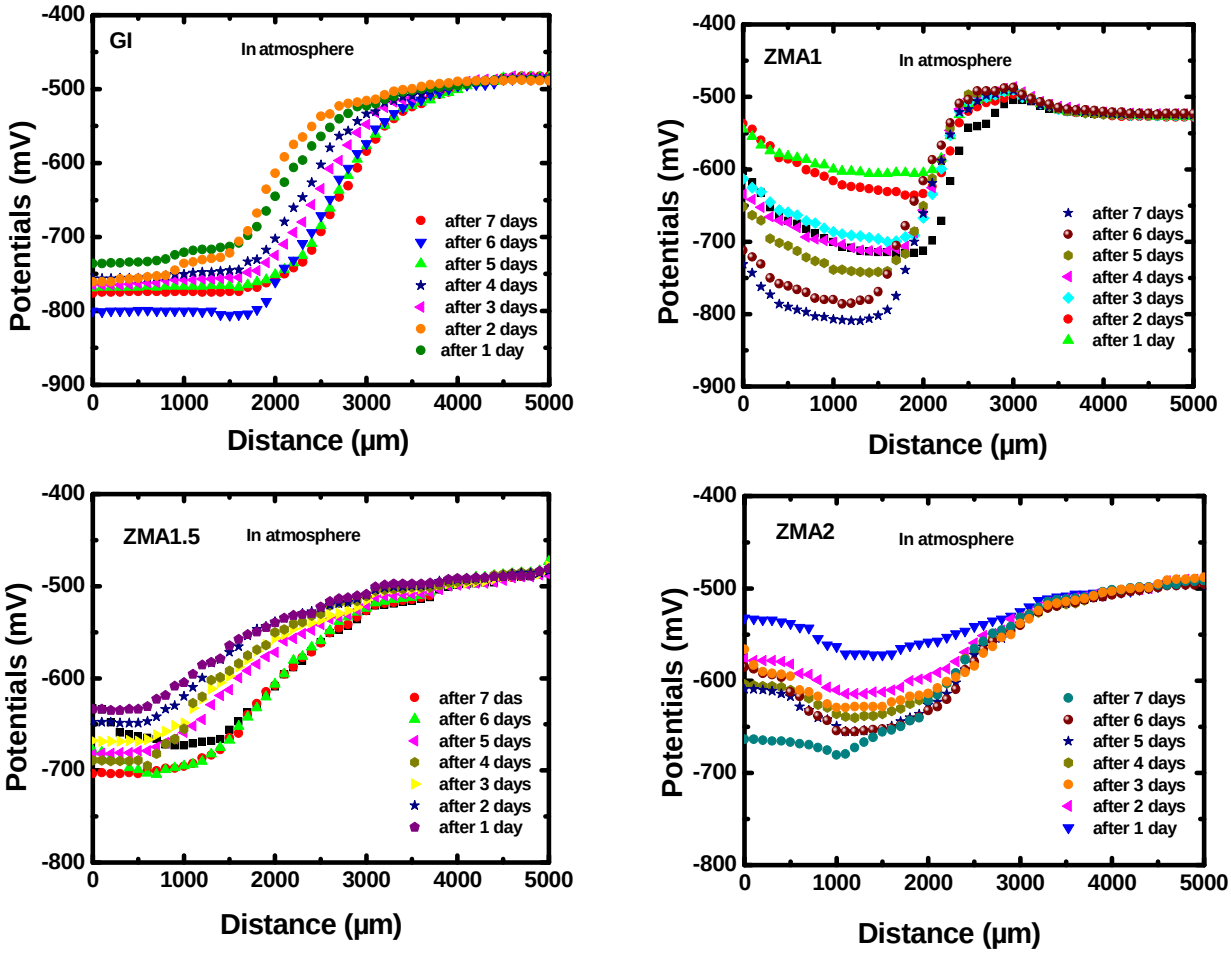

Figure 32: Evolution of the delamination distance from the defect (simulated by a large steel surface) on ED coated phosphated ZMA1, ZMA1.5 and ZMA2 as a function of exposure time in humid air. Potential profiles obtained by SKP in V/SHE.

In a second step**, two different organic coatings** were applied directly on the solvent cleaned (10 min THF, 10 min acetone, 10 min isopropanol in ultra-sonic bath) metallic coated samples (e.g. no surface treatment was applied) and the same experiments as described above were carried out. Coating 1 was of 2 component acrylate based coating while Coating 2 was a 2 component polyurethane based one, without additives. Both coating systems were applied with a thickness of about 24 µm.

The results obtained with coating 2 are presented on Figure 33 and Figure 34 upon the nature of the artificial defect e.g. zinc or steel. As expected, these coating systems were not as delaminated resistant as the phosphated/ED-coating systems. From the results obtained in the delamination experiments in with a large simulated defect down to the zinc, the delamination rate was nearly two orders of magnitude faster than for the phosphated and ED coated samples. Other than for the latter samples, for the just painted samples, differences in the behavior are discernible, that are assumed to be correlated to the oxide structure at the metal coating/organic coating interface. However, the variations were not very large and did not show a systematic pattern. Interestingly, for the case of the large simulated defect down to the steel, similar delamination rates were observed as for the phosphated and ED-coated samples, which were expected if the delamination rate was determined by the anodic dissolution of zinc

(alloy). Contrarily to ED coated phosphated samples, differences in the delamination behaviour upon the metallic coating were observed, see *Figure 33*. After 3.5 days of exposure, ZMA coated samples showed a delaminated area ranging from 1 and 2 mm, while it was around 3 mm for GE and 2 mm for HDG (GI). These findings indicate that the oxide layer on ZMA seems to have some positive effect, but it was not that significant and no clear trend could be observed. Nevertheless, much less delaminated area was observed on phosphated and ED-coated ZMA samples with less than 0.5 mm in 60 days. Thus, avoiding phosphatation is obviously not possible.

For the simulated large defect down to the steel, similar delamination rates as for the phosphated samples were observed with about 1-2 mm in the first day (see Figure 34). The exception was ZMA 1.5 sample, which showed much faster delamination for an unknown reason.

Rather similar results were also obtained with the acrylate base coating named Coating 1.

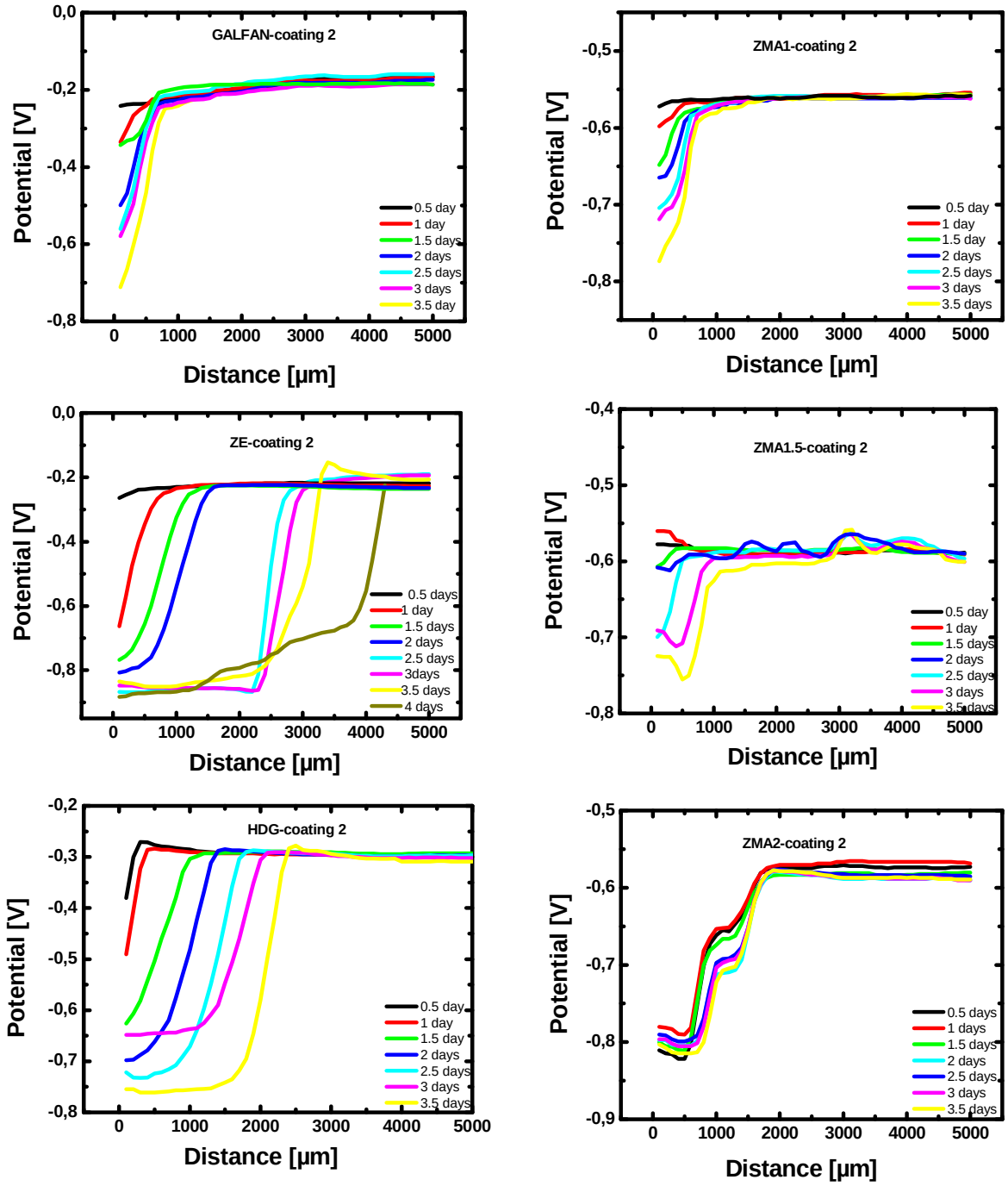

Figure 33: Evolution of the delamination distance from the defect (simulated by a large zinc surface) obtained on ZMA and conventional zinc metallic coating covered with coating 2 (no

phosphate layer) as a function of exposure time in humid air. Potential profiles obtained by SKP in V/SHE.

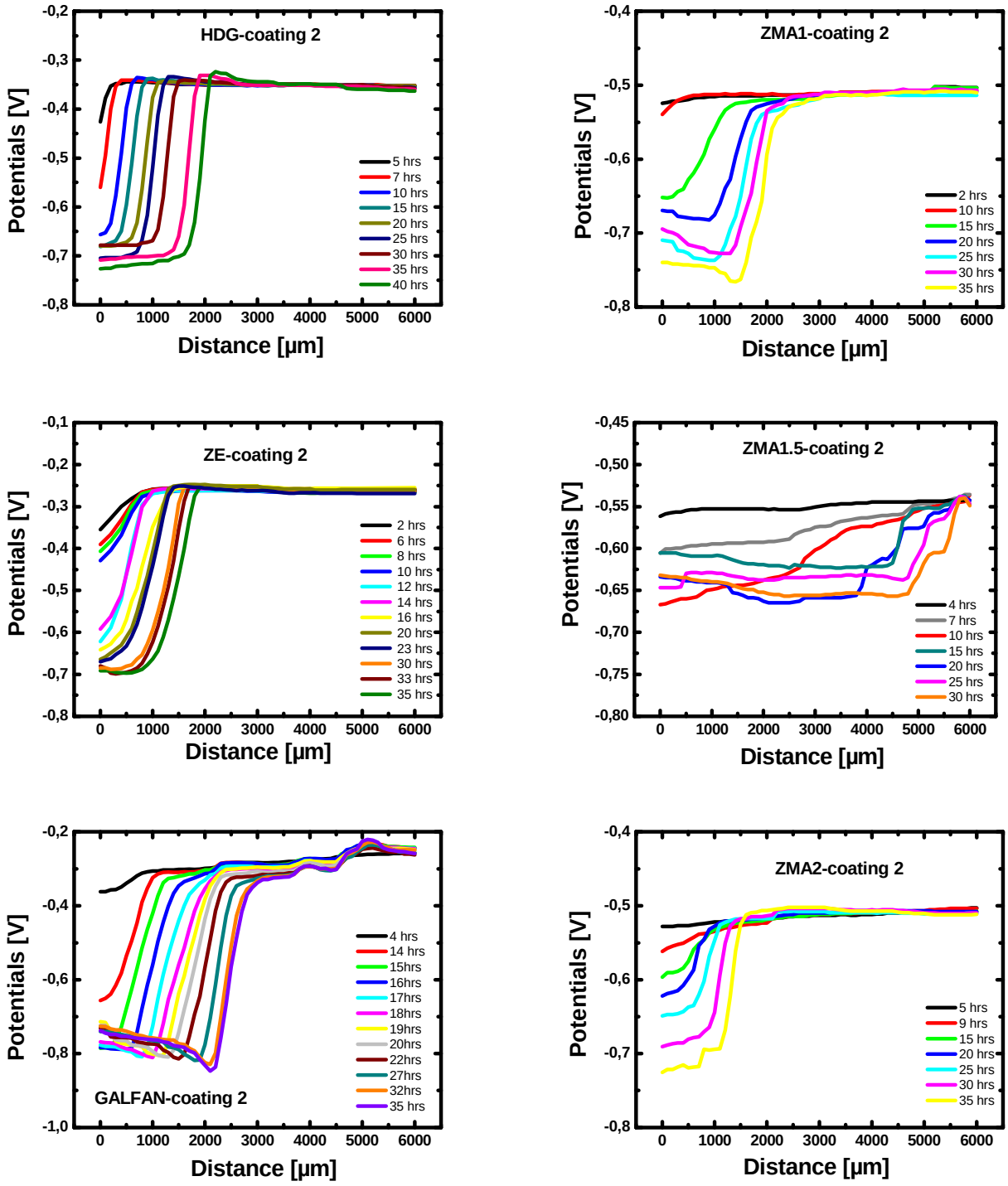

Figure 34: Evolution of the delamination distance from the defect (simulated by a large zinc surface) obtained on ZMA and conventional zinc metallic coating covered with coating 2 (no phosphate layer) as a function of exposure time in humid air. Potential profiles obtained by SKP in V/SHE.

2.3.4 **WP4 Long term corrosion properties**

The objectives of WP4 are to obtain reliable and full-scale data on performance of novel Zn-Mg-Al hot dip coated materials in a wide variety of real conditions, including on-vehicle exposures and exposure in stationary field sites.

2.3.4.1 Task 4.1: Testing at field stations

2.3.4.1.1 Experimental

Three field sites were selected for outdoor exposure which all started in July 2010 (see Table 10). As indicated in Table 11, the yearly metal loss was measured on cold rolled steel CRS (DCO1) and pure zinc (98.5%) in order to evaluate the degree of aggressiveness of the different sites. Obviously, the marine site of Brest was the most aggressive one as expected from its location, while Linz appears the mildest.

Table 10: list of the outdoor field stations

Site manager	Location	Atmosphere	Angle of exposure
IC	Brest, France	Marine & temperate	45° south
TKSE	Dormund, Germany	Industrial & Urban	45° south
voestalpine	Linz, Austria	Continental (-20/+30°C)	45° south

Table 11*:* Yearly metal loss on steel and zinc in Brest, Dortmund and Linz

g/m²(µm)	Brest (IC)	Dortmund (TKSE)	Linz (voestalpine)
CRS	700 (90)	104 (13)	50 (6)
Zinc	10 (1.5)	5 (0.7)	2.5 (0.35)

2.3.4.1.2 Results

Figure 35 presents the average scribe creep measured on cosmetic samples after 12 and 24 months of exposure in Dortmund and Brest sites. Data from Linz site were not plotted as no creep from scribe was observed as expected from the extremely low corrosivity of the site (see Table 11).

The results indicated rather low creep from the scribe line after the exposure in Dortmund with equal or less than 0.5 mm whatever the metallic coatings. No major increase of the corrosion was noticed between 12 and 24 months. Much longer exposure durations should be conducted to draw safe conclusions for this site. Regarding the exposure in the marine site of Brest, more significant scribe delamination was measured and its extent slightly increased with exposure time. Obviously, no major differences were observed between the different metallic coatings. Surprisingly, important scribe creep was observed on the 1 mm wide scribe on ZMA1.5 coating but no explanation could be given. Excluding this event, no influence of the thickness of ZMA coating (between 7 and 11 µm) could be observed.
However, it is believed that two years of exposure on field are obviously insufficient to draw safe conclusions.

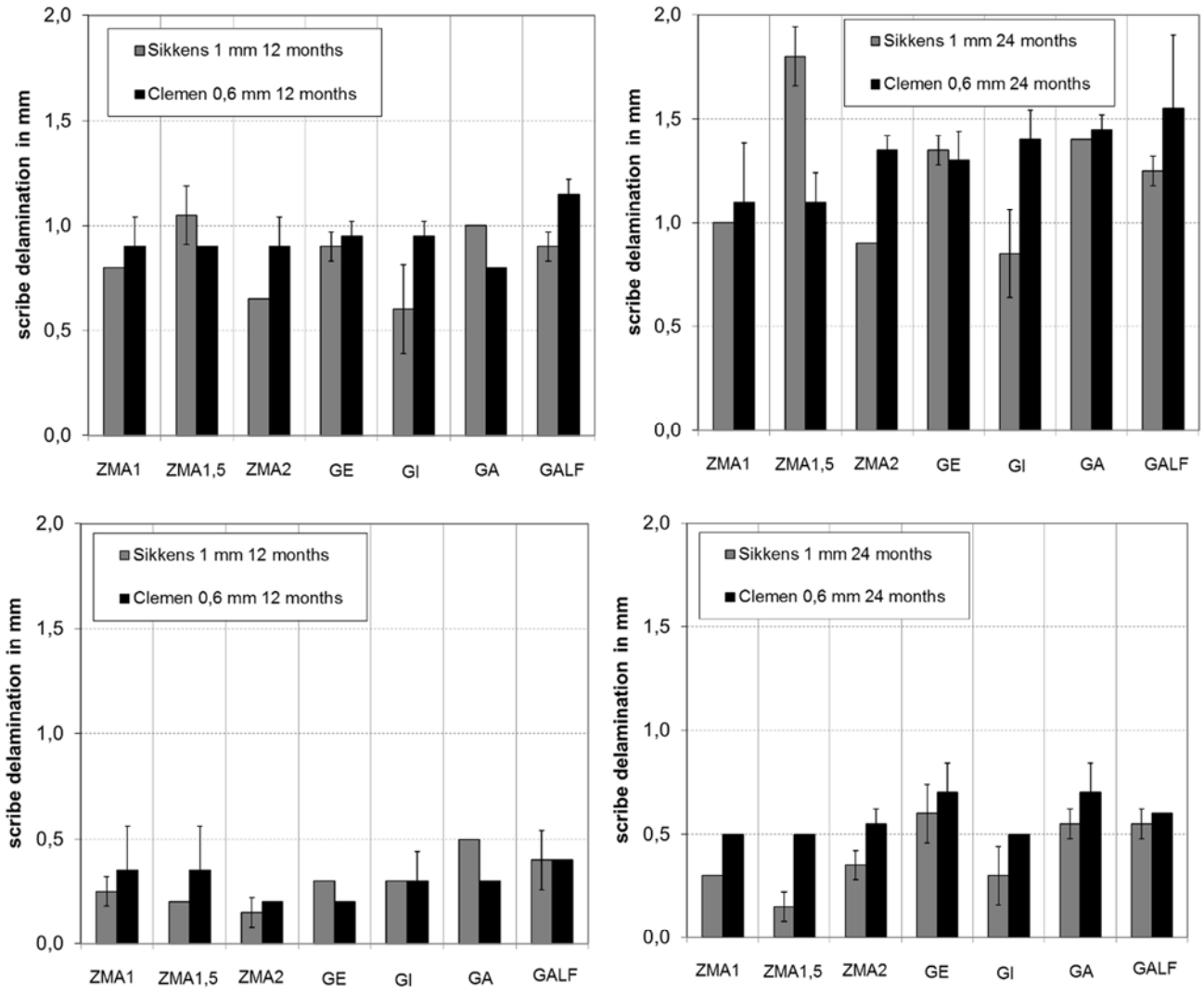

Figure 35: Mean delamination from scribe after 12 (left) and 24 (right) months of outdoor exposure in Brest (top) and Dortmund (bottom).

Regarding the behavior of unpainted materials in open and confined configuration after 1 and 2 years of exposure in the different stationary field sites, the metal loss is plotted in Figure 36 as a function of the different metallic coatings. As expected from the corrosivity class on zinc for the different sites (Table 11), the marine site of Brest induced the most important damages, followed by Dortmund and Linz and a global increase of the metal loss was observed with the exposure duration whatever the site.

When considering **open surfaces** (Figure 36 top), the results clearly showed an improvement of ZMA coating in comparison to conventional zinc coatings GI, GE or GA, by a factor of 2 approximately, whatever the exposure site after 1 year of exposure. However, one should be careful to draw any definitive conclusions when low corrosion was measured e.g. for Linz and Dortmund to some extent. The improvement factor has a tendency to decrease to 1.5 after two years of exposure when GE is excluded from the comparison. The results also showed that the improvement is comparable to galfan coating. The influence of Al and Mg content was not obvious unless after exposure in the marine site of Brest, neither the thickness of ZMA coating if ZMA 1.5 (11 µm) is compared to the ZMA1 and ZMA2 (~7µm).

In **hem-flange configurations** (Figure 36 bottom), similar observations may be done regarding the aggressiveness of the different site, the marine site being the most aggressive one. In this configuration, the improvement of ZMA coatings is not manifest as comparable data were obtained on GI and GA coatings. Electrogalvanised substrates were the most affected ones, particularly after exposure in the marine site where spots of red rust were formed.

Note also the large deviation between replicates in case of hem-flange configuration which has been reported several times elsewhere despite many effort to design reproducible samples. The design of the

confined surface and variation upon the replicate is indeed very much influencing the results. It is thus not evident to attribute the better behavior of ZMA1.5 compared to ZMA1 and ZMA2 after 2 years of exposure in the marine site to the thicker layer of metallic coating.
From a comparison of open and confined configurations, it is obvious that confined situations induced more corrosion as reported in previous works and also from data obtained in accelerated corrosion tests performed in this project (WP 6).

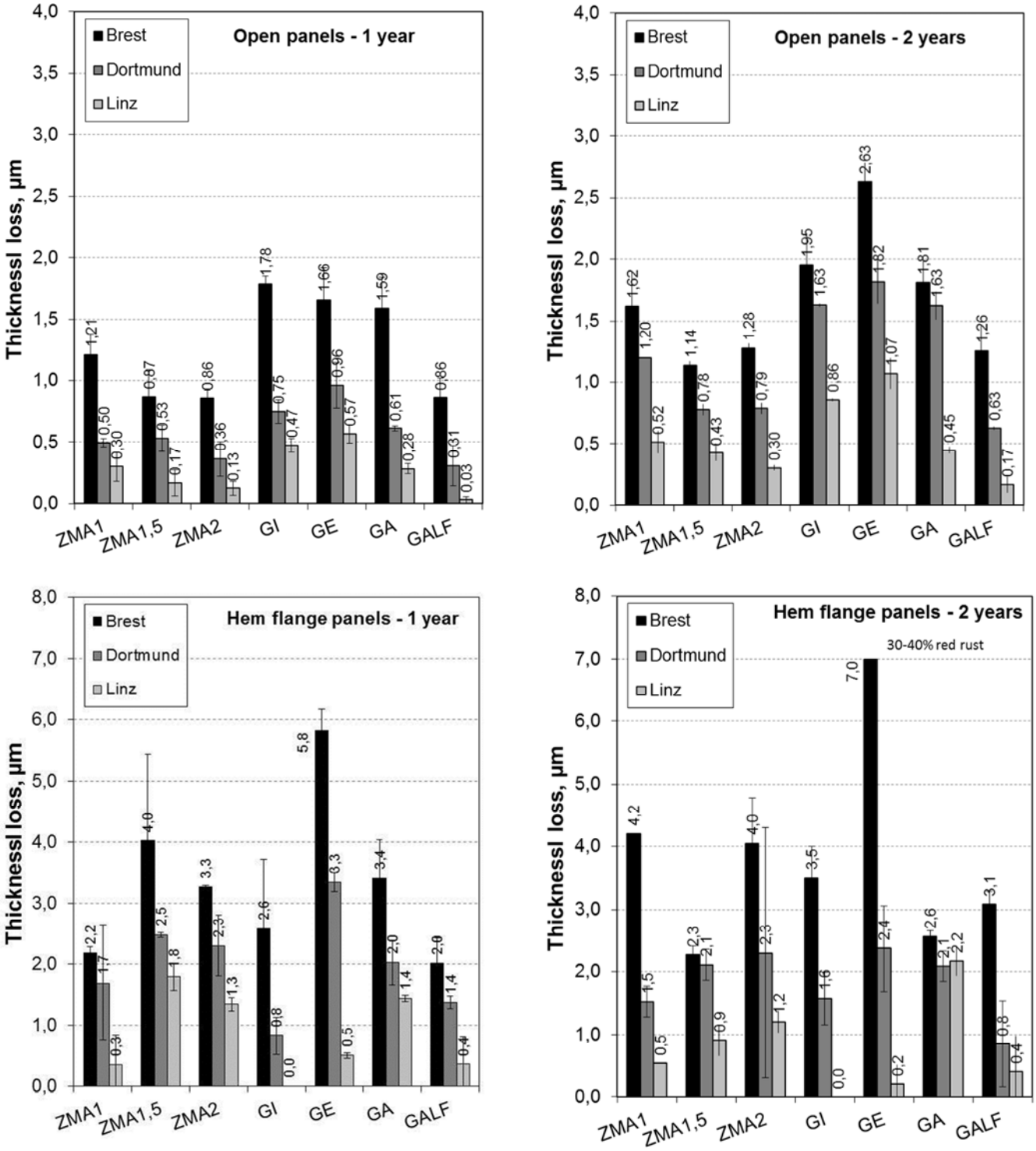

Figure 36: Metal loss of metallic coating in open configurations (top) and hem-flanges (bottom) after 12 (left) and 24 (right) months of outdoor exposure in Linz, Dortmund and Brest sites. Note that ZMA1.5 thickness was around 11 µm versus 7 µm for the other coatings.

As regards to red rust at cut-edge which is presented on Figure 37 for samples exposed 2 years in the marine site, it is obvious that no much difference was observed between ZMA, GI and Galfan coating

while more significant extent of red rust was formed on GE coating. This would indicate a beneficial effect of aluminium in the coating.

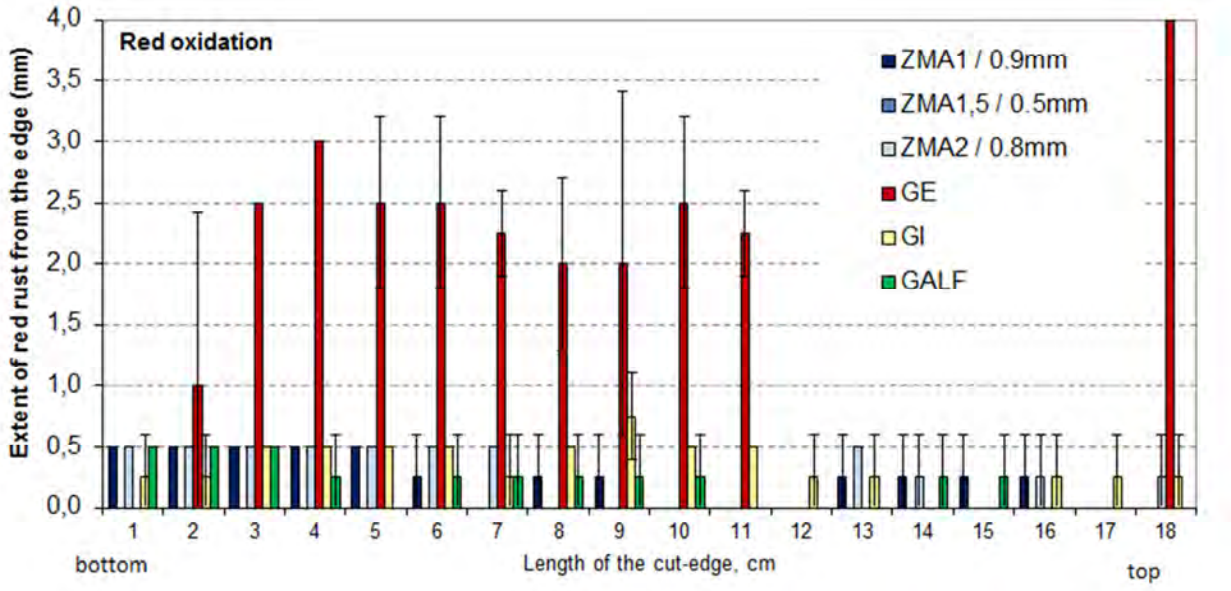

Figure 37: Extent of red rust at cut-edge after 2 years of exposure at the marine site.

2.3.4.2 Task 4.2: On-vehicle testing

2.3.4.2.1 Experimental

Two on-vehicle exposures were conducted, one under a truck driving in Switzerland and one at a FIAT proving ground test.

Truck exposure - The samples have been exposed under a trailer of a truck driving in the Swiss Alps around Zürich area on October 22, 2010, see photograph on Figure 38. Due to space restriction under the trailer, the number of samples has been limited. Thus, only one reference line hot dip coating was exposed e.g. GI, and 2 replicates per exposure duration and materials. One set of samples was removed after 1 year and a second one after two years. In addition to Autocoat samples, CRS and pure zinc panels were exposed to measure the yearly metal loss, which results are given in Table 12. Despite such results are highly dependent on many parameters (driving location and conditions, distance, service of the truck, garage parking), the data are typical for roads with moderate use of de-icing salts [7].

Figure 38: Photographs of the samples exposed under the trailer

Table 12: Metal loss on CRS and zinc after one year of exposure under the truck (mean of year 1 and 2)

	g/m²	µm
CRS	353	45
Zinc	25	3.5

Proving ground at FIAT - A proving ground test was performed at FIAT. It consisted of 40 days of driving on different road conditions for a total run of 6000 km. However, full completion of the test may need up to 6 months. Figure 39 presents a description of FIAT proving ground. The aggressiveness of the proving ground was evaluated towards bare CRS and zinc (see Table 13), showing rather hard conditions for zinc materials with 16 µm of metal loss. This is 4 times more than what was observed on real driving situation in Switzerland.

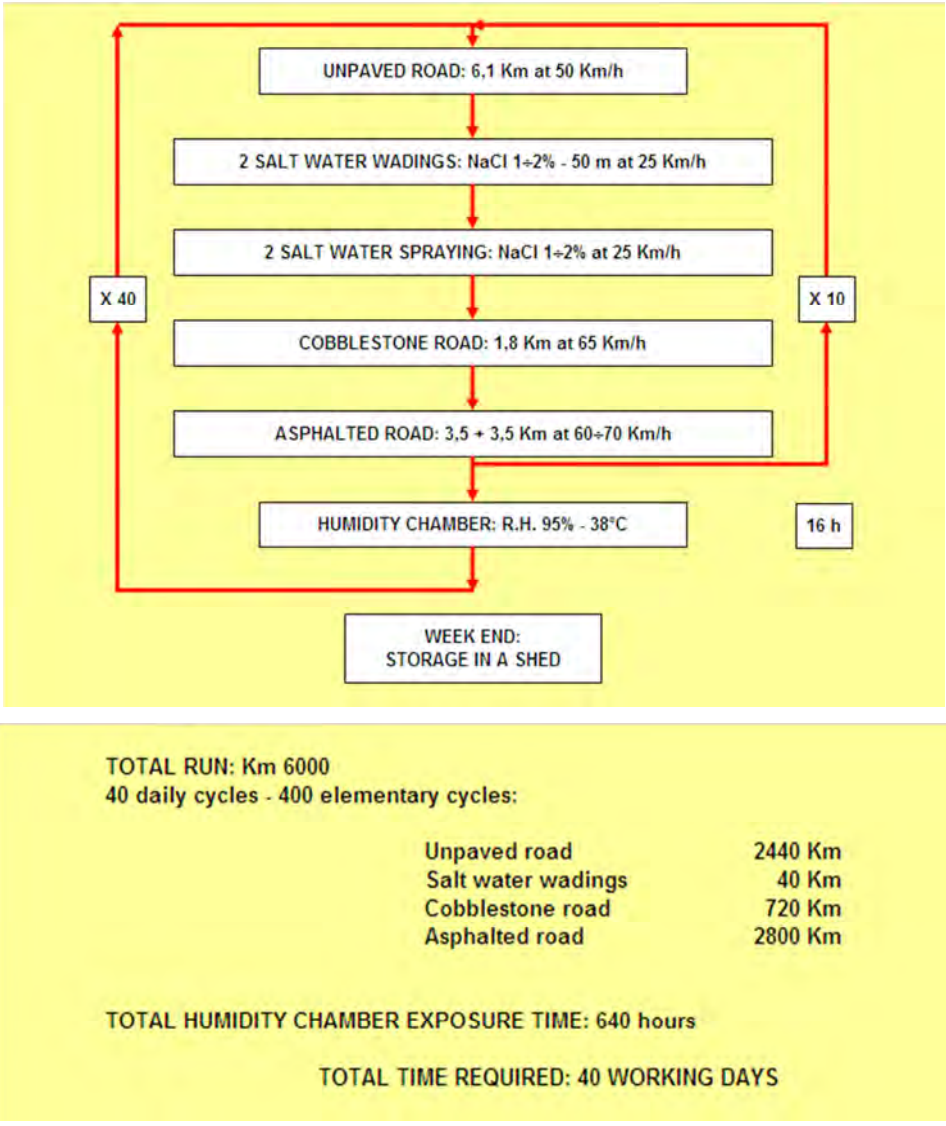

Figure 39: Main characteristics of FIAT proving ground

Table 13: Metal loss on CRS and zinc after Fiat proving ground

	g/m²	µm
CRS	750	95
Zinc	119	16

It should be mentioned that a first trial was conducted in June 2011 and a second one had to be performed in 2012 because of some technical problems in the first trials (all hem-flanges samples were broken and some samples were lost). Thus, new hem-flanges samples with a metallic cover panels had to be prepared using GI, ZMA1 and ZMA2 coated steel only. All the samples were carefully fixed on a 1x1 m² plexiglass panel in such a way that the replicates were distributed along the vertical side, see on Figure 40. This frame was positioned at an angle of about 25° to the vertical on a truck platform (see on Figure 40).

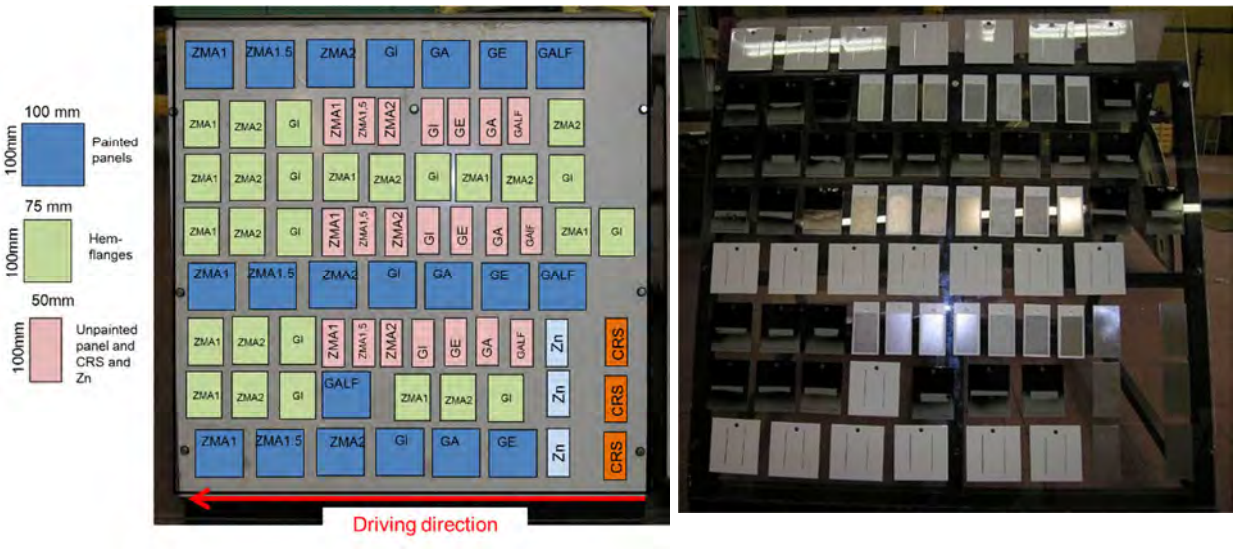

Figure 40: Position of the samples on the plexiglass located on the lateral side of a truck platform (scheme and photos).

2.3.4.2.2 Results

For cosmetic samples exposed on operating vehicles, two conditions of tests were carried out resulting in two different results which are presented in Figure 41. The exposure under a trailer of a truck driving in Zürich area in Switzerland induced rather low corrosion damage as the scribe creep was globally around 0.5 mm or less (see Figure 41b), thus in the range of what was measured in Dortmund area. In such situations, no difference was observed upon novel and conventional zinc coating.

On the contrary, significant differences were observed when the cosmetic samples were exposed in a proving ground test. As shown in Figure 41a, ZMA coating presented twice less scribe creep than conventional coatings. Such results are typical of tests involving significant salt load and wetness such as in the VDA test (see WP 6). In the FIAT proving ground described in Figure 39, the vehicle is operating on various types of road and indeed exposed to salt solution (e.g. salt wading and salt spray) and climatic conditions at regular intervals. In such aggressive conditions on operating vehicle, ZMA coatings showed undoubtedly better performance than conventional zinc coatings. One should also point out the significant deviation of the results which were explained by the position of the samples along the vertical side.

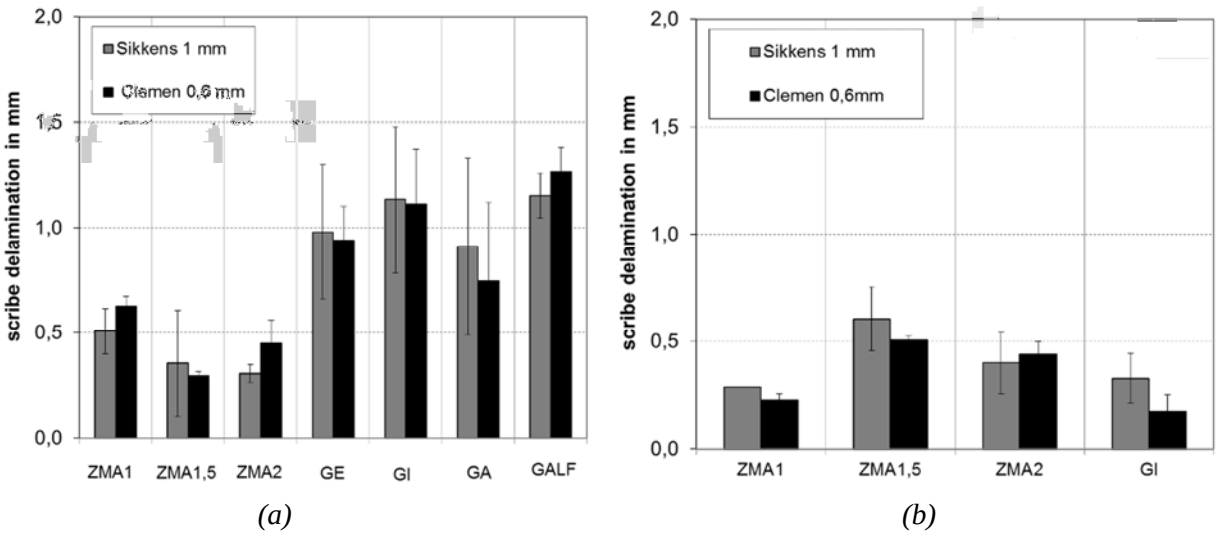

Figure 41: Mean delamination from scribe after 40 days of Fiat proving ground test (a) and 24 months of exposure under truck driving in Switzerland (b).

The results obtained after 12 and 24 months of exposure on **real mobile situation** e.g. under the truck driving in Switzerland are plotted in Figure 42 for open and confined situations. As indicated in the experimental section, only four coatings including the three ZMA and GI ones were exposed due to space restrictions. In agreement with data observed on stationary field sites, confined situations induced significantly more corrosion than openly exposed surfaces. Red rust was indeed observed on GI coatings after 1 and 2 years with 40 to 60% but also on some of ZMA1 replicates upon their locations under the trailer (distance to the wheels), which explains the large deviation on the metal loss. Note that when red rust is formed, it is not possible to estimate the metal loss of the coating by pickling/gravimetric technique, thus full consumption of the coating is plotted, even if the corrosion is generally localized. The deepest corrosion attack in steel was found in GI coated steel. No red rust was however observed on ZMA1.5 and ZMA2 which both showed better performance than GI. The results also indicated no major increase of the corrosion between 1 and 2 years, which may appear somehow surprising. When such geometry of samples are exposed to road conditions, obstruction of the confinement with road mud often occurs obviously influencing the corrosion rate and inducing deviations in the results upon the samples/location. This is probably why no major changes were obtained between 1 and 2 years. More replicates should probably have been exposed in order to get more statistically data.

When considering openly exposed surfaces on Figure 42a, the corrosion has significantly increased with exposure duration and there are no doubts on the better performance of ZMA coatings compared to GI one, as it has been observed also in field stations (see Figure 36). It is interesting to note that the improvement of ZMA coating decreased significantly from approximately 6 to 2.5-3 when doubling the exposure duration. The same trend was also noticed after exposure in stationary sites, reminding that the improvement coefficient was lower e.g. below or equal to 2 approximately. As it has been shown in WP 6 (accelerated corrosion testing) which results were reported in deliverable 10, the improvement factor of ZMA versus GI coating seemed to be linked to the salt load: the more salt load, the more improvement of ZMA versus GI coatings. Whereas it has not been measured, it is very likely that the amount of salt (from de-icing salt) accumulated on mobile exposure is more important than on the stationary field sites where the samples are also regularly washed with rain leaching aggressive species, which is not true under the trailer. It would thus be interesting to evaluate the behavior of such material on longer exposure duration in order to verify how the ZMA improvement coefficient evolves.

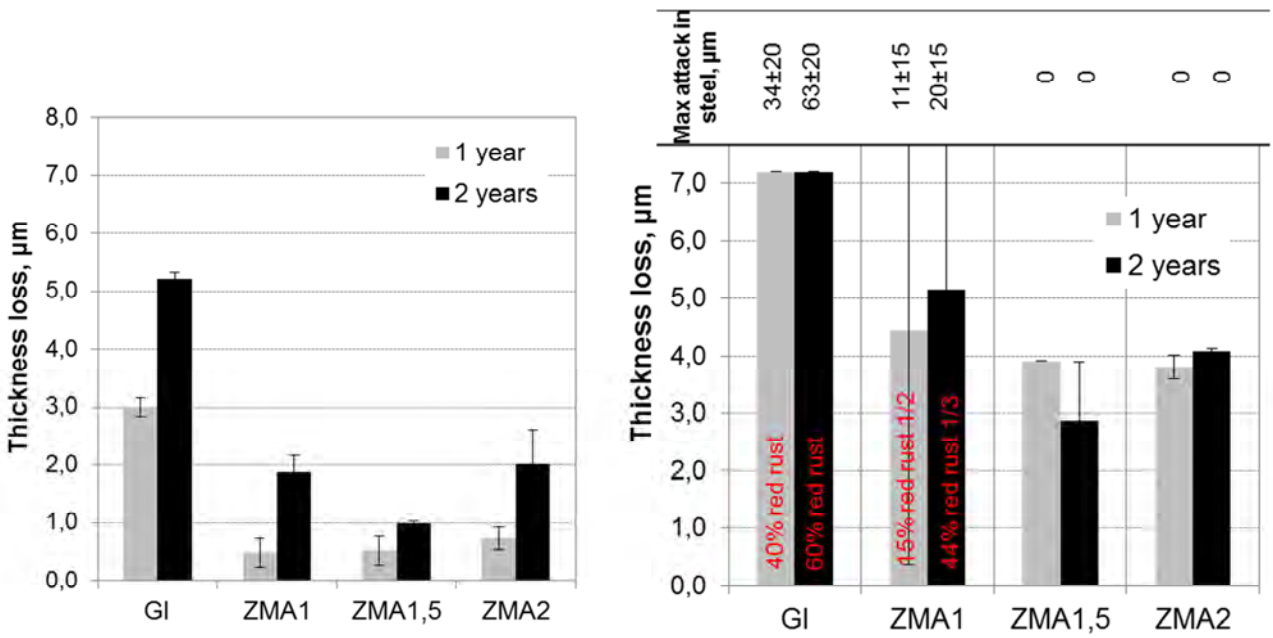

(a) *(b)*

Figure 42: Metal loss of metallic coating in open configurations (a) and hem-flanges (b) after 12 and 24 months of outdoor exposure under the truck driving in Switzerland. The maximal depth of corrosion in steel is also given for samples red rust.

When ZMA coatings are exposed to **Fiat proving ground test** in open configuration, they also showed better performance compared to conventional coatings as can be seen in Figure 43 which presents the mean metal loss together with the extent of red rust. As indicated previously, when red rust covered more than 5 % of the surface, the thickness loss was plotted equal to the thickness of the metallic coating and the deepest attack in steel was indicated, which was the case of GE, GI, GA and Galfan coatings. It can be noticed that less red rust was yet observed on Galfan coating than on the other conventional coatings while none of ZMA ones were affected. The corrosion in steel was also less deep on Galfan coatings than on GI, GE or GA ones.

Large deviations were also obtained on ZMA metal loss. This was clearly attributed to the position of the samples as exemplified on Figure 44 which presents the metal loss of each replicate as a function of its position to the truck platform. Indeed, more corrosion was developed on replicates located on the top of the frame. In Fiat proving ground, the vehicle drives in salt water wading (15 cm) which cannot splashed on the samples in such position. However, the vehicle is also spayed with salt solutions from top sides which would explain such position dependency of the results. One should thus consider the results as a general trend as regards to the position dependency.

It is likely that different results would have been obtained if the samples were exposed under the vehicle due to salt splashing when driving in salt pools.

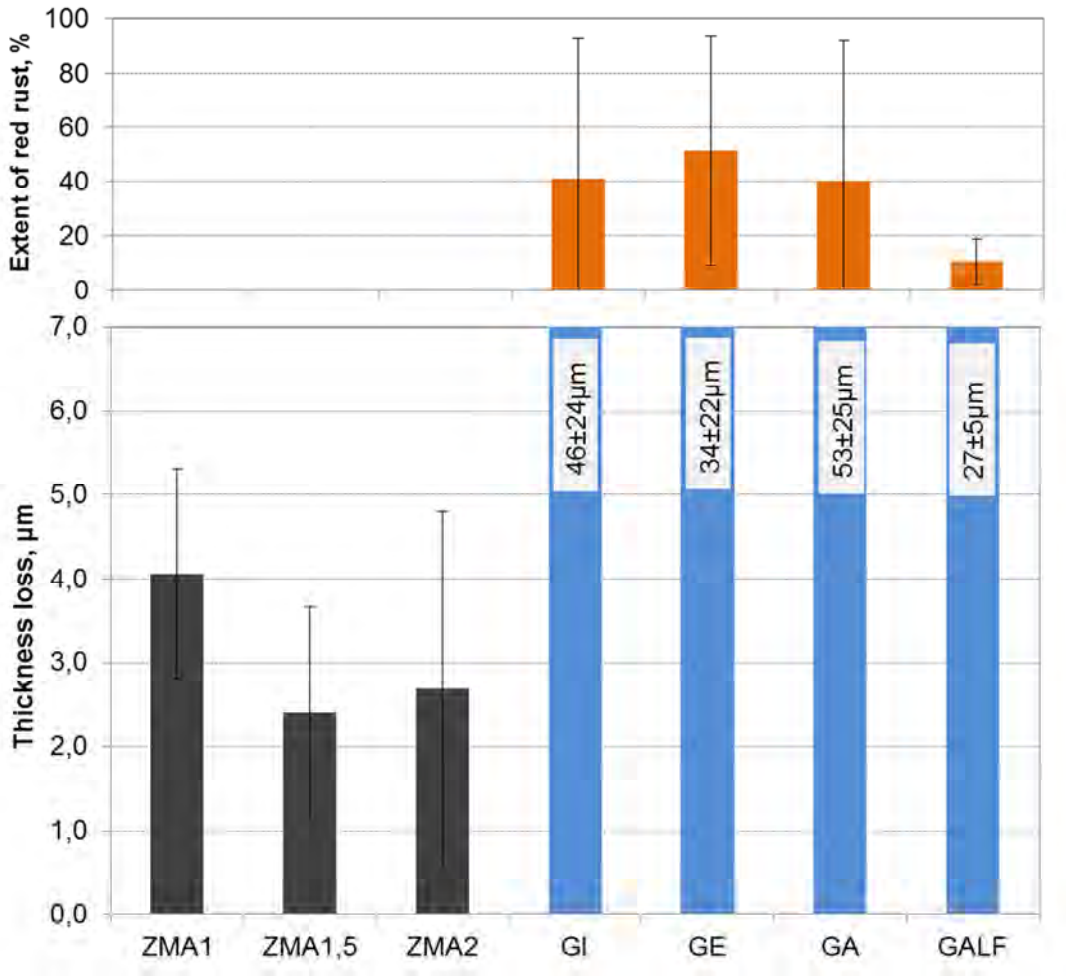

Figure 43: Extent of red rust (top) and metal loss of metallic coating in open configurations after Fiat proving ground. The maximal depth of corrosion in steel is also given on the bar (bottom).

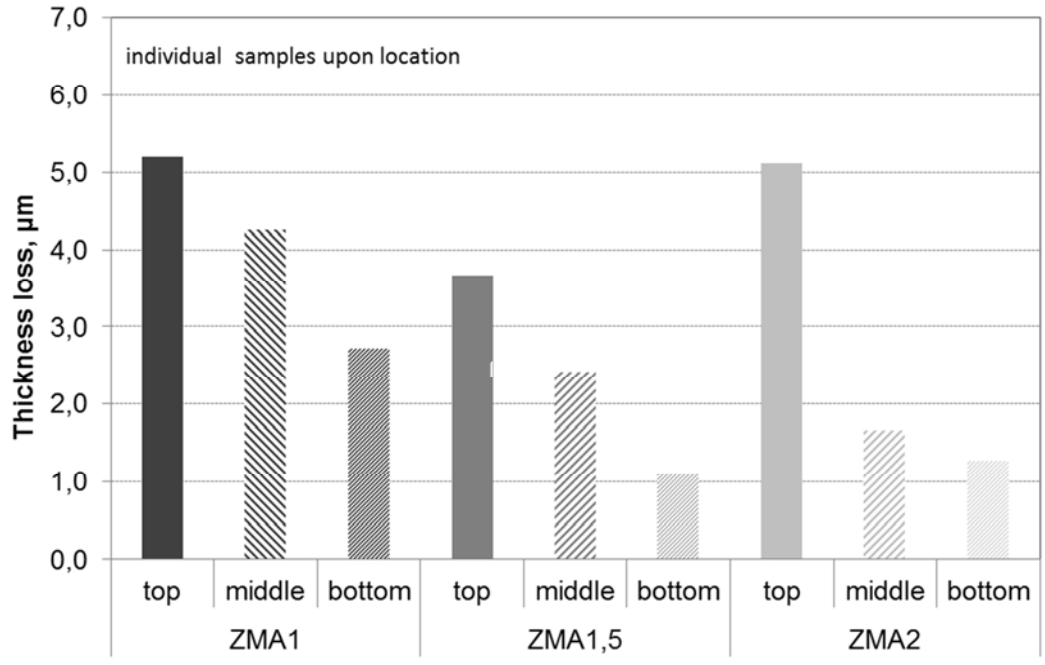

Figure 44: Metal loss of individual ZMA coated samples in open configurations as a function of exposure location after Fiat proving ground.

The results obtained in confined situations seem very much confusing as shown on Figure 45 which gives the metal loss of individual samples and corresponding extent of red rust for ZMA1, ZMA2 and GI coatings. But the spreading of the metal loss becomes comprehensible considering that the salt spray is more concentrated at the top than at the bottom. 9 replicates of each coating were exposed at different locations on the frame (see Figure 40). Indeed, red rust was formed on all coatings at different degree on some of the replicates as indicated in Figure 45 (top). In general, ZMA1 were the most affected coatings showing red rust up to 35% on 6/9 of the samples corresponding to 35 µm of maximal attack in steel substrate. ZMA2 samples were less affected by red rust (3/9) and the corrosion attack in steel was between 15 and 27 µm.. More than 50% of GI coatings presented red rust estimated at a moderate level of 5 to 15%. The depth of corrosion in steel was however scattered ranging from 30 to 100 µm.
Giving a mean value of the metal loss would imply an important deviation for all coatings. It is thus impossible to draw any clear trend on the basis of such results which probably demonstrate that ZMA coatings do not provide any improvement compared to GI in confined situations as it has been observed on samples exposed in stationary field stations and also in accelerated corrosion tests (see WP 6). It is clear that confined surfaces are under different conditions compared to open surfaces with different rate of drying and wetting, transportation of reactants which would determine the corrosion rate generally enhancing it in a more localized way. In such situations, much more alkaline conditions are obtained subverting the formation of stable zinc corrosion products whatever it concerns conventional zinc coating or novel Zn-Mg-Al coatings.

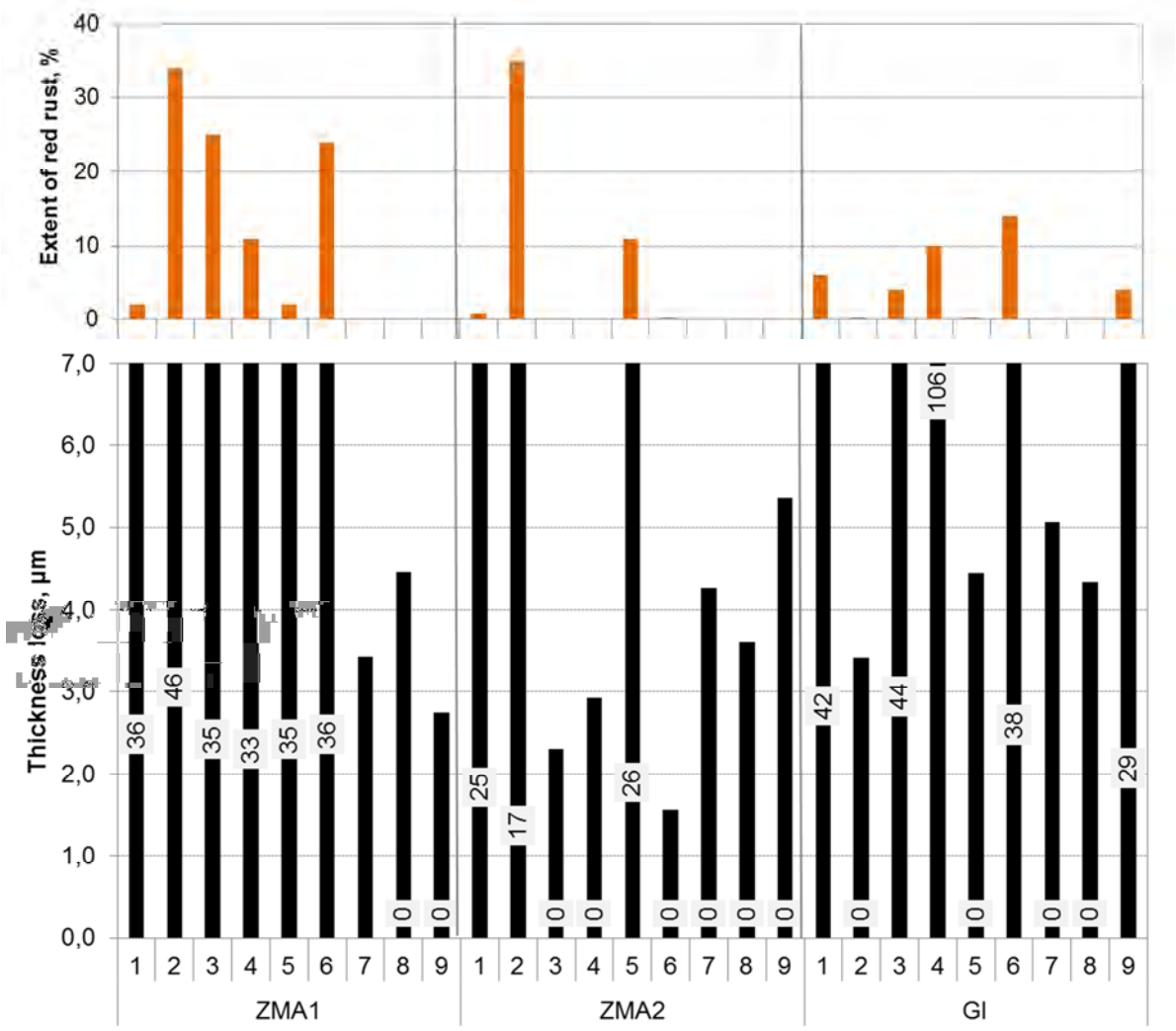

Figure 45: Extent of red rust (top) and metal loss (bottom) of individual ZMA and GI coated samples in hem-flange configurations as a function after Fiat proving ground. The maximal depth of corrosion in steel is also given on the black bar (bottom).

2.3.5 **WP5 Application properties**

The main objective of WP5 was to obtain evidence that ZnMgAl (ZMA) coatings can be applied in mass automotive production as regards to important properties such as formability and joining.

2.3.5.1 **Task 5.1: Formability**

Formability of coatings was studied in **cross die test** by FIAT and in **Erichsen test** by Ruukki. The surface of formed samples was investigated and photographed under Scanning Electron Microscopy. Formed samples were further tested in accelerated corrosion tests by FIAT (Scab test) and TKSE (New VDA test) in order to evaluate the effect of forming on the corrosion resistance. The results were reported in **deliverable D9**.

2.3.5.1.1 Cross die test

Cross die test parameters were as follow:

- sample size 115x115 mm
- blank holder force 4 tn
- pressure 6 bar
- sample height 18 mm
- no lubrication

Materials tested in cross die test are presented in Table 14.

Table 14: Materials tested in cross die test

Label	**Steel grade/ thickness, mm**	**ZMA metallic coating**	
		Composition	**Thickness, µm**
ZMA1	DX56 / 0.9	Zn1%Mg1%Al	~7.5
ZMA1.5	DX53 / 0.6	Zn1.5%Mg1.5%Al	~11
ZMA2	DX54/ 0.79	Zn2%Mg2%Al	~7.5
Z100 (GI)	DX56/ 0.9	Zn0.2%Al	~7

Photo of cross die sample is presented in Figure 46. Locations of SEM inspection are indicated by arrows i.e. A, B and C.

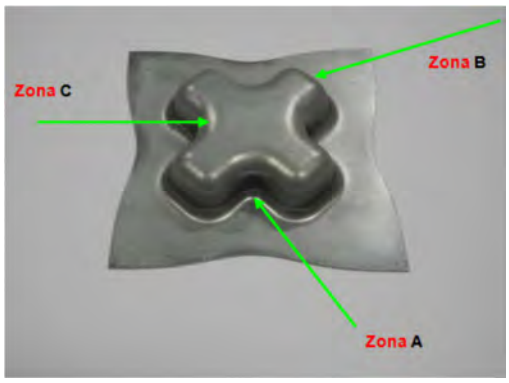

Figure 46: Photograph of the cross die sample and identification of inspected area

2.3.5.1.1.1 SEM inspections of cross die samples

SEM images of sample surface of ZMA1, ZMA2 and ZMA1.5 in these different locations are presented in Figure 47 and 48. Note that ZMA1 coating is compared to conventional HDG.From the SEM images, it is obvious that ZMA coatings cannot resist cracking in severe forming. Especially in the location B, the crack network covers the whole coating and the cracks go through the coating down to the steel. However, delamination or galling of the coating was not observed.

On HDG coating, few cracks could be noticed in location B using higher magnifications but otherwise HDG coating was free of cracks. Delamination of coating was not observed.

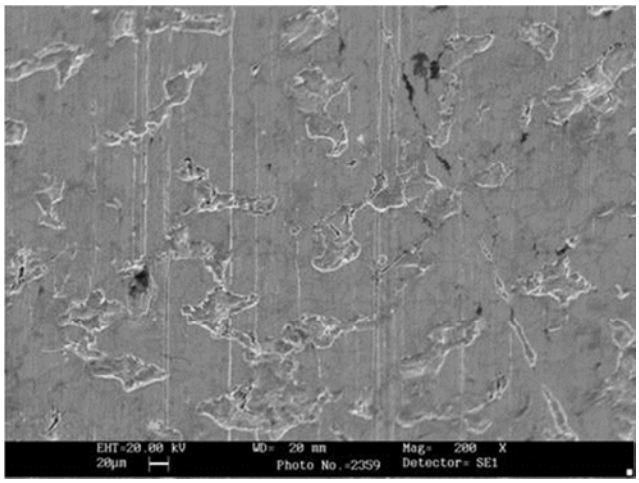

a) ZMA1, location A.

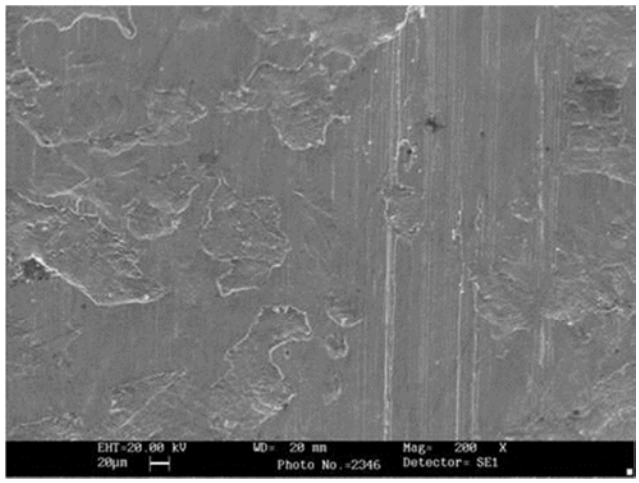

d) Z100MB, location A

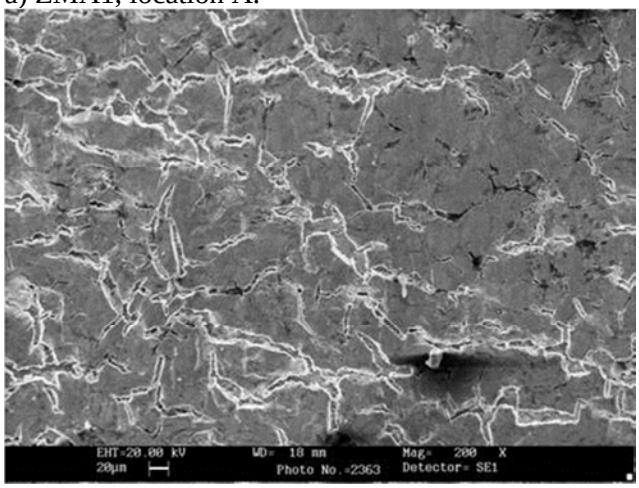

b) ZMA1, location B.

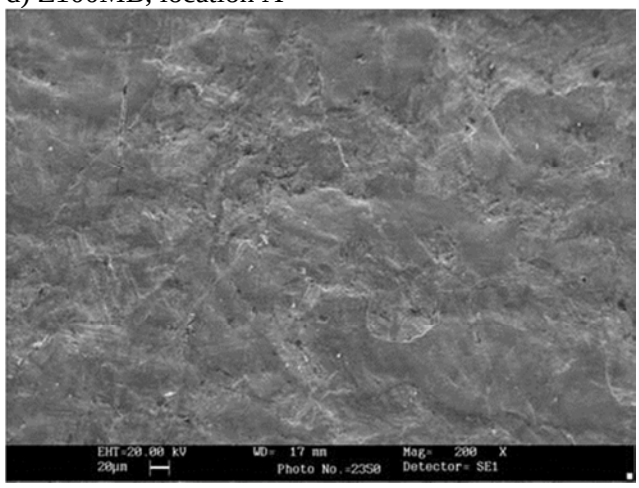

e) Z100MB, location B

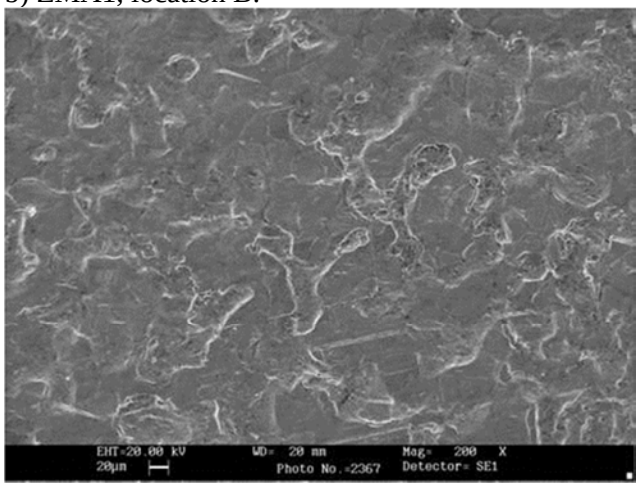

c) ZMA1, location C.

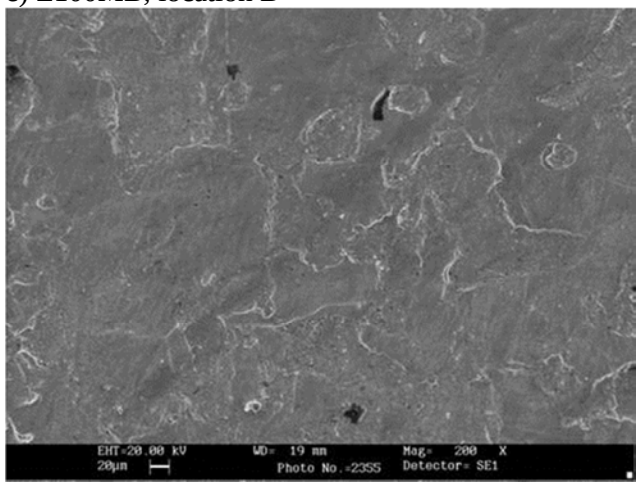

f) Z100MB, location C

Figure 47: SEM images of cross die cup surface of ZMA1 coating (left column) and corresponding HDG reference coating (right). Magnification X200.

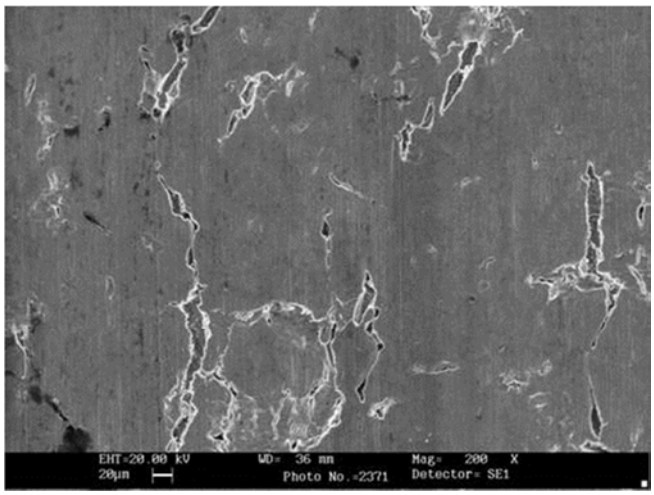

a) ZMA1.5, location A.

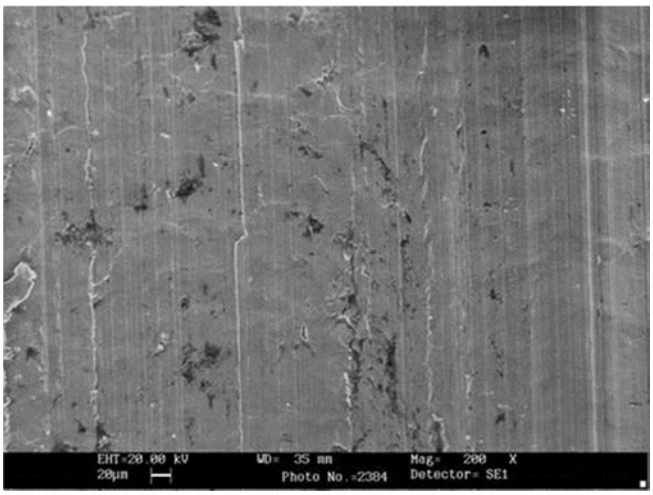

d) ZMA2, location A

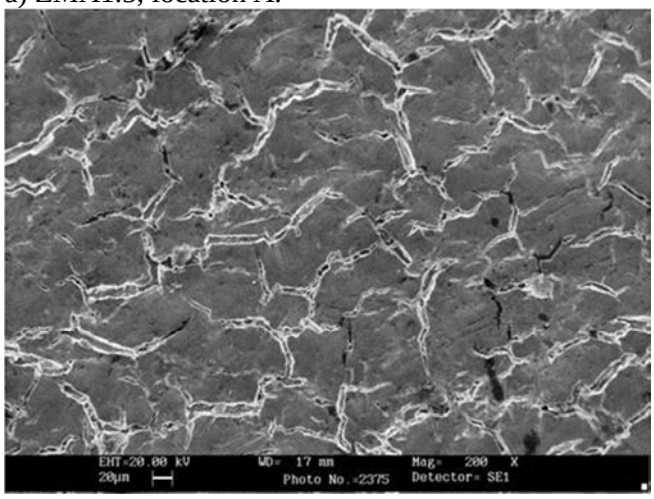

b) ZMA1.5, location B.

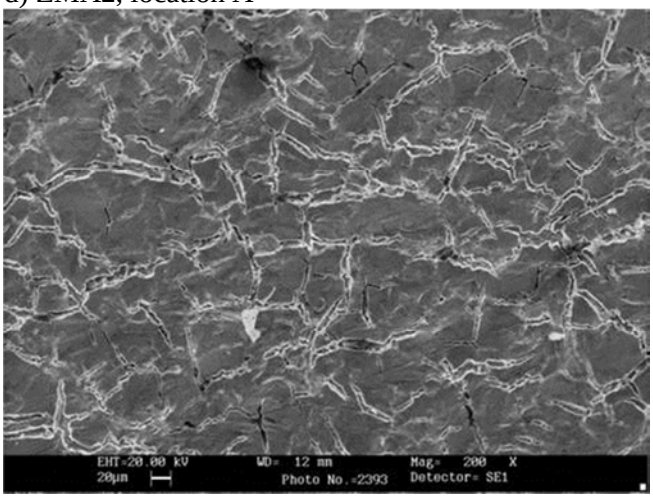

e) ZMA2, location B

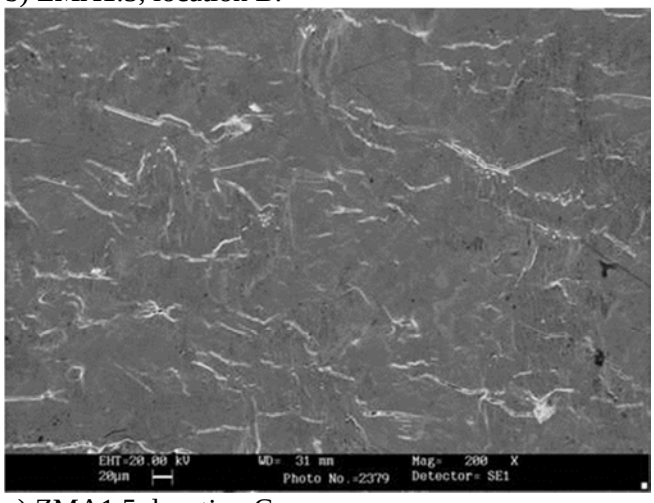

c) ZMA1.5, location C.

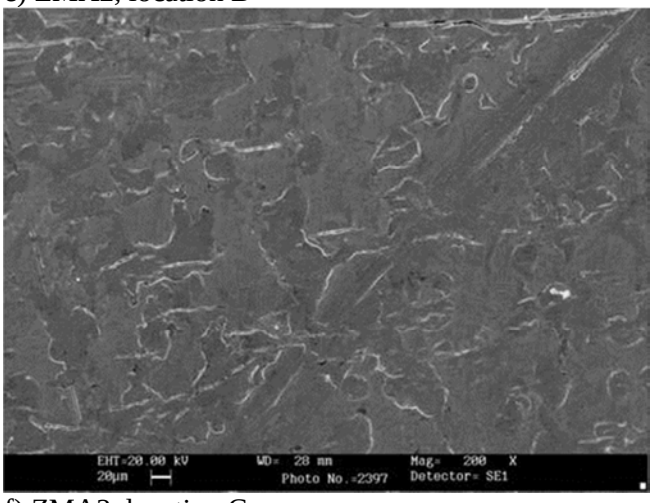

f) ZMA2, location C

Figure 48: SEM images of cross die cup surface of ZMA1.5F (left) and ZMA2 coating (right). Magnification X200.

2.3.5.1.1.2 Corrosion behaviour of cross die cups

In order to check the effect of forming and of the cracking of the coating on the corrosion performance, cross die cups were tested in SCAB indoor corrosion test by FIAT and in N-VDA test by TKSE. The SCAB test consisted of repeated cycles of 20 minutes at 40 ± 2°C and R.H. > 95% + spray of salt solution (NaCl 0,5% - pH = 6 to 6,5) followed by a phase of 30 minutes at 55 ± 2°C (no R.H. control). The test duration was 150 hours. It should be mentioned that this test is systematically performed by Fiat in order to evaluate the corrosion resistance of formed panels. The New VDA test is described in WP 6. 5 replicates of cross die sample per coating were exposed in each test.

The evaluation of samples was done by visual inspection and photographing. Besides, a numeric "corrosion performance index" was evaluated by a method used by FIAT which consisted of measuring the number of squares affected by red rust (see Figure 49). A corrosion index close to 100 indicates a good corrosion performance of the coating.

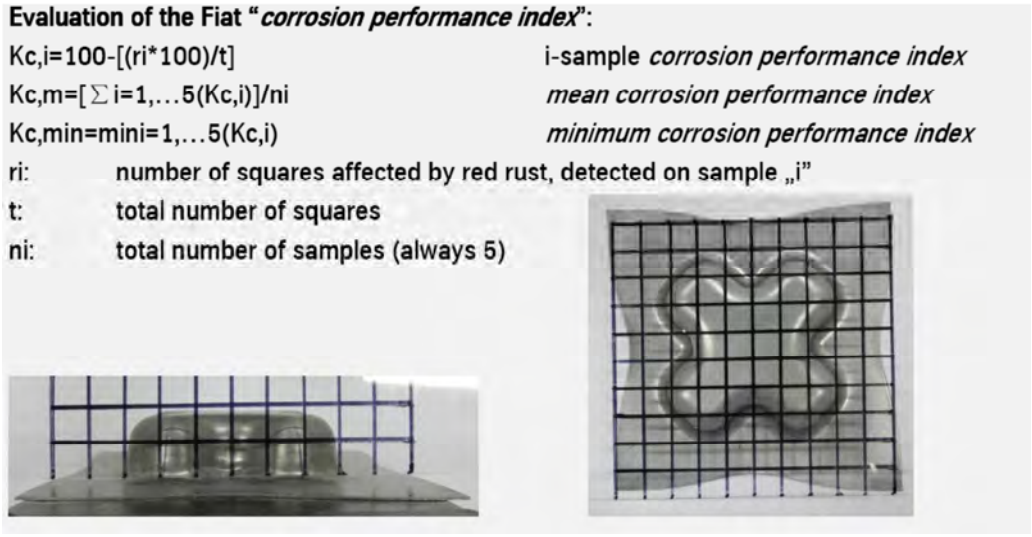

Figure 49: FIAT evaluation method for cross die corrosion samples.

SCAB test results after 150 hours test are presented in Figure 50. Three conclusions can be drawn from the results of SCAB test. Firstly, ZMA1 coating outperforms HDG coating in this test. Secondly, ZMA1.5F coating resisted red rusting best which is naturally due to thicker coating. And finally, cracks in ZMA coating seem not to have an effect on red rust initiation. It is more related to sample position in the chamber and always starts from uppermost corners of the "cross".

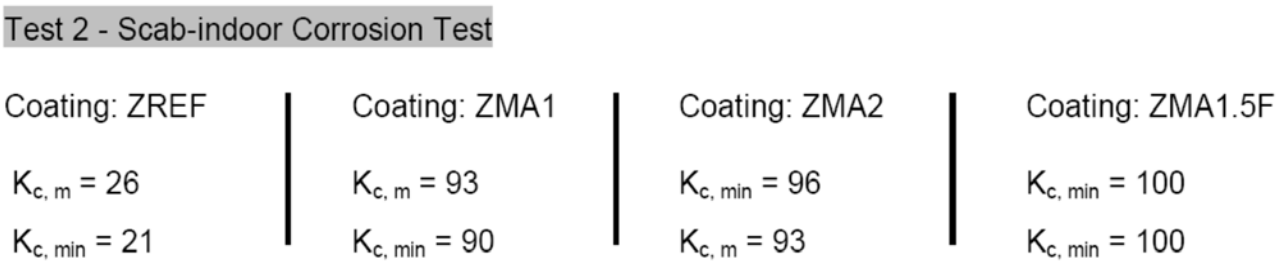

Figure 50: Calculated corrosion index for coatings after SCAB test.

Figure 51 presents the corrosion index results plotted as a function of exposure duration in new VDA test.

While no obvious difference was noticeable after 1 cycle (e.g. 1 week), ZMA coatings were superior to HDG one (Z100) after longer exposure durations. Among ZMA coatings, ZMA1.5 was performing best because of the larger coating thickness e.g. 11.6 µm against 7.2 µm for ZMA1 and 7.8 µm for ZMA2. The coating thickness difference between ZMA1 and ZMA2 is approximately 8 % and the corresponding difference in corrosion index was about 7 % after 2 cycles, 14 % after 3 cycles and 28% after 4 cycles. Therefore, the difference in coating thickness can explain the difference in corrosion performance only after two cycles but not beyond that because red rust propagation is faster on ZMA1 coating.
Cracking of the coating does not seem to have a noticeable effect on the corrosion initiation and propagation. Red rusting always starts from the upper corner of the cross die cup on both ZMA and HDG coating, not depending on the coating cracking but depending on sample geometry.

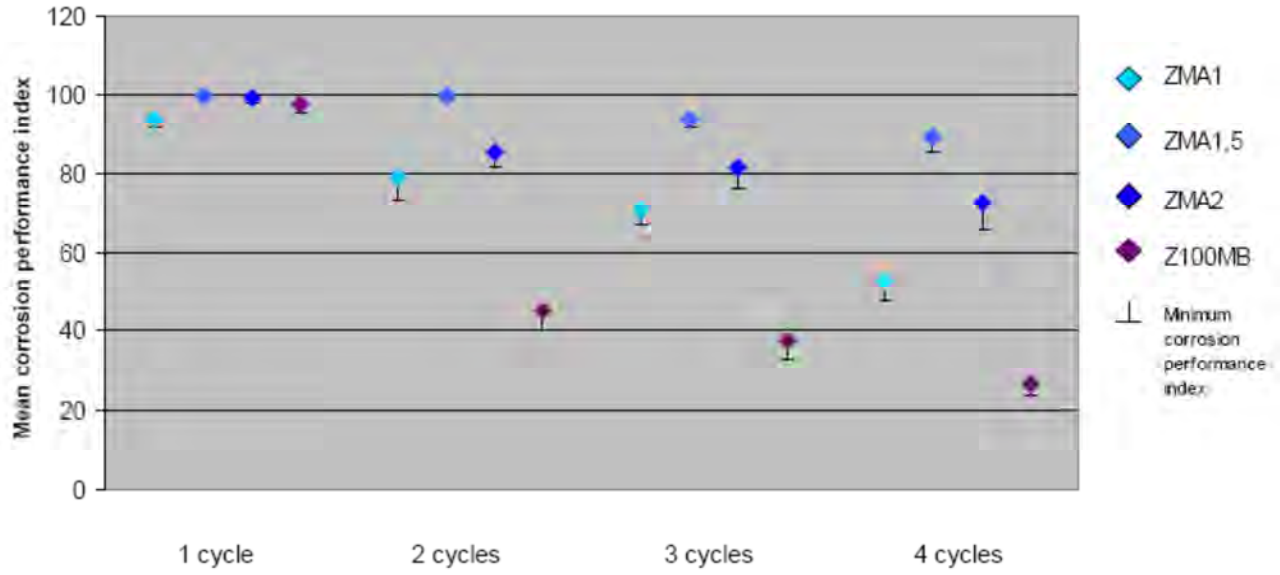

Figure 51: Fiat corrosion indexes after each cycle (= week) in new VDA test.

2.3.5.1.2 Erichsen cup test

Erichsen 142-40 Sheet Metal Testing Machine was also used to evaluate the formability of ZMA coatings. The side of samples was lubricated with Divinol 85000 lithium based grease. The diameter of the press was 10 mm, blank holder force 10 kN and drawing speed 20 mm/min. First, the maximum cup height (i.e. steel rupture) as an average of three draws was measured. However, due to the different steel grades and thicknesses, the maximum cup height was different for each material. Therefore, in order to ensure the comparability, it was decided to use the lowest measured value as the maximum for all materials. The lowest value 8.6 mm was measured for ZMA1.5F (DX53, 0.6 mm). From this value, 25, 50 and 75% was calculated and cups with height of 2.2, 4.3 and 6.5 mm were prepared for all materials.
Table 15 presents the characteristics of materials tested using Erichsen equipment. As indicated in the table, for each ZMA coating, its corresponding reference with HDG coating was tested.

Table 15: description of materials used for formability using Erichsen equipment

ZMA coating				**Corresponding reference with HDG coating**		
Label	**Steel grade/ thickness, mm**	**ZMA metallic coating**		**Label**	**Steel grade/ thickness, mm**	**Thickness of Zn coating, µm**
		Composition	**Thickness, µm**			
ZMA1	DX56 / 0.9	Zn1%Mg1%Al	~7.5	ZMA1ref	DX56 / 0.9	~7.5
ZMA1.5	DX53 / 0.6	Zn1.5%Mg1.5%Al	~11	ZMA1.5ref	DX53 / 0.6	~11

ZMA2	DX54/ 0.79	Zn2%Mg2%Al	~7.5	ZMAref	DX54 / 0.76	~7.5

The coating surface was photographed under SEM on the location of highest deformation shown by an arrow in Figure 52.

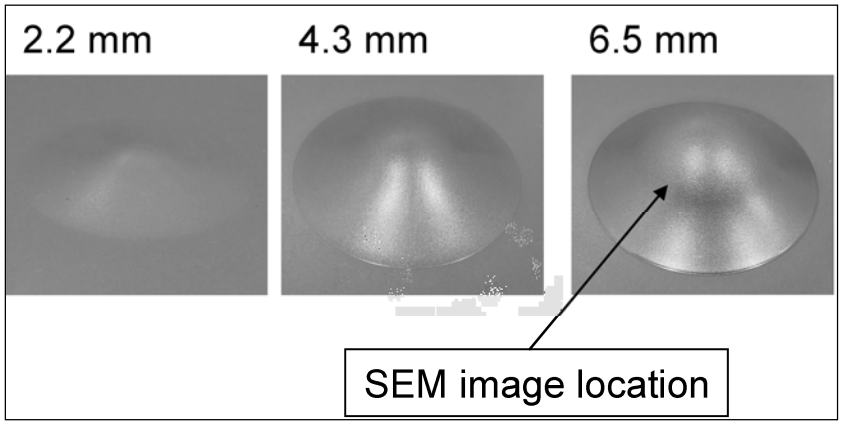

Figure 52: Erichsen cups prepared for materials.

2.3.5.1.2.1 SEM inspections of Erichsen cups

SEM images of the different coatings upon cup height are presented in Figure 53 to Figure 55 for ZMA1, ZMA1.5 and ZMA2 respectively. For each coating, its corresponding galvanized reference is presented as well.

From the surface images, it is clear that ZMA coatings are more prone to cracking compared to HDG coating. Difference can be seen best in 6.5 mm cups where there is a network of cracks covering the whole surface on ZMA coatings but only few unconnected cracks are visible on HDG coatings. Also relatively low deformation of substrate steel initiates cracks on ZMA coating as can be seen on 2.2 mm cups. Cracks seem to be wider on ZMA1.5 coating which can be explained by thicker coating 11.6 um versus 7-8 um on ZMA1 and ZMA2. No delamination or powdering of coating was observed.

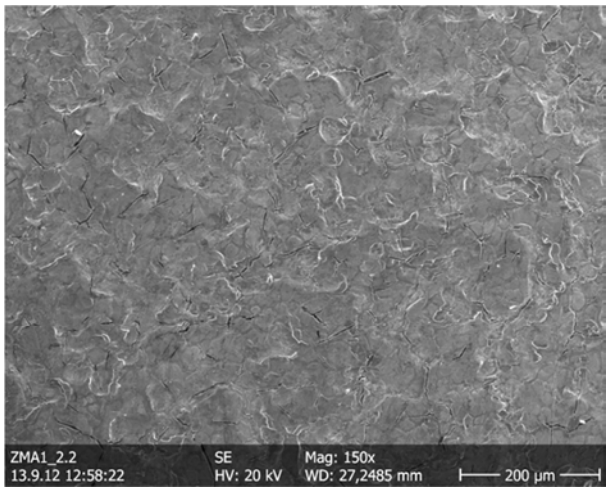

a) ZMA1, cup 2.2 mm.

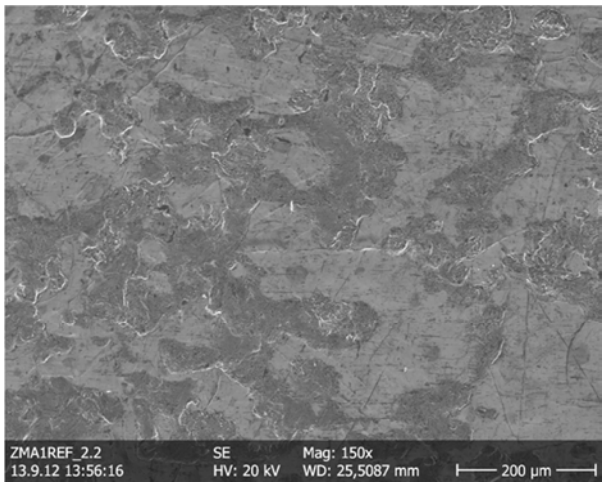

d) ZMA1ref, cup 2.2 mm.

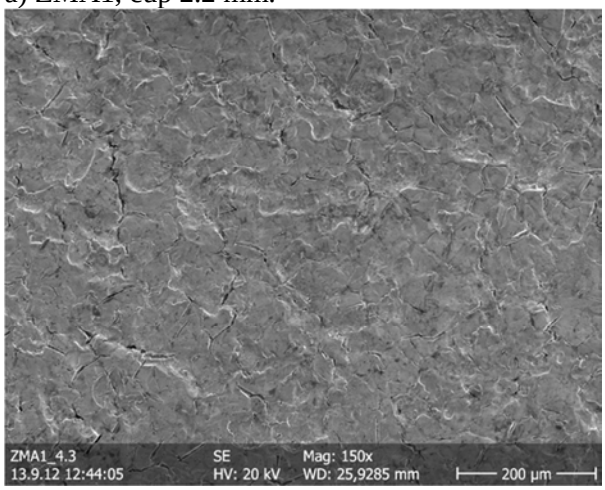

b) ZMA1, cup 4.3 mm.

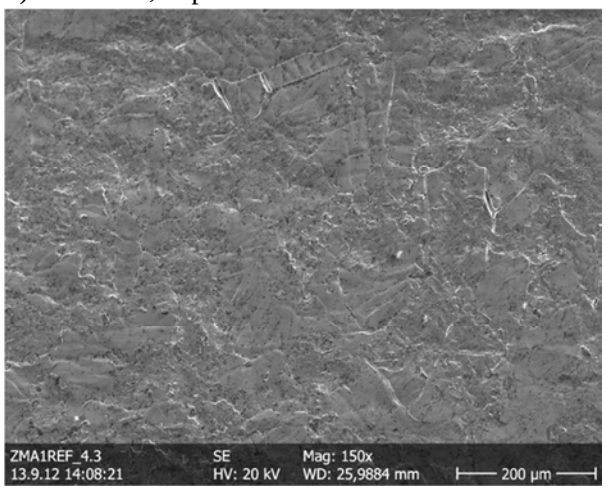

e) ZMA1ref, cup 4.3 mm.

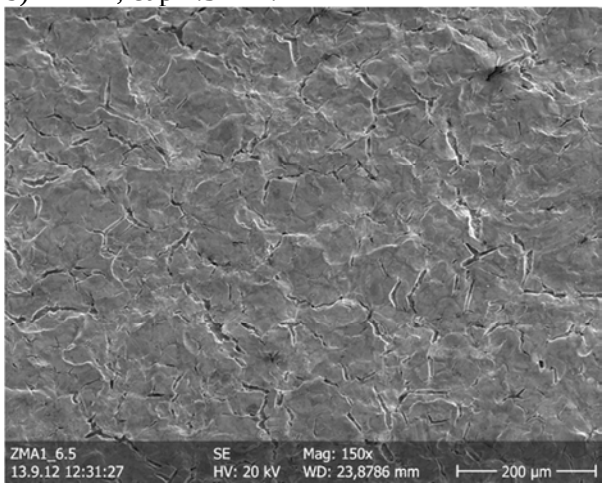

c) ZMA1, cup 6.5 mm.

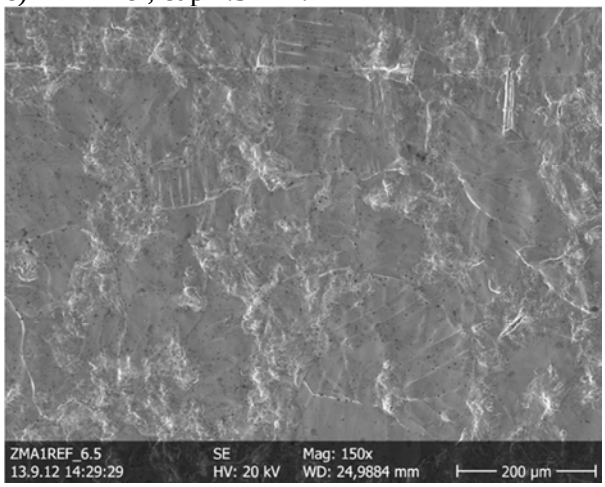

f) ZMA1ref, cup 6.5 mm.

Figure 53: SEM images of cup surfaces of ZMA1 coating (left column) and corresponding HDG references (right). Magnification X150.

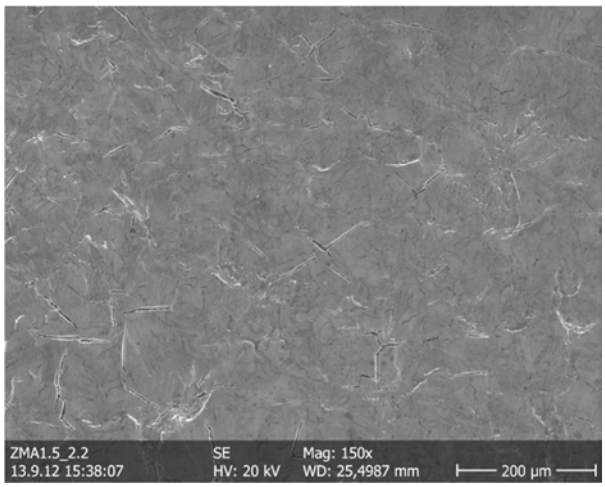

a) ZMA1.5F, cup 2.2 mm.

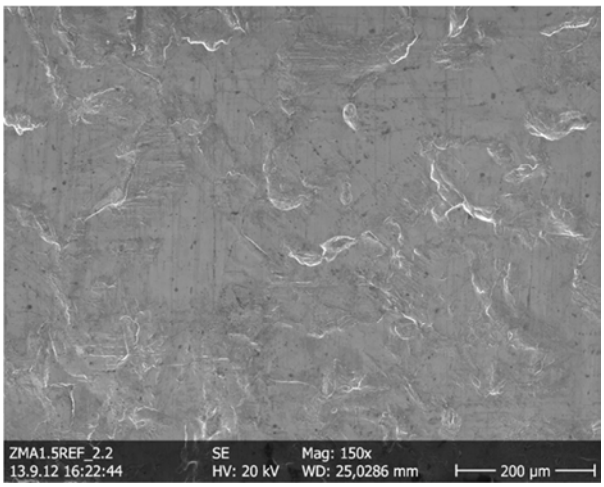

d) ZMA1.5Fref, cup 2.2 mm.

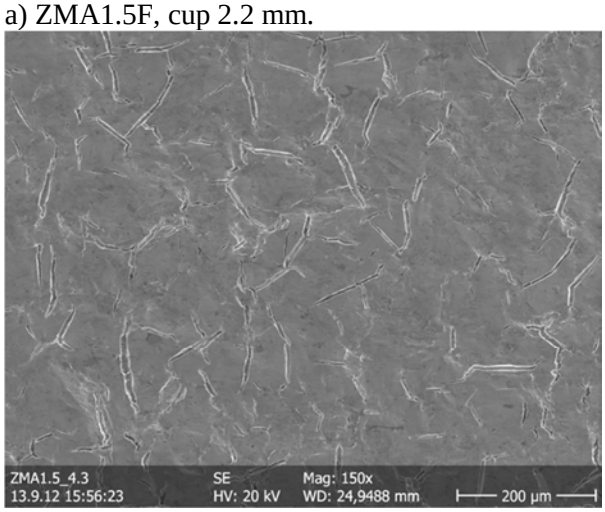

b) ZMA1.5F, cup 4.3 mm.

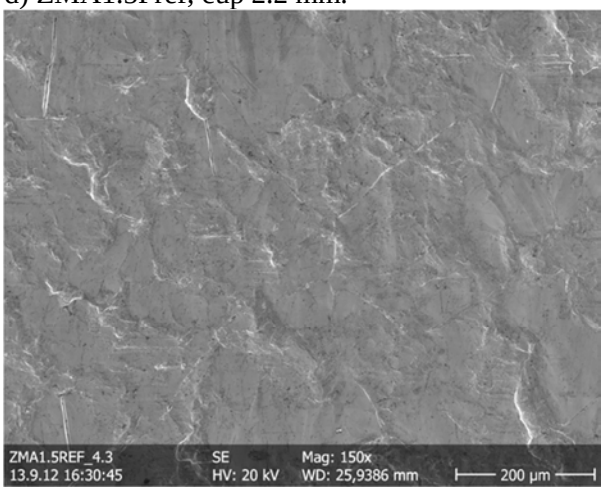

e) ZMA1.5Fref, cup 4.3 mm.

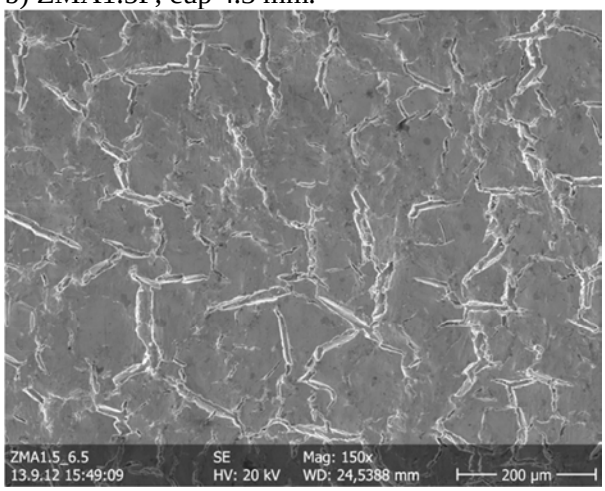

c) ZMA1.5F, cup 6.5 mm.

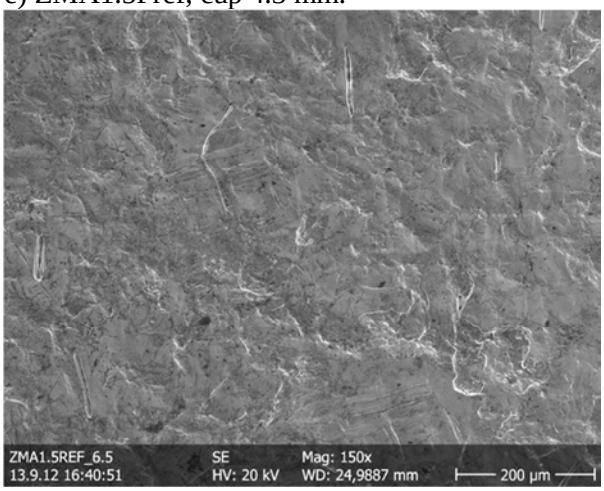

f) ZMA1.5Fref, cup 6.5 mm.

Figure 54: SEM images of cup surfaces of ZMA1.5F coating (left) and corresponding HDG references (right). Magnification X150.

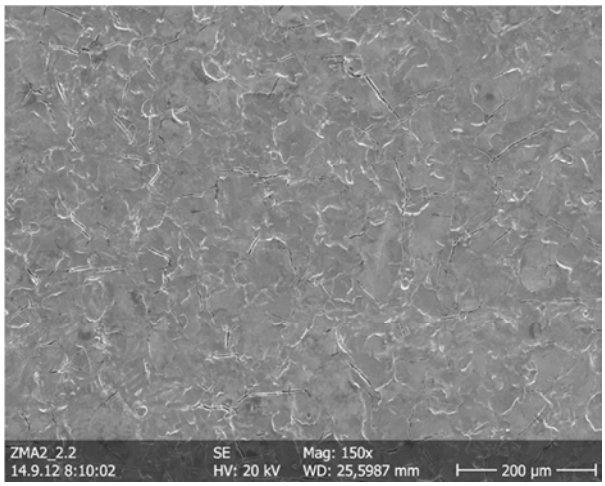

a) ZMA2, cup 2.2 mm.

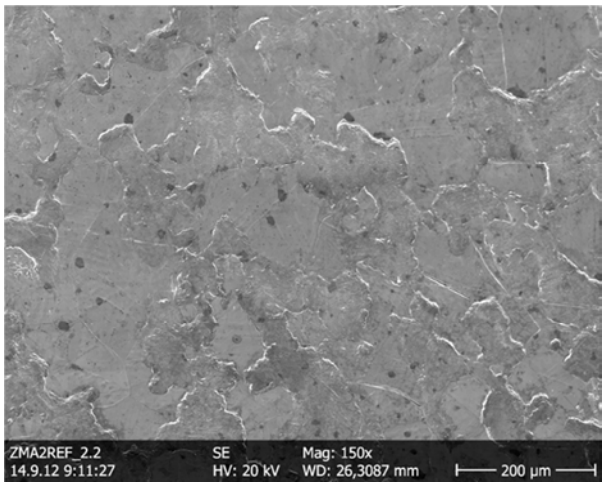

d) ZMA2ref, cup 2.2 mm.

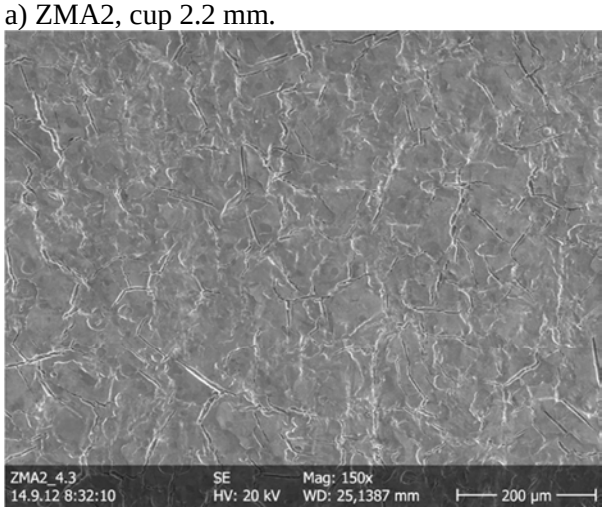

b) ZMA2, cup 4.3 mm.

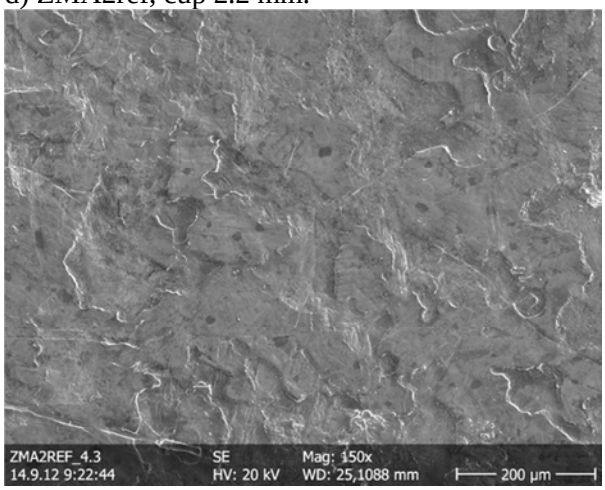

e) ZMA2ref, cup 4.3 mm.

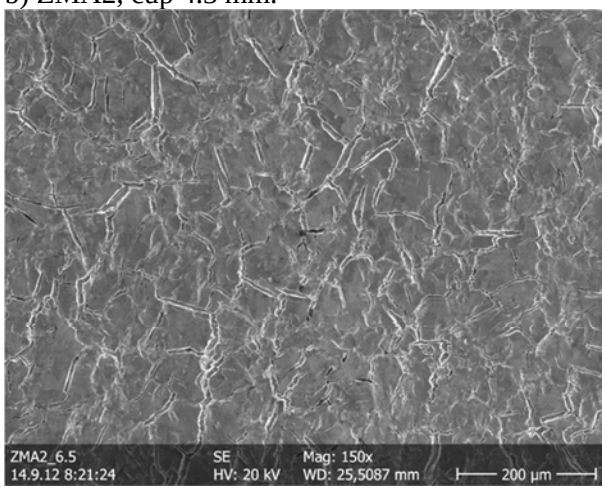

c) ZMA2, cup 6.5 mm.

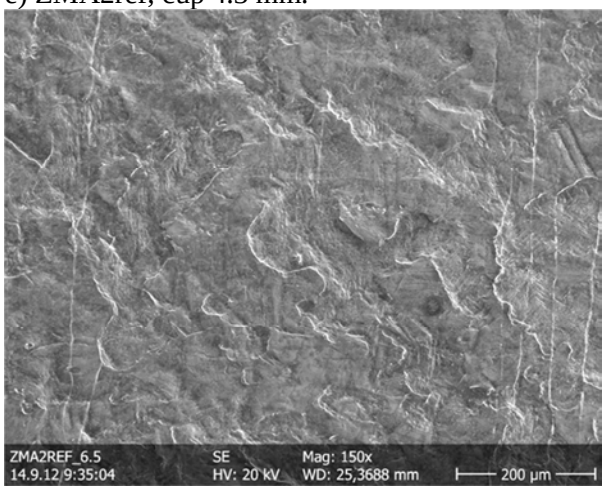

f) ZMA2ref, cup 6.5 mm.

Figure 55: SEM images of sample surfaces of ZMA2 coating (left) and corresponding HDG references (right). Magnification X150.

2.3.5.1.3 Corrosion behaviour of Erichsen cups

Erichsen cups were tested in the new VDA corrosion test by TKSE in order to check the effect of cracking on the corrosion resistance. All three line materials ZMA1, ZMA1.5F and ZMA2 with corresponding HDG references namely ZMA1ref, ZMA1.5Fref and ZMA2ref were tested. The samples were inspected once a week.
The results are presented in Figure 56 as regards to time to red rust for the different ZMA coatings and cup dimensions. Photos of the samples after 4 weeks of exposure are presented in Figure 93 to Figure 95 of appendix 2.

HDG reference coatings were already totally covered by red rust when ZMA coatings started to show the first red rust. The best performing coating was ZMA1.5 which can be explained by the highest coating thickness e.g. 11.6 µm. The measured coating thickness of ZMA1 and ZMA2 were 7.2 um and 7.8 um correspondingly. ZMA2 showed better red rust resistance compared to that of ZMA1 which is probably because of both thicker coating and richer alloying composition. For an unknown reason, HDG reference of ZMA1 2.2 mm cup sample was behaving differently and its resistance to red rust was even better than that of ZMA1.
On ZMA coatings, the first red rust was always observed on flat surfaces instead of cup area where coating was yet cracked. No explanation could however been given. It is likely that deeper investigations should have been done such as by SEM in order to visualize the coating aspect upon exposure. Based on this observation, it is obvious that forming does not increase the corrosion risk on formed parts. There seems to be a cup geometry related effect on red rust propagation analogically to cross die corrosion samples.

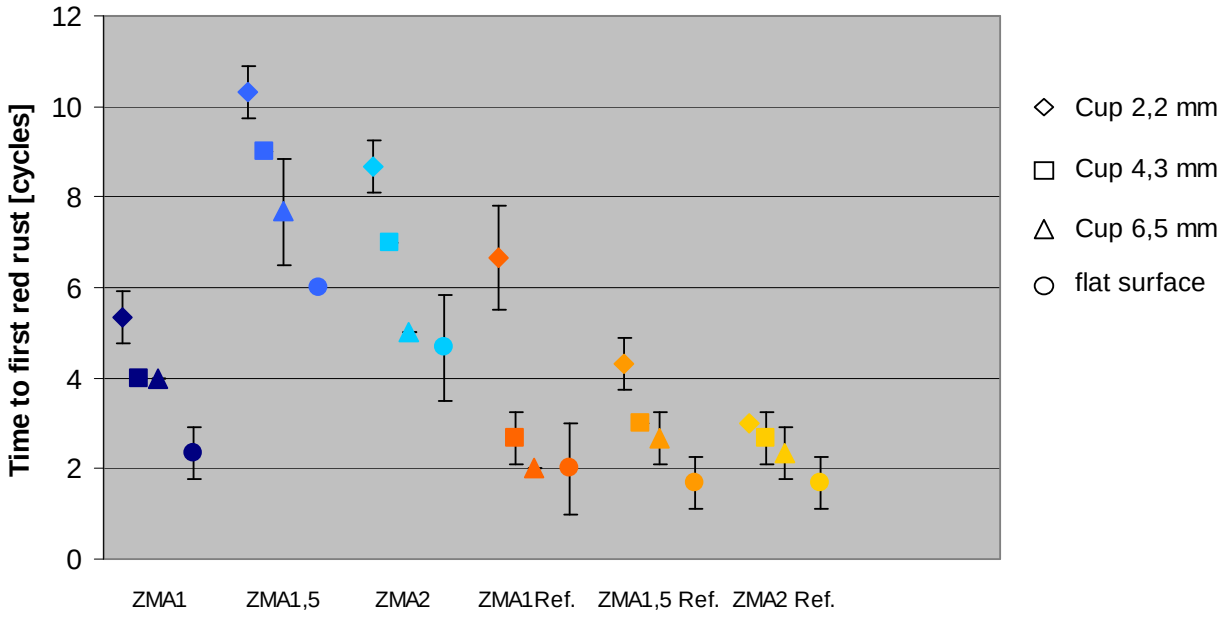

Figure 56*:* Time to red rust of ZMA and corresponding HDG reference coatings in new VDA test. Influence of cup height. ZMAx Ref corresponds to HDG coated steel (same grade and thickness of steel as ZMAx coating, x = 1; 1.5; 2)

2.3.5.1.4 Coating friction coefficient

Coating friction properties were evaluated in high frequency linear oscillation test (SRV=Schwingungs Reibverschleiss) at TKSE. German standard DIN51834 gives the general principles of the SRV test but the actual test parametres were internally selected by TKSE. A stainless steel ball with diameter of 10 mm was used as a counterpart and samples were lubricated with automotive prelube oil Fuchs Anticorit PL3802-39-S. Friction coefficients measured for the materials are summarized in Table 16. More details may be found in **deliverable D9**.

From Table 16, it can be seen that as a rule, friction coefficient decreased linearly with sliding speed in all coating groups. There was no correlation between Rhesca coating nor line ZMA coating composition and friction coefficient. Generally, ZMA line coatings seem to have slightly lower friction coefficient (0.123) compared to that of line HDG coatings (0.135) but on the other hand, ZMAR Rhesca coatings gave the highest value (0.148). Therefore, it was assumed that the differences in friction coefficient between HDG coatings and ZMA coatings probably arise from other parameters such as surface roughness rather than coating type. Rhesca coatings were not skin passed while all the other coatings were skin passed in galvanising lines at Ruukki, TKSE and voestalpine.

Table 16: Summary of SRV test results for Rhesca (ZMAR), line hot dip ZMA and corresponding HDG reference (ZMAxRef) and Galfan

Hz	(m/s)	ZMAR0.5	ZMAR1	ZMAR2	ZMAR2/1	ZMAR3	ZMAR4	Average
10	0.02	0.173	0.179	0.138	0.247	0.163	0.197	**0.183**
20	0.04	0.148	0.162	0.130	0.188	0.137	0.146	**0.152**
30	0.06	0.162	0.163	0.116	0.154	0.121	0.156	**0.145**
40	0.08	0.152	0.152	0.080	0.164	0.131	0.132	**0.135**
50	0.10	0.116	0.13	0.097	0.154	0.141	0.124	**0.127**
Average		**0.150**	**0.157**	**0.112**	**0.181**	**0.139**	**0.151**	**0.148**

Hz	(m/s)	ZMA1	ZMA1.5	ZMA2	Average
10	0.02	0.184	0.091	0.127	**0.134**
20	0.04	0.174	0.089	0.147	**0.137**
30	0.06	0.155	0.079	0.137	**0.124**
40	0.08	0.145	0.098	0.130	**0.124**
50	0.10	0.11	0.069	0.104	**0.094**
Average		**0.154**	**0.085**	**0.129**	**0.123**

Hz	(m/s)	ZMA1Ref	ZMA1.5Ref	ZMA2Ref	Average
10	0.02	0.205	0.159	0.155	**0.173**
20	0.04	0.162	0.123	0.126	**0.137**
30	0.06	0.144	0.110	0.128	**0.127**
40	0.08	0.138	0.106	0.131	**0.125**
50	0.10	0.129	0.094	0.111	**0.111**
Average		**0.156**	**0.118**	**0.130**	**0.135**

Hz	(m/s)	Galfan
10	0.02	0.161
20	0.04	0.140
30	0.06	0.142
40	0.08	0.149
50	0.10	0.140
Average		**0.146**

2.3.5.2 Task T5.2: Joining.

2.3.5.2.1 Resistance spot welding

The behaviour of hot dip Zn-Al-Mg materials during spot welding was evaluated by determining the welding window and electrode consumption. A Kemecweld KRW 81P spot welder at 50 Hz was used for all experiments.

The **weldability range** was measured for materials ZMA1, ZMA1.5F and ZMA2 together with reference material DX51+Z140MC according to the following parameters upon the material:

- ZMA1, 0.90 mm: electrode force 3.0 kN, tip Ø 6 mm
- ZMA1.5F and DX51D+Z140, 0.60 mm: electrode force 2.2 kN, tip Ø 4 mm
- ZMA2, 0.79 mm: electrode force 2.5 kN, tip Ø 5 mm

The results are presented in Figure 57. Direct comparison of welding ranges was only possible between materials ZMA1.5F and DX51D+Z140 because steel and metallic coating thicknesses were identical. From the figures, it can be seen that the optimum curves are not very far from each other but ZMA coating seems to give narrower current range with all welding times. However, when ZMA2 is compared to typical weldability ranges from FIAT in Figure 58 where similar steel thickness was used, comparable curves were obtained.

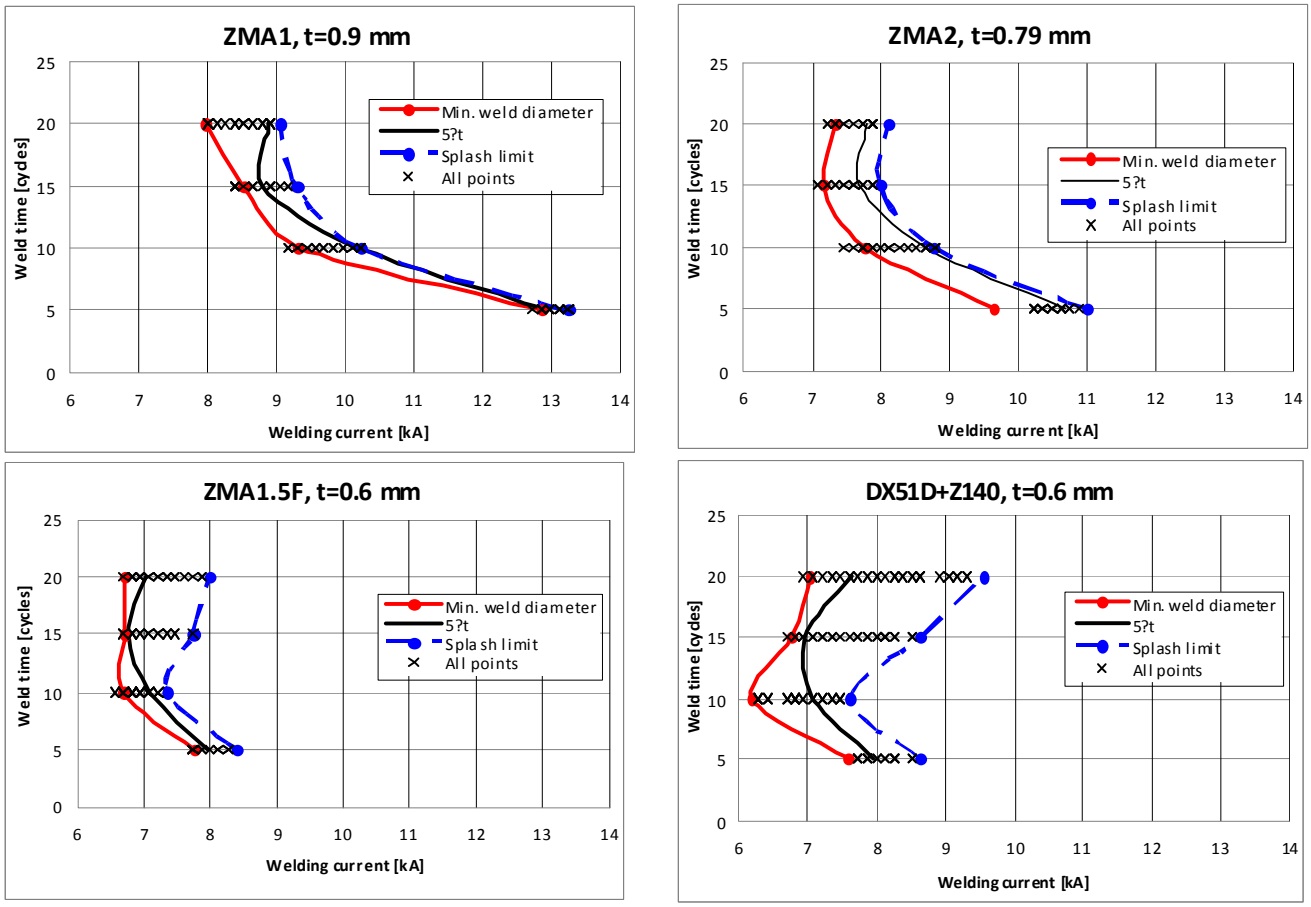

Figure 57: Weldability ranges for ZMA1, ZMA1.5, ZMA2 and HDG reference.

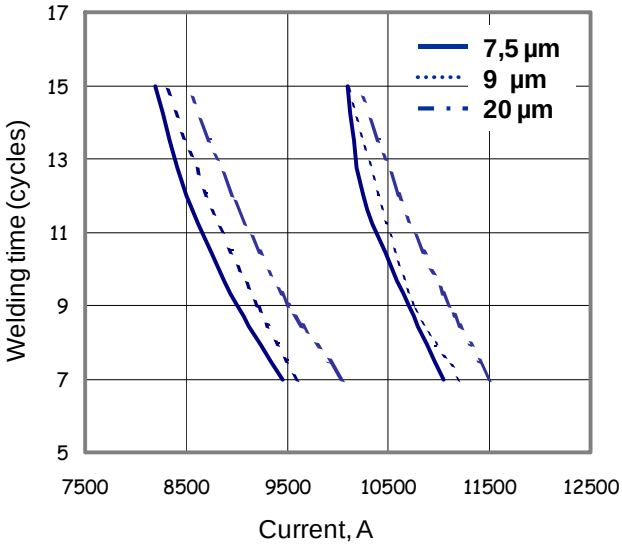

Figure 58: Typical weldability range of zinc coated steel 0.8 mm as a function of zinc thickness. Data from FIAT.

For the **electrode lifetime**, based on the first results presented in the mid-term report, it was decided that despite of recommendations given by the standard EN ISO 8166, the same electrode force had to be used for all coatings in order to ensure comparability of the results. Therefore, welding tests were finally done using fixed parameters as follow: electrode force 2.3 kN, diameter 5.5 mm and welding time 10 cycles for all materials. The results for ZMA1, ZMA1.5F and ZMA2 including galvanised references are presented in Figure 59 where lifetimes of 600 to 900 spots were obtained. When comparing ZMA coatings to galvanised ones, it is hard to see any consistent differences in lifetime and the electrode wear can be estimated to be the same for both types of coatings. The lifetime curve for the reference coating ZMA1.5F was however strange and the results should thus be taken with some caution. The number of welds was probably too low because in the first test (reported in mid-term report), the results obtained for ZMA1.5F were in good agreement with those of its reference. No evidence on the effect of alloying element was observed on the electrode wear when comparing zinc coatings with different amounts of Mg and Al,

Based on these results, we can conclude that the addition of Mg and Al from 1 to 2 % in the coating gives comparable welding properties which are clearly more sensitive to welding parameters and to coating/steel thickness than to coating composition in this range.

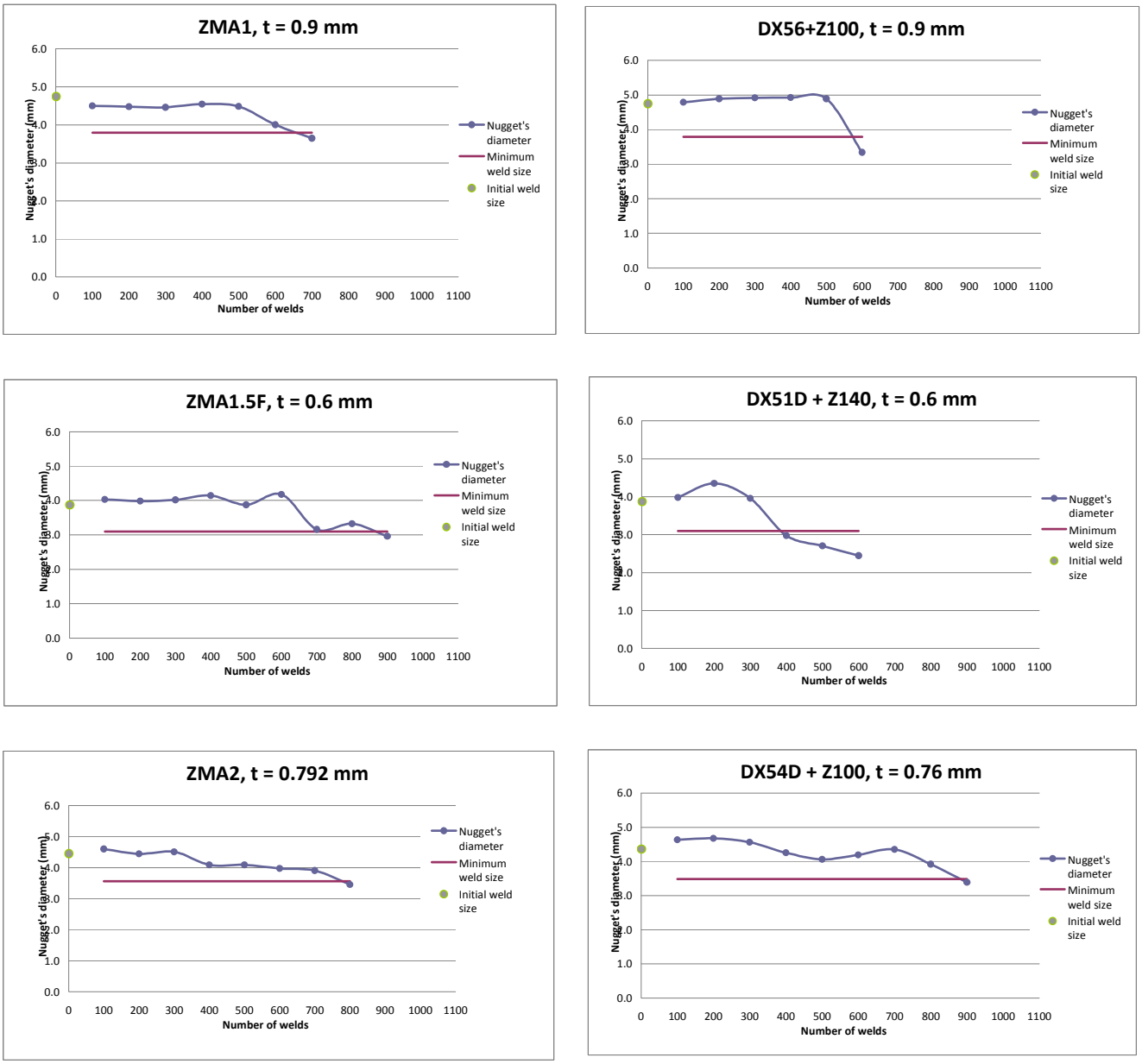

Figure 59: Electrode lifetime for coatings with electrode force 2.3 kN.

2.3.5.2.2 Adhesive bonding

Adhesive bonding of ZMA coating was tested by FIAT according to the internal procedure using a structural adhesive from PPG 851302. Two materials e.g. ZMA2 and its corresponding HDG coating reference were tested using three parallel samples. Sample size was 100x25 mm with overlapping length of 12 mm (see Figure 60). Target thickness of adhesive film was 0.2 mm.

Adhesive bonded samples were degreased, phosphatized and heat treated to simulate the painting procedure. During treatment, samples were heated to 160 °C for 30 minutes and let to cool down for another 30 min at ambient temperature (simulating cataphoretic baking), heated to 140 °C for 30 minutes and let to cool down another 30 min at ambient temperature (primer baking) and heated to 130 °C for 30 minutes and let to cool down 2 hours at ambient temperature (paint baking). So called overbaked samples were heated to 160 °C (instead of 140°C) for 30 minutes to simulate paint baking, otherwise the procedure being the same.

Table 17 summarizes the different test conditions systematically performed at FIAT to test the adhesive bonding properties of metallic coatings. The tensile tests were conducted at 3 different temperatures on un-aged samples and at one temperature for the overbaked samples. Three ageing tests of 500 h each

were also carried out and tensile tests were thereafter conducted at room temperature. The tolerance criteria upon testing conditions are also given.

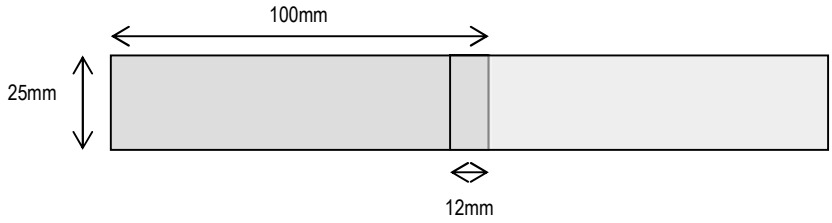

Figure 60: scheme of adhesive bonded samples

Table 17: description of ageing tests of adhesive bonded samples and tolerance criteria (From FIAT standard)

	Ageing	Test temperature		
Detachment resistance to cutting (N/mm^2)	– – –	at 23±2 °C	§ 2.8	≥ 10
	– – –	at 80±2 °C		≥ 9
	– – –	at −40±2 °C		≥ 10
	overbaking	at 23±2 °C		≥ 8
	500 h at 100 °C	at 23±2 °C		≥ 9
	500 h in D.H.C.	at 23±2 °C		≥ 9
	500 h in S.F.	at 23±2 °C		≥ 9

D.H.C.: Damp Humidity Chamber (95 ÷ 100% Relative Humidity; temperature 40 ± 2 °C) ; **S.F.** (i.e. S.S.T.): Salt Fog (sodium chloride 50 ± 5 g/l; pH 6,5 ÷ 7,2 ; temperature 35 ± 2 °C)

The strength of adhesive joint was evaluated in tensile test. Samples were clamped for a section of 50 mm at each end and drawn at a speed of 12 ± 2 mm/min. Test matrix and tensile test results are presented in Table 18 each result being the average of three tests. In addition, the fracture mode of the adhesive was estimated from visual inspection and the results are summarized in Table 19.
Calculating the average of tensile strength for all test environments, ZMA2 coating gives approximately 10 % of reduction in tensile strength compared to that of HDG coating. However, results deviation was relatively small and the same for both coatings. Both materials fulfill internal test requirements. As regards to the type failure (not considered in FIAT requirements), the failure is mostly adhesive on ZMA2 while it is cohesive on HDG. It is obvious that cohesive failure is preferred.

Table 18: Tensile test matrix and results for adhesive bonding test.

Ageing	Test temperature	ZMA2 (N/mm^2)	HDG reference (N/mm^2)
-	+23℃	11.27	14.78
-	+80℃	9.82	9.9
-	- 40℃	14.2	13.73
overbaking	+23℃	10.83	13.96
500h @ 100℃	+23℃	13.27	12.52
500h in D.H.C.	+23℃	9.48	11.88
500h in S.F.	+23℃	9.86	11.01
	Average	**11.2**	**12.5**
	Stdev	**1.8**	**1.7**

Table 19: Fracture mode of adhesive bonded ZMA2 and HDG as a function of testing conditions

Ageing	Test temperature, ℃	ZMA2	HDG
no	+23	Adhesive	Cohesive
no	+80	Adhesive	Cohesive
no	-40	Adhesive	Cohesive
overbaking	+23	Partially cohesive	Cohesive
500h @ 100℃	+23	Partially cohesive	Cohesive
500h in D.H.C.	+23	Adhesive	-
500h in S.F.	+23	Partially cohesive	-

2.3.6 **WP6 Cosmetic corrosion and protection in hem flange**

The objectives of WP6 were to evaluate the corrosion performance of Zn-Al-Mg coated materials using several standard accelerated test procedures well accepted by the automotive industry. This was done on bare materials, cosmetic samples and samples simulating hem-flanges. The results were reported in **deliverable D10**.

2.3.6.1 **Description of accelerated corrosion tests**

Three different accelerated corrosion tests used by the Automotive Industry have been selected, namely Volvo (ACT STD423-0014), New VDA (VDA233-102) and VDA (VDA621-415) tests. The main characteristics of the 3 tests are summarized in Table 20. The tests differ by the salt solution (pH, concentration, deposition rate), the duration and the wet/dry levels and frequency. In VDA test, the concentration of NaCl of the salt solution is 5 or 10 times higher than in the other tests performed. The tests also differ by the mode of application of the salt solution. In the Volvo test, the application of the pollution was like a “shower” or a rain while a fog of salt solution is applied in New VDA and VDA. Range of temperatures differs from one test to the others. In particular, the New VDA test has a freezing phase once a week (-15°C) and reaches 50°C in a drying phase while in the other tests, the temperature varies from about 20°C to 60°C. It should be mentioned that the VDA 621-415 standard has been widely used since the 80’s to develop and qualify new corrosion resistant products and to select materials. However, this test fails in simulating on vehicle exposures [4-7]. Thus, to be more representative of natural exposure of automotive substrates, a new accelerated corrosion test namely N-VDA or VDA233-102 in replacement of the VDA 621-415 standard is currently in development by a working group of the VDA (German vehicle producers association) and the VDEh (German steel producers association) [6]. In addition to the standardized tests, a modified VDA621-415 test using NaCl 1wt% was also performed in order to evaluate the influence of the salt load. This test was conducted at TKSE.

The test duration was ranging from 10 (VDA) to 12 weeks (N-VDA) and even up to 18 weeks for the Volvo test where a kinetics of corrosion degradation was performed. Volvo test was performed in a fully automatic 2000 L ClimeArt chamber at IC. The New VDA test was performed in a fully automatic 2000 L Corrocompact 616/2000R cabinet from Erichsen at TKSE while a Weiss SC 1000/40-130 cabinet was used by voestalpine. VDA test was conducted in a conventional Weiss SC 1000 cabinet at voestalpine.

Table 20: Main characteristics of the accelerated corrosion tests performed

Test standard	Pollution			T.°C	R. H., %,	Approx time of wetness, %	Test duration weeks
	Salt solution pH deposition rate in 80cm²	Frequency T°C	Chloride deposition, mg/cm², test				
Volvo ACT STD 423-0014	NaCl 1% wt, pH4 120mL/h (15mm/h)	3x15 min twice a week 1.5h/week 35°C	27 (6w)	45.. 35..	..50, 4h ..95, 4h	44	Up to 18
New VDA VDA233-102	NaCl 1% wt, pH6.5-7.2 2mL/h	3h (3 times/week) 9h/week 35°C	8.1 (6w)	-15.. Up to 50	..50 Up to 100	53	Up to 12
VDA 621-415	NaCl 5%wt, pH 6.5-7.2 1.5mL/h	24h/ week 35°C	136 (10w)	40.. 18-28.. 23..	..100, 8h ..50, 16h ..50, 48h	35	10

2.3.6.2 Task 6.1: Cosmetic corrosion and protection in defects

2.3.6.2.1 Experimental

Details on materials, surface treatment and paint application are given in task 2.3.
Before testing the ED-coated cosmetic panels, two vertical scribes of 100 mm parallel to the longer side were applied at TKSE. The 0.6 mm wide Clemen was scribed with an electrical machine and the other one with 1.0 mm wide Sikkens applied by hand-scribing tool. The advantages of these two scribing tools are well known as scribing is relative easy through the surface and the reproducibility works well.

The average and maximum delamination from the scribe lines were evaluated as a function of exposure duration. At the end of the test, the measurements were also made after taking off the delaminated paint considering both sides of the scribe and minus the scribe width. The evolution of edge creep was also followed as a function of exposure time in the Volvo test.

2.3.6.2.2 Results

Figure 61presents the average scribe creep after twelve weeks of exposure in New VDA and 18 weeks of Volvo test, while results obtained after exposure in VDA621-415 and modified VDA 1wt% are given in Figure 62.
Regarding the **New VDA** test, the results indicated quite comparable material ranking whatever the testing chamber after twelve weeks with an obvious tendency to develop less creep on zinc-aluminium-magnesium coated steel than on conventional galvanized materials. Galfan coating showed the largest scribe delamination. Galvannealed steel (GA) showed intermediate behaviour between conventional galvanized and ZMA coatings. It must be noticed that with a larger thickness e.g. between 10 µm versus 7 µm ZMA1,5 showed a better resistance to corrosion creep than ZMA1 and ZMA2. However, no major differences could be noticed upon the content of aluminium and magnesium e.g. between ZMA1 and ZMA2. Both were tested with comparable metallic coating thicknesses (7 µm). Thus an improvement on cosmetic corrosion resistance of approximately 1.4 was measured on hot dip galvanized zinc coatings with 1-2 % magnesium and 1-2 % aluminium (e.g. ZMA1 and ZMA2) in comparison to conventional zinc coatings (GE and GI) after twelve weeks of New-VDA test. When examining the results after ten weeks of **VDA621-415**, which operates with a higher salt load (NaCl 5wt%), the beneficial effect of magnesium and aluminium was significantly better than after New-VDA test with an improvement of 3 in comparison to conventional galvanized coatings. The delaminated area was in the same range as after the New-VDA e.g. approximately 1 mm but larger scribe creep was developed on GE and GI coatings (e.g. 4 mm). It is interesting to note that less difference between

ZMA and conventional zinc coating was obtained when the samples were exposed in a **modified VDA test using NaCl 1wt%** (improvement of about 2 to 2.5), indicating an obvious influence of the salt load particularly on the corrosion of conventional zinc coatings (GI, GE and GA). For an unknown reason, an important scribe delamination was measured on the 1 mm scribed ZMA1.5 after VDA 1wt%. The ranking obtained in the VDA-tests (New, old or modified) are comparable with the ranking of previous results in the neutral salt spray test ISO 9227 [1, 6].
The results from 18 weeks of exposure in **Volvo test** did not reveal any significant improvement of aluminium and magnesium content in comparison to conventional zinc coatings. Nevertheless, the effect of coating thickness could be observed: ZMA1,5 with around 10 instead of 7 µm showed the best corrosion resistance. Regarding the influence of the scribe width, no major differences were observed unless after the Volvo test where larger scribe creep was observed on the 0.6 mm scribe with however rather scattered values.
In order to illustrate the above observations and compare the type of degradation from the defect upon the testing conditions and the metallic coating, details of the scribed area are also shown in Figure 96 of appendix 2 for all metallic coatings after 18 weeks of exposure in Volvo test.

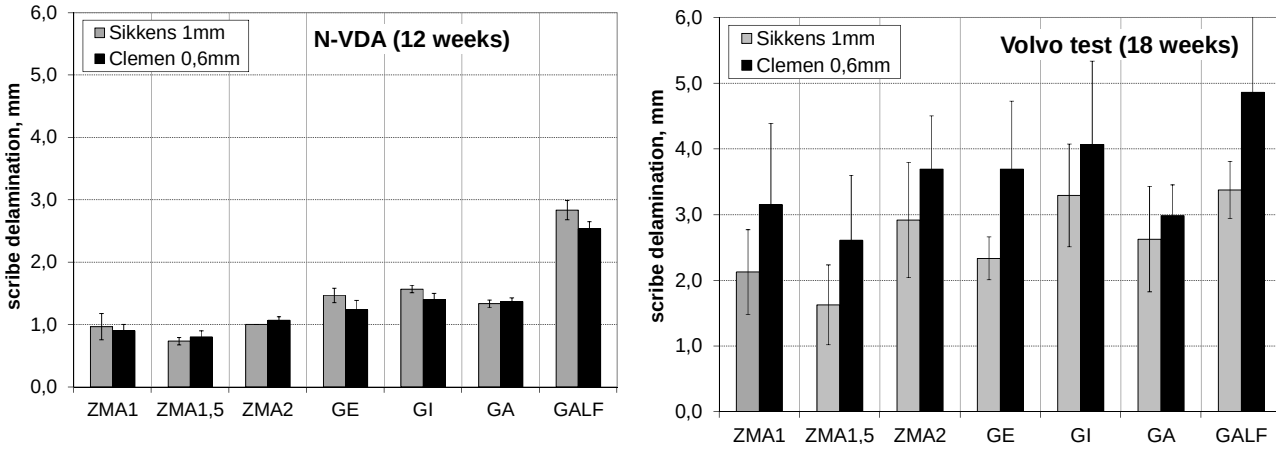

Figure 61: Mean delamination from scribe after 12 weeks of exposure in New VDA test (left) and 18 weeks of Volvo test (right)

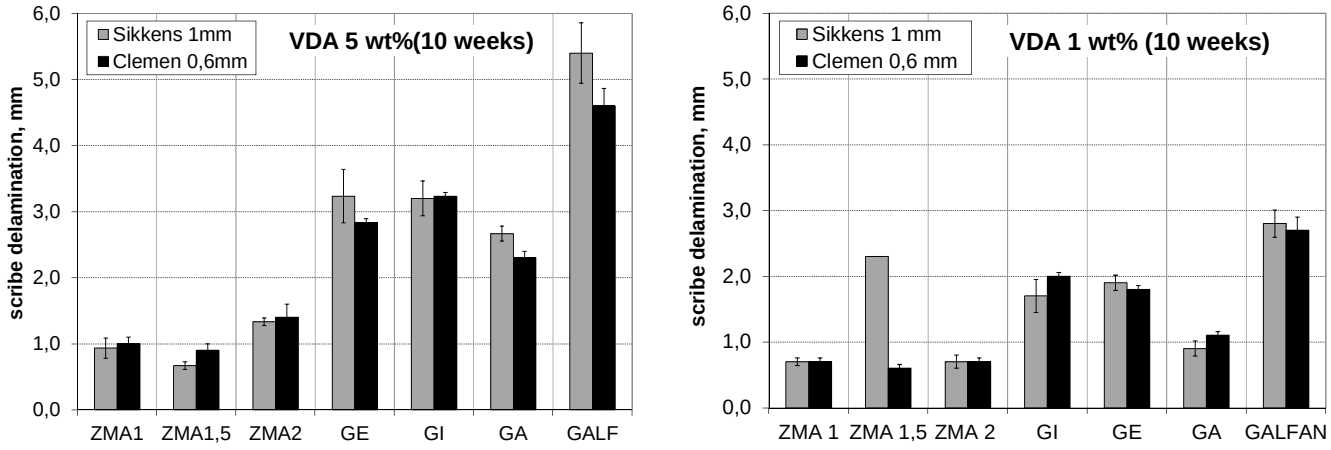

Figure 62: Mean delamination from scribe after 10 weeks of exposure in VDA test performed using NaCl 5wt% (left) and 1 wt% (right)

2.3.6.3 Task 6.2: Perforation corrosion

2.3.6.3.1 Experimental

Samples

For perforation corrosion, hem flange samples were used. The three parallel samples per material/configuration were exposed together with the cosmetic samples in New VDA, VDA621-145 and Volvo test for various durations upon the test. In addition to hem flange samples, bare materials in open situation were also exposed as well as samples with a cut edge. Moreover several sets of samples were tested in order to follow the kinetics of degradation of the metallic coatings. In particular in the Volvo test samples were removed after one, three, six, twelve and 18 weeks in order to evaluate the metal loss as a function of exposure time. Rhesca samples were also tested in open configuration in the Volvo test. Again, two sets of samples were exposed, one for 6 weeks and another for 18 weeks.

Evaluation

Intermediate inspections of the samples with photographs were performed and the extent of red rust was evaluated using an image software analysis. For red rust at cut-edges, the percentage was evaluated on a 10 mm wide area along the vertical cut-edge. On completion of the tests, all the samples were sent to IC for evaluation. The samples were photographed and the corrosion products were collected for further analysis. Then, zinc corrosion products were removed by pickling the samples in saturated glycine solution. Thereafter, the remaining metallic coating was obviously calculated from a difference in the coupon mass before and after dipping in Clark's solution (20g of antimony oxide and 60 g of tin(II) chloride in 1 L of concentrated hydrochloric acid). It should be noted that the preciseness of the procedure decreases with the amount of red rust on the surface and no zinc coating metal loss was calculated when the extent of red rust was more than 5-10%. The maximum corrosion attack in steel substrate was measured using a micrometer gauge equipped with a sharp on three points on each sample.

2.3.6.3.2 Results

As mentioned in the experimental section above, the evolution of the corrosion degradation and particularly the extent of red rust were monitored by regular inspection in the 3 accelerated corrosion tests for the different configurations. Since the cover panel of hem-flange is transparent, it was possible to follow the red rust formation. Photographs showing the appearance of the metallic coatings upon the test and the configuration may be observed in Figure 97 to Figure 102 of appendix 2. The extent of red rust is plotted in Figure 63 as a function of exposure time in the Volvo, New VDA and VDA tests for the different metallic coatings unless the galvannealed one where the corrosion of Zn-Fe coating also produced rust coloured corrosion products difficult to distinguish with the corrosion of steel substrate. The results obviously indicated a kinetic of red rust propagation which was dependent on the testing conditions but also on the configuration of the samples. Thus, regarding **open surface,** whatever the tests, the propagation of red rust was lower on Zn-Mg-Al coatings in comparison to conventional ones, ZMA1.5 (10µm) showing the least amount as expected from the larger thickness e.g. 10µm versus 7.5µm. It may be observed a tendency to develop more red rust on ZMA1 particularly in New VDA test where the surface was almost entirely covered by red rust after 12 weeks. This was observed in both New VDA tests conducted at DOC and voestalpine. Clearly, New VDA testing conditions appeared the most aggressive ones towards open surface, while Volvo offered the mildest conditions.

In **hem-flange configurations**, the beneficial improvement of aluminium and magnesium is not obvious at all. Indeed, if the kinetics of red rust propagation on ZMA coatings are still lower than on conventional zinc coatings (GE, GI) in the Volvo test, less differences between the two coatings generations may be observed. Same observations may be drawn for samples exposed in the VDA test where Galfan coating appeared the less rusty one. However, in the New VDA test, no beneficial effect of the ZMA coating may be observed unless on the thicker one ZMA1.5. It should be mentioned that the exposure of hem-flange samples in New VDA were stopped after 10 weeks due to important corrosion in the confined area which lifted the cover glass panel. As only one set of samples was exposed in VDA test, the samples were removed after 6 weeks.

The extent of red rust at **cut-edge** was also examined in order to evaluate the efficiency of ZMA coatings to protect cut-edges. Again, whereas the results are dependent on the testing conditions, it may be observed an obvious tendency to better protect the cut-edges using Zn-Mg-Al coatings in comparison to classical zinc coatings. At comparable thickness of metallic coating (7.5 µm), the addition of 2% magnesium and 2% aluminium (ZMA2 – 0.8 mm steel) was about twice more efficient to red rust extent than coating with 1% of magnesium and aluminium (ZMA1- 0.9 mm steel) when exposed in Volvo or New VDA tests. When tested in VDA cycle, the extent of red rust at cut-edge was insignificant on ZMA coatings (less than 10% after 12 weeks) while it covered 100% of the cut-edge area in a short time on conventional GE and GI coatings.

From these inspections, the time to red rust appearance which is an important parameter in terms of protective ability of automotive coatings was evaluated considering open and hem-flange configurations for the different tests. As shown in Figure 64, the time before red rust formation varies upon the testing conditions and the configuration, with a tendency for ZMA coatings to delay the development of red rust. The beneficial effect of ZMA coatings was more pronounced in open situations than confined ones. In particular, when exposed in VDA test, the red rust formation was delayed by a factor of 10 in comparison to GI and GE coatings while it was significantly lower in New VDA or Volvo tests with an improvement ranging between 2 and 3 approximately in terms of delay to red rust formation. The protective ability of ZMA coatings to delay the formation of red rust was obviously altered in a confined area. The present results are in rather good agreement with previous work published by Prosek *et al.* who compared the behaviour of different metallic coatings at various thicknesses in a Volvo test using different designs of hem-flange [7]. According to recent works of Schuerz and *co-workers* who compared the behaviour of hot dip ZnMg2Al2 (7 µm) to conventional zinc coating HDG in open configuration exposed in neutral salt spray test ISO 9227, the formation of red rust on ZMA2 was delayed by a factor of 13 in comparison to HDG [8-10]. Traces of red rust were formed after 1320 hours of exposure while hot dip galvanised coatings was rusty only after 100 hours. From these results, it is possible to summarize the improvement of ZMA coatings versus conventional zinc coatings as a function of testing conditions in Table 21.

The results showed that the beneficial effect of ZMA in delaying red rust formation increases in the following order:

Volvo ~ New VDA << VDA621-415 < NSST.

This may be partly related to the chloride load.

In order to verify that the chloride load influences the corrosion of metallic coatings, it was decided to conduct accelerated corrosion tests at different salt loads mainly on bare material in open configuration. Thus a test according to VDA621-415 was conducted using a salt solution of 1 wt% NaCl instead of 5 wt%. In addition, a test according to Renault ECC1 D17 2028 standard (NaCl 1wt%, pH 4) was performed at IC. As shown in Figure 65 which presents the improvement of ZMA versus GI regarding the time to red rust formation as a function of the salt load, the influence of the salt load seems to be a key factor on the degradation of ZMA coatings. Volvo was not considered as the salt solution is applied as a rain and it is difficult to compare with pollution applied as a fog. A new order of the tests relative to their property of the beneficial effect of ZMA in delaying red rust formation is the following:

Volvo ≈ New VDA < ECC1 < VDA1%wt NaCl << VDA621-415 (5%) < NSST.

In order to study the influence of the alloying elements Mg and Al, the Rhesca samples that were produced with composition ranging from 1 up to 4 wt% were exposed in the Volvo test in bare configuration. Two sets of samples were exposed one for 6 weeks and one for 18 weeks. The results are presented in Figure 66 together with data obtained on line hot dip coatings ZMA and GI after 6 weeks of exposure in the test. It should be remembered that Rhesca coatings were significantly thicker (11 -16 µm) than line hot dip ZMA. It is interesting to note that comparable metal loss was measured on both Rhesca and line hot dip coatings of equivalent composition e.g. Zn1%Mg1%Al and Zn2%Mg2%Al. Moreover, adding alloying elements resulted in a significant decrease of the corrosion of the metallic coating. When increasing the exposure duration (up to 18 weeks), the metallic coatings with the smallest amount of alloying elements e.g. ZMAR1and ZMAR2/1 showed an obvious poorer corrosion resistance compared to most alloyed coatings.

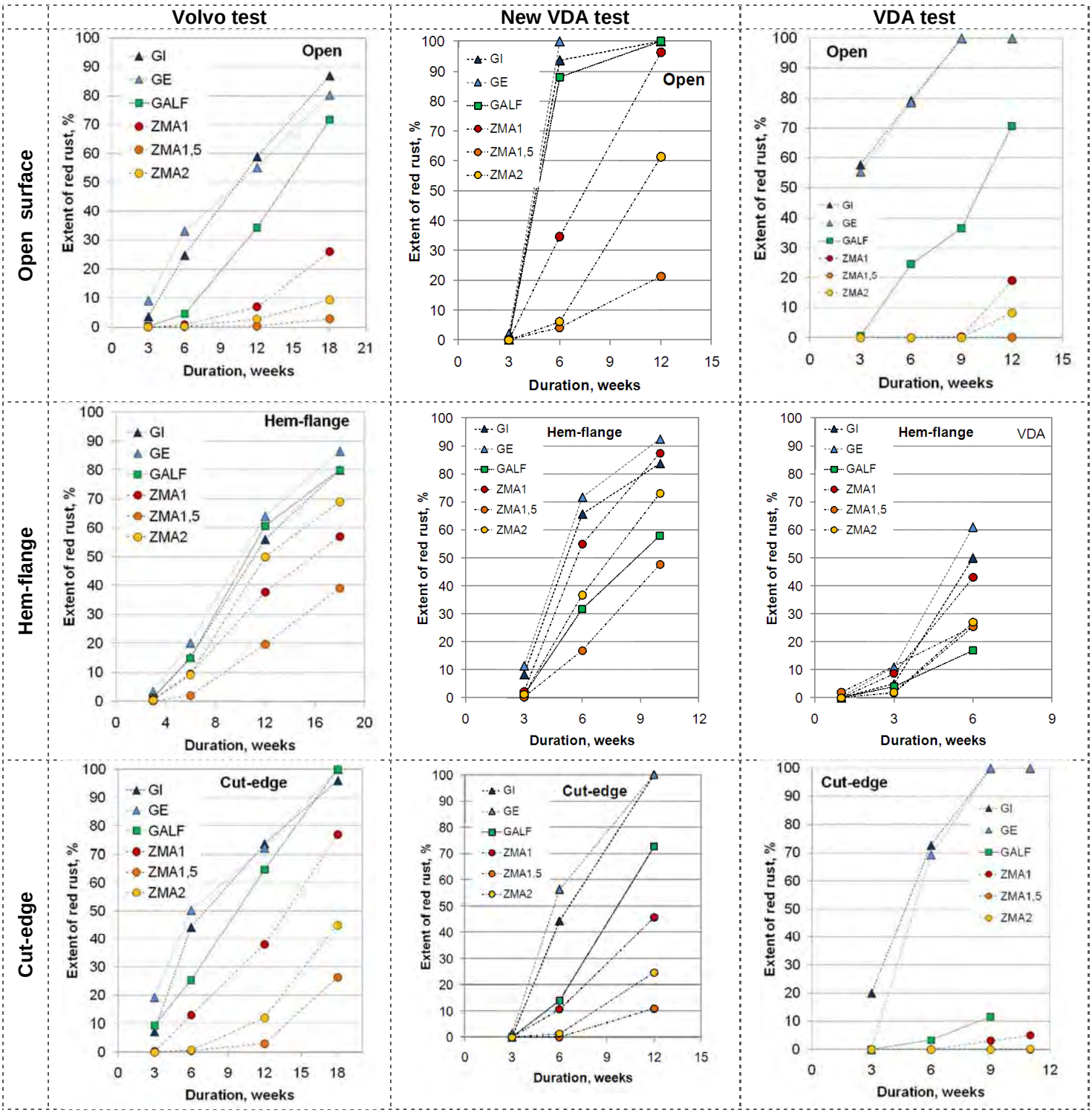

Figure 63: Extent of red rust as a function of exposure time in Volvo (left), New VDA (center) and VDA (right) tests and configurations e.g. open surface (top), hem-flanges (middle) and at cut-edge (bottom). All metallic coatings unless GA.

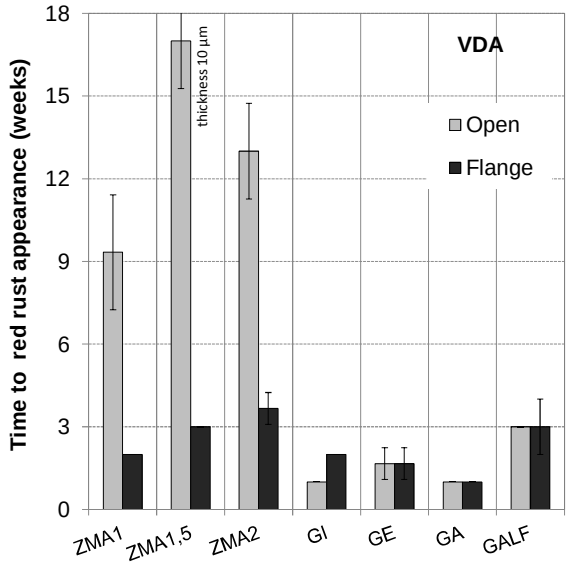

(a)

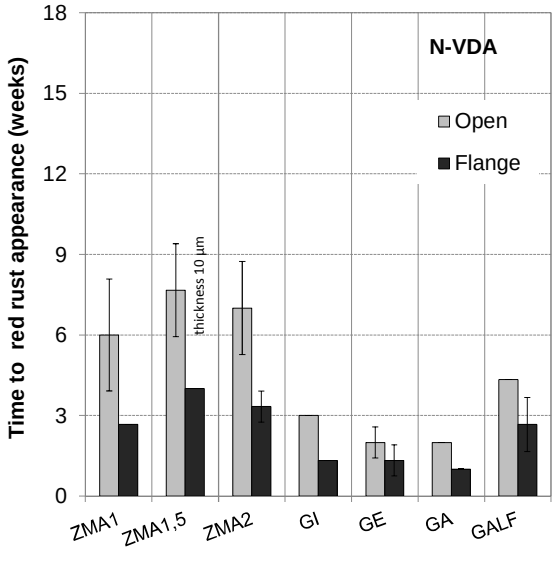

(b)

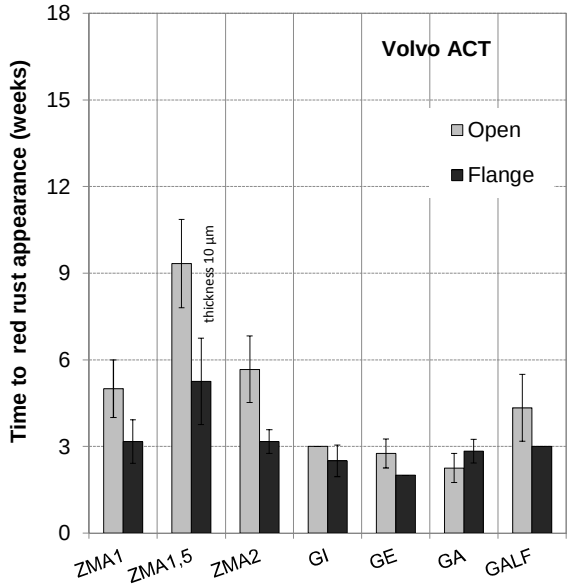

(c)

Figure 64: Time to red rust appearance on open and hem-flange configuration exposed to VDA (a), New VDA (b) and Volvo test (c).

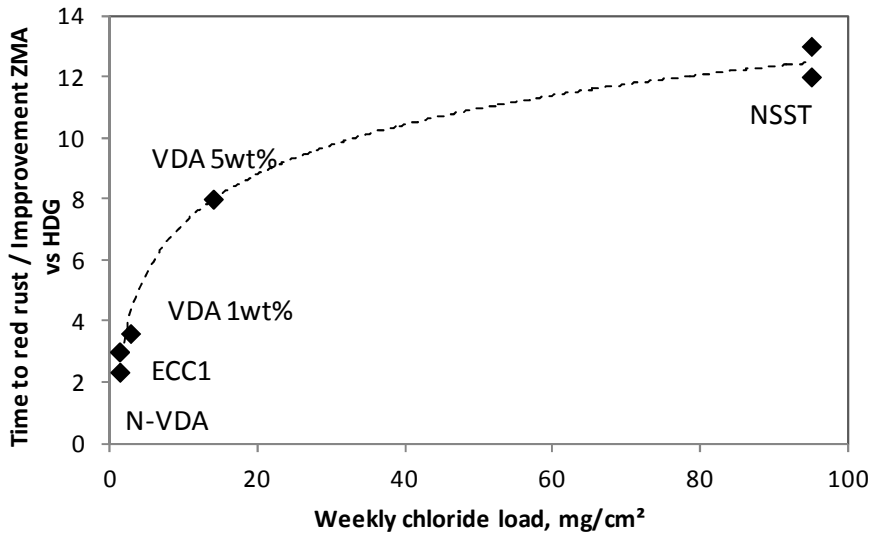

Figure 65: Time to red rust formation versus weekly chloride load in New VDA, VDA and NSST (Improvement of ZMA 7µm vs HDG 7µm on open panels)

Table 21: Time to red rust appearance as a function of testing conditions

Open	HDG 7µm	ZMA 7µm	Improvement *vs* HDG
Volvo test	3	5	1.7
New VDA test	1.5	3	2
Renault ECC1 test	2	6	3
VDA test	1.5	12	8
Neutral salt spray test (from [10-12])	0.6	8	13

In order to study the kinetics of metallic coating degradation, sets of samples were removed after different exposure durations in the Volvo test. Then, the weight loss of the metallic coatings was evaluated and plotted in Figure 66 versus the alloying elements. It should be mentioned that the evaluation of the weight loss was only possible when no or less than 5-10% of red rust was formed. Thus, over this level of red rust, it was considered that the metallic coating was fully consumed at least locally. The results indicated a dependency between the weight loss and the alloying elements which however changed with exposure time. After 1 week of exposure where no red rust was formed on any of the metallic coatings, ZMA coatings showed a weight loss about 5 times lower than conventional zinc coatings, in the same range as the Galfan coating. With longer exposure durations when identical material thickness is compared, ZMA2 showed less weight loss than ZMA1 and Galfan, while conventional zinc coatings presented significant red rust. Thus, the following classification from the least resistant to the most stable one can be established in the Volvo test on open panels: GI-GE<<Galfan<ZMA1<ZMA1.5~ZMA2.

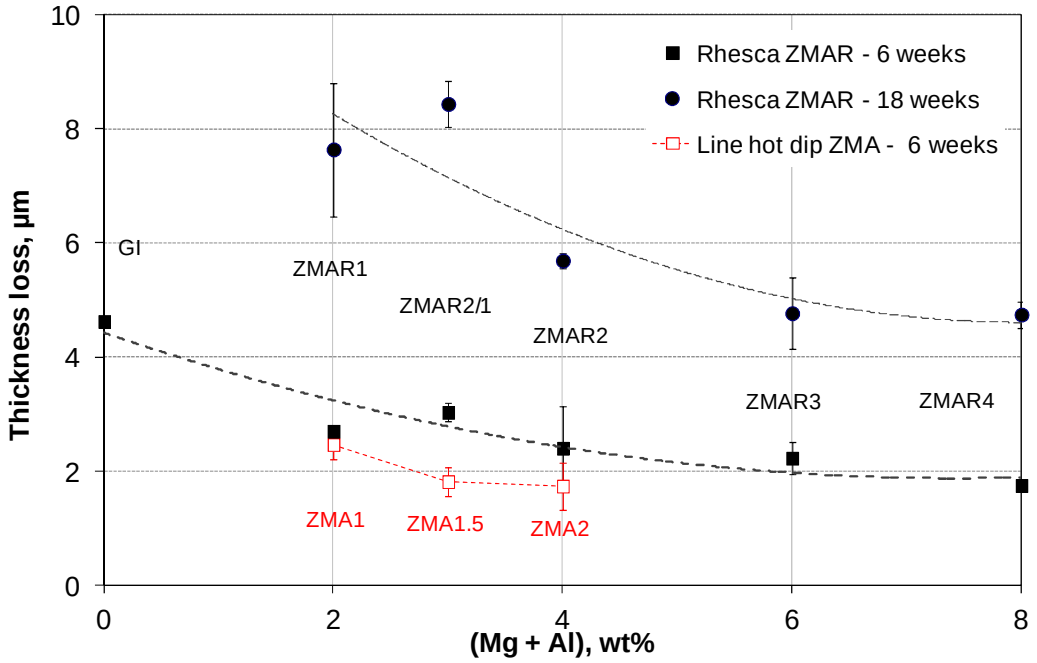

Figure 66: **Metal loss of metallic coated steel (Rhesca and line hot dip coatings) in open configuration versus alloying element after exposure in Volvo test.**

As mentioned before, the depth of corrosion attack in steel substrate was also evaluated using a micrometre gauge on samples which presented red rust. Again, these measurements were performed as a function of exposure time up to 18 weeks in the Volvo test both on open and hem-flange panels while one or two exposure durations were considered in the New VDA and VDA tests. The results are given in Figure 67 to Figure 69 for Volvo, New VDA and VDA tests respectively. In good agreement with the extent of red rust, the depth of attack in steel logically increases with exposure time in the accelerated corrosion tests. Considering **open panels**, the best corrosion resistance was observed for ZMA1.5 and ZMA2 in all testing conditions. In particular, no attack in steel was observed after 18 weeks of Volvo test and 12 weeks of VDA on these two coatings while conventional zinc coatings were significantly degraded with attacks up to 400 µm and 500 µm on the galvannealed steel. The results obviously showed fewer differences between ZMA coatings and conventional ones when exposed in the N-VDA test (see Figure 68). In addition, it is interesting to note that a rather comparable behaviour may be observed between ZMA1 and Galfan coatings.
In the case of **confined areas,** the corrosion resistance of ZMA coatings was definitively poorer than in open situations showing less pronounced differences with conventional Zn coatings (GI and GE). Thus, ZMA1 and ZMA2 showed rather comparable corrosion attacks than Galfan in the Volvo test while the thicker layer of metallic coating in ZMA1.5 provided a better corrosion resistance. These observations are not that obvious when examining the results of New-VDA test where significant deviation was noticed.
The influence of **NaCl concentration** in a VDA cycle on the corrosion resistance of ZMA and conventional coatings in open configurations is illustrated in Figure 70 considering the weight loss (a) and the depth of corrosion in steel substrate (b) after 12 weeks of exposure. The beneficial effect of ZMA coatings is obvious whatever the concentration of NaCl, VDA with 1wt% NaCl being less aggressive than the conventional VDA test using 5wt% NaCl in term of red rust, metal loss and attack in steel substrate. Yet, as indicated in Figure 65, the red rust formation on ZMA coating was delayed by a factor of 4 in comparison to GI when NaCl 1wt% was used in VDA test while a factor of 10 was found using NaCl 5wt%.

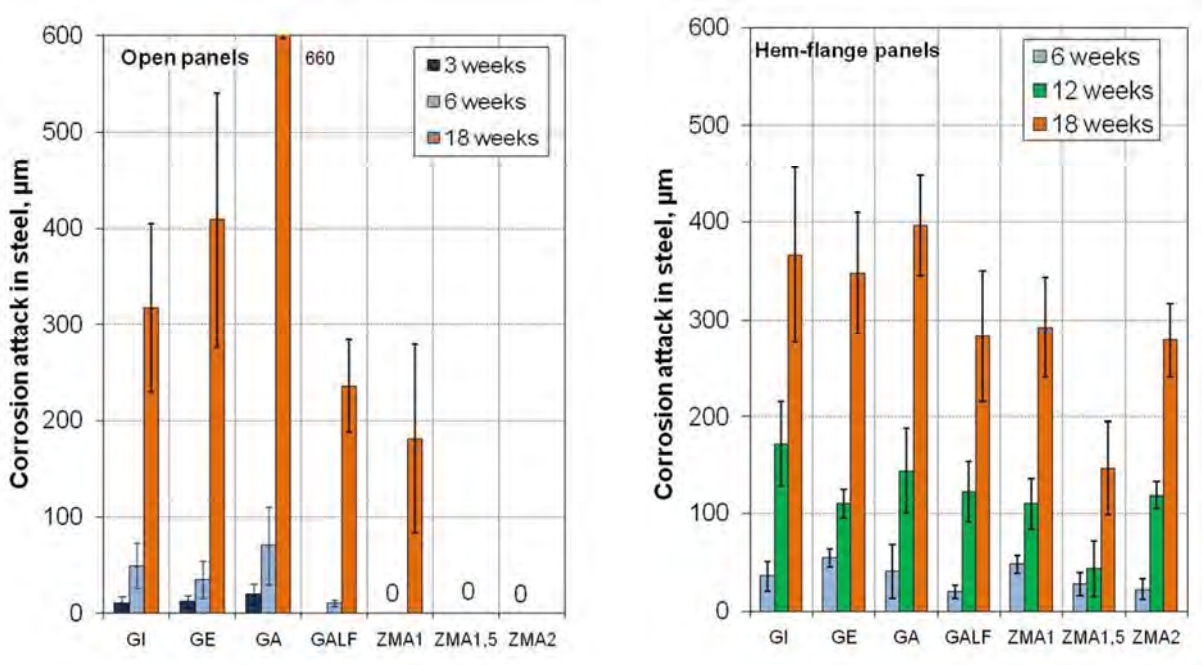

Figure 67: Maximal depth of corrosion in steel as a function of exposure time in the Volvo test for metallic coatings in open (left) and hem-flange (right) configurations.

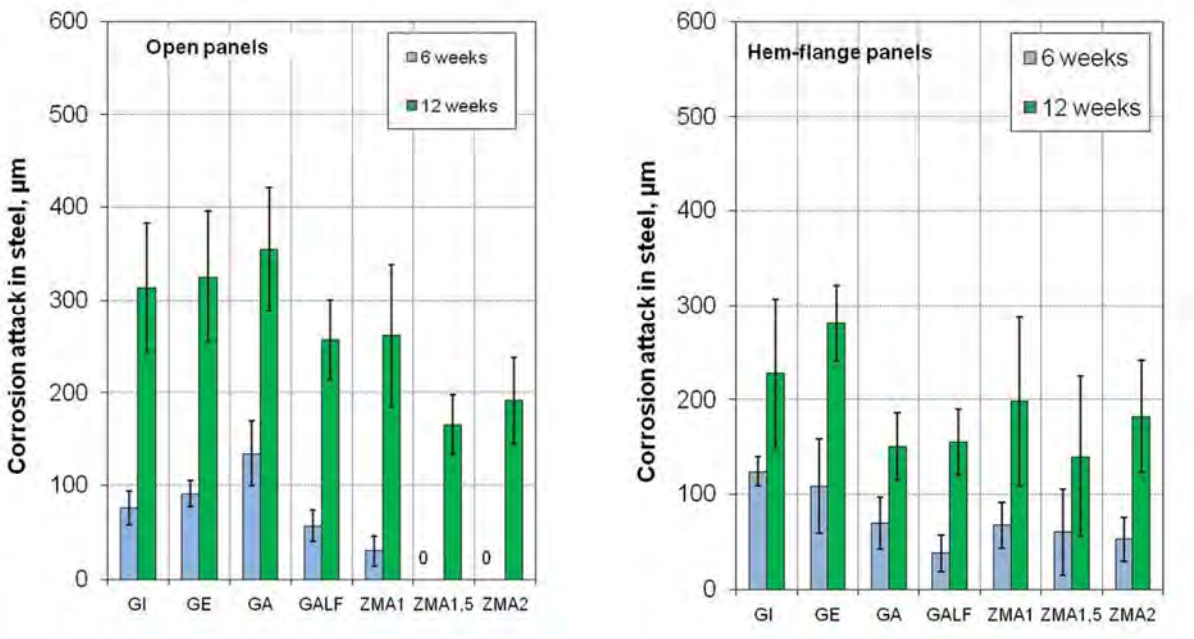

Figure 68: Maximal depth of corrosion in steel as a function of exposure time in the New VDA test for metallic coatings in open (a) and hem-flange (b) configurations.

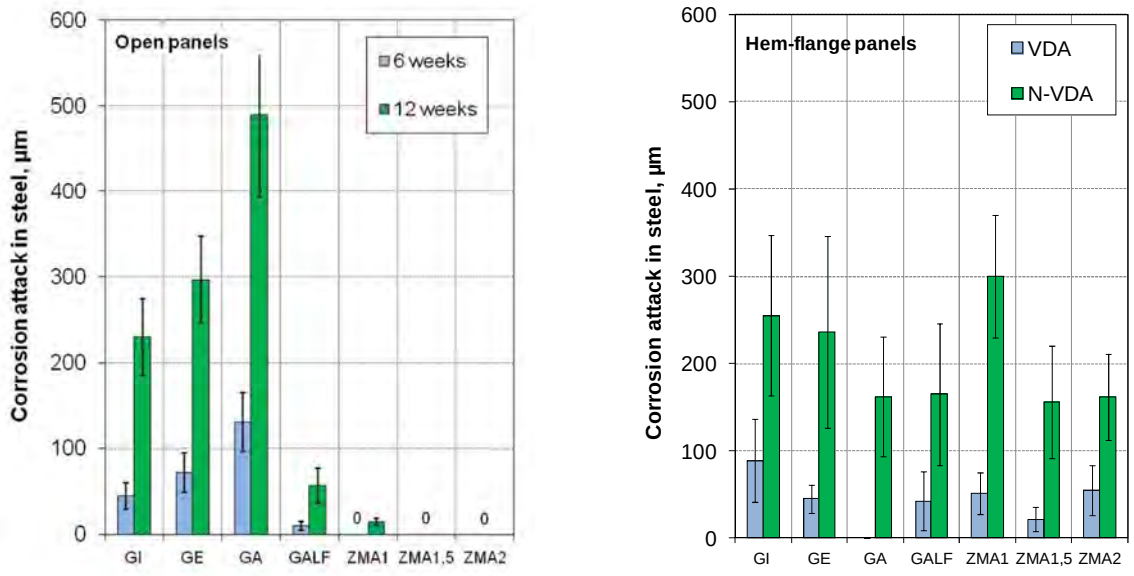

(a) *(b)*

Figure 69: Maximal depth of corrosion in steel as a function of exposure time in the New VDA test for metallic coatings in open (a) and hem-flange (b) configurations.

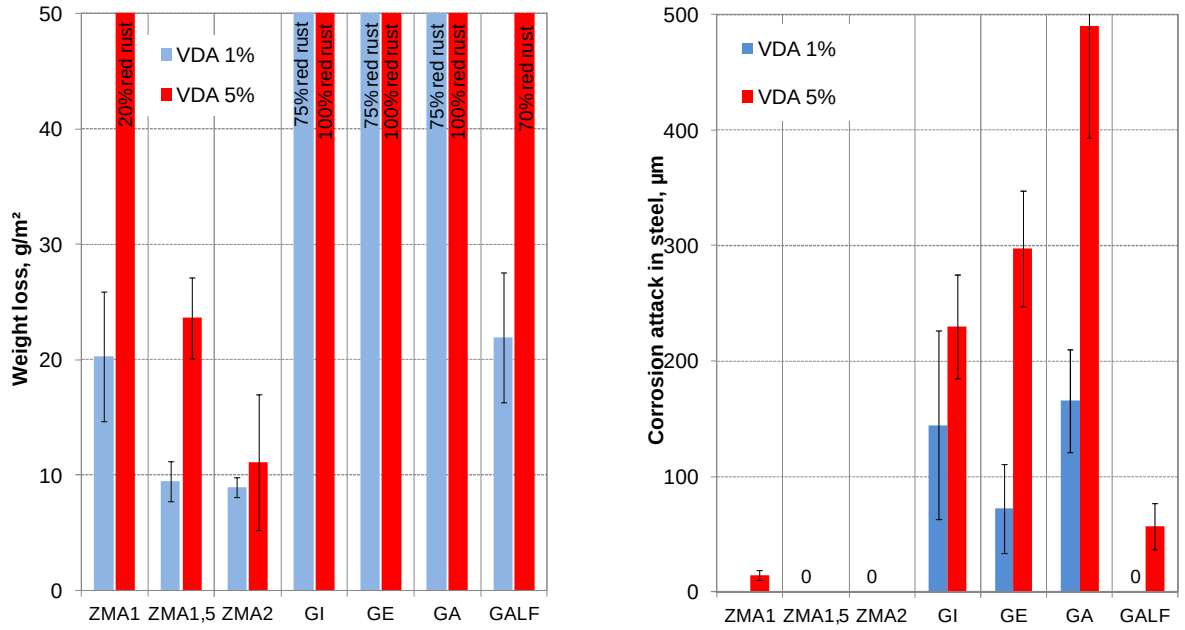

Figure 70: Influence of NaCl concentration (NaCl 5 and 1wt%) in VDA 621-415 cycle on the corrosion of metallic coatings in open configuration. (a): weight loss and (b): maximal depth of corrosion in steel after 12 weeks of test.

2.3.7 WP7 Galvanic protection by Zn-Mg-Al coatings and effect of carbon dioxide

The objectives of WP7 were to understand the role of specific parameters such as carbon dioxide in the corrosion mechanism and the effect on the protective ability of Zn-Mg-Al coatings and to measure the galvanic effect of coupled ZMA and various fasteners in comparison to conventional zinc coatings. The results were reported in **deliverable D13**.

2.3.7.1 Task T7.1: Effect of carbon dioxide

The experiments and FTIR analysis were conducted at IC while XRD and SEM/EDX analysis were further carried out at MPIE.

2.3.7.1.1 Experimental

Sample preparation - **ZMA2**, **GI** and **Galfan** coated steel were used in these experiments. In some cases, pure aluminium and pure magnesium were also tested. The samples had a geometry of 50x50 mm with a test surface of approximately 16 cm² (40x40 mm) due to the edge protection. Before exposure, the samples were ultrasonically cleaned in heptane, dried in air and stored in a dessicator over silica gel for 24 hours before being weighed. Then, the edges were protected in order to avoid any corrosion of steel at the cut-edge. NaCl was added by spraying a given volume of solution of methanol containing NaCl to get three different surface concentrations e.g. 1, 0.5 and 0.2 g/m² of chloride (Cl^-). The surface concentration of NaCl was verified by weighing the samples after 24 hours storage in dessicator. In each experiment, 5 parallel samples were exposed among which 3 were used for the metal loss calculation and 2 for the corrosion products analysis. In addition, two samples without chloride were used as blanks.

Experimental set-up - The experimental set-up consisted of a transparent cell of 39 L immersed in a water tank held at a selected temperature e.g. 20 or 30 °C. The samples were exposed in horizontal position. The gas flow was 5 L/min. Relative humidity was regulated by mixing dry air and air saturated in vapor to get 85-90 % R.H.. In the experiments without CO_2 or with low CO_2, the air was purified by letting it pass through filters before entering the system. A concentration of less than 3 ppm was achieved. In the experiments with CO_2, no CO_2 adsorber was used, thus a concentration of 350-400

ppm of CO_2 was measured. In all cases, the exposure duration was limited to 14 days in order to avoid red rust to form. Preliminary experiments in CO_2 free atmosphere with 1g/m² of chloride have indeed shown that red rust was formed after 15 to 16 days of exposure on ZMA2.

Methods of evaluation - After completion of the exposure, the sample were dried into the exposure cell for about 4 days by introducing dry air or CO_2 free air (RH < 10 %) before being weighed (dry mass gain). Water soluble corrosion products and unreacted NaCl were first removed by leaching in pure water for 3 min. Then, the samples were pickled in saturated glycine for up to 20 min in order to remove the corrosion products and the weight loss of the metallic coating was gravimetrically calculated. The amount of Cl^- in water or glycine was determined by ion chromatography (detection limit below 12 mg/m²). On one sample, the surface pH was visually mapped by placing a thin layer of agar containing a wide range of pH indicator (WRI). Details on the preparation of the WRI agar may be found elsewhere [13]. This allowed a visualization of the anodic and cathodic area upon the material and exposure conditions. FTIR, XRD and SEM/EDX techniques were also used to analyze the corrosion products.

2.3.7.1.2 Results

Figure 71 presents the metal loss of the different metallic coatings e.g. ZMA2, GI and Galfan after 2 weeks of exposure at 90% R.H. with or without CO_2 in presence of different concentrations of chloride. The experiments in CO_2 free atmosphere were carried out at 20 and 30 °C. The results of Figure 71 show an obvious impact of carbon dioxide on the corrosion of zinc coatings where an enhancement of the corrosion rate may be observed in low CO_2 conditions whatever the coating. This is in good agreement with the work of Lindström and co-workers which studied the influence of CO_2 on pure zinc [14]. The metal loss increases with the concentration of surface chloride as expected. It is also interesting to note that no major differences were observed upon the metallic coating and testing conditions e.g. with or without CO_2 when the samples were contaminated with a low amount of chloride e.g. 0.2 g/m². For higher chloride concentrations, the metal loss varies upon the metallic coating and CO_2 level. Thus, in air conditions, GI presented as expected a higher metal loss than Galfan and ZMA2, ZMA2 showing the best behavior, in good agreement with previous studies conducted in similar conditions [15]. The situation is totally reversed when the experiments are conducted in CO_2 free atmosphere, here ZMA2 coating showed more metal loss than conventional zinc coating. These results were observed at both temperatures 20 and 30 °C with an obvious tendency to induce more metal loss when increasing the temperature, as expected. The importance of CO_2 on the corrosion of the different zinc metallic coatings is indeed clearly visible on the photographs of the samples after the test at 30°C in presence of 1 g/m² of chloride, see Figure 72.
In order to highlight the influence of CO_2, the ratio of the metal loss low CO_2/Air was plotted in Figure 73 for the different metallic coatings versus chloride concentration after 2 weeks at 90 % R.H.. Thus, in the absence of CO_2, the metal loss was approximately 2 times higher on GI coating whatever chloride concentration compared to CO_2 containing air. It is remarkable to underline that this ratio is higher when considering ZMA2 or Galfan coating and is increasing with chloride concentration, particularly on ZMA coating where a metal loss 12 times higher was measured at the highest concentration in CO_2 free atmosphere compared to air.
Additional experiments on the influence of CO_2 have also been conducted on other ZMA coatings using Rhesca samples in order to study the effect of Zn and Mg content (from 1% to 4%). Similar observations as for ZMA2 were drawn for ZMAR1 and ZMAR4 in terms of corrosion behavior versus GI coating, with however a trend to form more localized corrosion on ZMAR4.

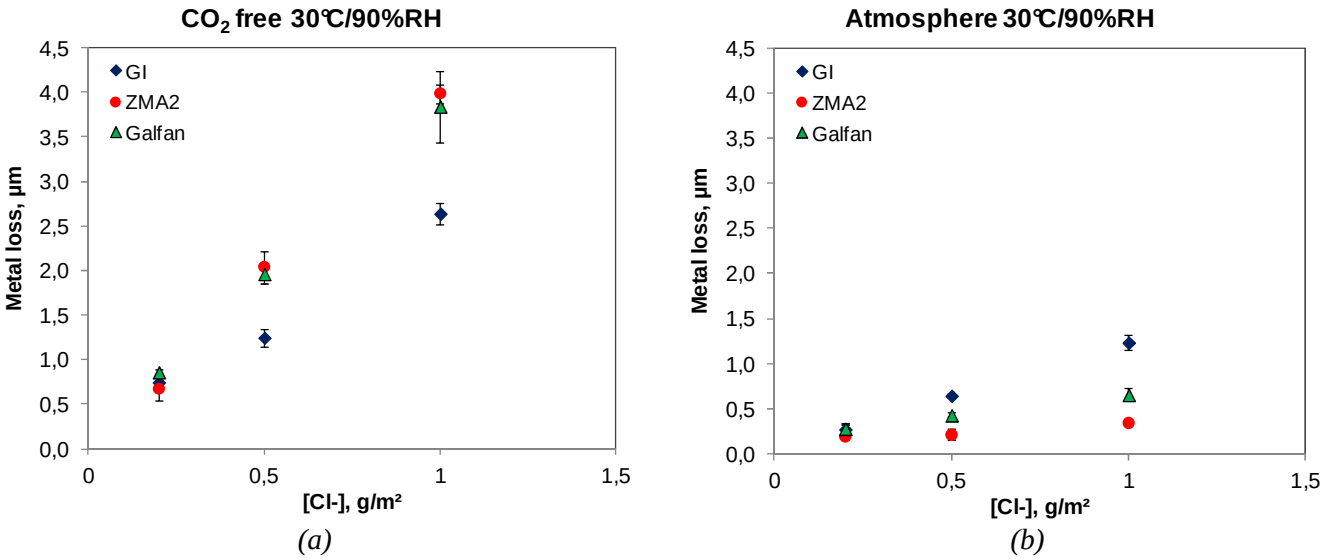

Figure 71: Influence of CO_2 and temperature on the weight loss of metallic coated steel in open configuration exposed 14 days at 85-90 % R.H.. (a): CO_2 free – 30 °C, (b): Atmosphere – 30 °C, (c): CO_2 free – 20 °C.

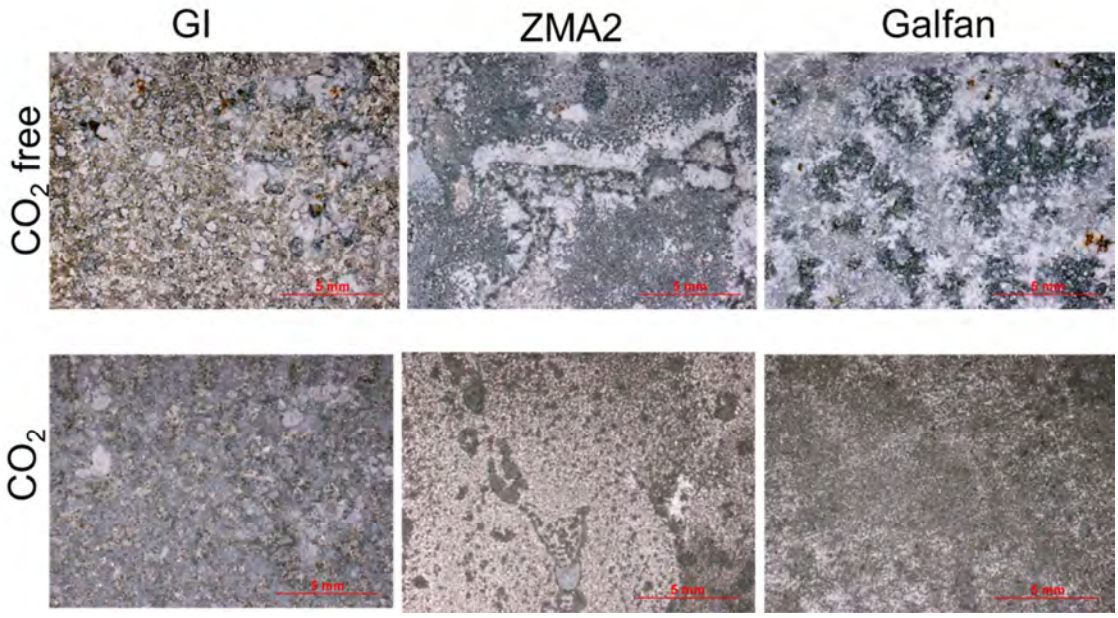

Figure 72: photographs of GI, ZMA2 and Galfan coated steel after 2 weeks of exposure at 30°C and 90% R.H. in presence of 1 g/m² of chloride. Influence of CO_2 content.

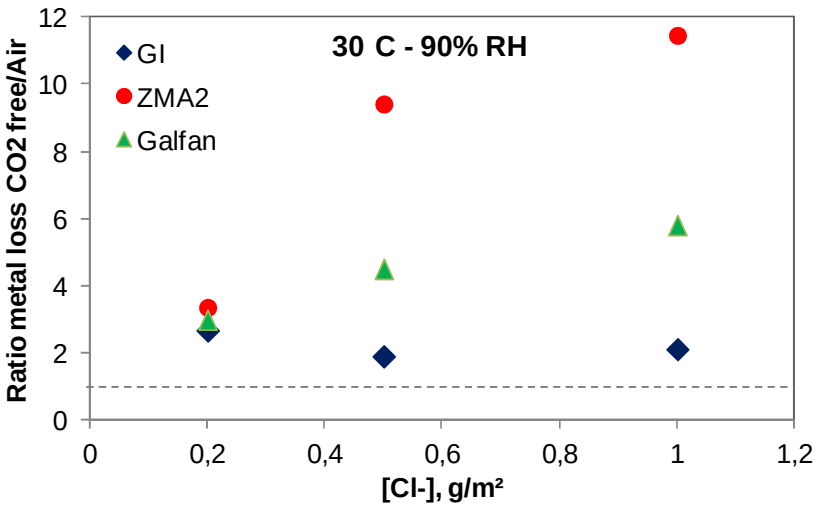

Figure 73: Ratio of the metal loss CO_2 free/Air as a function of NaCl concentration. 30 °C, 90 %R.H..

As indicated in Figure 74, the fraction of water soluble chloride was also measured upon testing conditions and metallic coatings. Thus, only a small fraction of water soluble chloride was found on GI coating in CO_2 containing air indicating that most of the chloride is incorporated in the corrosion products as insoluble form, while in CO_2 free atmosphere, most of chloride was water soluble. This is in line with the composition of the corrosion products summarized in

Table 22 which are extracted from FTIR analysis and XRD measurements (Figure 107 of appendix 2). This last figure shows the relative amount of zinc corrosion products on GI coated steel as a function of exposure conditions, based on XRD measurements in three locations of the corroded surface. Indeed, a predominance of zincite (ZnO) was noticed on GI in the absence of CO_2 while simonkolleite ($Zn_5Cl_2(OH)_8$ H_2O) and hydro-carbonates ($Zn_4CO_3(OH)_6$ H_2O) were the main compounds formed in CO_2 containing conditions. Some traces of carbonate containing compound were also found in CO_2 free atmosphere probably because the concentration of CO_2 was not zero. Note that hydrozincite was not detected in XRD presumably due to its amorphous structure.

Regarding ZMA2 and Galfan coatings, it is interesting to note that the fraction of water soluble chloride is significantly more important when exposed to CO_2 containing air than in low CO_2 conditions, while it was opposite on GI materials. This is in line with the low metal loss measured on ZMA2 in air. As summarized in

Table 22, layered double hydroxides (LDH) and simonkolleite were identified on ZMA2 as the main compounds in the absence of CO_2 while some hydroxy carbonate and simonkolleite were dominating in air. These observations are based on FTIR spectra (Figure 108) and XRD analysis (Figure 109) presented in appendix 3. On Figure 109, as for ZMA2, the relative amount of zinc corrosion products (from XRD measurements) was plotted as a function of exposure conditions (with or without CO_2) on ZMA2 coatings. The figure undoubtedly shows the presence of LDH in CO_2 free conditions, its amount increases with the concentration of NaCl.
An obvious pH effect was noticed on Figure 75 which shows the surface pH measured using an agar containing pH indicator that was applied on the different samples after the experiments. From the figure, it is clear that in the absence of CO_2, the pH became very alkaline (see the dark blue area) for all investigated metallic coatings. From this figure, it is also obvious that most of the exposed surface is at alkaline pH. This is in contrast to the pH measured in air with CO_2, which remained in the neutral region apart from some localized areas indicated by a blue colour in the picture.

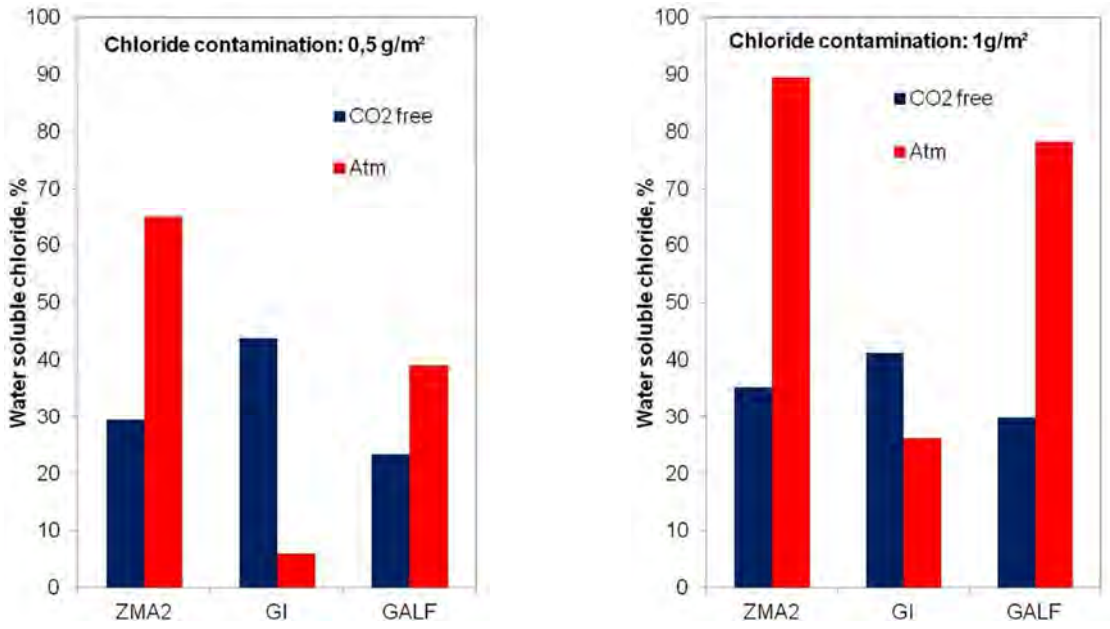

Figure 74: Water soluble chloride in corrosion products formed on zinc coated steel after 2 weeks if exposure at 30 °C and 90 % RH. Influence of CO_2 and chloride concentration.

Table 22: Summary of major compounds identified by XRD and FTIR spectroscopy in the corrosion products formed on GI and ZMA2 upon CO_2 level and NaCl concentration. The main corrosion products are in bold.

Material	Exposure conditions	Chloride concentration	Detected phases
ZMA2	Low CO_2	0.2 g/m^2	**$Zn_{0.61}Al_{0.39}(OH)_2(CO_3)_{0.195}\cdot H_2O$ (LDH)** $Zn_5(OH)_8Cl_2\cdot H_2O$ **ZnO**
		1 g/m^2	$Zn_{0.61}Al_{0.39}(OH)_2(CO_3)_{0.195}\cdot H_2O$ (LDH) $Zn_5(OH)_8Cl_2\cdot H_2O$ **ZnO**
	Ambient	0.2 g/m^2	$Zn_5(OH)_8Cl_2\cdot H_2O$ $Zn_5(OH)_6(CO_3)_2$
		1 g/m^2	$Zn_5(OH)_8Cl_2\cdot H_2O$ $Zn_5(OH)_6(CO_3)_2$ LDH (traces)
GI	Low CO_2	0.2 g/m^2	$Zn_5(OH)_8Cl_2\cdot H_2O$ **ZnO**
		1 g/m^2	$Zn_5(OH)_8Cl_2\cdot H_2O$ **ZnO**
	Ambient	0.2 g/m^2	$Zn_5(OH)_8Cl_2\cdot H_2O$ **$Zn_5(OH)_6(CO_3)_2$**
		1 g/m^2	$Zn_5(OH)_8Cl_2\cdot H_2O$ **$Zn_5(OH)_6(CO_3)_2$**

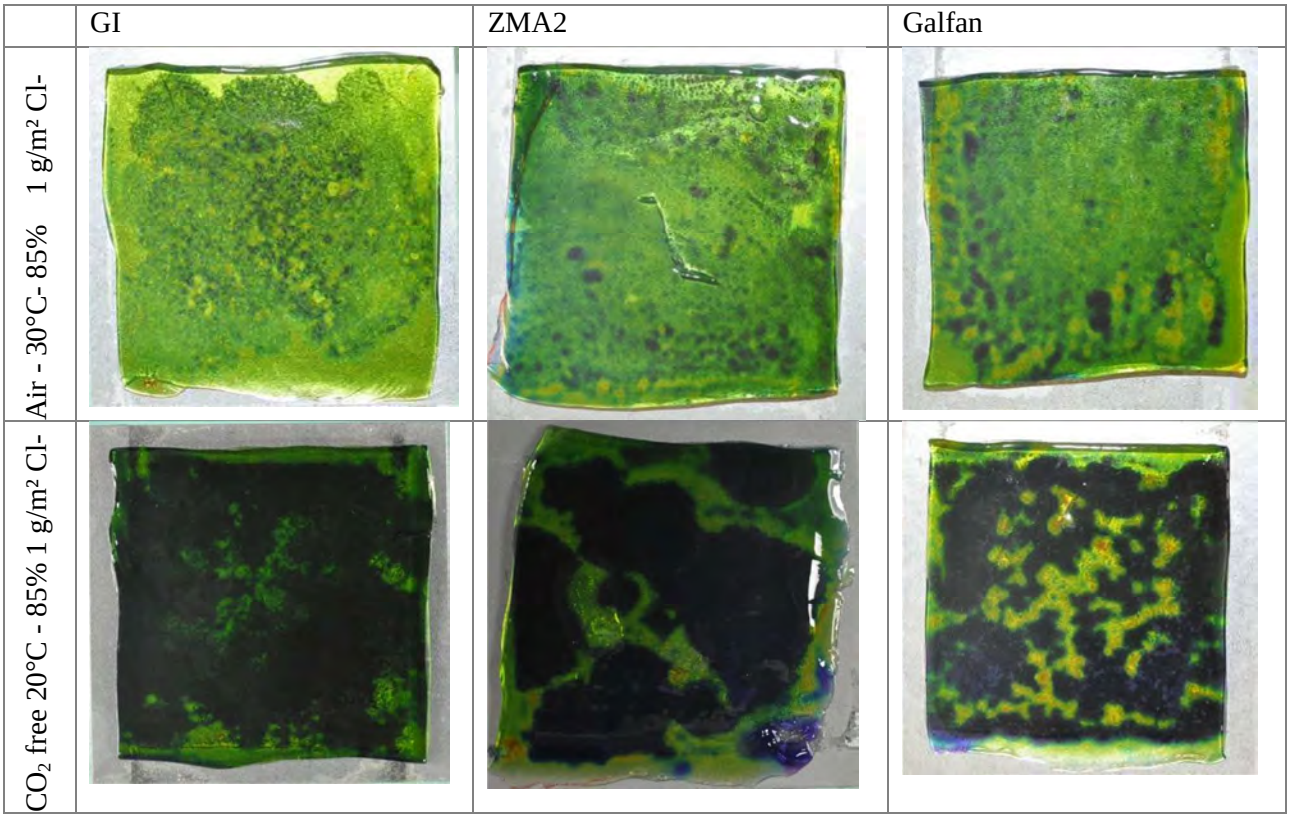

Figure 75: Photograph of surface pH from WRI containing agar after exposure on corroded GI, ZMA2 and Galfan metallic coating in top: Air at 30°C/85% RH and bottom: CO_2 free at 20°C/85% RH. 1 g/m² Cl^-. Dark blue = pH 10 or more; green: pH 7; red: pH 4.

2.3.7.1.3 *Discussion*

- Atmospheric corrosion of ZMA2 in the presence of CO_2

The mechanisms of atmospheric corrosion of zinc and hot-dip galvanised steel in chloride containing conditions have been studied in details by different authors [14, 16-20]. The corrosion of zinc starts with the oxidation of zinc at anodic sites. The hydrolysis of the Zn cations may locally lead to a slight decrease in pH locally according to equation (1) and explains the formation of ZnO. Simonkolleite is thus formed at anodic sites due to migration of chloride to anodic sites according to equation (2) or (3):

$$Zn^{2+} + H_2O \rightarrow ZnO + 2H^+ \quad (1)$$

$$5ZnO + 2\,Cl^- + 6H_2O \leftrightarrow Zn_5(OH)_8Cl_2H_2O + 2OH^- \quad (2)$$

$$5Zn^{2+} + 2Cl^- + 9H_2O \rightarrow Zn_5(OH)_8Cl_2H_2O + 8H^+ \quad (3)$$

Due to the presence of CO_2 in air (typically 350-400 ppm), carbonates are often reported as corrosion products of zinc and hot-dip galvanised steel. The formation of carbonates depends on the adsorption of carbon dioxide into the surface electrolyte and the formation of bicarbonate and carbonate according to reactions (4-6) resulting in a decrease of the surface pH.

$$CO_2(g) + 2OH^- \leftrightarrow CO_3^- + H_2O \quad (4)$$

$$CO_2(aq) + H_2O \rightarrow HCO_3^- + H^+ \quad (5)$$

$$HCO_3^- \leftrightarrow CO_3^{2-} + H^+ \quad (6)$$

The formation of zinc hydroxicarbonates at the cathodic sites is possible according to reactions (7):

$$5\,Zn^{2+} + 2CO_3^{2-} + 6OH^- \leftrightarrow Zn_5(OH)_6(CO_3)_2 \quad (7)$$

It should also be noticed that even simonkolleite may undergo some transformations into hydrozincite during the carbonatization of the surface according to reaction (8).

$$Zn_5(OH)_8Cl_2H_2O + 2HCO_3^- \leftrightarrow Zn_5(OH)_6(CO_3)_2 + 3H_2O + 2Cl^- \quad (8)$$

The results obtained in this work for hot-dip galvanised steel are in good line with the literature on the subject. Indeed, simonkolleite and hydrozincite were found as the main corrosion products, independently on the applied chloride concentration. As shown in Figure 75, the surface pH remained rather neutral promoting the formation of these corrosion products. In the case of ZMA2, similar corrosion products were found as on GI. It should be noticed that under these exposure conditions, the relative performance of ZMA2 compared to GI steel was largely dependent upon the surface chloride concentration (e.g. better performance at higher chloride concentrations). This is in good agreement with data presented in WP 6 as well as on the literature on the subject showing that the relative performance of zinc magnesium aluminium coated steel is generally superior to HDG in harsh environments [21]. It is generally accepted that Mg and Zn are dissolved selectively from the coating whereas the dissolution of aluminium is linked to an increase of the local pH at cathodic sites. In a recent paper, Persson *et al*. have shown that LDH are formed on ZMA2 coating within a few hours of exposure under rather similar exposure conditions, indicating under these exposure conditions that the local pH increases sufficiently to dissolve Aluminium [22]. This is in contrast to the results reported by Volovitch *et al.* who indicate two steps mechanisms of corrosion of Zn2-4%Mg2-4%Al coating with the formation of LDH at the later stage [23]. It should be noticed that a direct comparison of the work of Persson *et al.* [22], Volovitch *et al*. [23] and the present work is rather difficult as exposure conditions and duration are different as well the composition of Zn-Mg-Al coating in [23]. As seen in Figure 2.3.2-9 of task 2.4, Al was enriched in the surface layer of ZMA2. It is thus possible that at the very initial stage as reported by Persson *et al.,* more aluminium is dissolved favouring the formation of LDH. At later stage, the corrosion rate seems to be more governed by the dissolution of zinc with the formation of zinc corrosion products as observed in this work.
On the other hand in very harsh conditions such as the VDA corrosion test or the neutral salt spray, LDH seems to be formed probably due to an increase of the local pH leading to a higher dissolution of the surrounding aluminium phase [12, 21]. Thus, from this work as well as other work on the subject, it seems that the nature of the corrosion products formed on ZMA2 depends largely upon exposure conditions and are most likely only the reflect of the local pH generated at the cathodic sites. As presented in Figure 71, the corrosion rate of ZMA2 in CO_2 containing atmosphere was low independently on the surface chloride concentration. On the contrary, a strong dependency of chloride surface concentration was seen for HDG coated steel. Moreover, as inferred from Figure 74, most of the chloride is bonded in the corrosion products for HDG steel whereas it is unreacted in the case of ZMA2 coated steel. It is likely that this reflects an increasing surface pH on HDG steel compared to ZMA2 when increasing the surface chloride concentration.

- Atmospheric corrosion of ZMA2 in the absence of CO_2

In the absence of CO_2, the corrosion rate of HDG steel increased by a factor of 2-3 depending upon the surface chloride concentration. This is in good agreement with the data of Lindström *et al.* obtained on pure zinc [14]. It should be noticed that a similar ratio (e.g. 2-3) was also found for pure magnesium in the present study. The presence of up to 40-45% water soluble chloride without CO_2 compared to 5-20% with CO_2 seems to indicate a decrease in the amount of simonkolleite formed and that the surface conductivity was high in low CO_2 environments. It should be noted that in CO_2 free environments, the corrosion became more localised (see Figure 76) with large cathodic areas. As summarized in

Table 22, zincite was the dominating corrosion products for HDG steel in CO_2 free environments indicating a high pH on the surface due to an increase cathodic activity (as also observed in Figure 75). The results obtained with ZMA2 coating in CO_2 free environments clearly indicate that the performance of this coating was inferior to HDG steel under these conditions. It should also be noted that the

corrosion rate of ZMA2 was close to that of Galfan at both 20 and 30°C and independent on the surface chloride concentration. This seems to indicate that the poor performance of ZMA2 in this environment is linked to its aluminium content. Indeed, as observed by Bengtsson *et al.*, aluminium and aluminium alloys show a rapid corrosion in CO_2 free environments due to an increased pH at the cathodic sites [24, 25]. The increased rate of dissolution of aluminium in the case of ZMA2 coating in CO_2 free atmospheres was confirmed by the presence of large amounts of LDH in the corrosion products. This together with the presence of zincite seems to indicate that the pH was very alkali under these conditions. This has been confirmed by the surface pH measurements as shown in Figure 75. Hence, it is possible that under these conditions, aluminium is dissolved due to an increase pH at the cathodic areas. In a recent paper by Persson *et al.*, a mechanism of corrosion of ZMA2 was proposed for the first stages in chloride containing atmospheres [22]. In that situation, the corrosion product formation is a result of the anodic dissolution of Zn-$MgZn_2$ phases and cathodic oxygen reduction taking place on the Zn phase. It is proposed here that the high pH at the cathodes also leads to significantly higher pH at the boundaries where Al-rich phases are located which induces a rapid dissolution of the aluminium oxide. It cannot be excluded that the cathodic reaction of oxygen reduction also takes place on the aluminium rich phase. This has led to a poor performance of ZMA2 under these conditions. A similar mechanism is probably valid for Zn-5%Al coating as this material also shows very poor performance in CO_2 free atmospheres.
The present results are important for the application of zinc magnesium aluminium coated steel as situations where CO_2 can be depleted may be encountered in practical applications such as in hem-flanges. This is the subject for further investigations in our laboratory.

The present results constitute key indications on the mechanisms of corrosion of ZMA coatings and will be discussed in task 8.1 as well.

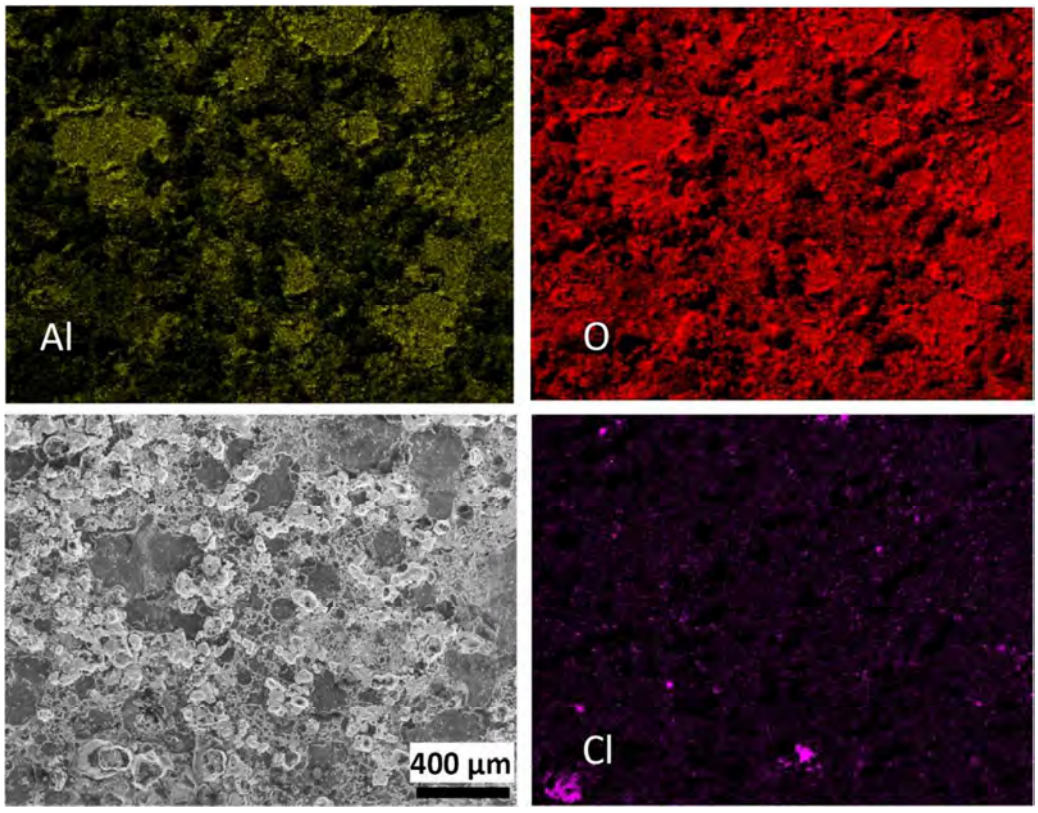

Figure 76: SEM and EDX map of the surface of a ZMA2 sample contaminated with 1g/m^2 Cl^-, exposed to low CO_2 atmosphere.

2.3.7.2 Task T7.2: Galvanic protection

2.3.7.2.1 Experimental

The galvanic protection of ZMA coating was compared to conventional zinc coatings in assemblies with fasteners of different natures in order to simulate on-vehicle situations. Thus, fasteners of steel, austenitic stainless steel A70 and Zn-Ni (16-18% Ni), Geomet, ZEC coat 888 (Zn flake + silane top coat) coated steel were used and mounted on different zinc coated plates following a Renault standard (02.00.006) currently used to study bi-metallic corrosion with screws. It should be mentioned that steel screws were selected as reference where the strongest galvanic coupling was obviously obtained. The screws were mounted on the different plates at a given torque of (10 ± 0,2) Nm. See Figure 77.

The corrosion of the ZMA plate around the fastener was evaluated by assessing the extent of white and red rust using an image analysis software as well as the corrosion attack in the substrate by measuring the maximum depth of attacks in steel using a micrometre gauge once the corrosion products have been removed by pickling. The corrosion attack in steel substrate was only possible when the metallic coating was fully consumed.

Figure 77: photograph of parts (galvanic corrosion), M8 fastener and evaluation areas around the hole.

The extent of corrosion of ZMA coatings in galvanic coupling with different fasteners has been studied in accelerated corrosion tests (N-VDA) and in field exposures including stationary sites (for 1 and 2 years), under the trucks driving in Switzerland as well as after FIAT proving ground test.

In addition, the galvanic current between ZMA1.5 coating and the different bolt materials was measured in 3% NaCl solution using a Gamry 600 potentiostat. The area of ZMA1.5 was 10 cm² while that of the bolt was about 1 cm².

2.3.7.2.2 Results

2.3.7.2.2.1 Accelerated corrosion tests

Photographs of the samples after 6 weeks of New VDA test are presented in of the annex for the different metallic coatings, see Figure 103 of appendix 1. It may be observed full coverage of red rust on GI (and GE) and GA coatings while ZMA coatings and to some extent Galfan are obviously less affected. From the photographs, it is not easy to see how much affected is the area around the screws. However, the evaluation of the corrosion attacks in steel in the vicinity of the different screws once the corrosion products were chemically removed allows drawing some conclusions (see Figure 78). As expected, steel screws induced the deepest corrosion attacks on all metallic coatings with a tendency for ZMA and Galfan coatings to be less affected, particularly on ZMA1.5 due the thicker coating (11 µm). The corrosion attack was in general more pronounced under the screw head (distance 0.5 cm) where a confined area was generated. A rather satisfying behaviour of ZMA coatings as well as Galfan when in contact with stainless steel, Zn-Ni coated steel, ZEC 888 or Geomet coated steel screws was noticed, while conventional coatings provided less galvanic protection. It should be noted that GE coating was highly degraded whatever the nature of the screws, showing corrosion attacks in the range of measured value on open and hem-flange panels (see mid-term report). It cannot be excluded that the torque of 10 Nm may have damaged the metallic coating locally.

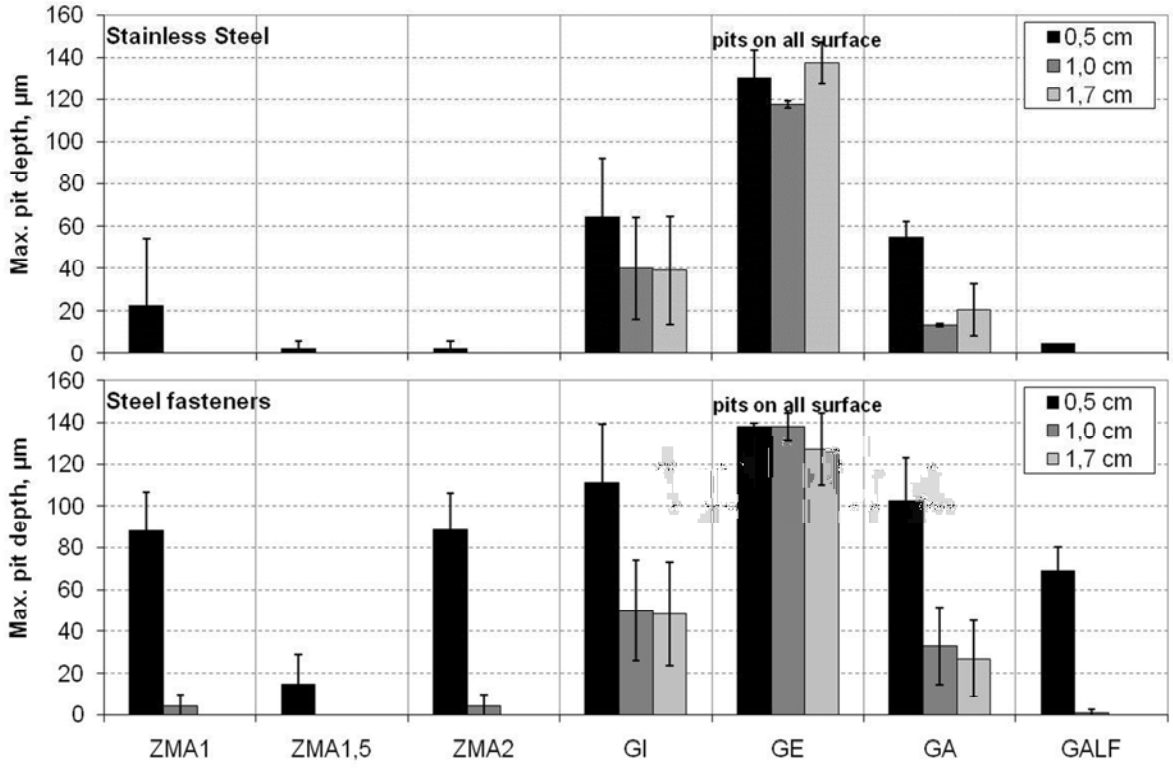

Figure 78: Max depth of attacks in steel around the screws after 6 weeks of NewVDA test. Examples of galvanic coupling with steel and stainless steel fasteners.

2.3.7.2.2.2 Field exposures

Contrarily to what was observed in the accelerated corrosion test (New VDA) where significant corrosion attack was measured when connected to steel screw, rather low extent of corrosion was generally noticed on ZMA and conventional zinc coatings whatever the field exposure.

In particular, one and two years of exposure on **operating truck in Switzerland** did not induce much corrosion even when galvanic coupled to steel fasteners. Photographs of the different samples may be observed in Figure 104 of appendix 1. The kinetics of degradation are obviously slow.

The situation was different on the materials exposed in **FIAT proving ground** where more significant corrosion extent could be observed. Nevertheless, it was difficult to visually evaluate the corrosion exclusively due to the galvanic coupling from the corrosion of the coating itself. The depth of attack in steel substrate ranged between 10 and 20 µm whatever the metallic coating when coupled to steel fasteners. When in contact with the other types of fasteners, no attack in steel substrate was noted.

As shown in Figure 105 of appendix 2, the exposure in **marine atmosphere** resulted in localized corrosion of the metallic coating in the vicinity of the fastener forming a ring of white or/and rust corrosion when connected to steel fasteners in particular. GE coating was visually the most degraded coating followed by ZMA1. Rather comparable results were observed on GI and ZMA1.5 and ZMA2. Much less attacks were observed when galvanic coupled to stainless steel fasteners where only GE showed some red spots. White rusting was visible around the fastener on ZMA coating in quantity slightly larger than on GI. Same observation may be drawn when connected to Zn-Ni coated steel fasteners. After two years of exposure in the marine site, more corrosion of the metallic coatings may be observed. The extent of white and red oxidation around the different fasteners has thus been quantified using an image analysis software. The results are given in Figure 79 for all fasteners and all metallic coatings after 2 years of exposure while Figure 80 presented results with steel fasteners where the strongest galvanic coupling was obviously obtained. As regards to the galvanic coupling with steel fastener, whereas there are no major differences between ZMA and GI at comparable thickness, the extent of white and red oxidation formed on ZMA coatings has a tendency to be slightly larger than on GI coating. A slightly better protection was observed with thicker ZMA coating (ZMA1.5). Galfan

coating provided slightly better protection (less red rust) and comparable extent of white oxidation while GE and GA coatings where the most affected ones. No or very low degradations were observed on ZEC 888 and Geomet coated steel fasteners, commonly used by the car industry in the manufacturing of vehicles.

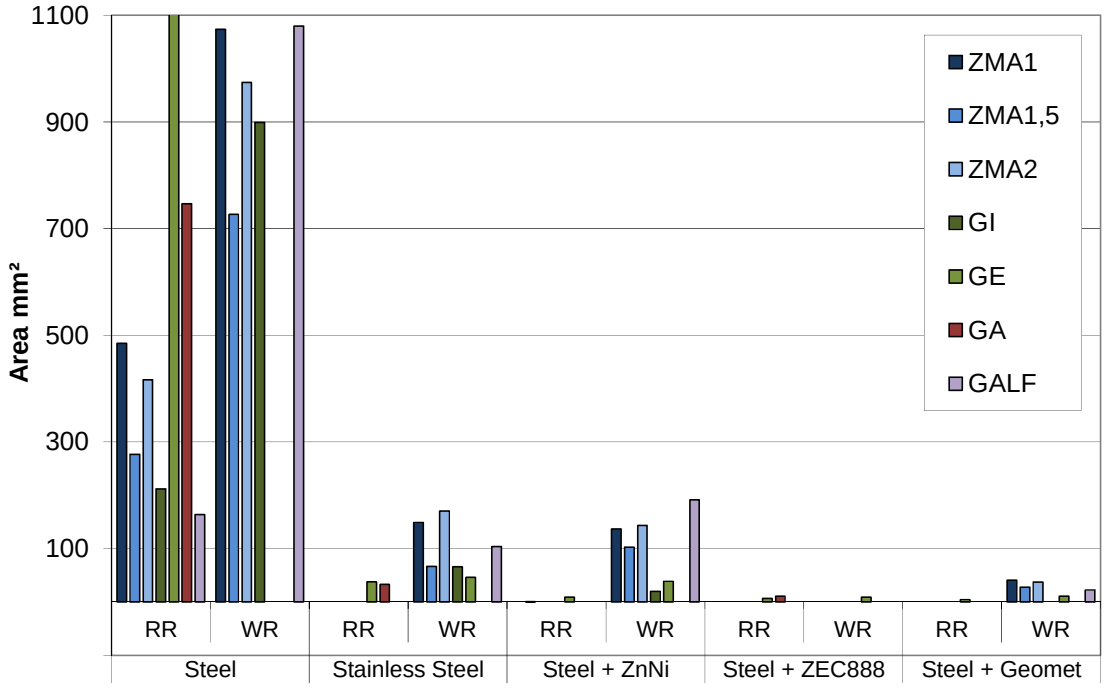

Figure 79: Extent of white and red oxidation around different fasterners in galvanic contact to ZMA, GI, GE, GA and galfan coated steel panels after 2 years of outdoor marine exposure.

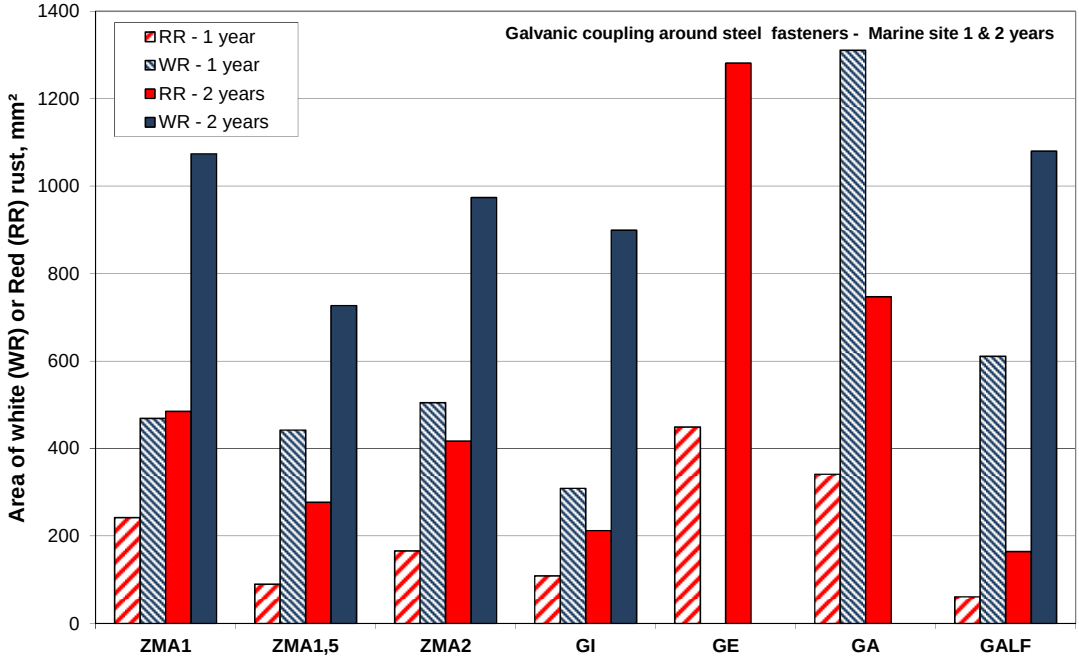

Figure 80: Extent of white and red oxidation around steel fasterners in galvanic contact to ZMA, GI, GE, GA and galfan coated steel panels after 1 and 2 years of outdoor marine exposure. WR: white rust; RR: red rust.

The other field exposures in **Dortmund** and **Linz** sites did not reveal much degradation after 2 years of exposure, as expected from the lower corrosiveness of the environment compared to the marine site.

Photographs of the metallic coatings around the different fasteners are presented in Figure 106 of appendix 2. Additional exposure duration will be conducted after the end of the project.

The results obtained in the field are explained by the strength of the galvanic coupling between zinc coatings and the fasteners. Few electrochemical experiments in NaCl solutions were indeed conducted focusing on one ZMA coating e.g. ZMA2. The results are presented in Figure 81 concerning the galvanic current and the potential. As regards to the potential difference measured in NaCl solution, the most dangerous coupling was obviously observed with uncoated steel fasteners while no important potential differences were obtained with ZEC and Geomet coatings, both being based on zinc. When measuring the galvanic current between ZMA and the different fasteners, the highest current was measured with uncoated steel bolt as expected, which induces in a higher zinc coating consumption as it has been observed in accelerated tests and marine field exposure. Much lower galvanic currents were observed with zinc coated fasteners as expected. It is interesting to underline that excepted on ZnNi coating, the galvanic current showed a tendency to increase when half of the bolt was removed from the solution. This is explained by the enhanced access of oxygen to the cathode surface in presence of a thin electrolyte film for area of the fasteners in atmosphere. The ratio cathode/anode will also influence the consumption of the coatings. Considering ZnNi coated bolt, rather low galvanic current was measured while the potential difference was high.

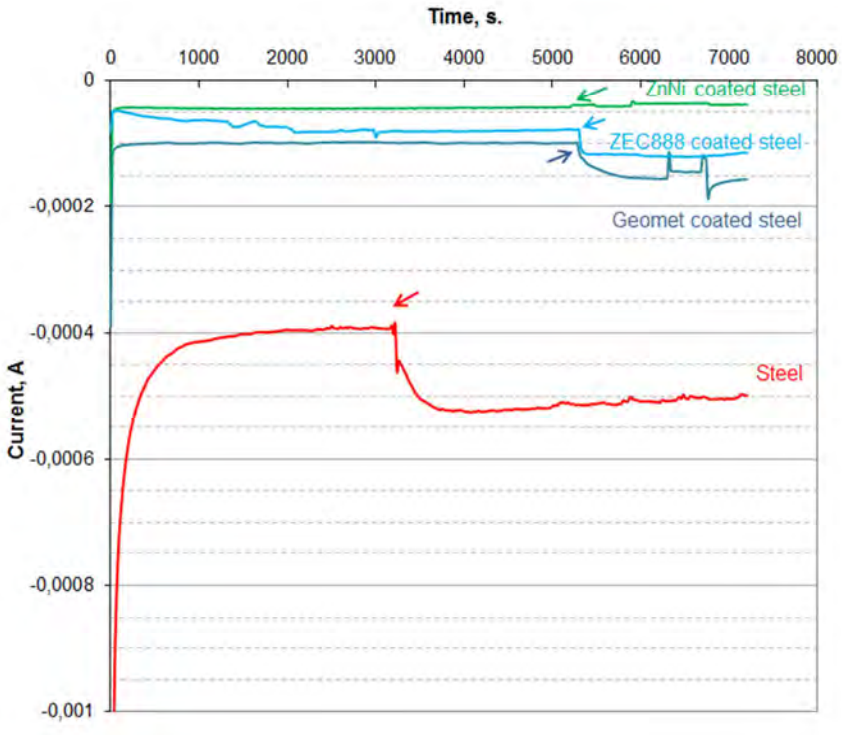

Rest potential and potential difference comp. to ZMA

mV/SCE	E	ΔE
ZMA2	-1080	
Geomet	-1050	30
ZEC 888	-1040	40
ZnNi	-840	240
C-steel	-620	460

A: bolt in solution

Galvanic current

µA	A	B
Steel	400	500-520
Geomet	90-100	150-160
ZEC 888	80	110
ZnNi	40-45	35

A: bolt in solution
B: ½ of the bolt is out of the solution

Figure 81: Left: galvanic current vs. time between ZMA and bolts in 3% NaCl solution. The arrow indicates the time when half of the bolt is taken out of the solution. Right: summary of potential and potential difference in 3% NaCl and galvanic currents.

2.3.8 **WP8 Modelling, life prediction and application guidelines**

The main objectives of WP 8 were to compile data from laboratory, accelerated, and field tests and to propose mechanisms of metal and paint degradation in order to formulate models describing the corrosion mechanism of ZnAlMg coated materials as a function of exposure conditions, composition, and microstructure. This work package constitutes thus the conclusions of the project.

2.3.8.1 Task T8.1: Mechanism and modelling

In this work package, the possible mechanisms of corrosion protection ZMA coatings, based on the results obtained in WP3 - WP7, are analysed and models for corrosion at initial and later stages are proposed. This analysis will be divided in three subgroups, as sketched out in Figure 82.

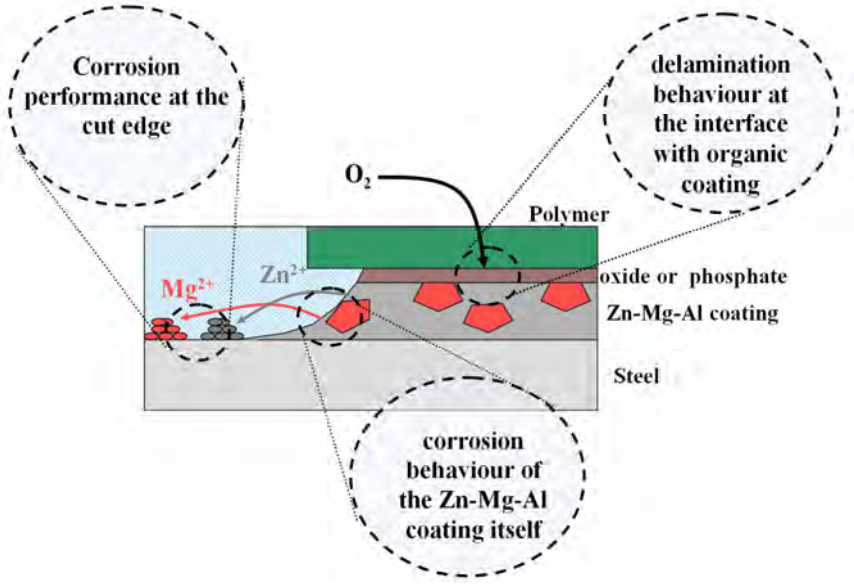

Figure 82: Schematic description of the overall corrosion behaviour of zinc alloy coatings involving (1) the performance at the cut edge (or defect down to steel), (2) the delamination behaviour and (3) the corrosion of the coating itself.

2.3.8.1.1 Part 1: Corrosion performance at the cut edge or scribe

For the corrosion at the cut edge, significant improvements are reported as an effect of Mg additions to the zinc coating, as emphasized in a recent paper from Krieg et al. where a factor of 5 was indeed noticed in chloride containing electrolyte [26]. In this project, relatively high improvement factors of protection at defects were found when testing ZMA coatings in conditions with high salt load (see Figure 61and Figure 62 of WP 6). From the figures, it was also noted that the improvement depends on the aggressiveness of the test: the more aggressive the test, the more significant the effect of Mg addition. Furthermore, it is quite clear that the effect is really a consequence of the magnesium, as aluminium has no effect on the cut edge: GI behaves more or less like GE and Galfan is even performing worst. The reason for the low or even negative effect of aluminium is that, at the alkaline pH established at the defect to steel (cut-edge or scribe), no effect of aluminium is to be expected, as its oxides are stable only in the pH range 4-8. It has been shown that much higher pH are prevailing locally on steel surface at the cut edge [see reference 26 and literature cited therein). The high pH levels are most likely the reason for the especially poor performance of Galfan, as the high content of Al-rich phases is the weak point at high pH.

Interestingly, the positive effect of Mg addition was reached already at the lowest tested amount (e.g. 1wt% Mg) and remains at the same level even up to 2wt% Mg. This is in accordance to the findings recently reported by Krieg *et al.*, where it was found that already very low concentrations of magnesium cations in the corrosive environment are sufficient to enhance the effect that is provided by zinc cations [26]. The effect of the zinc cations is also known as cathodic self-healing as described by Ogle *et al.* [27] and Thébault *et al.* [28]. The precipitation of zinc corrosion products would indeed inhibit the oxygen reduction on the exposed steel, resulting in a decrease of the galvanic current between the large steel surface and the small zinc edge at the cut edge or scribe down to steel, and accordingly a reduction

of the corrosion of zinc coating. Ogle *et al.* also pointed out that the inhibiting effect of the denser zinc corrosion product film formed close to the zinc edge was much better than the one of the more loose looking film formed further away [27]. This difference is certainly due to differences in pH: at the very high pH levels that are prevailing far away from the zinc edge on the steel surface, the precipitating of zinc oxides are not stable and consequently looser films are formed. According to Krieg *et al.*, significant inhibition of oxygen reduction occurred in this region not mainly as a consequence of zinc corrosion products, but due to a modification of the iron oxide covering the exposed steel surface at the high pH values. Even at the low potentials, steel was polarized by zinc: Fe^{2+} cations, which are mainly responsible for the high activity of the iron oxide *vs* oxygen reduction, were exchanged with Zn^{2+} cations from the electrolyte. Thus, the oxygen reduction rates on the surface were significantly inhibited. This effect was obviously enhanced by the presence of Mg cations by a factor of 5 and more, although Mg cations by themselves had only negligible inhibition effect. It is assumed that the explanation for this synergetic effect may lie in the precipitation of MgO on the steel surface which is supposed to facilitate this exchange process. Note that Krieg et *al.* reported that Mg cations without Zn cations did not show a notable protection. It was also reported that the less active the corrosion was and hence the less alkaline the pH on the steel surface, the higher the concentration of zinc cations in the electrolyte on the steel surface and thus, the more pronounced was the effect by the zinc itself. In that situation, the additional synergetic effect by the magnesium cations was less significant; see Krieg et al. [26]. This directly means that the more active the overall corrosion reaction, i.e. the more aggressive the test, the higher should be the effect of the Mg additions.

Hence, it is also to be expected that at later stages of corrosion, where only low activity also of oxygen reduction prevails, the Mg effect vanishes because the effect of the zinc cations themselves cannot be optimized further and also already, a thick corrosion product layer will significantly limit the diffusion of oxygen to the reactive surface, see Figure 83**.**

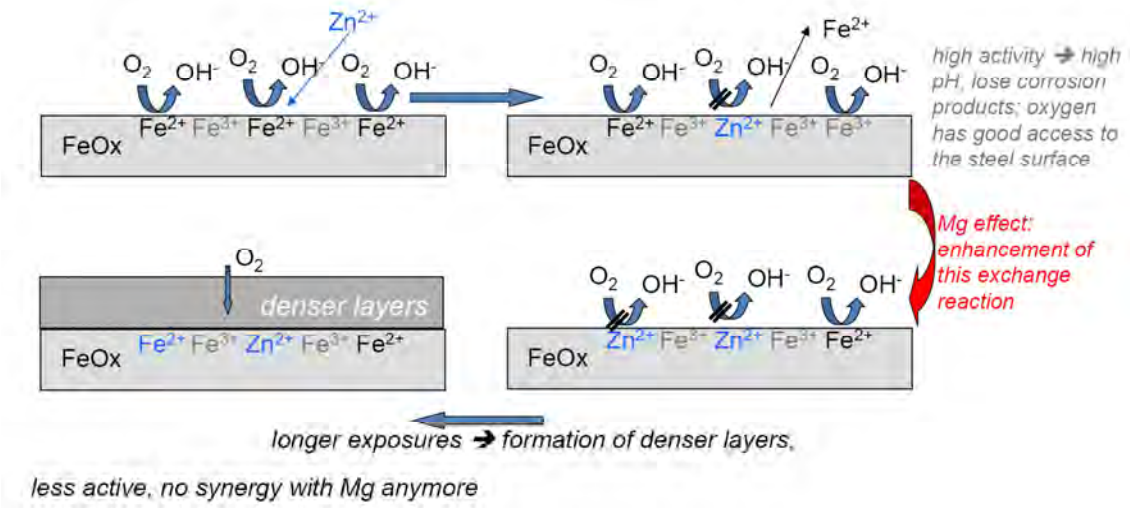

Figure 83: Schematic sketch of the inhibition of oxygen reduction on the exposed steel by zinc cations; at initial stages, it is mainly a modification of the steel surface (which is mainly iron oxide at the prevailing high pH), while at later stages, thicker zinc corrosion product layers have built up, providing a barrier for diffusion of O_2, thus decreasing the overall activity.

This was indeed observed in the field exposure tests (see WP 4, Figure 35). As soon as a dense and thick corrosion product layer is formed on the steel surface, as it is the case here, the promoting effect of Mg is not relevant any more. Also, the appearance of red rust at the cut edge was not much different for ZMA compared to GI after 2 years of exposure in a marine site, see Figure 35 of WP 4. However, these results show that contrarily to the initial stages, aluminium has obviously a positive effect at later stages, as can be seen by the better performance of Galfan in these long term tests. The appearance of red rust is related to the loss of cathodic protection either due to too high loss of zinc coating (according to the scribe delamination, it is not the case) or due to weak protection of the steel surface by the

corrosion product layer covering it during periods of limited protection such as during wetting/drying. Obviously, at later stages once a thick corrosion product layer has formed on the steel surface, the incorporation of stable aluminium corrosion products, thanks to less alkaline conditions, leads to this superior performance. The efficiency seems to be linked to the amount of Al in the metallic coating which is the highest in Galfan (5 wt% Al).

In conclusions, the initial effect of Mg at the cut edge or scribe down to steel is significant and already present for low Mg contents in the ZMA coating, as clearly shown in accelerated corrosion testing. The results of the accelerated tests also show that this is really an effect due to Mg and not Al. After longer exposure times, however, the Mg effect is vanishing. These findings are in accordance with the hypothesis sketched out in Figure 83.

2.3.8.1.2 Part 2: Delamination behaviour at the interface with the organic coating

The results obtained in WP3, T3.3 clearly show that the delamination behaviour under cathodic delamination conditions (performed with model experimental set-up with large artificial zinc defect) as well as the behaviour under conditions with strong anodic delamination driving forces (large artificial steel defect) is not much different for ZMA coatings compared to conventional coatings such as GE or GI. This confirms that the phosphate layers on ZMA coatings are of somehow similar quality than on GE or GI.
Studying the delamination performance of non-phosphated samples was envisioned based on previous findings of an inherent complete inhibition of cathodic delamination as reported by Hausbrand *et al.* for very high Mg-contents such as for $MgZn_2$ phase [3, 29, 30] or of a significant decrease in delamination rate, for medium alloys including Galfan and Zn-Mg-Al alloys in the RFCS project "Zinc Alloys" [2]. However, as described in task 3.3 of WP3, no significant inhibition of the delamination rate was observed on painted non-phosphated ZMA compared to conventional coatings. It was assumed that the alloying content of the line hot dip ZMA coatings investigated in this project (e.g. between 1 and 2 wt% of Al and Mg) was obviously too low in order to produce oxide layers which would ensure inherent delamination-resistant polymer metal interfaces.

2.3.8.1.3 Part 3: Corrosion performance of Zn-Mg-Al coating itself

Introduction

The explanations for an improved corrosion protection of ZMA coatings in comparison to Zn coatings reported in the literature are manifold. In two recently published papers, an effect of the Mg on the formation of a better performing corrosion product layer is proposed [31, 23]. The authors indeed proposed that for Mg-containing coating, the improved corrosion resistance is achieved by a stabilization of protective simonkolleite and zinc hydroxysulfate. According to these authors, Mg^{2+} ions bind the excess of carbonate preventing the formation of soluble or less-protective products. On the other hand, Schuerz *et al.* attributed the improved corrosion performance of ZMA on the formation of zinc aluminium carbonate hydroxide (a layered double hydroxide, LDH) or aluminium rich oxide layer in general [10, 12]. This exemplifies several hypotheses on the possible working mechanisms of Zn-Mg-Al coatings. Already in 2007, Hosking et al. pointed out that obviously the actual improvement of the corrosion performance of Zn-Mg alloy coatings in comparison to zinc coatings depends critically on the corrosion conditions [33].

Other possible mechanisms for the improved performance of ZMA coating can be found in the literature. Some authors proposed that the semiconducting properties of magnesium oxides may play a role in the inhibition of the oxygen reduction rate, as well as in the inherent delamination resistance of polymer coated Mg-rich Zn-Mg-alloys [3, 29, 30, 32]. In the work by Prosek *et al.*, a Mg-rich corrosion product layer was observed to be formed between the metal and the zinc corrosion products [32]. However, under corrosion conditions where water soluble corrosion products can run off the sample, usually no significant amounts of Mg containing corrosion products are found on the corroded samples, as these are quite soluble. Hosking *et al* suggested that the main beneficial effect of magnesium could

be the precipitation of magnesium hydroxide on the surface of the coating, which would reduce the oxygen reduction activity at the cathodic sites. For later stages of corrosion, Hosking *et al.* suggested a gradual conversion of these $Mg(OH)_2$ deposits to more soluble hydroxycarbonates by uptake of atmospheric carbon dioxide. The decrease of the pH by the inhibition of the oxygen reduction is further suggested to promote the formation of simonkolleite on the surface, which is supposed to be very corrosion resistant. This is quite similar to the proposal of Volovitch *et al.*

However, Prosek *et al.* reported that in their experiments, a mixture of simonkolleite and hydrozincite was present in the corrosion products on zinc, while, besides the above mentioned Mg based film adjacent to the metal surface, only hydrozincite was found in the corrosion products on Zn-Mg alloys, i.e. no simonkolleite [32]. Nevertheless, the Zn-Mg alloys were still performing better than the zinc, which questions whether the simonkolleite really can be the key to an explanation for the improved performance of ZMA coatings.

Recently, Diler *et al* [34] suggested that the differences between the results reported by Prosek *et al.* [32] and those of Hosking *et al.* [33] and Volovitch *et al.* [31] are most likely due to the corrosion testing conditions. Indeed, no wet and dry changes were carried in the test of Prosek et al. contrarily to the other studies [31, 33]. Moreover, the vertical arrangement of the samples in the latter works enables corrosion product run-off, while in the work of Prosek *et al.*, the samples were exposed horizontally. Diler *et al.* confirmed that under the testing conditions of Prosek *et al.*, magnesium corrosion products, in the form of magnesium carbonates and hydroxycarbonates were indeed found. In addition, they identified zinc hydroxycarbonate but no simonkolleite. The $Zn(2p_{3/2})$ XPS peak of the latter was found to be at a higher binding energy than for the hydrozincite found for corrosion of zinc in the absence of Mg. Based on their findings on the stability of ZnO and $Zn_{1-x}Mg_xO$ in alkaline solution, they suggested that the inclusion of Mg induces a stronger adsorption of OH groups on the surface, which they propose also to increase resistivity and inhibit charge transfer.

In a recent paper, Persson *et al.* reported the formation of LDH on ZMA coating at very initial stage of atmospheric corrosion (e.g. less than 24 hours) using *in-situ* FTIR spectroscopy [28].

As further possible explanation, Volovitch *et al.* suggested that also the crystallinity of zinc oxides and thus also the morphology and porosity of the corrosion product layer might be indirectly affected by the presence of Mg cations during precipitation even when no Mg is incorporated [31].

In conclusions, it can be stated that depending on the severity of the testing conditions as well as the duration of the test, not only the corrosion performance but also the corresponding corrosion products may vary. Some of the proposed mechanisms, such as buffering of the pH or consumption of CO_2 for stabilizing simonkolleite were usually developed on the basis of results obtained from high Mg-content alloys and certainly require certain minimum amounts of magnesium cations which can be present initially due the surface enrichment of Mg. In others, an effect on the precipitation of zinc corrosion products, i.e. indirectly affecting the crystallinity might work already at lower concentrations and/or longer exposure durations.

Discussion of the results obtained in this project

In this project, quite significant differences were also found in the corrosion performance of ZMA coatings upon testing conditions and configurations. In the following, the performance will be discussed regarding two evaluation criteria: metal loss and time to red rust.
The first criteria refers to the corrosion performance of the coating itself, while the second criteria is rather a mixture of corrosion performance of the coating itself and galvanic protection (as it is the main aspect of cut edge performance).

a) Metal loss on open surfaces

Concerning the corrosion performance of the coating itself, experiments carried out at constant temperature and relative humidity named "static experiments" shall be firstly discussed. Such experments may be taken as reflecting early stages of corrosion under relatively active conditions. Some effect of Mg content is discernible in these tests, although it is not as significant as that observed for cut-edge performance in accelerated corrosion tests. In static experiments conducted in air, the highest protection factor compared to GI (i.e. about 4) was observed in presence of high salt loads, but it should be noted that this improvement factor was just twice better compared to Galfan coating (Figure 71b in WP 7).

In atmosphere with significantly reduced CO_2 content, the performance of ZMA coating was even inferior to that of GI (See Task 7.1), and interestingly, Galfan coating behaved rather similarly to ZMA2 coating. From XRD analysis of the corrosion products formed during static experiments in atmosphere containing CO_2, no evidence was found that hydrotalcites (LDH) or a stabilisation of simonkolleite plays a crucial role. Indeed, lower amounts of simonkolleite was found on ZMA than on GI coating (in accordance with the observations of Prosek et al. [32]), although ZMA coatings performed very well under these conditions. Interestingly, large amounts of hydrotalcites were especially detected at lower carbon dioxide contents, where ZMA coatings showed very poor corrosion resistance (see XRD results in Task 7.1).
Under field exposure conditions, XPS and XRD analysis performed on the bulk ZMA2 and Zn samples showed that at initial stages, in agreement with Persson et al. [28], hydrotalcite may form on the ZMA2 while after one year, no hydrotalcite could be found by XRD, but higher amounts of simonkolleite than on Zn, again ruling out hydrotalcite as an important factor (see Task 7.1). These measurements showed a clear tendency of a higher ratio of O:Zn on ZMA as compared to Zn, indicating a higher zincite amount on the zinc sample although that was not found by XRD (hence maybe amorphous).

Hence, although a better performance of the ZMA was observed for all these testing conditions, the corrosion products found on the surface were different in all cases.

From this statement, it seems obvious that **the superior behaviour of ZMA coatings is not strictly linked to the formation of a certain corrosion product** (neither hydrotalcite as reported by Schuerz *et al.* for the very aggressive salt spray test [10] nor simonkolleite) although for some testing conditions, they may indeed be favoured on ZMA compared to Zn coating. In the static tests, the amount of simonkolleite was more important on GI than on ZMA coating under atmospheric conditions where ZMA performed better, while hydrotalcite was found in low CO_2 atmosphere where ZMA fails. Hence, the explanation has to be found elsewhere.

It is further proposed, that the formed phases are rather an indication for the actual corrosion conditions, especially **the pH prevailing on the surface**. It is quite likely that not only the phases are governed by the pH, but also the compactness and hence the protective character of the corrosion product film. In principle, ZnO is a relatively wide gap semiconductor and there is no reason why zincite should not provide good corrosion protection, if the thickness of the layer is sufficient enough. However, the usual observation is that zincite does not provide good protection. Due to the buffering effect from atmospheric CO_2, the pH is more alkaline directly on the surface, where the oxygen reduction occurs, than in the bulk of the electrolyte (note that the zinc cation is only slightly acidic and its dissolution has only a small buffering effect). Hence, corrosion products precipitating in the electrolyte over the surface may not be fully stable directly on it, which leads to the formation of loose layers. Note that the $O:Zn^{2+}$ ratio decreases towards the interface with the metallic substrate, indicating significant ZnO like precipitates at this internal interface (see e.g. the XPS sputter profiles obtained on the field exposure bulk ZMA and Zn shown in task 3.2). These precipitates at this inner interface should be accordingly of better quality for conditions where hydrotalcite can be formed. Indeed, directly on the surface, the pH should be less alkaline and hence at least be also in a more stable range for these Zn rich corrosion products such as ZnO, leasing to denser layers than at higher pH.

In the absence of atmospheric CO_2, no buffering effect takes place. Thus, the pH can rise to extreme alkalinity, which is proposed as the main reason for the worse performance of the coatings in CO_2 free atmosphere (see surface pH on Figure 75 in task 7.1). Mg cations are also proposed to be able to buffer the pH (see in references 31 and 33). However, it should be borne in mind that Mg content in zinc alloy coatings investigated in this project is relatively low (i.e. 1 to 2 wt%) and that Mg cations are only very mildly acidic. Yet, the surface composition of Mg can be relatively high and thus have an effect at initial stage.

Nevertheless, there is another aspect where the addition of magnesium as an alloying element in the metallic coating might have an important effect: **the alloying dramatically changes the microstructure of the coatings** as can be observed in Task 2.4 on the cross sections of Figure 4 and Figure 11 for line hot dip ZMA and Rhesca compositions respectively. This should have an effect on the formation of local cathodes and anodes: with decreasing feature size of the microstructure, more anodes are expected to form as the Mg-containing intermetallics are more reactive than the zinc phase (see in the work of Elvins *et al*. [35]). Prosek *et al.* also reported such an observation when comparing the microstructure of their different alloys [32]. This provides by far a higher density of corrosion initiation sites when compared to GE or GI, where the corrosion phenomenon is more a "statistical effect". Similar to pitting corrosion, the statistical initiation sites on GE or GI coatings are stabilised by the related pH changes (less alkaline at the anodes, more alkaline at the cathodes). Hence, on GI coating, large anodes and cathodes are established while on ZMA coating, the size of anodes and cathodes is much smaller. This is exemplified on EDX mapping of chloride in Figure 84 where indeed large anodes and cathodes are visible on GI contrarily to ZMA coating where the anodes and cathodes are of obvious smaller sizes homogeneously distributed over the surface. This will lead to less extreme alkalinity on the cathodes of ZMA coating. This buffering effect is even more important that corrosion activity is high (i.e. more alkaline pH). This is in accordance with the observation that for ZMA the performance gain over GI or GE increases with increasing aggressiveness of the corrosion test. Of course, this reasoning should also be applied to Galfan coating, which has also a relatively fine microstructure (see Figure 85). However, for Galfan, the Al-rich phases themselves are not the most active ones. Hence, on Galfan such an effect is not direct by offering active phases, but indirect by possibly offering more nucleation sites at the boundaries between phases, which is not expected to be that effective. Indeed, even on ZnAl coated steel, the corrosion resistance increased as dendritic microstructure become finer [36]. Possibly, for ZMA, this microstructure related buffering effect, which is already effective at relatively low alloying degrees, is further enhanced by a buffering effect through Mg cations, but most likely only at the initial stages of the corrosion process, as Mg is quickly de-alloyed from the surface region [37]. A schematic representation of surface pH upon anode/cathode size is sketched out in Figure 86.

It should be emphasized that at later stages of the corrosion such as after 1 to 2 years of field exposures, no Mg effect can be discerned as Galfan always performs better than the ZMA samples (see results on open surface in Figure 36). The main reason for this is that the role of distribution of active sites at the metal surface becomes less important on less active surfaces, i.e. when they are covered by thick layers.

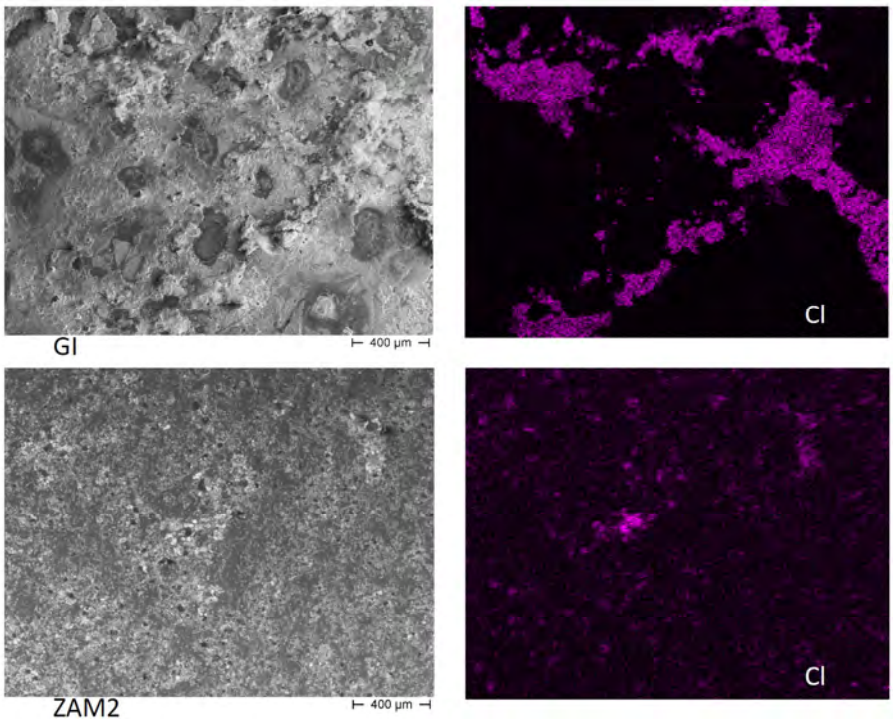

Figure 84: SEM images and chloride map obtained on a GI sample (top) and ZMA2 sample (bottom) after corrosion testing in static test (Cl^- 1g/m^2, atmosphere).

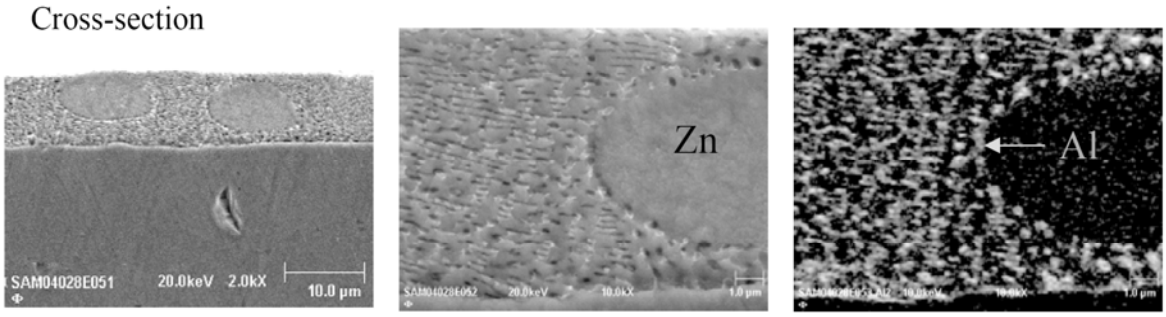

Figure 85: Cross sectional SEM images of Galfan from [2]

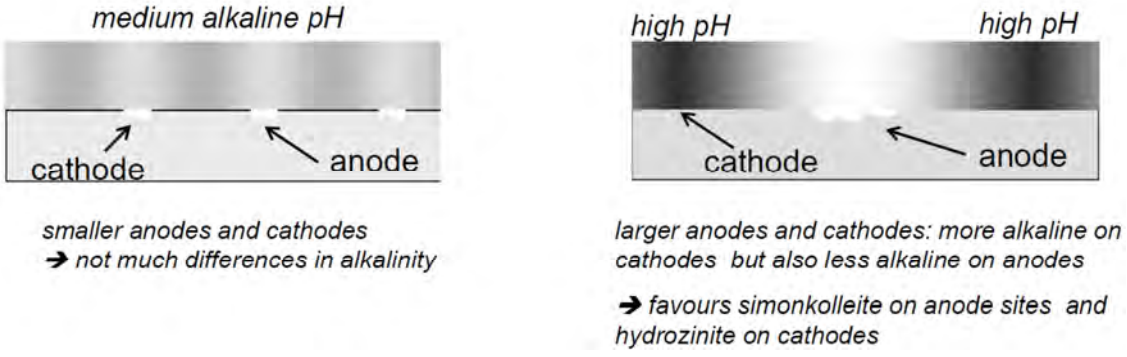

Figure 86: Schematic distribution of the pH over the surface upon cathodes and anodes size. Left: case with small anodes and cathodes (ZMA); Right: case with large anodes and cathodes (GI). Note that far away from the surface the average pH in the electrolyte might reach by averaging similar values for both depicted cases.

Influence of CO_2 (and consequences for hem-flange performance):

As can be seen from Figure 71 for low CO_2 conditions, ZMA but also Galfan coating show even inferior corrosion performance compared to GI one. In the absence of the buffering effect of CO_2, the pH on the surface raised to much higher value than in atmosphere. Obviously, these alkaline conditions do not allow the formation of dense zinc based corrosion product layers, even if some buffering is provided by the above discussed microstructure based averaging effect and possible additional direct buffering by magnesium cations. Such high pH values, however, destabilize the aluminium rich phases, which become very active. Hence, the enhanced corrosion of ZMA and Galfan compared to GI coating is proposed to be due to the inferior performance of these Al-containing compounds under these conditions. This was further confirmed by a series of simple control experiments: cast Zn-Mg model alloys and Zn-Mg-Al model alloys were immersed in electrolyte (aqueous 0.1M NaCl) and the evolution of the polarisation resistance was followed over time. During exposure, the electrolyte was purged either with oxygen (no access of CO_2) or with ambient air. The specimens were exposed simultaneously in separate cells. As can be seen from Figure 87, in the case of oxygen purging, Zn-Mg alloy with 2% of Mg (ZM2) shows a steady increase in resistance which indicates a build-up of an increasingly protective layer. Zn-1%Mg-1%Al (ZAM1) alloy showed comparable behaviour for some time but the resistance finally decreases. It is interesting to note how the addition of 4.26% Al to Zn-2%Mg decreases the performance in CO_2-free electrolyte (or O_2 purging), while the performance of the Zn-2%Mg is not much affected. In air purging conditions, the Al-containing alloys showed resistances close to the ZM2 and ZAM1. Note that in bulk electrolyte, the transport of CO_2 to the surface is still much lower than in the atmospheric corrosion tests performed in this project, where only a thin layer of electrolyte was covering the surface, which explains the still slightly inferior performance of the Al containing alloys.

This is also the explanation why in general the performance of the ZMA coatings in hem flange conditions is not as good as in open exposure conditions.

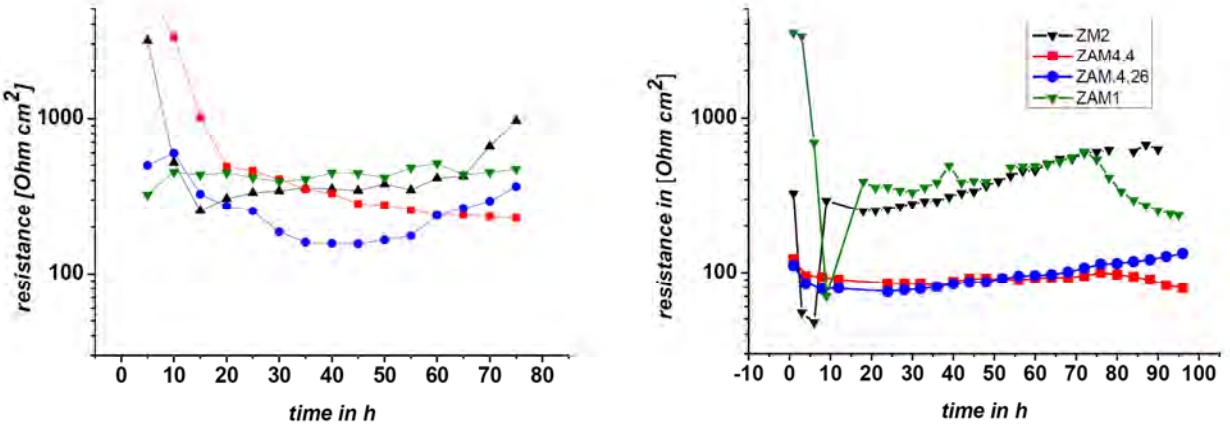

Figure 87: Evolution of the polarisation resistance over time for samples immersed in aqueous 0.1 M NaCl with (left) air purging and (right) O_2 purging. (Samples: ZM2: Zn-2%Mg; ZAM1: Zn-1%Mg-1%Al; ZAM4.26: Zn-4.26%Al-2.13%Mg; ZAM4.4: Zn-3.6%Mg-4.4%Al).

Additional experiments were thus carried out in order to emphasize a possible effect of CO_2 depletion and high alkalinity in confined situation. As shown in Figure 88a, a long crevice area of 185 mm in length was created by fixing a glass cover panel with a gap of 120µm on top of ZMA2 coated steel. The design was chosen with only one aperture in order to create conditions with a long air diffusion path in a confined area and examine how the corrosion of Zn coated steel was developing from the aperture to the bottom of the crevice. Once contaminated with NaCl, the samples were exposed to wet and dry cycles at 40°C and regularly inspected. It is interesting to note that significant corrosion products were formed at the extremity of the confinement far from the aperture with local attack of steel substrate (see Figure 88). This was connected to alkaline pH as shown on the WRI containing agar, while more neutral conditions and less corrosion attacks were observed closer to the aperture of the flange.

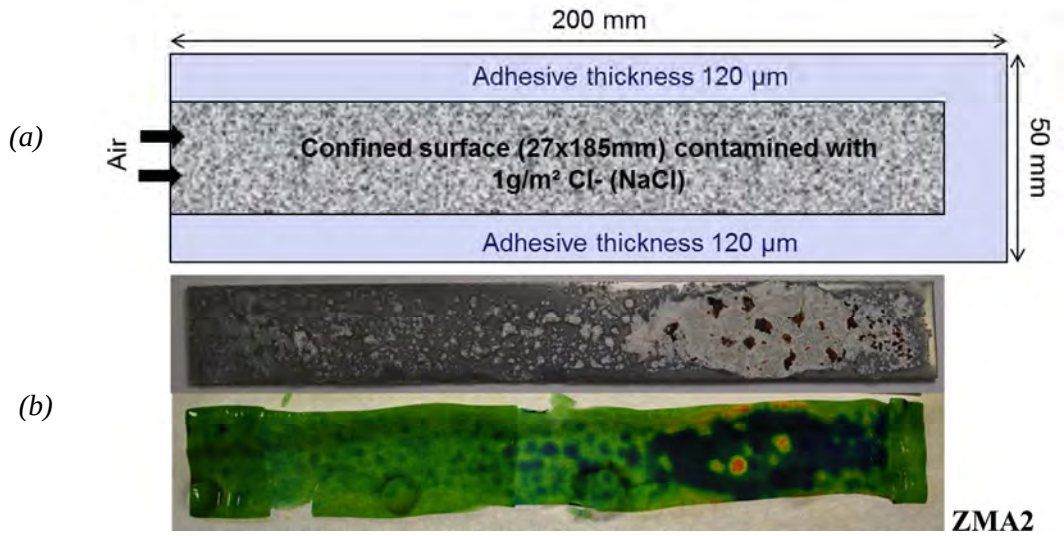

Figure 88: Photographs and corresponding surface pH (WRI containing agar) of NaCl contaminated confined surface of ZMA2 after 10 weeks of exposure at 40°C and wet/dry cycle (6h-50% / 6h-95% RH). (a): scheme of the confined set-up with long air diffusion path.

b) Time to red rust and galvanic protection

The time to red rust appearance in corrosion testing of open panels is determined by the corrosion resistance of the zinc alloy coatings themselves and by the cathodic protection of areas with exposed steel by the remaining zinc coating. According to the above discussed mechanisms for the cathodic protection (performance at the cut edge) and the corrosion of zinc alloy coating itself, it can be safely proposed that an enhanced protection effect of ZMA against red rust and attack into steel should be more pronounced for the most aggressive tests, such as the VDA test. This is indeed true if we consider the time to red rust as a function of testing conditions presented in Figure 89. The delay of red rust appearance on ZMA2 was indeed 13 weeks while it was 1 on GI after VDA test. Similar factors were also obtained by Schuerz *et al*. in a neutral salt spray test ISO 9227 [10-12]. However, surprisingly the high protection factor that can be seen in Figure 89 is not because the performance of the ZMA coatings just slightly decreases with the aggressiveness of the test while for GE, GI, GA and Galfan it decreases much more significantly, as it is the case for the weight loss (see Figure 70 in WP 6). Instead, the time to red rust for ZMA even increases in the VDA test while for all other coatings, it is the shortest of the three tests.

Hence, the role of cathodic protection of steel substrate by zinc alloy coatings plays an important role here. The main factor is proposed to be due to the Mg effect already discussed for the cut-edge protection, i.e. the synergetic enhancement of the inhibition of oxygen reduction at exposed steel sites by zinc cations, which was also shown by Krieg *et al.* to be higher for conditions representing more active corrosion conditions [26].

It is proposed that for the inhibition of red rust appearance, this cathodic protection enhancement and the decreased metal loss of the alloy coating are combined leading to the significant improvement of ZMA coatings under very aggressive conditions.

The relation between performance of ZMA and aggressiveness of the test was presented in Figure 65 of WP6.

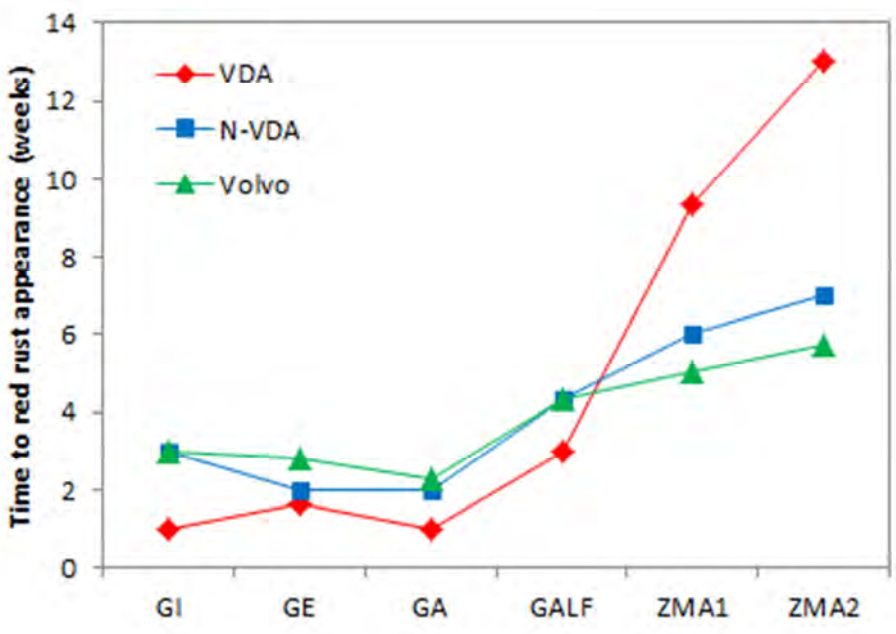

Figure 89: Time to red rust in weeks as obtained from the Volvo, New VDA and VDA.

2.3.8.2 Task T8.2: cost analysis, lifetime prediction and guidelines for industry

Based on the outcome of the project, **application and corrosion guidelines for the automotive industry** have been issued in a comprehensive way. It should be underlined that the presence of a European carmaker FIAT (CRF) in the consortium has definitively helped in orientating the structure of the project for further application of these novel ZnMgAl coatings in manufacturing of car body. Thus, FIAT procedures have been followed such as for studying the adhesive bonding properties of the metallic coating but also in forming process. In general, FIAT opinion on the corrosion behaviour of these coatings was essential.

The ability of line hot dip ZnMgAl coatings (Mg and Al in the range of 1 to 2%) to conventional automotive process is thus summarized in Table 23 as regards to phosphatation, process forming, spot welding and adhesive bonding. As can be seen, ZMA coatings do show general satisfying behaviour similar to conventional hot dip galvanised (GI) coatings unless on deformed panels where cracks in the coating were observed. Yet, no effect on the corrosion behaviour was further noticed. It was also noted a narrower welding range when spot welding ZMA in comparison to GI. Globally, ZMA coatings fulfilled FIAT requirements as regards to automotive process which were assessed in the project.

The corrosion resistance of ZMA compared to GI is summarized in two additional tables.

Table 24 summarizes the corrosion performance of ZMA upon various testing conditions in laboratory and in real situations taking into account unpainted coating in open and hem-flange configurations but also painted materials (corrosion from a defect). When tested in bare open configuration, ZMA coatings showed obvious superior corrosion resistance compared to conventional GI coating in various testing situations including field exposures (stationary sites and mobile exposures – 2 years). Only, the absence of CO_2 has a detrimental effect on the stability of the coating resulting in poorer behaviour than GI as a consequence of high alkalinity. It is likely that the situation in hem-flange configurations where no major differences were observed on ZMA compared to GI coating, is also linked to the pH inside the confined area. One should however underline that the corrosion performance in confined situations is highly dependent on the geometry of the samples and the testing conditions, which explains why ZMA is either equal or slightly better than GI coating. From this outcome, it seems difficult to use ZMA for hem-flange without additional anti-corrosion protection such as wax in areas where de-icing salts are used.

As regards to cosmetic corrosion on painted materials, ZMA showed better or equal behaviour compared to GI coating, upon testing situations accelerated tests or field exposure. One should note that ZMA coatings were phosphated prior to E-coat application. The situation of ZMA was however worse than GI coating when they were covered with artificial NaCl containing dirt, which could be observed on real situation on vehicle where road mud accumulated, close to the wheels for example.

Additional results considering the corrosion resistance of unpainted ZMA in galvanic coupling with fasteners of different natures and in deformed configuration are given in Table 25. While ZMA coatings showed better resistance to galvanic corrosion in accelerated corrosion test, no significant differences were observed in field exposures after 2 years. For formed panels, ZMA coatings were also better than GI at least in accelerated corrosion test despite the presence of cracks on severe deformations. Obviously, these types of samples have not been tested in all conditions.

In summary, the application window of ZMA seems larger than for conventional zinc coating which is obviously an advantage in the car industry but also for other applications such as building or infrastructure.

Table 23: Application guideline as regards to automotive process for phosphatation, forming, and joining established on results from WP3 and WP5. ZMA (1-2% of Mg and Al). ☺: Acceptable, similar behavior than GI; 😐: medium; ☹ : problems)

T	Behavior of ZMA compared to GI			↴	Comments
5.1	**Formability**	**Type of deformation**	**H, mm**		
		Cup (Erichsen tool)	2.2	☺	No cracks
			4.3	☹	Cracks on ZMA but no effect on corrosion
			6.5	☹	Cracks on ZMA but no effect on corrosion
		Cross Die Samples	18	☹	Cracks on ZMA but no effect on corrosion
		Friction coefficient		☺	
5.2	**Welding (RSW)**	Electrode lifetime		☺	
		Welding range		😐	Narrower current range
	Adhesive bonding	Structural adhesive (FIAT procedure)		☺	Fulfilled FIAT requirements (but adhesive failure)
3.1	**Phosphatation**	Commercial solution (Granodine, Henkel) – automotive process		☺	
		Robustness to process variations (T℃, time, free acid)		☺	

Table 24: Corrosion guideline established on results from WP4, WP6 and T7.1 and data from IC projects. ZMA (1-2% of Mg and Al)

	LABORATORY TESTS						FIELD TESTS			ZMA *vs* GI is		
	Chloride		Static high R.H.	Cyclic Wet/dry	CO_2		Artificial dirt NaCl	Real Exposures (2 years)		☺	😐	☹
	High	Low			Ambient	Low		Static Marine Urban	Mobile Under truck (Alps)	better	equal	worse
Open bare panels	x		x		x					●●		
	x			x	x					●		
	x					x						●●
		x	x		x					●		
		x		x	x					●	●	
		x	x			x						●
								x		●		
									x	●		
Hem-Flanges	x			x	x					●	●	
		x		x	x					●	●	
								x			●	
									x	●	●	
Cosmetic painted panels	x		x				x					●
	x			x	x					●●		
		x		x	x					●		
								x			●	
									x		●	

Table 25: Corrosion guideline established on results from T7.2 (galvanic coupling with fasteners) and T 5.1 (formed panels). ZMA(1-2% of Mg and Al)

Task				LABORATORY TESTS					FIELD TESTS		ZMA *vs* GI is		
				Chloride		Cyclic Wet/dry	CO_2		Real Exposures (2 years)		☺	😐	☹
				High	Low		Ambient	Low	Static Marine Urban	Mobile Under truck (Alps)	better	equal	worse
7.2	Galvanic coupling* with fasteners of :	Steel			x	x	x				●		
									x	x		●	
		Stainless steel			x	x	x				●		
									x	x		●	
		ZnNi coated steel			x	x	x				●		
									x	x		●	
		ZEC (Zn flakes)			x	x	x				●		
									x	x		●	
		Geomet coated steel			x	x	x				●		
									x	x		●	
5.1	Formed panels *	Cross Die Test	18		x	x	x				●		
		Erichsen cup	2.2		x	x	x				●		
			4.3		x	x	x				●		
			6.5		x	x	x				●		

*: The samples were tested in bare conditions (unpainted), the value refers to the height of the deformation

As regards to **cost analysis aspect**, it has been impossible to get exact figures from the Steel industry on the economic impacts of the application of ZMA in car body. Due to compliance restriction, *Thyssen Krupp Steel* and *voestalpine* were unfortunately not allowed to give any details on the financial impacts of using ZMA in the manufacturing of vehicles. Indeed, the sales volume for automotive application is too low to predict a saved estimation.

It is obvious that a cost advantage caused by a reduced thickness of ZMA in comparison to GI is not quantifiable because it is depending on different production parameters such as the amount of produced material, the surface quality, the coating weight etc..

From the results obtained in the project, the situation can thus be summarized as follows:

- A cost reduction by eliminating additional corrosion protection such as wax in hem-flanges is not possible
- A cost reduction by eliminating surface treatment such as phosphatation is not possible
- A cost reduction by lowering the coating weight is not certain. This is depending on the conditions of production (as mentioned before) and on the used coating weights (e.g. depending on the thickness reduction : 275 g/m^2 to 140g/m^2 or 100g/m^2 to 70g/m^2)

The point of view of *FIAT* was however interesting. They indicated that ZMA could be an advantage for parts of vehicle in which the thickness of the E-coat is lower than the expected value. These parts represent about 14 to 18 % of the body in white. ZMA could also be an advantage for E-coated parts representing about 20 to 30 % of the chassis components which have to fulfill the more and more stringent requirements of corrosion resistance.

3 Conclusions

Line hot dip materials including conventional zinc coatings (GI, GE, GA and Galfan) and new ZMA coatings (ZnMg1%Al1%, ZnMg1,5%Al1,5%, ZnMg2%Al2%) were selected in order to produce cosmetic samples (unpainted and painted); hem-flanges and galvanic panels. In addition, a Rhesca galvanizing simulator was used to prepare ZMA coating with various compositions of Mg and Al ranging from 0.5 to 4%.

The main achievements of the project can be summarized as follows:

- ZMA substrates were suitable for standard **phosphatation** process and showed good robustness in respect to process variations. This was confirmed by further SKP measurements. Delamination experiments without surface treatment on ZMA coatings were not conclusive. Thus avoiding phosphatation is not recommended.
- As regards to **weldability of ZMA,** the addition of Mg and Al from 1 to 2 % in the coating gave comparable welding properties as on conventional GI coating
- **Adhesive bonding** of ZMA showed comparable results as on GI coating for tensile strength which fulfill Fiat requirements; however, the failure was mostly adhesive on ZMA2 while it was cohesive on GI.
- Concerning **formability tests**, cracks were formed on ZMA coating in cup and cross die tests unless on weak deformations, but no effect of the corrosion performance was observed.
- **Stationary field exposures** (1 and 2 years) showed no improvement on painted cosmetic panels. Slight improvement was observed on ZMA in bare open situations (factor of 2) and a trend for slight improvement in hem flange configurations.
- **Exposure on vehicle** (1 and 2 years driving) showed no improvement on painted cosmetic panels (very little delamination on all samples), improvement of ZMA coatings on bare open configurations (factor of 4 to 2) as well as in hem flange (factor of 2) with however some deviations
- **When exposed in accelerated corrosion tests**, large differences were observed upon testing conditions and configuration. The advantageous effect of ZMA was more pronounced in open situations than in confined ones, particularly in test with significant salt load. The beneficial effect was indeed less pronounced in tests with lower salt load as noted in field exposures
- An enhancement of corrosion of zinc coatings in CO_2 free atmosphere, ZMA coating being more affected than GI in chloride containing media, in the range of Galfan. This suggested an effect of the surface pH. Layered double hydroxide (LDH) and simonkolleite were mainly formed on ZMA2 in low CO_2 conditions
- **In galvanic situation** with bolts of different composition (steel and coated steel) in field tests, ZMA presented comparable results as conventional coatings
- **Mechanisms of corrosion** of ZMA were discussed: the corrosion of the coating itself seems to be governed by the microstructure of the coating more than strictly the formation of certain corrosion product.

Finally, the main results of the project were summarized in a comprehensive way in **guidelines** for the automotive and steel industry.

4 Exploitation and impact of the research results

The main impact of the project is to provide new data on the application properties of ZMA coatings for automotive applications (e.g. phosphatation and E-coating, forming and joining) as well as on their corrosion behaviour both in accelerated corrosion tests used by car manufacturers but also in various field exposures including various outdoor stationary sites and mobile exposures. In addition, original data on the influence of CO_2 on the corrosion behaviour of ZMA coatings have been obtained helping in understanding the corrosion mechanisms of such coatings. The results clearly highlight that the corrosion behaviour of zinc (alloy) coated materials are dependent on the testing conditions and in particular the salt load (WP 6 and WP4).

It is believed that the results obtained in the project may be used as a guideline for the application of ZMA coated steel in the manufacturing of vehicles but also for other applications such as building and infrastructures. Such guideline is given in details in task 8.2.

Some results obtained in the project have been presented at Eurocorr 2012 Conference and also published in journals:

- N. LeBozec, D. Thierry, A. Peltola, S. Reiter, L. Luxem, G. Luckeneder, G. Marchiaro, M. Rohwerder, Proc. of Eurocorr 2012, Istanbul, 2012.
- G. Luckeneder, M. Rohwerder, P. Keil, A. Bashir, Proc. Of Eurocorr 2012, Istanbul, 2012.
- N. LeBozec, D. Thierry, A. Peltola, S. Reiter, L. Luxem, G. Luckeneder, G. Marchiaro, M. Rohwerder, Material and Corrosion, in Press, 2013.
- N. LeBozec, D. Thierry, M. Rohwerder, D. Persson, Influence of CO_2 on the corrosion performance of Zn-Mg-Al coated steel, Corrosion Science, 74, 379-386, 2013.
- M. Rohwerder, N. LeBozec, D. Thierry, A. Peltola, G. Luckeneder, L. Luxem and G. Marchiaro, The performance of zinc-magnesium-aluminium alloys in accelerated corrosion test and long term field exposures: discussion of possible underlying mechanisms. In preparation for submission in Corrosion Science.

5 List of figures

6 List of tables

7 List of acronyms and abbreviations

Abbreviation or unit	Full term
ACT	Accelerated Corrosion Test
CRS	Cold rolled steel
EDS/EDX	Energy Dispersive X-ray Spectroscopy
FTIR	Fourier Transformed Infra-Red
ED	Electro Deposited (Paint)
GA	Galvannealed steel
GALF	Galfan coated steel
GE	Electro-galvanised steel
GDOES	Glow Discharge Optical Emission Spectroscopy
GI	Hot-dip Galvanised steel
HDG	Hot dip galvanised
LDH	Layered Double Hydroxide
NSST	Neutral Salt Spray Test
PVD	Physical Vapor Deposition
R.H.	Relative Humidity
RSW	Resistance Spot Welding
SCE	Saturated Calomel Electrode
SEM	Scanning Electronic Microscope
SHE	Standard Hydrogen Electrode
SKP	Scanning Kelvin Probe
T	Task
THF	TetraHydroFuran
VDA	(Verband Der Automobilindustrie) for VDA 621-415
WP	Work package
WRI	Wide Range Indicator (pH)
XEAES	X-ray Excited Auger Electron Spectroscopy
XPS	X-ray Photoelectron Spectroscopy
XRD	X-Ray Diffraction
ZMA	Zinc Magnesium Aluminium (line hot dip)
ZMAP	Zinc Magnesium Aluminium (by PVD)
ZMAR	Zinc Magnesium Aluminium (by Rhesca)

8 References

1. S. Feliu Jr., V. Barranco, *Acta Materialia* 51, 5413, 2003.
2. RFCS Project Zinc Alloys, RFSR-CT-2003-00028
3. R. Hausbrand, M. Stratmann, M. Rohwerder, *J. Electrochem. Soc*., 155, C369, 2008.
4. N. LeBozec, N. Blandin, and D. Thierry, *Materials and Corrosion*, 59, 889-894, 2008.
5. N. LeBozec, A. LeGac, and D. Thierry, Fourth International Seminar in the field of Automotive Corrosion, Stockholm, Sweden, 5-6 May 2010.
6. F. Beier, K-H. Stellnbberger, and S. Geisler, Eurocorr 2009, Nice, France, 6-10 September 2009, Paper 8412.
7. B. Rendhal and N. LeBozec, Eurocorr 2009, Nice, France, 6-10 September 2009, Paper 8395.
8. M. Vlot, R. Bleeker, T. Maalman, E. Van Perlstein presented at Galvanized Steek Sheet Forum, Düsseldorf, Germany, May 30-31, 2006.
9. T. Prosek, N. Larché, M. Vlot, F. Goodwin and D. Thierry, *Materials and Corrosion*, 60, 412–420, 2010.
10. S. Schuerz, M. Fleischanderl, G. Luckeneder, K. Preis, T. Haunschmied, G. Mori and A.C. Kneissl, *Corr Science* 51, 2355-2363, 2009.
11. S. Schuerz, G. Luckeneder, M. Fleischanderl, K.-H. Stellnberger, K. Preis, and G. Mori, Eurocorr 2010, Moscow, Russia September 13–17, 2010.
12. S. Schuerz, G.H. Luckeneder M. Fleischanderl P. Mack H. Gsaller A.C. Kneissl G. Mori Corrosion Science 52, 3271-3279, 2010.
13. Isaacs H.S., Adzic G. And Jeffcoate C.S., *Corrosion*, 56, 971-978, 2000.
14. R. Lindström, J.E. Svensson, L.G. Johansson, *J. Electrochem. Soc*., 147, 1741-1757, 2000.
15. T. Prosek, D. Thierry, D. Persson, J. Stoulil, Galvatek 2011, Genova (Italy).
16. T. Falk, J.E. Svensson and L.G. Johansson, *J. Electrochem. Soc*, 145, 2993-2999, 1998.
17. T.E. Graedel, *J. Electrochem Soc*, 136, 193C-203C, 1989.
18. I. Odenwall and M. Westdahl, *Corr Science*, 34, 1231-1242, 1993.
19. I Odnevall and C. Leygraph, *Corr Science*, 34, 1213-1229, 1993
20. D. Thierry and N. Le Bozec, *Corrosion*, 65, , 718-725, 2009.
21. D. Thierry, T. Prosek, N. Le Bozec and E. Diler, Proceedings of Galvatech'11, International Conference on Zinc and Zinc Alloy Coated Steel, June 21-24, Genova, Italy, 2011.
22. D. Persson, T. Prosek, N. Le Bozec and D. Thierry, accepted for publication in Corrosion Science (2013)
23. P. Volovitch, T.N. Vu, C. Allély, A. Abdel Aal, K. Ogle, *Corr Science* 53, 2437–2445, 2011.
24. D. Bengtsson Blücher, R. Lindström, J.E Svensson and L.G. Johansson, *J. Electrochem. Soc*., 148, B127-B131, 2001
25. D. Bengtsson Blücher, J.E Svensson and L.G. Johansson in: Proceedings of the 15th ICC conference, September 22-27, Granada, Spain, 2002, 523-530.
26. R. Krieg, M. Rohwerder, S. Evers, B. Schuhmacher, J. Schauer-Pass, *Corr Science* 65, 119–127, 2012
27. K. Ogle, S. Morel, D. Jacquet, *J. Electrochem. Soc*. 153, B1–B5, 2006.
28. F. Thébault, B. Vuillemin, R. Oltra, C. Allely, K. Ogle, *Electrochimica Acta* 56, 8347– 8357, 2011.
29. R. Hausbrand, M. Stratmann, M. Rohwerder, *Steel Research International*, 74(7), 453, 2003
30. R. Hausbrand, M. Stratmann, M. Rohwerder, *Corr Science*, 51, 2107–2114, 2009.
31. P. Volovitch, C. Allely, K. Ogle, *Corr Science* 51, 1251, 2009.
32. T. Prosek, A. Nazarov, U. Bexell, D. Thierry and J. Serak, *Corr Science*, 50, 2216, 2008
33. Hosking, M. Ström, P. Shipway and C. Rudd, *Corr Science*, 49, 3669, 2007.
34. E. Diler, S. Rioual , B. Lescop , D. Thierry , B. Rouvellou , *Corr Science*, 65 , 119, 2012.
35. J. Elvins, J. A. Spittle, J. H. Sullivan, D. A. Worsley, *Corr Science* 50,1650–1658, 2008.
36. A.E. Ares, L.M. Gassa, Corr Science, 59, 290-306, 2012.
37. S. Oliver Klemm, J.-C. Schauer, B. Schuhmacher, A.W. Hassel, *Electrochimica Acta* 56, 9627–9636, 2011.

9 Appendix

9.1 Appendix 1: SKP maps

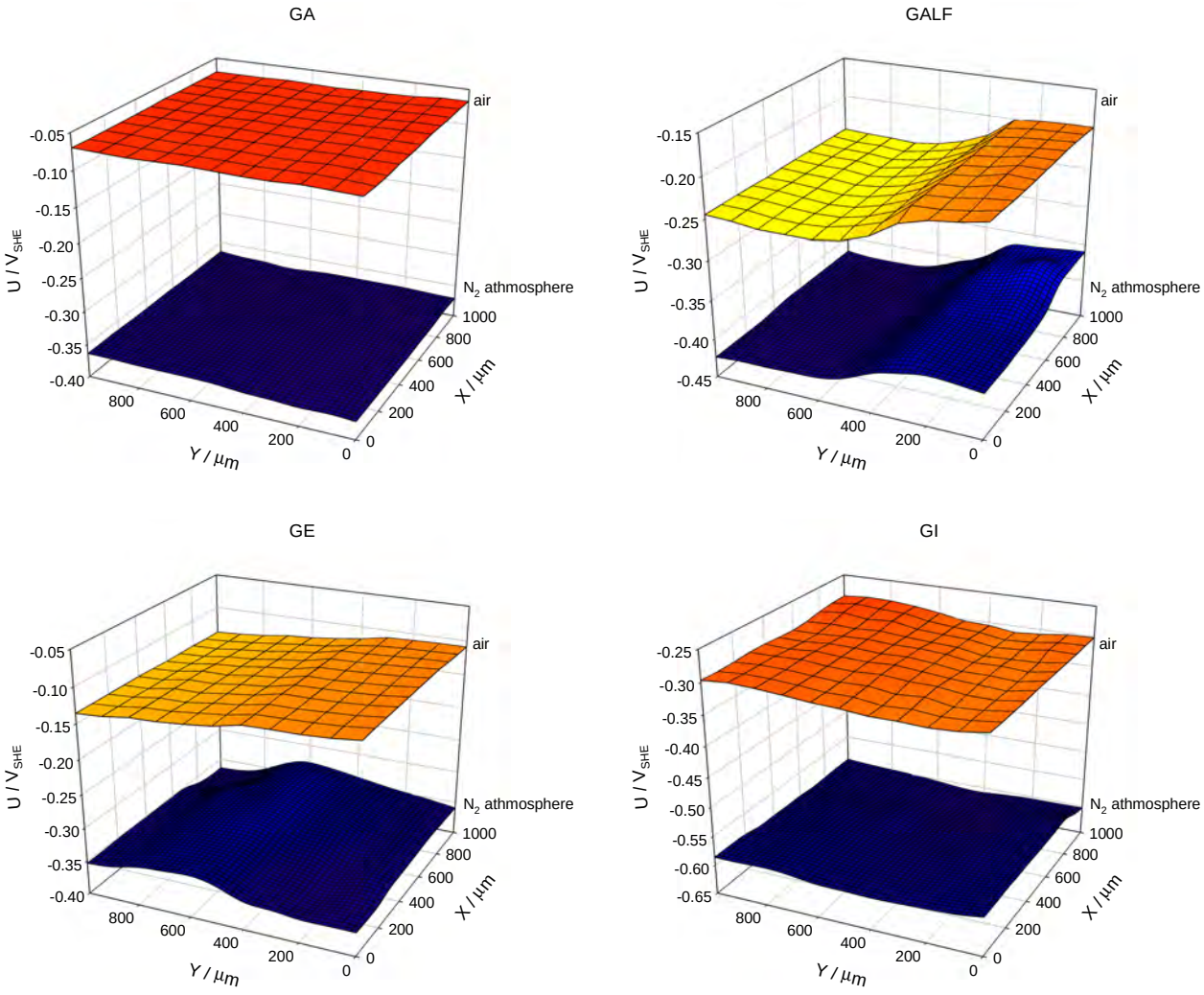

Figure 90: Surface potential maps of the reference coatings (GA, GALF, GI, GE) in water saturated N_2 and air.

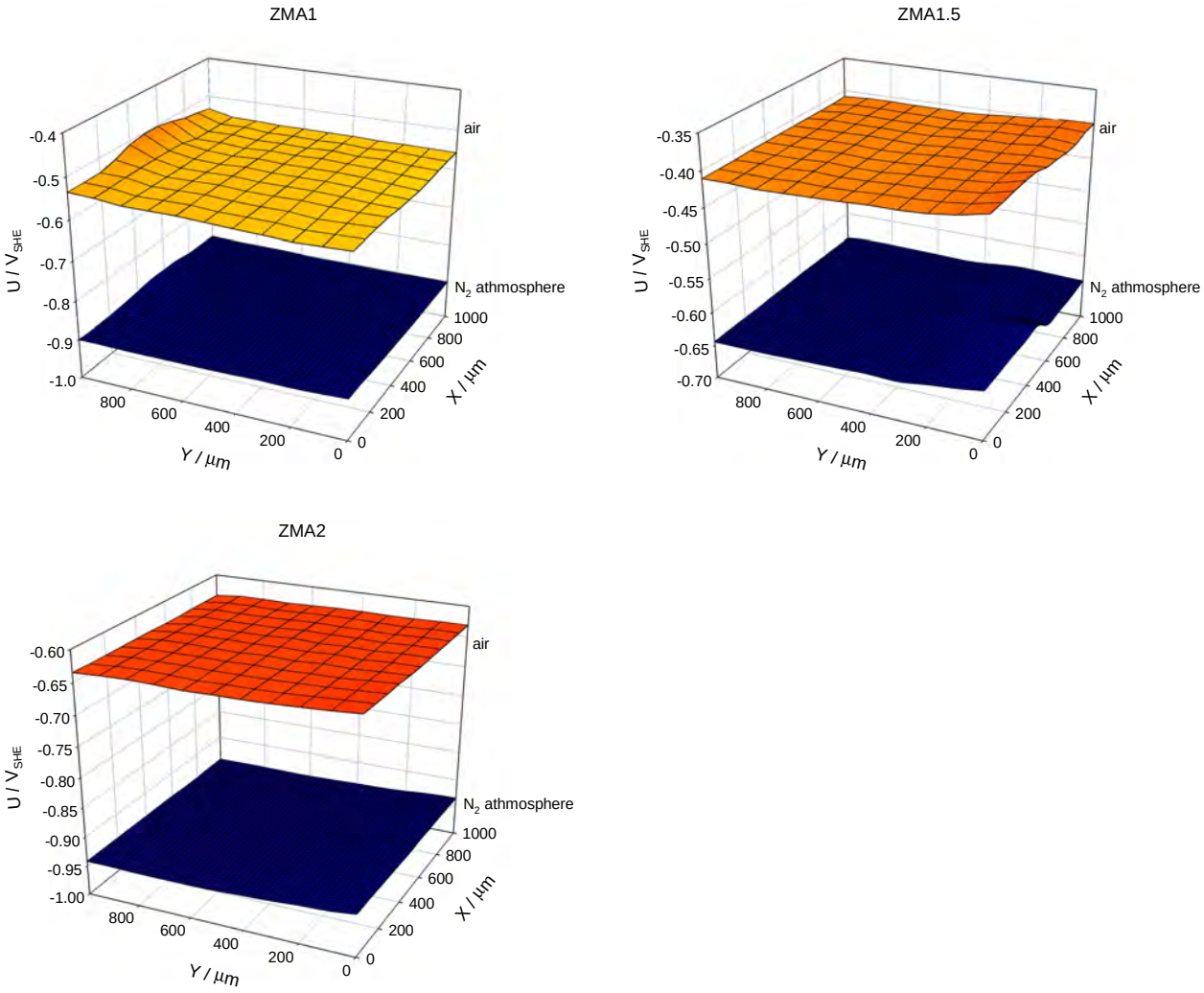

Figure 91: Surface potential maps of the line hot dip coatings (ZMA), ZMA1.5 and ZMA2) in water saturated N_2 and air.

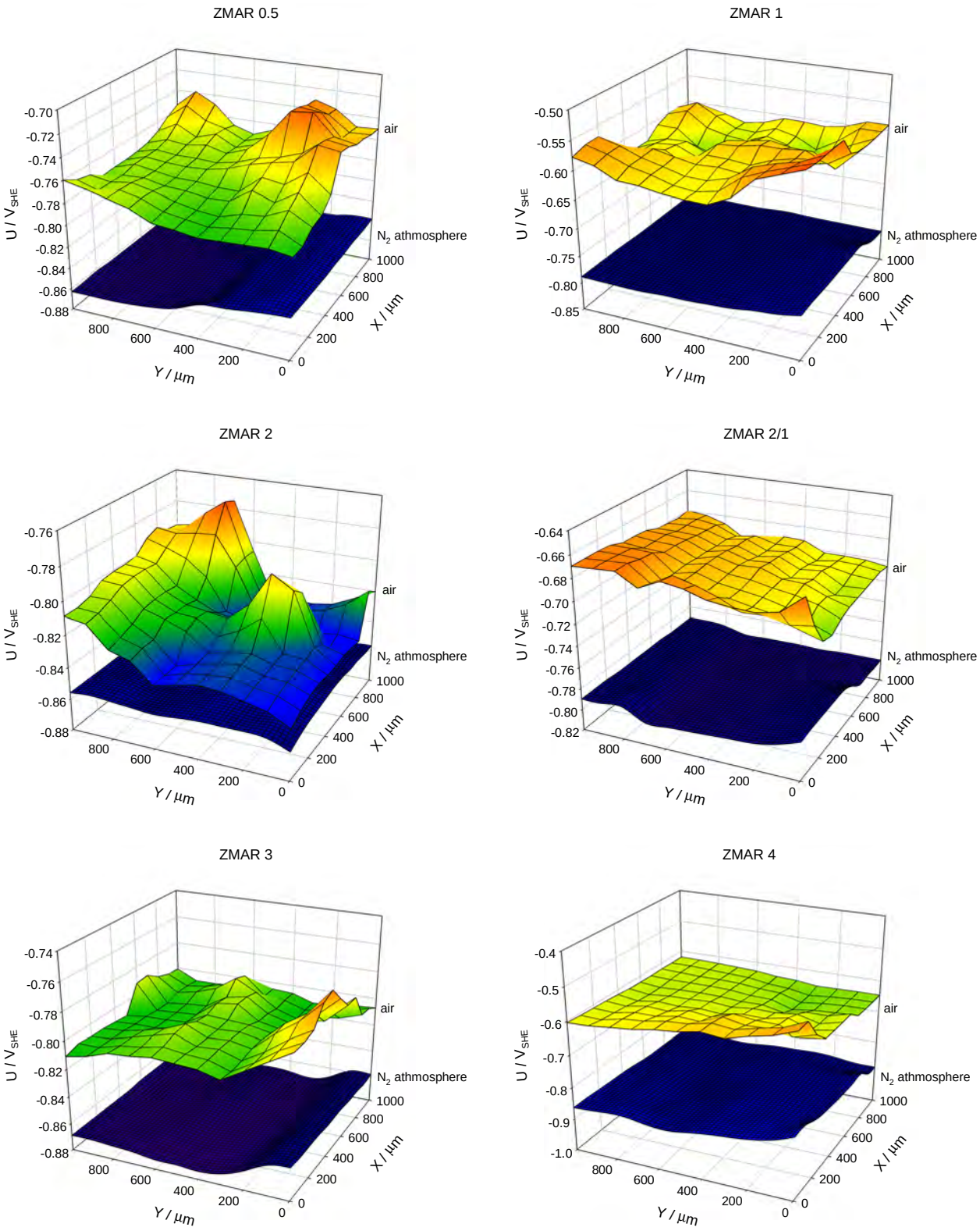

Figure 92: Surface potential maps of Rhesca simulator coatings (ZMAR1-4) in water saturated N_2 and air.

9.2 Appendix 2: Photographs of the samples

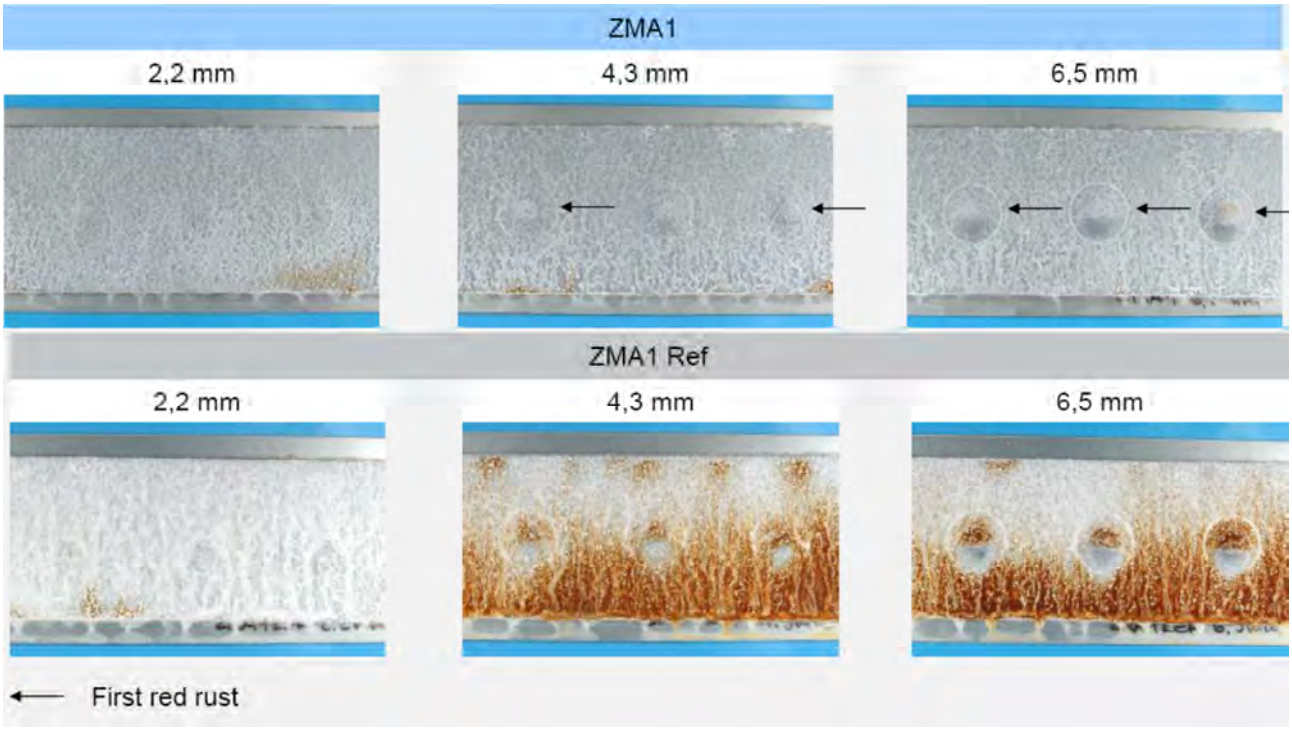

Figure 93: ZMA1 and ZMA1ref samples in cup shapes of 2.2, 4.3 and 6.5 mm height after 4 cycles in new VDA.

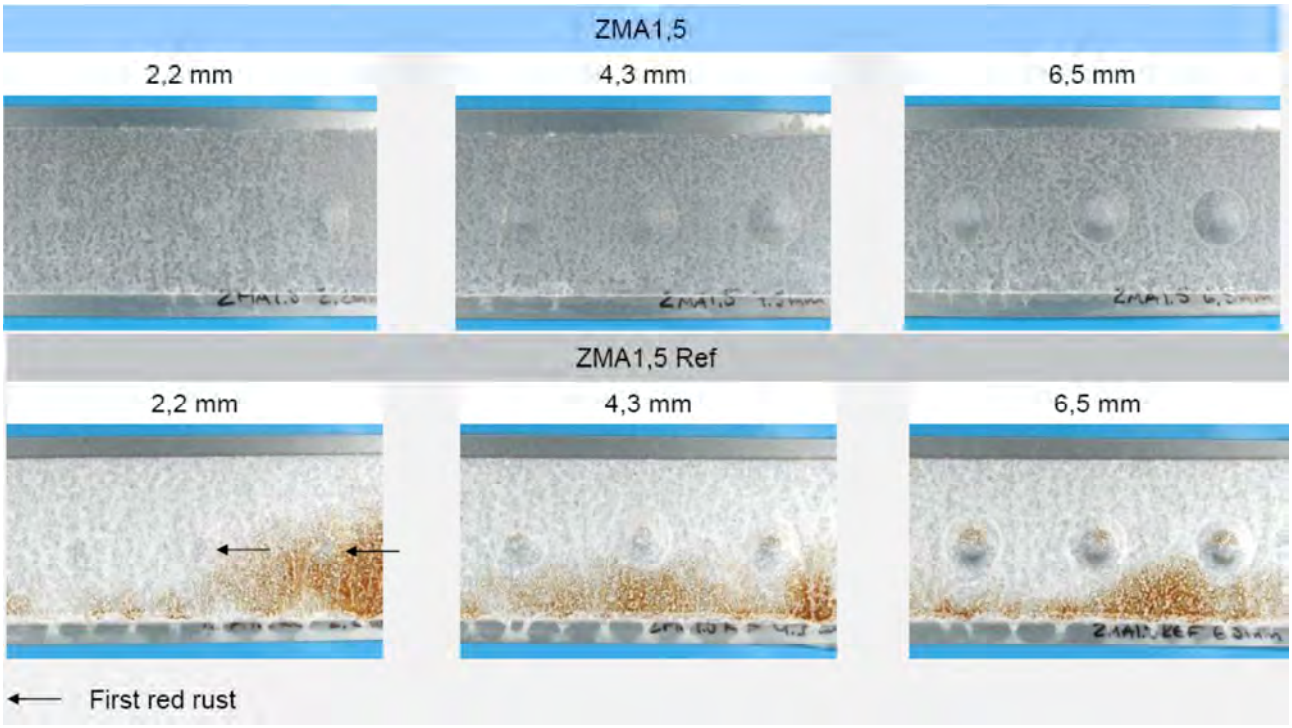

Figure 94: ZMA1.5 and ZMA1.5ref samples in cup shapes of 2.2, 4.3 and 6.5 mm height after 4 cycles in new VDA.

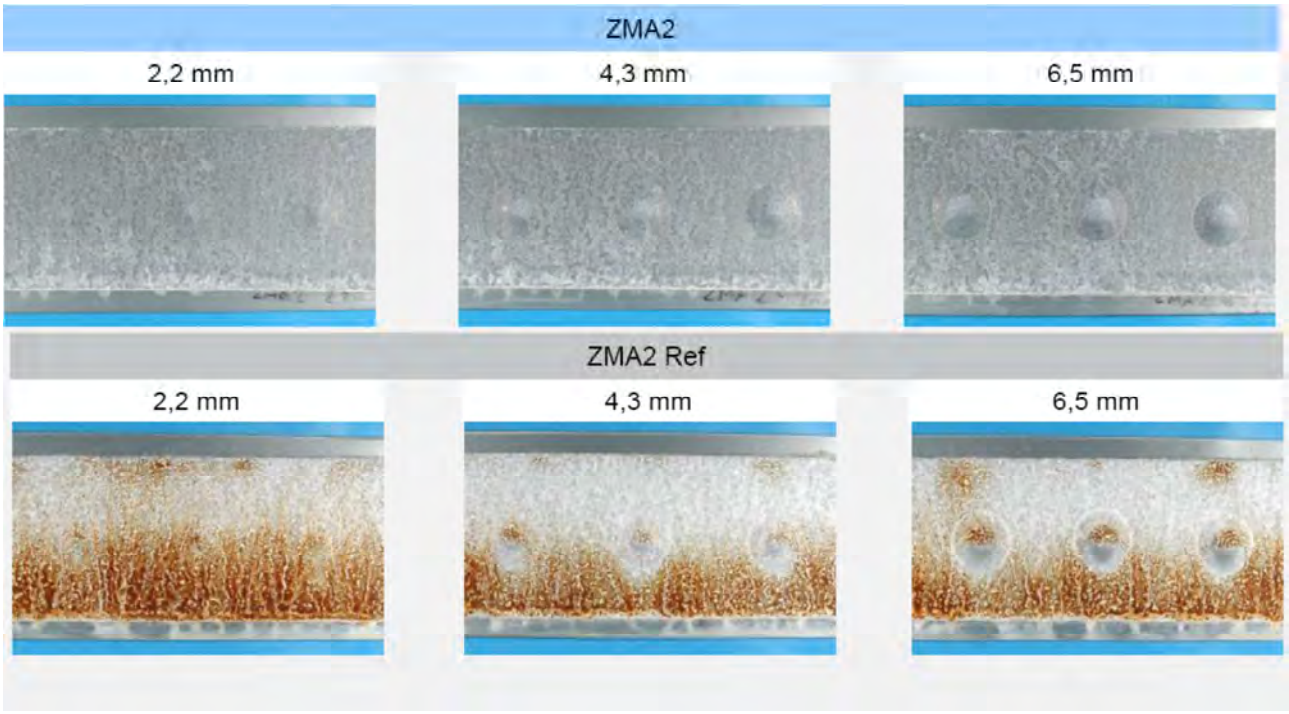

Figure 95: ZMA2 and ZMA2ref samples after 4 cycles in cup shapes of 2.2, 4.3 and 6.5 mm height after 4 cycles in new VDA.

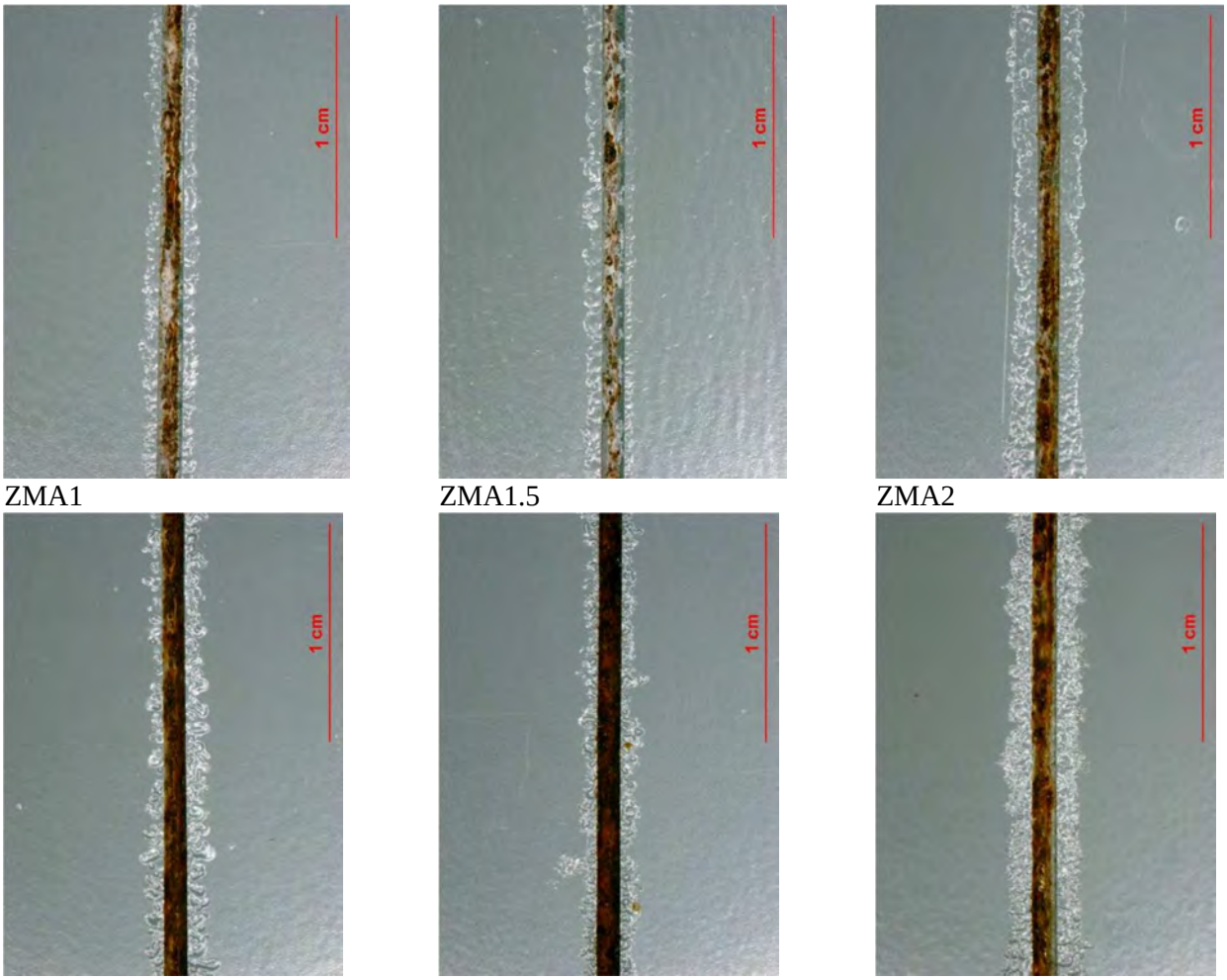

ZMA1 ZMA1.5 ZMA2

GE GA GALF

Figure 96: Photographs of creep from 1mm wide scribe line after 18 weeks of Volvo test

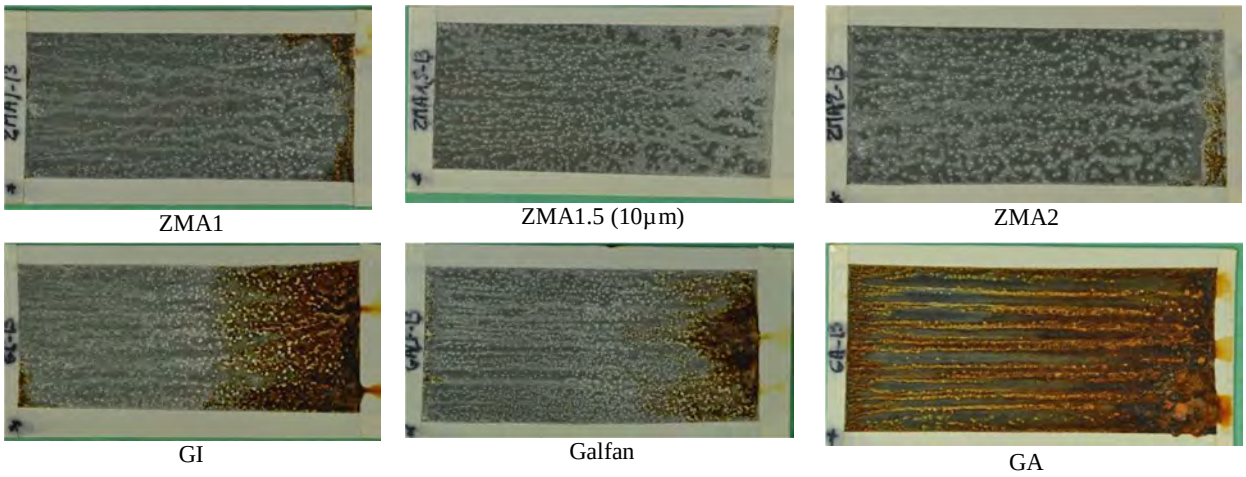

Figure 97: Photographs of open panels after 12 weeks in Volvo test (size of a sample 100x50mm)

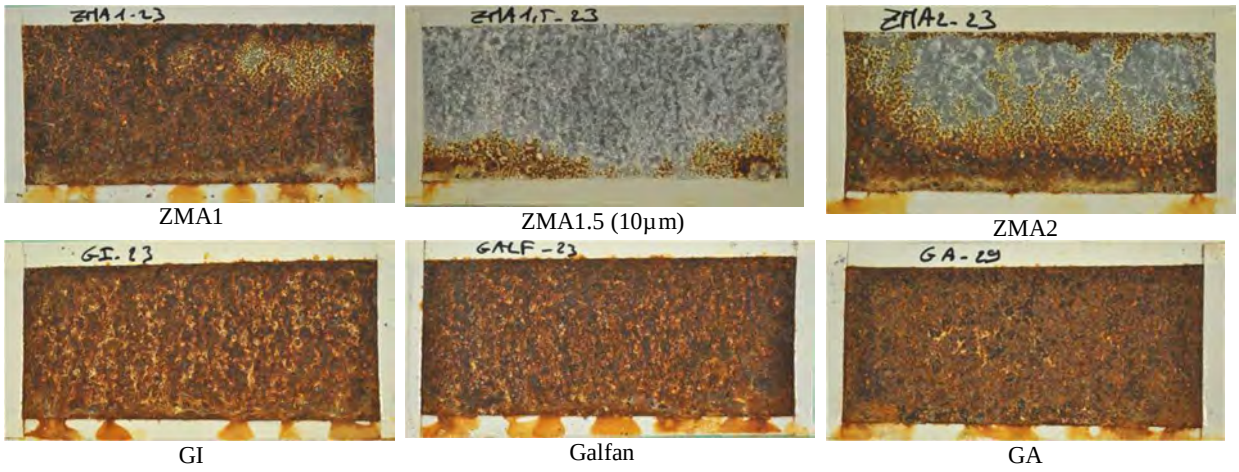

Figure 98: Photographs of open panels after 12 weeks in New VDA test (size of a sample 100x50mm)

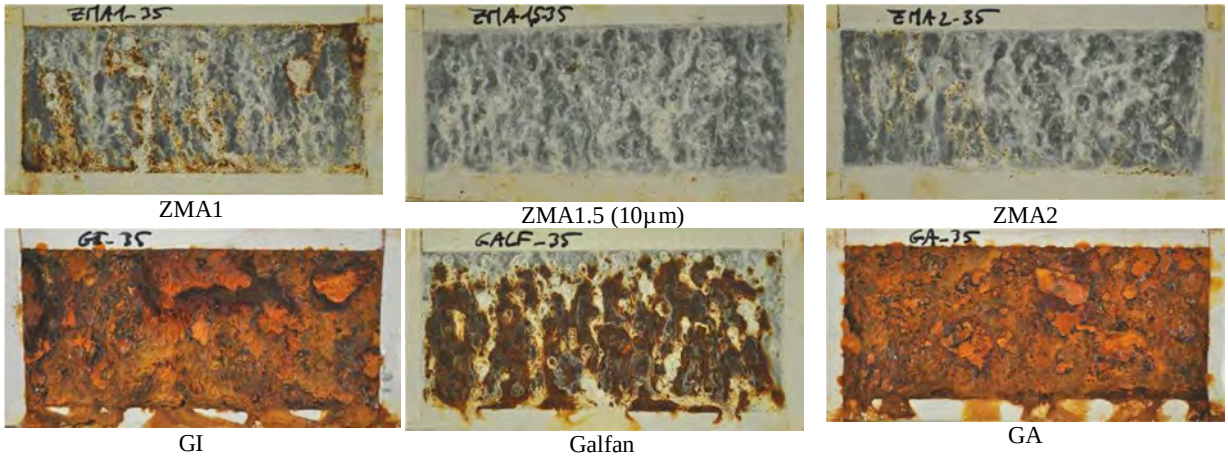

Figure 99: Photographs of open panels after 12 weeks in VDA test (size of a sample 100x50mm)

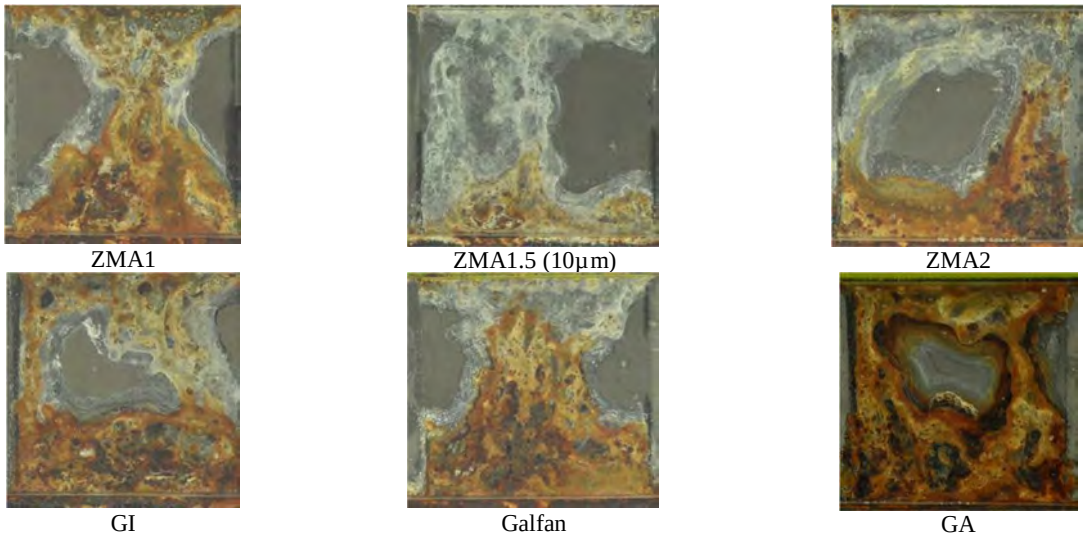

Figure 100: Photographs of hem-flange panels after 12 weeks in Volvo test (size of a sample 40x40mm)

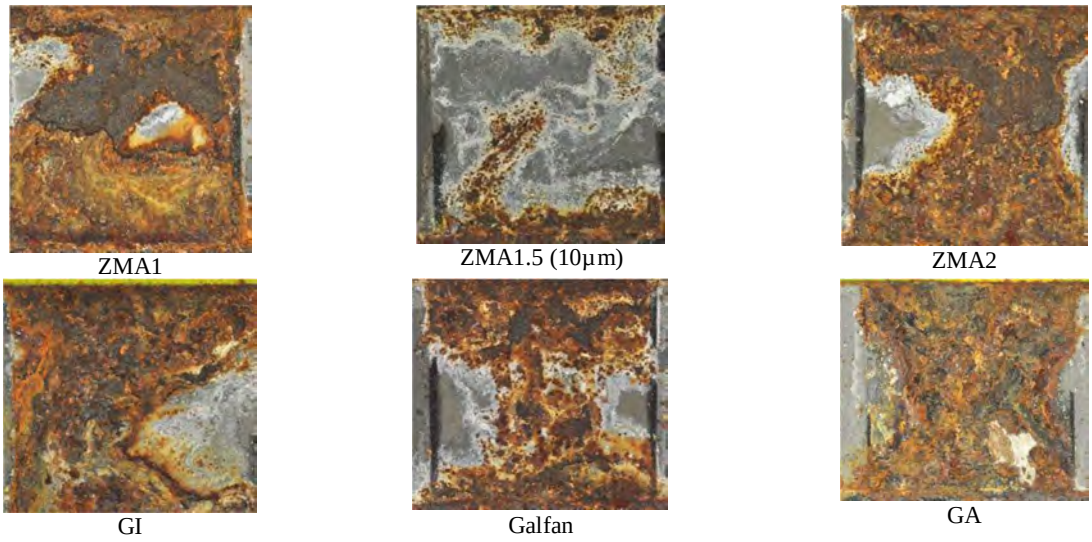

Figure 101: Photographs of hem-flange panels after 10 weeks in New VDA test (size of a sample 40x40mm)

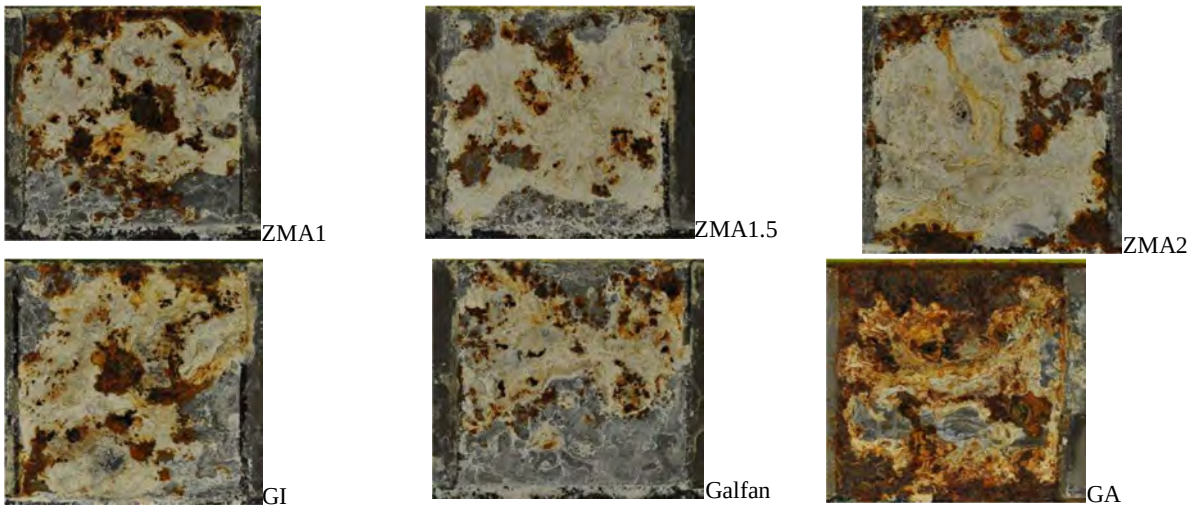

Figure 102: Photographs of open panels after 6 weeks in VDA test (size of a sample 40x40mm)

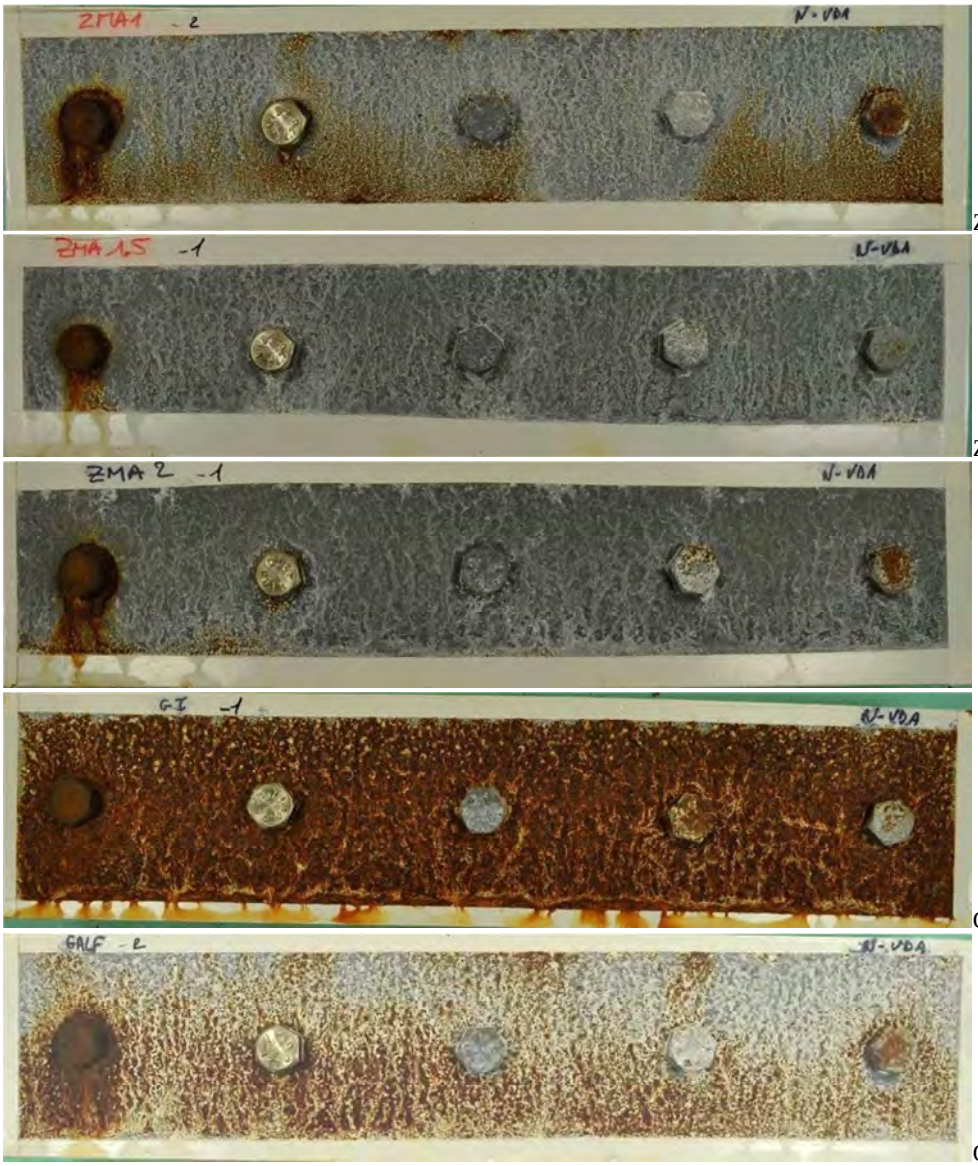

ZMA1

ZMA1.5

ZMA2

GI

Galfan

Figure 103: Photographs of galvanic panels after 6 weeks in NewVDA test (from left to right: steel, stainless steel, Zn-Ni coated steel, ZEC888 coated steel and Geomet coated steel).

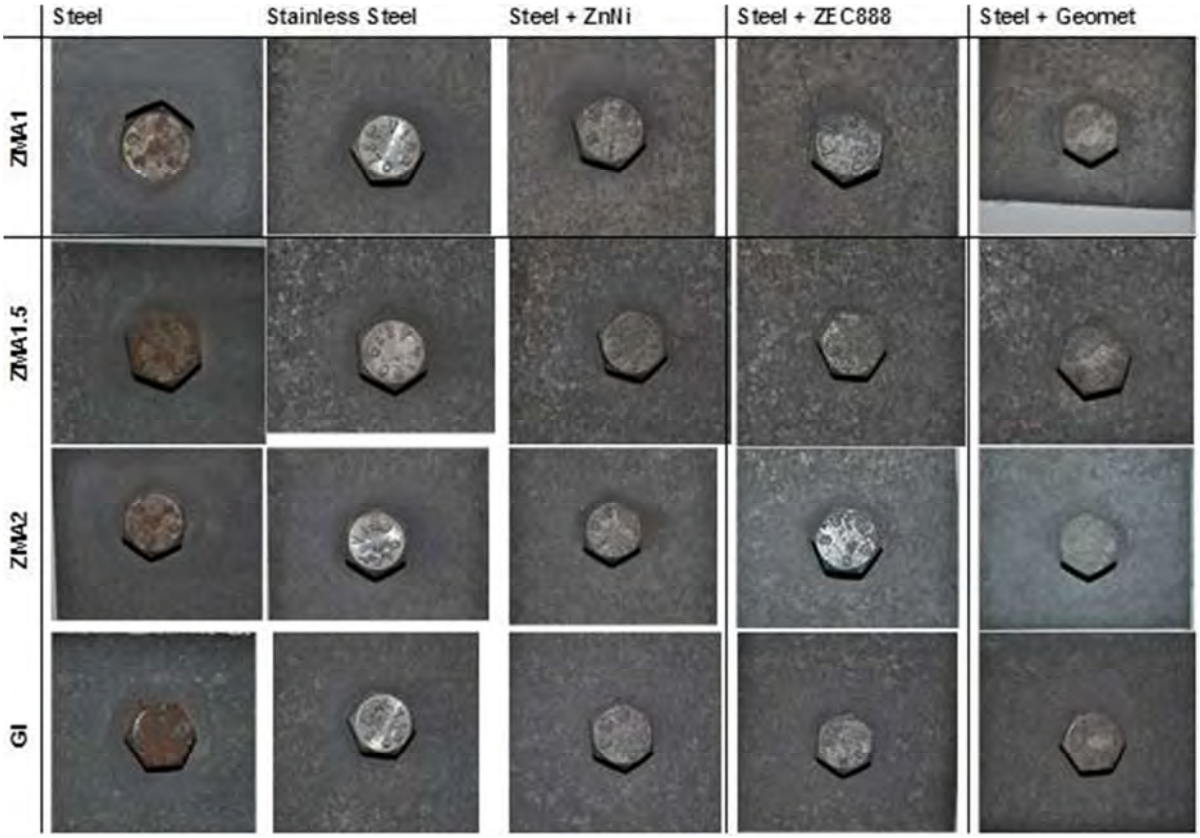

Figure 104: Photographs of ZMA and GI coated steel panels in galvanic couple with steel, stainless steel and Zn-Ni coated steel after 2 years of exposure under a truck driving in Switzerland. (On-site photographs)

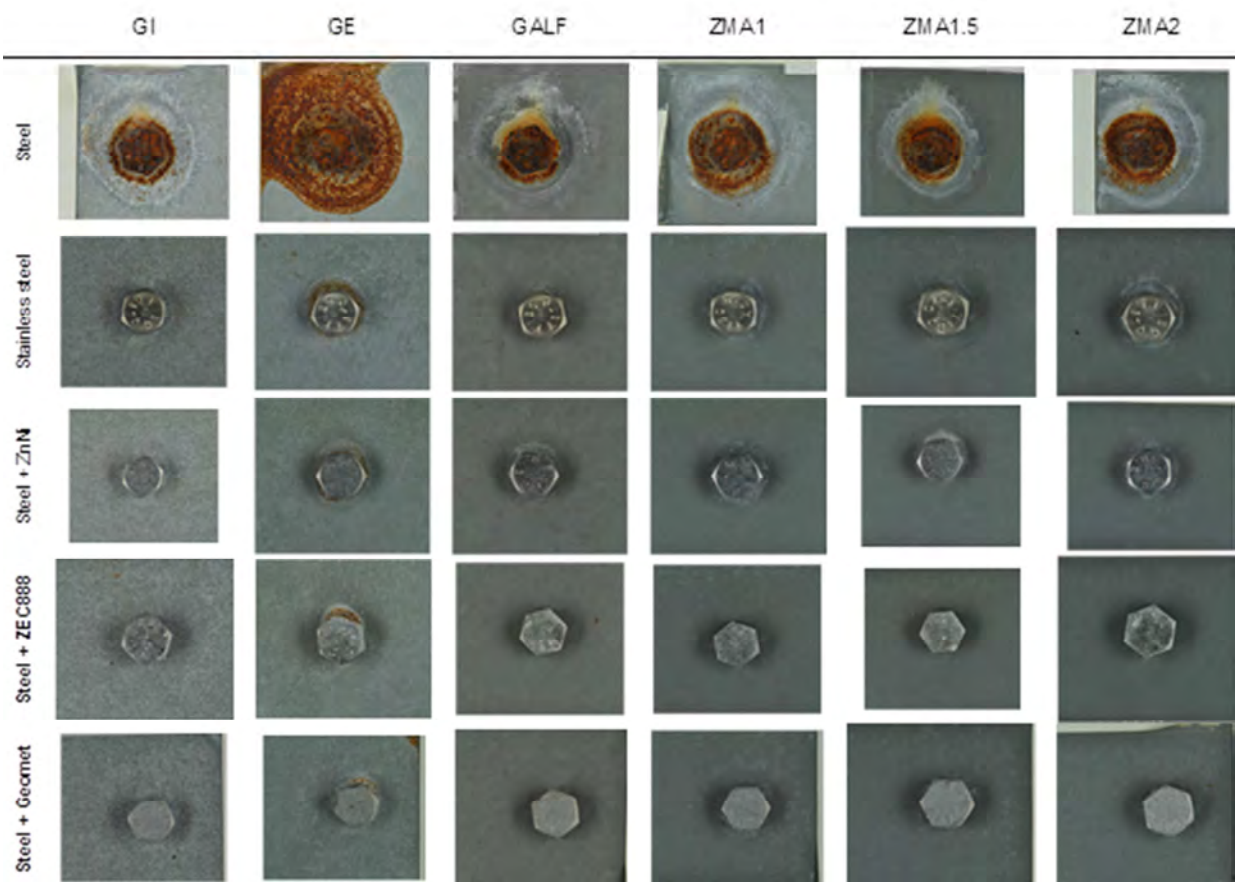

Figure 105: Photographs of ZMA, GI, GE and galfan coated steel panels in galvanic couple with different nature of fasteners after 2 years of marine exposure.

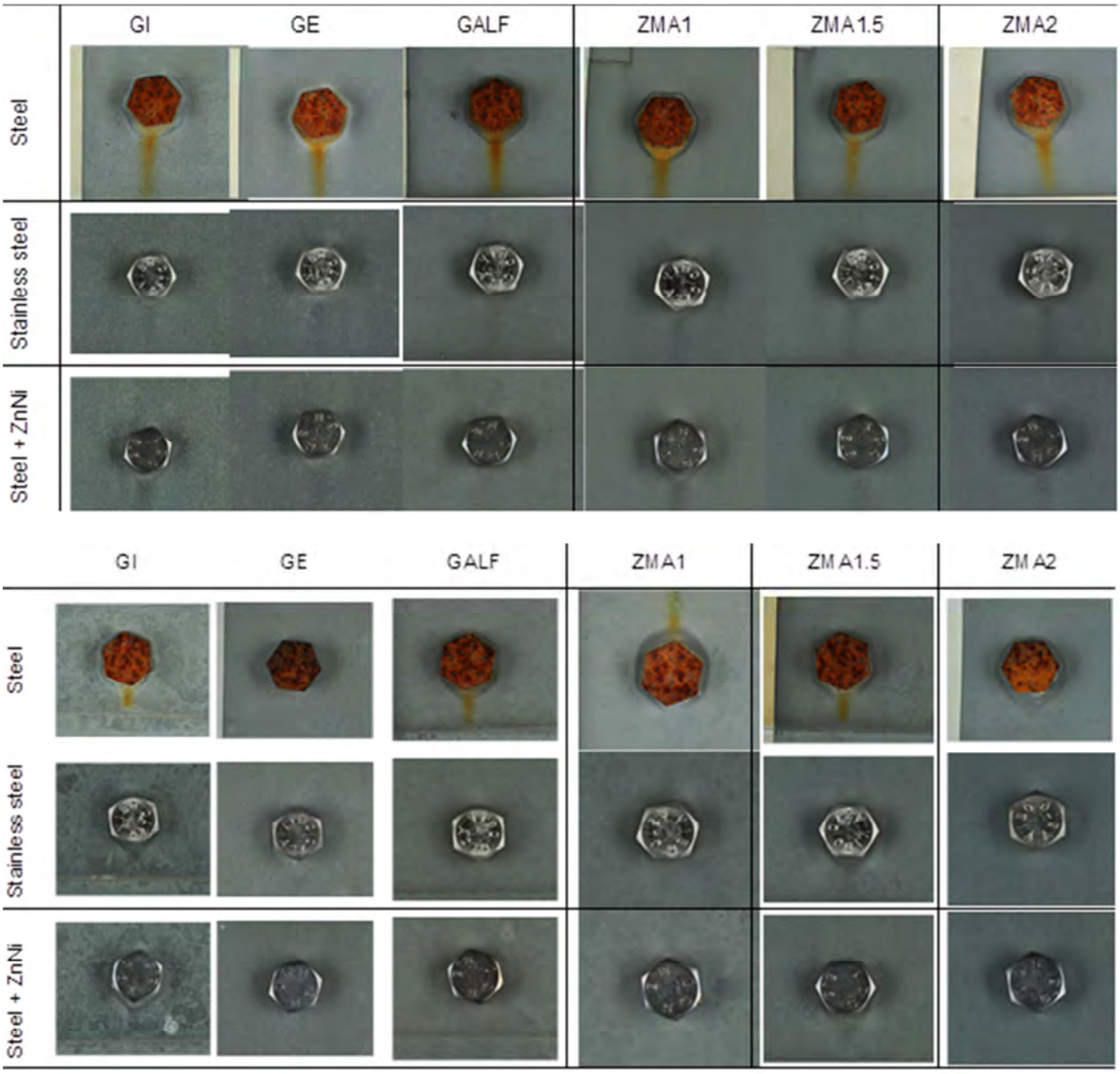

Figure 106: Photographs of ZMA, GI, GE and galfan coated steel panels in galvanic couple with steel, stainless steel and Zn-Ni coated steel after 2 years of exposure in Dortmund (top) and Linz (bottom).

9.3 Appendix 3: FTIR and XRD analysis for WP 7

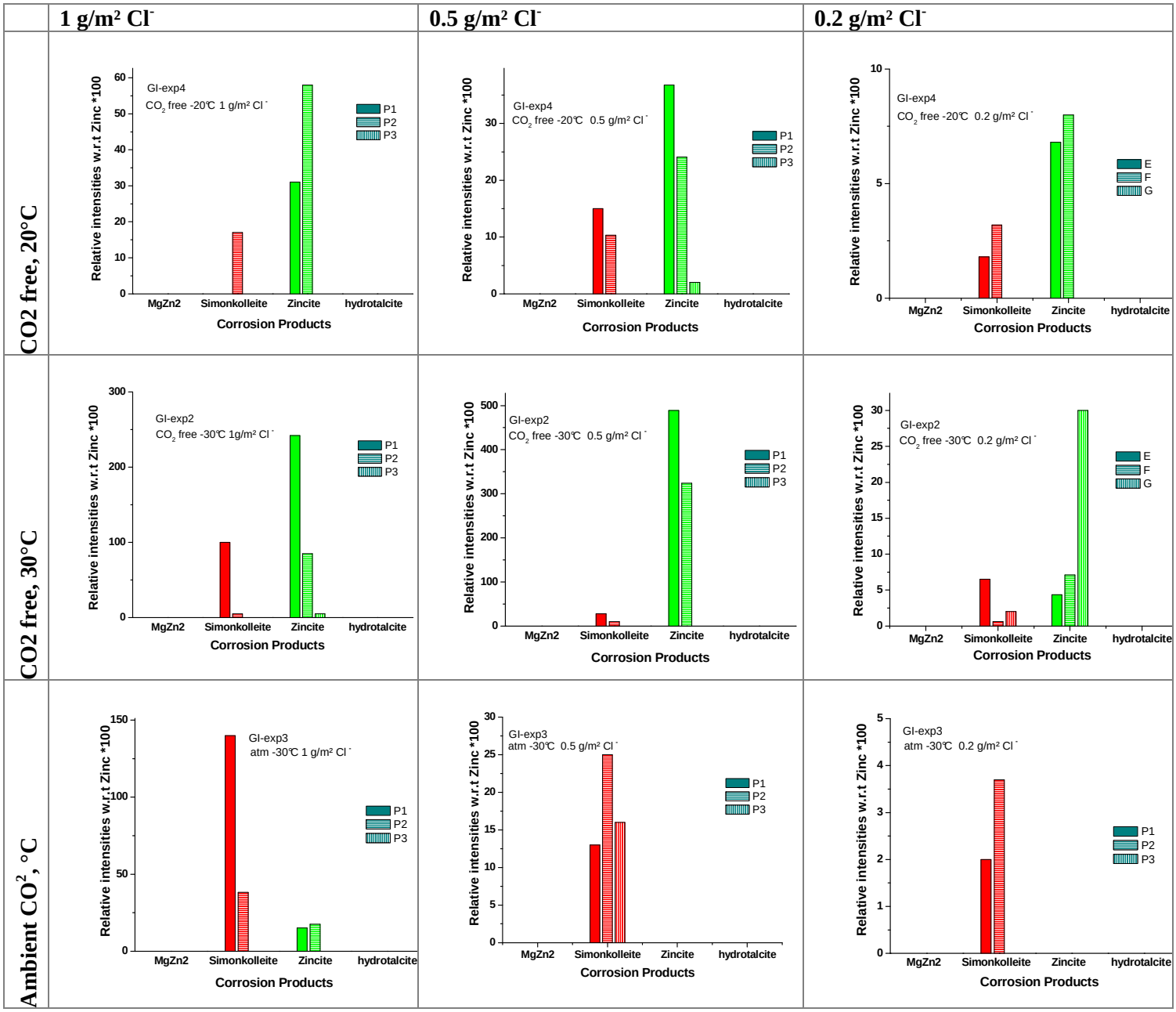

Figure 107: Relative amount of zinc corrosion products on GI coated steel as a function of exposure conditions (from XRD measurement). P1 to P3 refer to several points of measurements.

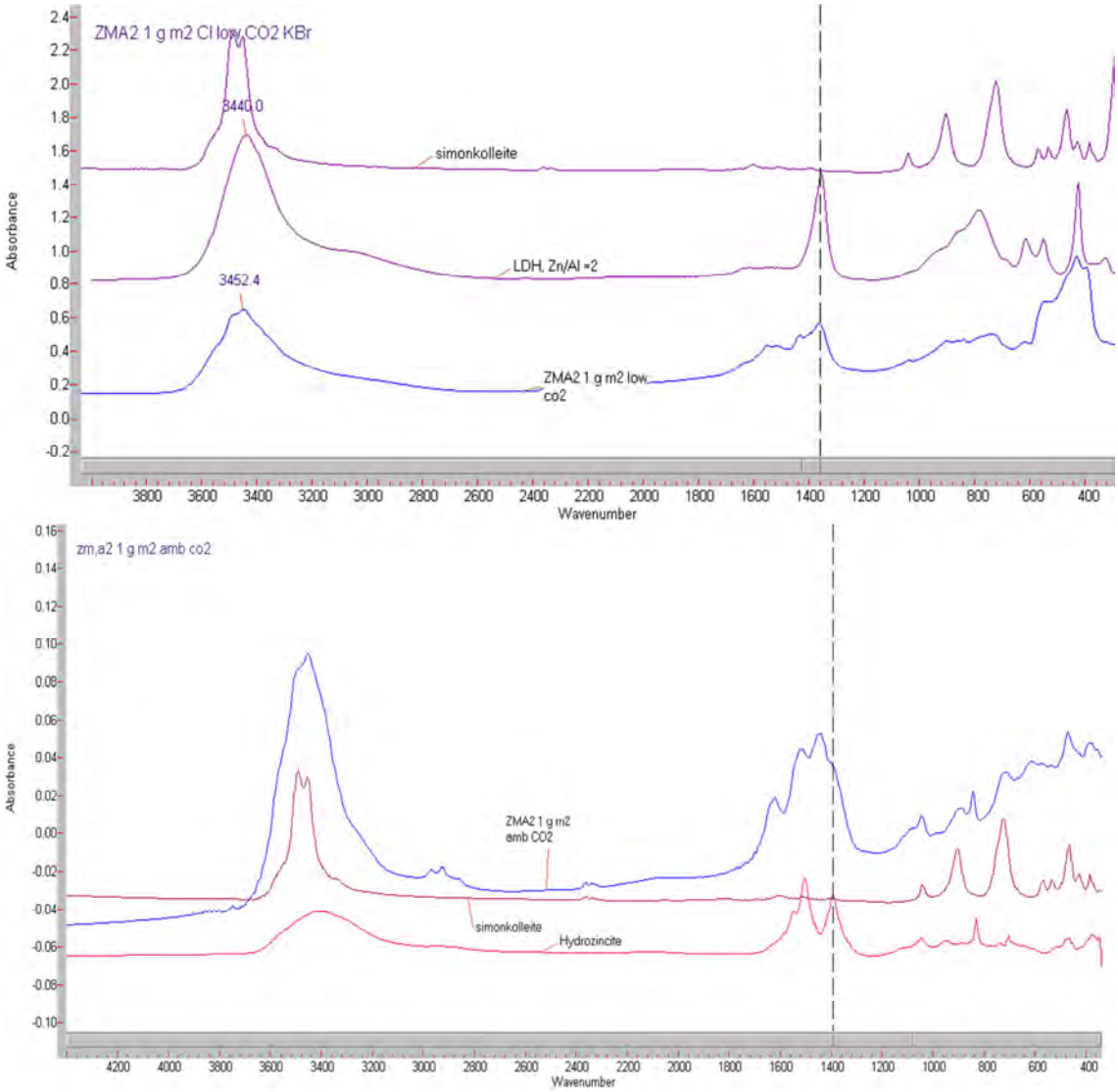

Figure 108: Transmission FTIR spectra of corrosion products formed on ZMA2 in low CO_2 atmosphere (top) and air (bottom). Comparison with reference spectra of simonkolleite, LDH and Hydrozincite.

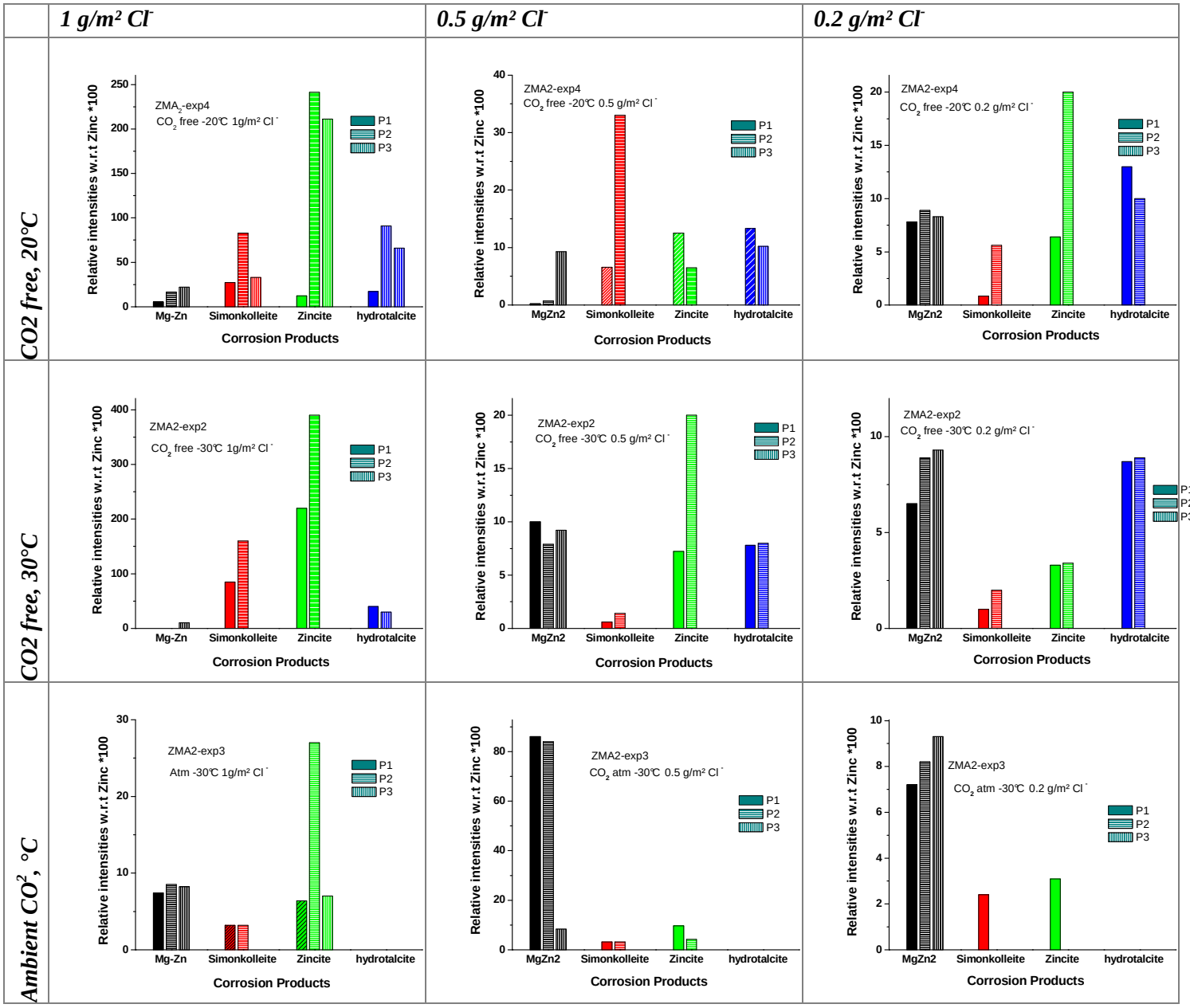

Figure 109: Relative amount of zinc corrosion products on ZMA2 coated steel as a function of exposure conditions (from XRD measurements). P1 to P3 refer to several points of measurement. Note the thinner corrosion product layer (Y axis) at ambient carbon dioxide amounts.

European Commission

EUR 26323 — Advanced zinc-based hot dip coatings for the automotive application (AUTOCOAT)

Luxembourg: Publications Office of the European Union

2013 — 127 pp. — 21 × 29.7 cm

ISBN 978-92-79-34587-6
doi:10.2777/50368

HOW TO OBTAIN EU PUBLICATIONS

Free publications:

- one copy:
  via EU Bookshop (http://bookshop.europa.eu);
- more than one copy or posters/maps:
  from the European Union's representations (http://ec.europa.eu/represent_en.htm);
  from the delegations in non-EU countries (http://eeas.europa.eu/delegations/index_en.htm);
  by contacting the Europe Direct service (http://europa.eu/europedirect/index_en.htm) or calling 00 800 6 7 8 9 10 11 (freephone number from anywhere in the EU) (*).

  (*) The information given is free, as are most calls (though some operators, phone boxes or hotels may charge you).

Priced publications:

- via EU Bookshop (http://bookshop.europa.eu).

Priced subscriptions:

- via one of the sales agents of the Publications Office of the European Union (http://publications.europa.eu/others/agents/index_en.htm).

KI-NA-26323-EN-N

The aims of this project were to establish connections between the coating composition, microstructure, pre-treatment and corrosion performance of ZnAlMg 'ZMA' coatings both in accelerated tests and field exposures. Line hot dip materials including four conventional zinc coatings and three ZMA coatings (ZnMg1%Al1%, ZnMg2%Al2%, ZnMg1.5%Al1.5%) were selected. In addition, a galvanising simulator was used to prepare ZMA coatings with different compositions of Mg and Al (up to 4 %).

ZMA coatings were suitable for standard phosphatising process and showed good robustness in respect to process variations. ZMA coatings also showed rather comparable application properties to HDG regarding formability, spot welding and adhesive bonding.

Significant improvements of ZMA over standard coatings were observed to be more pronounced for the most aggressive tests and especially for early stages of corrosion. ZMA coatings exposed in stationary sites and on-vehicle showed an improvement of 2 compared to HDG when tested unpainted in open configurations, while no differences were observed on painted samples after 2 years. For hem-flange designs, the improvement of ZMA was not obvious whatever the tests. The corrosion performance of ZMA was not linked to the presence of a specific corrosion product (simonkolleite or hydrotalcite). Rather, it is suggested that the effect of the alloying element is in the change of the microstructure and resulting anode/cathode ratio that will profoundly affect the pH of the cathode and explain the improved corrosion behaviour. This also explains why the improvement after long-term field exposure tests is less pronounced, as this effect is mainly active in the initial stages.

Studies and reports

ISBN 978-92-79-34587-6

Publications Office

doi:10.2777/50368